Western Australia's Weather and Climate

A Synthesis of Indian Ocean Climate Initiative Stage 3 Research

Manuscript ID: EP125374

Climate Adaptation Flagship

Citation

Indian Ocean Climate Initiative (2012) Western Australia's Weather and Climate: A Synthesis of Indian Ocean Climate Initiative Stage 3 Research. CSIRO and BoM, Australia.

Editors: Bryson Bates, Carsten Frederiksen and Janice Wormworth.

Drafting authors*: Doerte Jakob, Agata Imielska, Steve Charles, Guobin Fu, Carsten Frederiksen, Jorgen Frederiksen, Meelis Zidikheri, Pandora Hope, Kevin Keay, Catherine J. Ganter, Yun Li, Aloke Phatak, Mark Palmer, Janice Wormworth, John McBride, Richard Dare, Sally Lavender, Debbie Abbs, Leon Rotstayn, Tony Rafter

N. B.: The order of authors presented here corresponds to the sequence of presentation in the report body, and is not intended to reflect the level of contribution of individual authors.

Copyright and disclaimer

Important disclaimer

Foreword

It is with considerable pride that I see Stage 3 of the Indian Ocean Climate Initiative (IOCI3) conclude with this report, a synthesis of four and half years of research on Western Australia's climate. As both a farmer and former policymaker, I am aware of the important role these results will play in informing decisions to help Western Australians avoid the losses and realise the benefits of a changing climate.

I have been involved in IOCI since 1997 when, as Deputy Premier, I launched this Initiative. Its catalyst was the dramatic decline in south-west Western Australia winter rainfall – the major research focus of IOCI's first two stages. The third stage of IOCI continued to build on this important work, but also extended the scope of its inquiry to the climate systems of the economically important north-west of our state.

The new scientific results contained in this report are compelling. IOCI3 has improved our knowledge of extreme events in the North West: heat waves, intense rainfall and tropical cyclones. It has provided state-of-the art climate projections for both the North West and South West. And it has shed further light on the regional weather systems and hemispheric drivers implicated in the continuing and expanded drying of the South West. It has also advanced our understanding of the root causes behind these large-scale changes.

A 2011 report by consultants ACIL Tasman found that IOCI scientists have accomplished all this while providing good value for money, confirming that our leaders have invested public funds wisely. Their independent report also documents IOCI's uptake by decision makers, demonstrating the Initiative's influence on policy or management decisions in areas including water supply, agriculture, fisheries, health and emergency services, and mining safety.

I have personally witnessed the value of the Initiative to farmers who, thanks to IOCI results, have greater confidence when they make important decisions to grapple with weather and climate related risks. Whilst the relevance and value of its scientific results are clear, I believe IOCI is also a valuable demonstration of how Western Australians can successfully tackle adversity: by driving scientific innovation, new knowledge and skills.

I would like to thank the many people from the CSIRO, BoM and Government of Western Australia who contributed to this effort, but whom are too numerous to name here.

Hon Hendy Cowan

Chair, Indian Ocean Climate Initiative Stage 3

Contents

List of Acronyms

ACORN-SAT - The Australian Climate Observations Reference Network Surface Air Temperature dataset.

APC - Anomaly pattern correlation

AWAP - Australian Water Availability Project

CCAM - CSIRO Conformal-Cubic Atmospheric Model (see glossary)

CMIP3 - Coupled Model Intercomparison Project Phase 3 (see glossary)

CMIP5 - Coupled Model Intercomparison Project Phase 5 (see glossary)

DTD - Dew point temperature depression

ECMWF - European Centre for Medium Range Weather Forecasts

ENSO - El Niño – Southern Oscillation (see glossary)

ERA - ECMWF Reanalysis

GCM - Global climate model

GHG - Greenhouse gas

IBTrACS - International Best Track Archive for Climate Stewardship

IFD - Intensity-frequency-duration - see Box 6

IPCC - Intergovernmental Panel on Climate Change (see glossary)

NHMM - non-homogeneous hidden Markov model

NWWA - north-west Western Australia

NCAR/NCEP reanalysis - National Center for Atmospheric Research/National Center for Environmental Protection Reanalysis Project - see Box 2, sub-section 4.1.2.1

RCM - Regional climate model

RCP - Representative Concentration Pathway

SAM - Southern Annular Mode / Southern Hemisphere Annular Mode; also known as the Antarctic Oscillation, or the High-Latitude Mode (see glossary)

SWAC - Southwest Western Australian Circulation

SWWA - south-west Western Australia

SRES – IPCC Special Report on Emissions Scenarios - see Box 3

TC - Tropical cyclone

Acknowledgments

For all projects we appreciate the knowledge and input from the climate section, forecasters and severe weather staff at the Western Australian Regional Office of the Bureau of Meteorology.

Project 1.1: We acknowledge the modelling groups, the PCMDI and the WCRP's Working Group on Coupled Modelling (WGCM), for their roles in making available the WCRP CMIP3 multi-model dataset.

Project 1.2: We thank Pauline Treble from the Australian Nuclear Science and Technology Organisation for providing data and collaborating on the paleoclimate study within this project. Alan Wain from the Bureau of Meteorology did the backward trajectories for that study.

We thank Ming Feng and Evan Weller from CSIRO and Nick Caputi from Western Australian Department of Fisheries for their knowledge of puerulus life cycle that helped guide the study of 'spring' weather systems.

Project 1.3: We would like to acknowledge Professor Xiaogu Zheng, College of Global Change and Earth System Science, Beijing Normal University, Beijing, China, who collaborated on the results on the predictability of Western Australian rainfall and temperature.

Project 2.1: This project would not have been possible without a large contribution from staff at the Queensland Climate Change Centre of Excellence, in particular Stephen Jeffrey. Funding from the centre and matching funds from CSIRO were also essential for completion of the project; staff at CSIRO (Leon Rotstayn, Mark Collier and Stacey Dravitzki) were partly supported from these funds. The Queensland Government Department of Environment and Resource Management provided the high performance computing facilities for the CSIRO Mk3.6 simulations. The National Computational Infrastructure Facility in Canberra provided storage and processing resources for analysis of the CSIRO Mk3.6 simulations.

P**rojects 2.3 and 3.1:** The NHMM stochastic downscaling model code is developed and maintained by Sergey Kirshner, Purdue University, USA. His ongoing collaboration and assistance is gratefully acknowledged.

The GCM data used to generate stochastically downscaled projections were obtained from the Program for Climate Model Diagnosis and Intercomparison (PCMDI) www-pcmdi.llnl.gov. We acknowledge the modelling groups, the PCMDI and the WCRP's Working Group on Coupled Modelling (WGCM), for their roles in making available the WCRP CMIP3 multi-model dataset. Support of this dataset is provided by the Office of Science, U.S. Department of Energy. We also thank Mark Collier, CSIRO Marine and Atmospheric Research (CMAR), for maintaining a local archive of this data.

The CCAM temperature projections used in the generation of stochastically downscaled daily maximum and minimum temperatures were provided by Jack Katzfey, CMAR. His assistance is gratefully acknowledged.

Project 2.4: We acknowledge with thanks Jack Katzfey, Marcus Thatcher and Kim Nguyen for providing the CCAM outputs used in the analyses on tropical cyclones.

The hot spell model used in this report was jointly developed with Rick Katz from the Institute for Mathematics Applied to Geosciences at the National Center for Atmospheric Research (NCAR), Boulder, USA during Yun Li's two NCAR visits: the first visit was supported by a visiting scholar grant of the NCAR in 2010; the second was supported by a travel award from the Australian Academy of Science for Scientific Visits to North America in 2011.

Project 3.2: We thank the Western Australian Department of Water and Department of Agriculture and Food Western Australia for their supply of pluviograph data.

Key IOCI3 Research Findings

What *changes* to Western Australia's climate systems have been observed?

- South-west Western Australia's May-to-July rainfall decline has intensified and expanded in geographic extent during the last ten years[1]. In the far south-west, year-to-year rainfall fluctuations also declined along with rainfall totals.
- Winter (July) rainfall increased over central north-west Western Australia, and in central Western Australia.
- At Perth Airport the mean hot spell[2] frequency increased from approximately six events in 1958 to eight events in 2011. However, over the same period the mean duration of hot spells declined, from approximately two days to 1.5 days. There was no trend in hot spell intensity over this period.
- No trend can be detected thus far in the frequency or intensity of South Indian Ocean tropical cyclones for the 1992/93 to 2006/07 seasons, the period for which records can be considered consistent.

What do we understand about the *causes* of these changes?

South-west Western Australia rainfall declines:

- During the past 60 years there has been a 17% decrease in the strength of the subtropical jetstream, which is vitally important for the generation of storms in winter.
- Also during this period, significant warming south of 30° S reduced the atmospheric temperature gradient between the equator and South Pole, particularly over the Indian Ocean.
- Since 1950, these changes have increased the stability of the atmosphere during winter (and other seasons) in regions important for the formation of storms that affect south-west Western Australia. The result is fewer storms impacting on this region and the trend of observed rainfall decrease.
- Modelling shows that these large-scale changes are consistent with those expected in an atmosphere influenced by increasing concentrations of greenhouse gases. This is a major signature of climate change on the global climate system.
- Since the year 2000, south-west Western Australia's continuing May-to-July rainfall decline has been driven by a 15% increase in the prevalence of high-pressure systems. (Prior to this, the rainfall decline had been driven by a decreased incidence of deep low-pressure weather systems.) There has also been a reduction in the atmospheric moisture content of the lower troposphere.

North-west Western Australia rainfall increases:

- The amount of rainfall associated with each tropical cyclone increased during the period 1970 to 2009 in north-west Australia, most markedly from 1989 to 2009.
- The amount of rainfall from other forms of closed low weather systems also increased in north-west Australia from 1989 to 2009.

---

[1] Compared to averages for 1969 to 1999.

[2] Defined as one or more consecutive days of maximum temperature exceeding 37 °C.

- In the Kimberly region, weather patterns associated with very wet conditions became more common, and those with very dry conditions less common, during the summer wet season since 1960. In the Pilbara, weather patterns associated with summer dry conditions have also decreased since 1980, and some associated with summer wet conditions have increased since 1960.
- The formation of large-scale weather systems known as north-west cloud bands and intraseasonal oscillations has increased during winter over the past 60 years, a trend consistent with rainfall increases observed in central north-west and central Western Australia.
- Modelling studies suggest that aerosols (fine particles of air pollution from human activity) have contributed to the rainfall increase observed in north-west Western Australia. This finding is based on one climate model, and should be further tested using a range of climate models.
- The influence of Antarctic ozone depletion may have had a similar (but less pronounced) effect to that of aerosols, and natural variability is also likely to be important.

What can we say about anticipated *future* changes to South-west Western Australia's climate?

- Multiple approaches used to provide rainfall projections suggest south-west Western Australia's drying trend will continue under future scenarios of rising greenhouse gas emissions, as follows:
  - Modelling of large-scale changes to the atmosphere indicates that, as greenhouse gas concentrations continue to increase, the stability of the atmosphere in regions important for the formation of storms affecting south-west Western Australia will continue to increase over this century, with corresponding reductions in rainfall in all months of the May-October half-year. Reductions could exceed 20 millimetres in some months.
  - Modelling studies of regional weather systems indicate that high-pressure systems could become more prevalent; some models indicate that their incidence could increase 70% by the period 2081 to 2100 (compared to the 1961 to 2000 baseline). The incidence of low-pressure systems is expected to decrease by almost as much.
  - Station-scale projections also indicate a drying of south-west Western Australia's climate by mid-century (2047 to 2064), continuing through to end of the century (2082-2099), compared to the present day (1962 to 1999).
- Station-scale climate projections for south-west Western Australia also suggest that both maximum and minimum temperatures will warm by mid-century through to the end of the century under a high greenhouse gas emissions scenario.

North-west Western Australia's climate?

- International actions may lead to a future reduction in aerosols. This reduction would be expected to partially 'unmask' the effect of increasing atmospheric concentrations of greenhouse gases, and lead to a drying influence in north-west Western Australia.
- Station-scale projections indicate a drying of Kimberley and Pilbara region climates by mid-century (2047 to 2064), continuing through to end of the century (2082 to 2099), compared to the present day (1962 to 1999), under scenarios of increasing greenhouse gas emissions.
- Station-scale modelling studies also project a warming of the Kimberley and Pilbara region climates by mid-century, and further warming by the end of this century, under a high greenhouse gas emissions scenario.
- Modelled projections indicate there could be a 50% reduction in the number of tropical cyclones in the second half of this century (2051 to 2090) compared to present day (1971 to 2000), under scenarios of increasing greenhouse gas emissions.
- However, this modelling also suggests a distinct shift towards more destructive storms; the most intense tropical cyclones would become still more powerful.
- These projections for the frequency and intensity of South Indian Ocean tropical cyclones are in line with global projections.

- The projections also suggest a 100-km southward shift in the region of tropical cyclone formation and decay, a decrease in tropical cyclone duration (by an average 0.6 days), and an increase in the intensity of rainfall associated with these storms.

Technical Report of the Indian Ocean Climate Initiative, Stage 3

1 Introduction

The Indian Ocean Climate Initiative (IOCI) is a strategic program of research and information transfer to support government decision-making. A research partnership between the Government of Western Australia, the Commonwealth Scientific and Industrial Research Organisation (CSIRO), and the Australian Bureau of Meteorology (BoM), IOCI completed its third stage in June 2012.

1.1 Science to Inform Adaptation

Western Australia is a land of droughts and fires, storms and flooding rains, with climatic regions that range from the tropics to latitudes influenced by the Roaring Forties. Our variable and sometimes extreme climate shapes our lives and livelihoods, economic activities, social well being and unique natural environment. Western Australians are accustomed to responding to fluctuating climatic conditions, but climate change will pose still greater challenges for the state's society and economy. To adapt requires an even more proactive approach to decision making: communities, business and government must make decisions to avoid the risks and take advantage of the opportunities presented by a changing climate. The Indian Ocean Climate Initiative aims to empower decision makers by delivering a strategic program of climate research to provide the best available scientific knowledge in a policy-ready form.

Figure 1.1 The key study areas for IOCI3 as declared by state agencies are indicated by orange lines. In NWWA this includes the major part of the Bureau of Meteorology's Kimberley and Pilbara forecast districts and parts of the Gascoyne and Interior. This region contains most of the economically important Pilbara and North West Shelf. In SWWA the study region lies south-west of a line approximately from Esperance to Northampton. It includes the eastern and northern parts of the wheat belt, areas not considered under IOCI Stages 1 and 2.

1.2 IOCI History and Achievements

IOCI has increased the State's capacity to understand and cope with climate change and weather variation through significant advances in knowledge about south-west Western Australia (SWWA) and more recently north-west Western Australia (NWWA) (see Figure 1.1). Its results, along with parallel initiatives stimulated

by its activity, have regional, national and international significance. IOCI has yielded important, fundamental research about the nature and causes of drying in SWWA. This includes establishing a human 'fingerprint' of global warming on shifts in storm tracks that bring rain to SWWA. As one of the few countries in the tropics with high-quality weather data and climate modelling capacity, Australia – and therefore IOCI – is well placed to advance our understanding of the key features of the tropical climate. Groundbreaking research by IOCI3 on NWWA, detailed in this report, provides new insights into these features.

1.3 Scientific Achievements

Commencing in 1998, Stage 1 of IOCI investigated the reasons for the winter rainfall decline in SWWA, and sought better understanding of how the climate varied across years and decades. IOCI1 did this by improving datasets, detecting change, and advancing understanding of the behaviour of extremes throughout the rainfall decline. IOCI1 also improved understanding of Indian Ocean climate variability.

Stage 2 of IOCI sought to discover the causes of the climatic changes detected by IOCI1. It also answered other related questions through collaborative work on topics including historical climate, river flows, groundwater, salinity, sea temperature, sea level, and the Leeuwin current.

IOCI3 (see below) sought to analyse both rainfall and temperature variability and change across the whole state and, in particular, aimed to improve understanding of NWWA's climate systems.

Since 1998, IOCI scientists have produced 152 research outputs, including more than 80 peer-reviewed book chapters, reports and other publications. By May 2011, IOCI's published works had been cited 741 times by papers published worldwide. Considerable effort was also expended to inform stakeholders and the general public about IOCI's findings.

1.4 Broader Community

Information from IOCI's independent and objective science permits policymakers to implement sound and rational regional policies in response to climatic changes. As a gauge of its policy influence, IOCI has been mentioned more than 50 times in the Parliament of Western Australia. IOCI results have been crucial to water, fisheries, and agricultural policy, and also informed policy related to health and emergency services (ACIL Tasman 2011). IOCI3 work on NWWA's climate will inform decision making in the mining and petroleum sectors. Chapter 7 provides further information on the application of IOCI3 results to policymaking and management in Western Australia.

1.5 About IOCI3

IOCI3 continued strategic research on the key features of SWWA's weather and climate, but also extended its scope to NWWA for the first time. Mining and energy companies are strongly investing in this region, yet relatively little is known about NWWA's climate, and even basic weather data are much sparser than in SWWA.

THEME 1: BASELINES AND PREDICTABILITY OF WESTERN AUSTRALIA CLIMATE AND ATTRIBUTION OF CLIMATE CHANGE

Theme 1 of IOCI3 focused on detecting changes to weather systems and factors that influence or are related to the large-scale drivers of circulation patterns in the atmosphere. It aimed to establish the causes of these changes to identify whether a fingerprint of anthropogenic (human-induced) climate change can be detected (Project 1.1). This theme also focused on SWWA's climate and weather systems, identifying the presence or absence of trends in rainfall totals and intensities, and changes in the different weather systems that affect this region (Project 1.2). Other work under this theme sought to determine the upper

limits of predictability of Western Australian rainfall and temperature across seasons (Project 1.3). Finally, an entire project under Theme 1 was dedicated to providing high-quality, high-resolution datasets on daily climate for both NWWA and SWWA (Project 1.4). A resource for stakeholders, these data also fed into other IOCI3 projects.

THEME 2: CURRENT AND FUTURE CLIMATE OF THE NORTH WEST INCLUDING EXTREME EVENTS

Theme 2 of IOCI3 focused on NWWA. It sought to investigate the possible role of aerosols (fine particles suspended in the atmosphere that are generated by human activity) in the rainfall increases observed in NWWA, and how they might affect rainfall in future (Project 2.1). This theme also aimed to improve our understanding of tropical cyclones (TCs) and their relationship to the region's climate, and develop techniques for forecasting TC activity along the Western Australian coastline (Project 2.2). The third project under this theme was dedicated to providing projections (see glossary) of the future climate at spatial and time scales commensurate with regional needs and applications. This included further developing statistical downscaling (Box 1) methods for the tropics, where little such modelling had been done (Project 2.3). New methods were also developed to provide projections of extreme events, including heat waves, intense rainfall events and TCs (Project 2.4).

THEME 3: VERY-HIGH RESOLUTION CLIMATE CHANGE PROJECTIONS FOR THE SOUTH WEST

Focussed on SWWA, the third theme of IOCI3 sought to produce downscaled projections of rainfall and temperature for the middle and end of this century, for use in climate change impact and vulnerability assessments (Project 3.1). It also aimed to develop scenarios of extreme rainfall and temperature for SWWA (Project 3.2).

THEME 4: SCIENCE LEADERSHIP AND SUPPORT

Theme 4 of IOCI3 addressed the need to provide holistic and integrated understanding of climate change and climate variability to state partners and stakeholders. Toward this goal, IOCI3's fourth theme sought to coordinate the program across the research providers and the state, make regular presentations to state agencies and public audiences, and provide a synthesis of emerging messages in policy-ready form.

1.6 About Western Australia's Changing Climate

The following brief overview of observed changes in Western Australia's climate provides some context for the IOCI3 results in this report. South-west Western Australia receives relatively high rainfall totals compared to other western edges of landmasses at this latitude (about 30° S to 35° S; Bates et al. 2008). However, substantial rainfall decreases since the mid-20th century have countered the longstanding perception that SWWA is a region of relatively reliable winter rainfall (IOCI 2002). Winter rainfall declined sharply since the 1960s, a decline accompanied by even more pronounced reductions in streamflows (Bates et al 2008; 2010).

Work done under IOCI Stage 1 and 2 indicated that these changes were associated with large-scale changes in atmospheric circulation, including a 17% reduction in the strength of the subtropical jetstream over Australia. This led to a reduced likelihood of storm development over SWWA compared to the period prior to the 1970s (Chapter 3 reports related new research developments). The number of weather patterns that bring wet conditions decreased, and the number of patterns that bring dry conditions increased (see Chapter 4 for further developments). IOCI research showed that a combination of natural variability and increases in greenhouse gas (GHG) concentrations had likely contributed to the observed SWWA rainfall decline. Annual mean temperatures have also increased in SWWA since the 1970s (Bates et al. 2008).

In contrast to SWWA's rainfall decrease, NWWA has undergone a marked increase in total annual rainfall since 1950. Temperatures warmed only slightly or even cooled in some parts of NWWA over the period 1950 to 2006 (BoM and CSIRO 2007; CSIRO and BoM 2012).

1.7 About this Report

The aim of this report is to provide a technical synthesis of the main IOCI3 research results and methodological advances. Each section provides project links so that readers seeking more detailed information may access the associated Milestone reports from the IOCI website: www.ioci.org.au/publications.html.

2 Improved climate data and modelling

Drafting Authors: Doerte Jakob, Agata Imielska, Steve Charles and Guobin Fu

Western Australia's climate varies greatly, from tropical regions to the desert interior, and on to the Mediterranean climate of the South West. Studying this diverse climate is a challenge because meteorological networks are sparse in many areas, and existing networks expanded considerably or underwent other changes during the 20th century. This challenge is particularly marked in NWWA. For example, prior to IOCI3 only two high-quality daily rainfall records existed north of 20° S. Under IOCI3 ten new records have been added. This chapter describes the results of work to fulfil one important IOCI3 goal: to improve the quality and extend the coverage of climate data.

Another major goal of IOCI3 was to increase the utility of climate model output to further the understanding of Western Australia's present-day and future climate. One important such advance, discussed in this chapter, is the application of statistical downscaling (see Box 1) to the tropics and subtropics of the North West. This provided high-resolution projections, which can be used to inform climate change impact assessment and adaptation planning.

2.1 Extending and Improving High-Quality Climate Datasets

Project Link: 1.4[3]

The Bureau of Meteorology records and collects meteorological observations through its networks and incorporates this information into its databases. BoM uses sophisticated data analysis techniques to develop reference datasets, also referred to as high-quality datasets, for use in climate monitoring. Here the term 'dataset' refers to a collection of records of a meteorological variable (e.g., rainfall) from a specified set of station locations.

High-quality climate datasets are vital for stakeholders in planning and management. These datasets describe the information necessary to understand our climate and its variability at fine spatial and temporal scales. Historical data also allow us to understand how well climate models are able to replicate the real world, and help us to improve them.

Under IOCI3 the spatial coverage of existing high-quality datasets was extended and their data quality improved. The accessibility and usability of existing datasets was improved and new datasets (e.g., on cloud cover) were added to the existing range of high-quality datasets.

The quality of long records of climate can be affected by changes that actually have nothing to do with climate or weather, such as the relocation of a weather station from a city centre to a local airport. Such changes can produce artefacts in the data that may severely contaminate further analysis. To address this problem, IOCI3 scientists performed statistical tests to identify 'break points' (points at which discontinuities in the data are detectable), using neighbouring stations as a reference and metadata[4] to confirm that the break points were due to non-climatic factors (e.g., a change in a station's location). Once these break points were identified, metadata were used to provide the documentation needed to allow scientists to validate (confirm) the break points. Where necessary, adjustments were derived using

[3] See Chapter 1 for a description of IOCI3 projects. Further information, including project-by-project milestone reports, may be found online at www.ioci.org.au.

[4] Metadata are 'data about data'. They provide information on how measurements were undertaken including changes in measurement processes, such as changes to instrumentation, location, or observing practices (e.g., a change from imperial to decimal units).

reference stations. This process of making adjustments to data to compensate for external influences is referred to as data 'homogenisation' (see glossary).

2.1.1 HIGH-QUALITY RAINFALL DATASET

South-west and northern Western Australia were identified as key study areas for improved coverage because rainfall changes have occurred in these regions in recent decades. The new high-quality station network consists of 157 stations (this number includes 12 locations for which records of two or more stations were merged to form one long record). This IOCI3 work significantly improved coverage in the state's south-west and north (Marinelli et al. 2012; Figure 2.1 below).

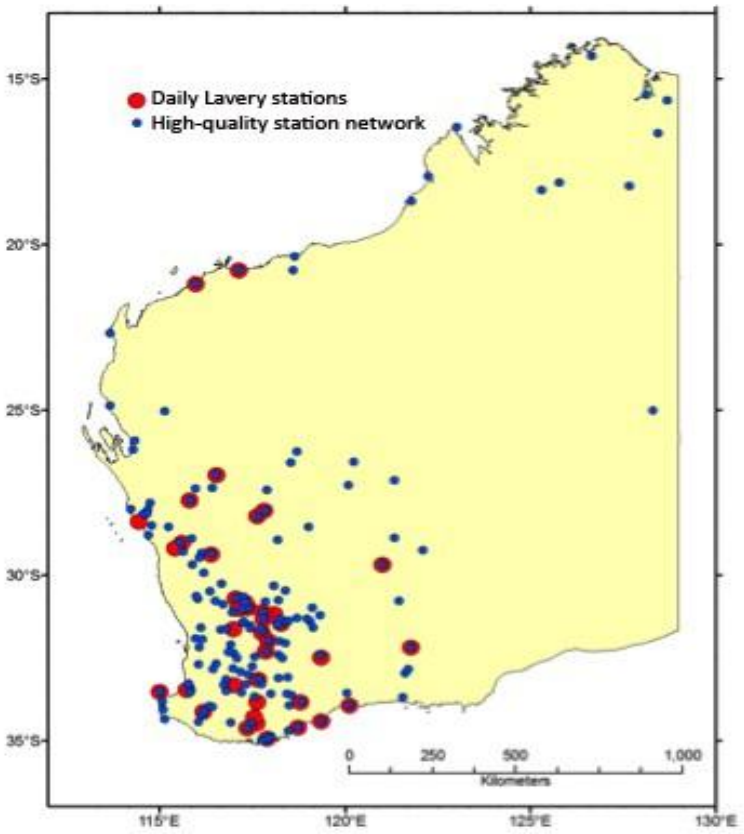

Figure 2.1 Expanded high-quality rainfall dataset. Red dots illustrate the location of stations described in Lavery et al. (1992), a network considered to be the 'gold standard' for high-quality rainfall data for approximately 20 years. Blue dots illustrate the newly developed high-quality station network for rainfall data, showing improved coverage in both the south-west and north of Western Australia.

All available daily rainfall records for stations located in Western Australia were checked for their completeness. Only stations with no more than 5% of their data missing for the period 1950 to 2008 were considered for further analysis. The data for this subset set of stations then underwent initial quality control. The statistical characteristics of the data from these stations was compared with neighbouring stations; if comparison revealed its data to be of inferior quality, the station was excluded from the high-quality network.

Once these steps were completed, a lack of suitable candidate stations was evident in the northern half of the state, especially the Kimberley. Where suitable records were available, the records of two or three stations were merged to produce composites.

The data from the selected stations then underwent further quality-control tests. This entailed automated checks (to identify values deemed suspect) followed by manual examination of suspect values (based on comparison against observations at nearby stations). The manual checks showed that only 5% of 1400 values flagged as suspect were subsequently identified as wrong. Where there was sufficient information at nearby stations, estimates were derived to infill missing values (Siriwardena and Seed 2010). The dataset is available at: http://www.bom.gov.au/climate/change/acorn-rainfall.

2.1.2 HIGH-QUALITY TEMPERATURE DATASET

The previously existing high-quality temperature dataset covered the period 1957 to 2009. IOCI3 made major advances by extending this dataset back to 1910 and adding six more stations for Western Australia (Trewin 2012a,b). This will facilitate the century-scale analyses of changes in temperature extremes. As was the case for rainfall data (see above), IOCI3 scientists applied rigorous and consistent quality control and homogenisation techniques, and documented the network as well as the corrections and adjustments they made.

In the first stage of dataset development, IOCI3 scientists subjected all historical data to detailed quality control procedures to check for: internal consistency between maximum and minimum temperatures, and between these and hourly or three-hourly data; and for consistency with surrounding stations. In the second stage, they identified inhomogeneities in the data at each station through a detailed search of metadata, to spot issues such as site moves. Statistical methods, such a comparison of data with that from nearby sites, were also used to locate such issues.

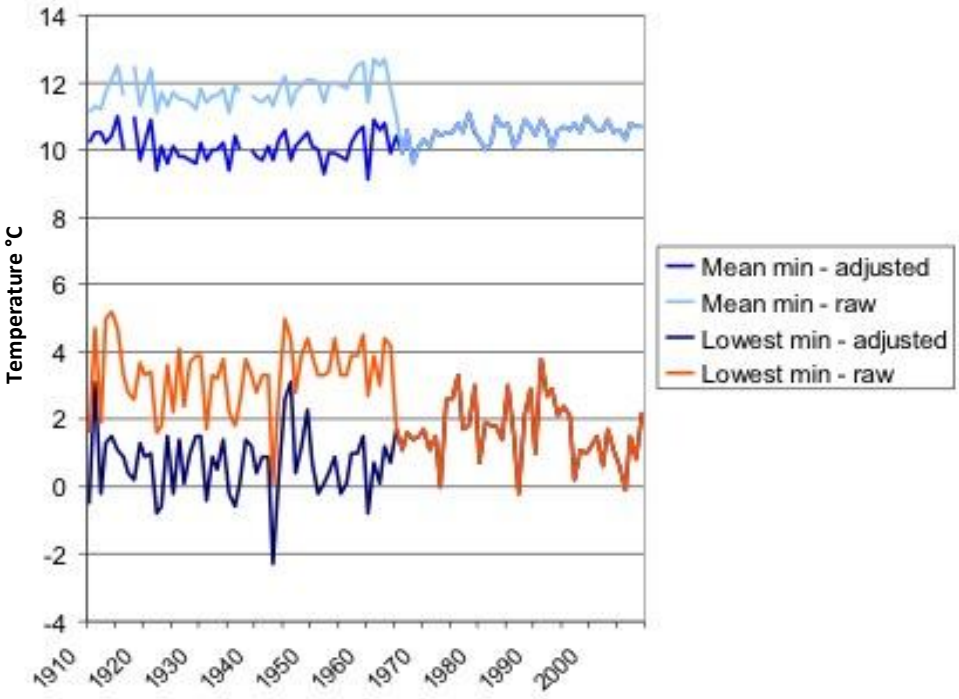

Figure 2.2 Inhomogeneity in minimum temperature data at Albany station. This example was caused by relocation of a weather station from Albany city centre (a coastal location) to Albany airport (about ten kilometres inland). This site move was made in 1965 and its influence is clearly evident in the raw (pre-adjustment) data for average minimum temperatures (pale blue, top series) and for lowest minimum temperatures (orange, bottom series).

This work underscored the need to correct inconsistencies in time series of temperature data that are caused when data collection sites are relocated. Moving a weather station can cause step changes of up to 2 °C in a series; data on extreme temperatures may be affected even more strongly. This problem is

illustrated in Figure 2.2 using the case of Albany, where a site was moved 10 kilometres (km) from a coastal, centre-town location to the airport.

In light of the intense public scrutiny of temperature data in Australia and abroad, the homogenised temperature dataset, named the Australian Climate Observations Reference Network - Surface Air Temperature (ACORN-SAT), was initially reviewed by a panel of experts convened by BoM. This review was followed by a further external review by international experts, who ranked BoM's procedures and data analysis as amongst the best in the world.[5] This international review also made recommendations on ACORN-SAT's future management; BoM implemented some of these recommendations ahead of the dataset's March 2012 public release. The dataset is available at www.bom.gov.au/climate/change/acorn-sat/.

2.1.3 HIGH-QUALITY CLOUD AND SOLAR RADIATION DATA

Uniquely among the various types of recorded weather data, cloud monitoring requires trained observers who must subjectively estimate the proportion of cloud cover. In order to validate these climatologies[6] and trends in cloud cover, IOCI3 scientists used three-hourly satellite data from the International Satellite Cloud Climatology Project for the period 1983 to 2006 as an independent dataset (Jovanovic et al. 2010). The resulting high-quality cloud data are available online at www.bom.gov.au/climate/change/hqsites.

Homogenised data are available for both morning and afternoon observations (09:00 and 15:00 hours) as well as daytime clouds (average of the two) for a range of time-scales (annual, seasonal, monthly). Time series of averages and anomalies can be selected from a point-and-click map and nearest alternate sites can easily be identified.

In addition, satellite-based estimates of surface solar radiation are now being provided in real time and at daily resolution on a 0.05° grid. These estimates of global solar exposure can be extracted free of charge from the Solar Exposure Archive[7] (daily grids), and through Climate Data Online at www.bom.gov.au/climate/data/. A map interface allows users to select locations to extract both daily and monthly solar exposure, for either a single year or for all available years of the record (extending back to 1 January 1990).

2.1.4 AN ENHANCED HOMOGENISED TROPICAL CYCLONE DATABASE FOR WESTERN AUSTRALIA

Ascertaining whether or not there are historical trends in TC frequency and intensity was an important area of investigation under IOCI3 (Chapter 5). To help answer these questions, IOCI3 scientists developed an enhanced homogenised TC database for Western Australia.

As was the case for the rainfall, temperature and cloud datasets, this required careful quality control. The dataset was developed (to the extent possible) with the aim of applying consistent practices throughout the record, e.g., with regard to categorising TCs. A tropical depression would be classified as a TC if its minimum central pressure dropped to 995 hectopascals (hPa) or less throughout its lifetime; and as a severe TC if this minimum dropped to 970 hPa or less. It was often necessary to reconcile multiple conflicting sources of data, both from Australia and elsewhere. Obvious errors were removed, and the procedures, biases and uncertainties associated with the dataset were documented. The resultant dataset can be considered generally homogeneous since the introduction of modern satellite observations in the early 1980s; prior to this date, the estimation of cyclone intensity had a high level of uncertainty, and in the

[5] The reports of this external review are available online at: www.bom.gov.au/climate/change/acorn-sat/#tabs=3

[6] Climatologies describe the average state of a climate, as well as its variability and extremes, over a period of time.

[7] www.bom.gov.au/jsp/awap/solar/archive.jsp?colour=colour&map=solarave&period=daily&area=nat

period up to the late 1960s, when satellite coverage was intermittent or non-existent, it is likely that some cyclones were missed altogether, especially those which did not approach land.

Based on this homogenised dataset, IOCI3 scientists determined that there are no significant trends in the frequency or intensity of TCs for the South Indian Ocean and the South Pacific over the last 30 years (Chapter 5), the period over which records are available. The results of this work were documented in a scientific paper (Kuleshov et al. 2010a) and the database is accessible online at: www.bom.gov.au/cyclone/history/tracks/.

Knowledge gaps and future directions

Most records for the high-quality rainfall dataset start around the year 1920. Information prior to 1920 is currently available only in paper form. If this earlier information were digitised and made available, additional stations could be included in the high-quality rainfall dataset. The selection of additional stations should be prioritised according to social, economic and environmental needs, with an emphasis on data-poor regions and regions sensitive to change. Other considerations for selection are aspects related to network maintenance (e.g., the cost and accessibility of a given location).

Regarding the high-quality temperature dataset, the above-mentioned review by international experts led to the recommendation that targeted investment be used to create a small number of additional sites. This would be a key improvement given that large parts of Western Australia, notably NWWA, still lack adequate coverage for high-quality temperature data.

2.2 Improved Application of Climate Models: Advances in Statistical Downscaling

Project Links: 2.3 and 3.1

IOCI3 scientists helped develop and apply an advanced statistical downscaling (Box 1) model that generates simulations of daily rainfall for multiple sites based on atmospheric predictors. Called the non-homogeneous hidden Markov model (NHMM; Charles et al. 1999a,b), it generates synthetic multi-site daily rainfall time-series based on the concept of 'weather states'. These weather states can be thought of as the dominant spatial patterns of rainfall occurrence over a network of stations. The daily sequences of these states are a function of the daily sequences of the selected atmospheric predictors.

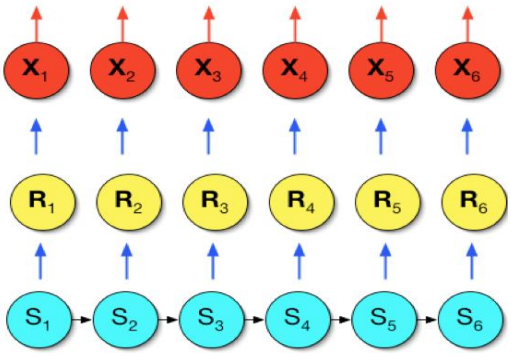

Figure 2.3 Conceptual view of the non-homogeneous hidden Markov Model. R_t represents multi-site rainfall on day t; S_t the sequence of daily weather states; and X_t the daily atmospheric predictors that influence the transitions between these states.

The NHMM is a stochastic[8] model, i.e., one able to generate multiple time-series for a given input sequence of atmospheric predictors. The day-to-day sequences of the NHMM weather states (S_t, t =1, ..., 6, in Figure

[8] Stochastic time series: sequences generated to have certain statistical characteristics but with a random component allowing for variation based on the observed probability distributions.

2.3) are influenced by atmospheric predictors (X_t) representing the key atmospheric processes producing the observed rainfall variability for the stations and seasons of interest (R_t). The set of atmospheric predictors (X_t) are selected in the NHMM calibration process. Selection entails assessing: statistical tests to avoid over-fitting; the ability to reproduce key rainfall statistics; and the physical realism of the resultant weather states' rainfall patterns and corresponding predictor field maps. Selected atmospheric predictors account for the position and strength of pressure systems and the degree of moisture saturation of the lower atmosphere. They are determined on a seasonal basis for a spatial domain encompassing a region on the order of 1000 by 1000 km, centred over the rainfall station network (see Appendix A and C).

BOX 1 SPATIAL DOWNSCALING EXPLAINED

Spatial downscaling is a process used to transform observed or modelled climate information at large spatial scales (hundreds of kilometres) into information at higher resolution (points to tens of kilometres). Global climate models (GCMs) typically have a horizontal resolution of between 150 and 300 km, but many sector-based process models used to inform management and planning require information at scales of 50 km or less. For example, hydrological models often require point-scale (i.e., individual station) inputs.

Statistical downscaling is one method used to bridge the gap between the coarse spatial scales simulated by GCMs and regional climate models (RCMs), and the finer scales required by process models, to produce the required high-spatial-resolution climate change information, typically at a daily time scale (Maraun et al. 2010; Figure 2.4 below).

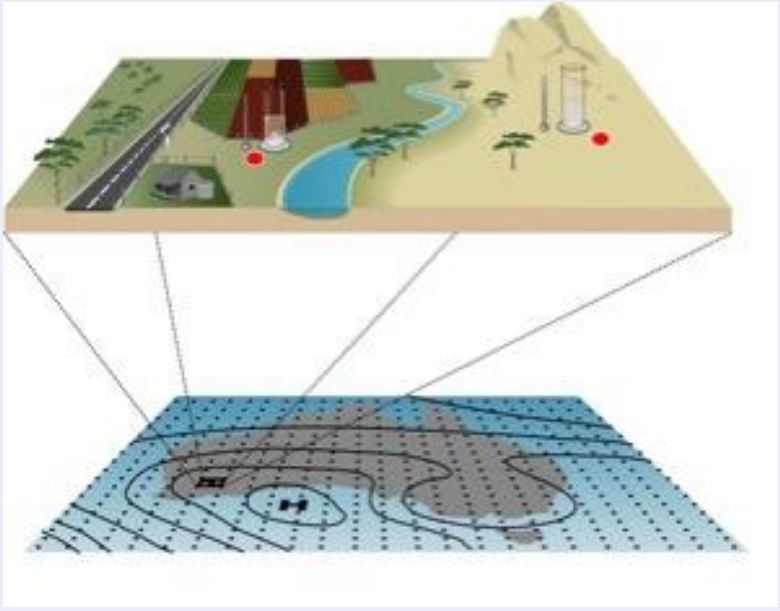

Figure 2.4 Downscaling is used to bridge the gap between the coarse spatial scales simulated by global and regional climate models, and the finer scales required by process models.

Statistical downscaling methods estimate this finer-scale information using observed statistical relationships between daily fine-scale variables (e.g., BoM weather station data) and daily larger-scale variables ('predictors') obtained from reanalysis datasets (Box 2, subsection 4.1.2.1) and GCMs. Analogue methods (circulation typing), regression analysis, or neural network methods are among several techniques used to accomplish this. Global climate model projections of future climate are used to provide the future time-series of these daily large-scale predictors. These are then used to drive the statistical relationships derived for the observed data to yield estimates of the fine-scale details of future climate. This approach assumes that these statistical relationships apply under changed climate conditions. Charles et al. (1999a) describe a method to assess this assumption's appropriateness.

Dynamical downscaling is a complementary spatial downscaling strategy that uses GCM output to provide the boundary conditions for finer-resolution RCMs; global models with 'stretched grids' that have higher resolution over the region of interest; or high-resolution global models. These RCMs provide a spatial resolution down to a few tens of kilometres; however, experience

has shown that even at their finest spatial scales their daily outputs still often require bias correction prior to their use as input for process models (Maraun et al. 2010).

Fowler et al. (2007) provide a detailed discussion of the relative advantages and disadvantage of statistical versus dynamical downscaling.

The NHMM's main advantage is its ability to provide multiple sequences of daily multi-site weather data suitable for input to process models (as presented in Chapters 4 and 5 for SWWA and NWWA, respectively). The use of these sequences allows a probabilistic risk assessment of climate impacts, for present-day and projected future conditions. However, this is not the only scientific advance provided by this methodology. An important additional benefit has been to use the NHMM to identify and understand changes to regional-scale atmospheric circulation that have influenced observed regional rainfall trends (e.g., Bates et al. 2010; Section 5.1.1).

Demonstrated usefulness of NHMM modelling advances

The NHMM stochastic downscaling methods developed under IOCI have informed sector-specific sensitivity studies in SWWA. In the water sector, NHMM projections of changes in rainfall patterns over key water supply catchments were used by the Department of Water (three reports available from the Department of Water website) to assess water supply vulnerability to climate change (Bates et al. 2010 and Charles et al. 2007). The NHMM was also used to help quantify the uncertainties in climate change projections of groundwater recharge; this work included a SWWA study site (Gnangara Mound; Crosbie et al. 2011). In the agriculture sector, downscaled projections have been used to assess scenarios for changes to crop yields at several locations on the Western Australian wheat belt (Farre and Foster 2009).

Knowledge gaps and future directions

The projections produced by different downscaling techniques (statistical and dynamical) are not always consistent. However, due to resource constraints, only a single statistical technique (the NHMM) was applied within this IOCI3 project. More research is required to compare projections from multiple downscaling techniques to attempt to determine reasons for any differences among their results.

One unresolved question is ‘which period of historical data should be selected to define a "baseline" climate against which to compare projections?' This question becomes problematic in regions of recent significant climatic change that is not reproduced in GCM historical simulations (e.g., in SWWA where autumn and winter rainfall has declined markedly during the past 60 years). This is because applying the projected changes to different baselines (e.g., as in studies related to water supply management) can produce a range of results, suggestive of different future impacts. To help inform baseline choice, further research is needed to quantify the proportion of observed change likely due to anthropogenic climate change versus that likely caused by natural climate variability alone (Chapter 3).

2.3 Other IOCI3 Modelling Advances

IOCI3 scientists have also examined how well climate models can replicate changes in large-scale atmospheric processes (Chapter 3). This question is important when considering possible future changes under scenarios of increased GHG emissions. Other IOCI3 work has focused on modelling techniques that provide a way to attribute the likely driving forces (known as forcing agents; see glossary) of observed climate change (Chapter 3). This is also the aim of new climate modelling performed under IOCI3 that sought to improve the understanding of the role of aerosols in NWWA's observed and future potential rainfall trends (Chapter 5).

Extreme climate and weather events have profound socio-economic and environmental consequences. Better information about these events is urgently needed, under both present day and projected future climate conditions. Toward this goal IOCI3 scientists sought to advance the application of statistical methods to examine hot spells and extreme rainfall (Chapters 4 and 5) and physical and statistical modelling methods to study TC characteristics (Chapter 5).

3 Large-scale Climatic Changes and their Attribution

Drafting authors: Carsten Frederiksen, Jorgen Frederiksen and Meelis Zidikheri

Project Link: 1.1

During the last sixty years there has been a marked and continuing reduction (about 20% to date) in autumn and winter rainfall over SWWA. This negative rainfall trend has coincided with major shifts in the structure of the large-scale circulation of the Southern Hemisphere (see Frederiksen and Frederiksen 2005, 2007), which has in turn changed the nature of the prevailing weather systems, including their growth rates and likelihood of development. In IOCI Stage 2, this three-way relationship between changes in large-scale circulation, weather systems and rainfall was only investigated for July and over the period 1948 to1994, when some of the largest changes occurred. In IOCI Stage 3, this research was extended to all months and into the 21st century. The issue of attribution (i.e., identifying the causes) of these changes was also addressed with the formulation of a new methodology to identify the forcing responsible.

This chapter summarises some of the IOCI3 research that links observed regional Western Australian rainfall changes to large-scale atmospheric changes. It also describes some of the consequences of these large-scale atmospheric changes for important weather systems, using dynamical models and mechanistic studies. The issue of attribution and future projections of changes are also discussed. The changes in the statistics of the different weather systems and their impacts on SWWA, as well as future projections of these systems, are discussed in Chapter 4.

3.1 Large-scale Changes in Climate: Subtropical Jet and Storm Tracks

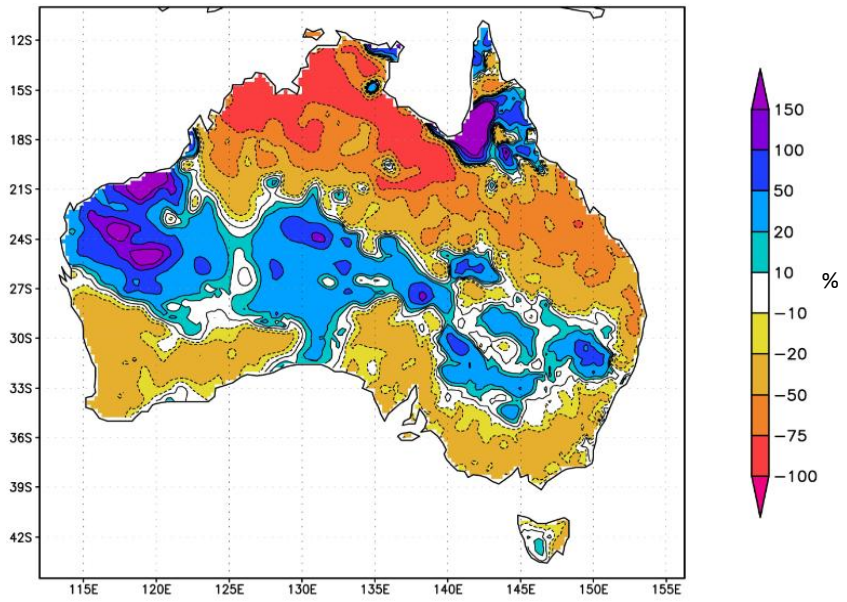

Figure 3.1 Percentage change in July rainfall between the periods 1997 to 2006 and 1949 to 1968. AWAP data.

Over the latter half of the 20th century some of the largest changes in winter rainfall, atmospheric circulation and weather systems have occurred in the month of July. Figure 3.1 illustrates the percentage change in July rainfall between the periods 1997 to 2006 and 1949 to 1968. Substantial reductions (greater

than 20%) are seen over SWWA and east and south-east Australia. Conversely, substantial positive percentage changes are observed over NWWA (Chapter 5) and over parts of central Australia (Section 3.2).

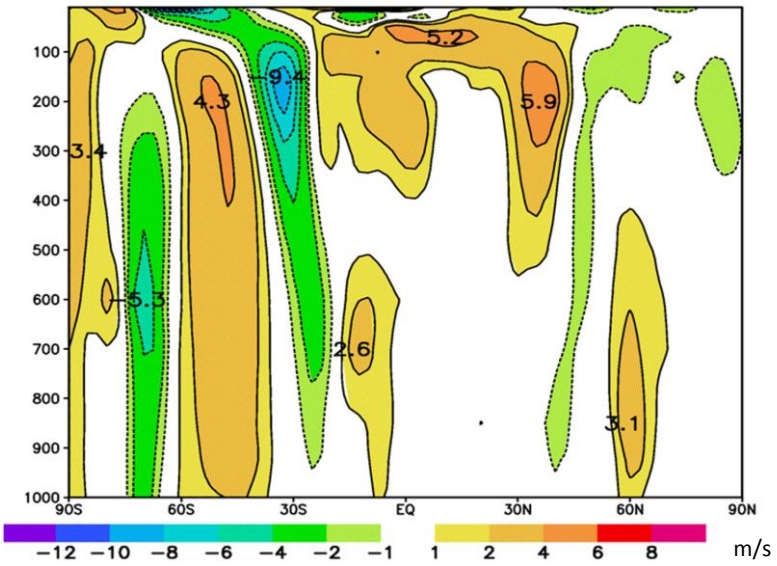

Figure 3.2 Change in July zonal wind. Averaged over the longitudes of 100° E to 130° E over the two time periods 1975 to 1994 and 1949 to 1968, in metres per second. The green to blue shading just to the left of the centre of the figure illustrates an up to 9.4 metre-per-second reduction in the wind strength in the subtropics near 30° S latitude. Y axis is atmospheric pressure level in hectopascals. NCEP data.

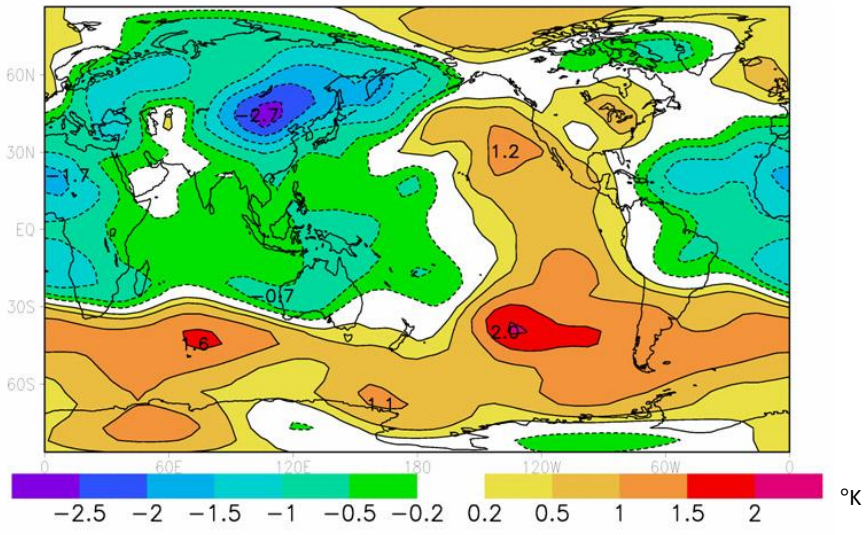

Figure 3.3 Reduction in the equator-to-pole temperature gradient. Change in the vertically averaged potential temperature between the periods 1975 to 1994 and 1949 to 1969. Warming (yellow to red shading) in the Southern Hemisphere south of 30° S and in the Eastern Hemisphere has reduced the equator-to-pole temperature gradient, particularly in the Eastern Hemisphere. In degrees Kelvin; NCEP data.

One important IOCI3 finding was that the SWWA rainfall reductions could be explained by marked changes in the mean state of the global atmospheric circulation and temperature. Some of the largest changes occurred between the periods 1949 to 1968 and 1975 to 1994, and coincided with large reduction of inflow into Perth dams. These atmospheric changes have in turn resulted in shifts in the Southern Hemisphere storm tracks (i.e., the paths along which the storms move; Frederiksen and Frederiksen 2005, 2007 and 2011; Frederiksen et al. 2009a, b). Figures 3.2 and 3.3 show the full extent of these changes in the circulation and thermal structure of the atmosphere over time, by comparing the change in climate across two periods: 1949 to 1968 and 1975 to 1994.

Over these two periods one significant difference was a 17% reduction in the peak strength of the Southern Hemisphere subtropical jetstream over the southern Indian Ocean 'upstream' (roughly west) of Australia (Figure 3.2). The subtropical jetstream is a belt of strong, upper-level westerly winds found roughly 12 km above regions of subtropical high pressure. It is a source of potential energy in the atmosphere; it is the conversion of this potential energy into kinetic energy that drives the formation of storms. Changes in the jetstream are a signal of changes in the circulation of the atmosphere, including changes to storms and high-pressure systems.

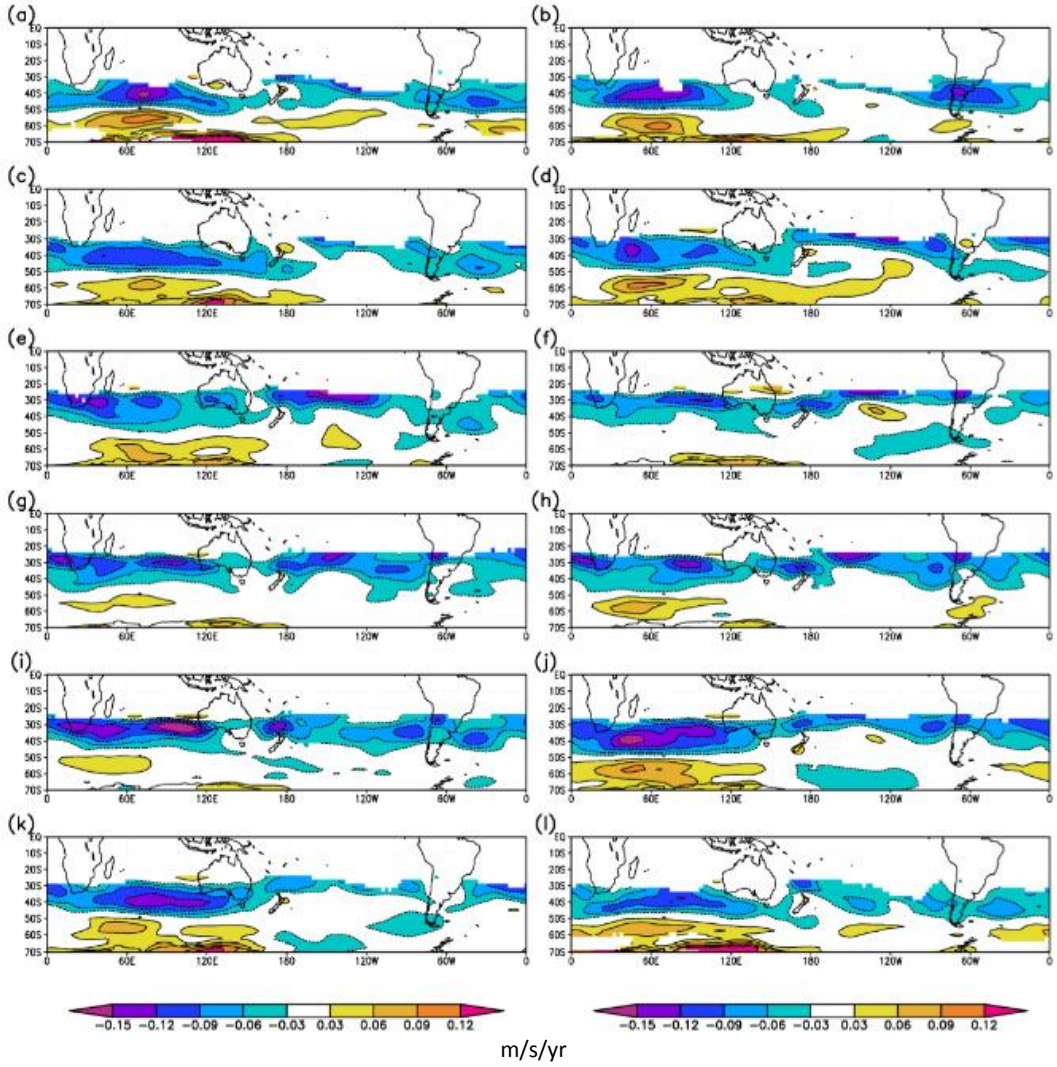

Figure 3.4 Trends in atmospheric instability. (a) to (l) for January to December over the period 1950 to 1999 in metres per second per year. Note the highly statistically significant negative trends 'upstream' (roughly west) of Australia (blue to purple shading), and the significant positive trends south of Australia (yellow to red), with maximum values near 60° S.

Figure 3.2 shows the elevation (in pressure units) and latitudinal cross-section of the zonal (i.e., westerly) wind, averaged over 100° E to 130° E longitude. In both periods, the zonal wind reaches a maximum strength in the subtropics (near 30° S) at an elevation that corresponds to approximately the 200-hPa-pressure level. In the later period (1975 to 1994), there was a reduction in the zonal wind of up to 9.4 m/s in this maximum. In fact, there was a hemisphere-wide reduction in the upper level zonal winds and vertical wind shear near this latitude of 30° S. However, at other latitudes the zonal winds have increased: in a hemispheric band near 50° S; in the upper troposphere near 45° S; and in the main Northern Hemisphere jet core (the jetstream maximum) near 35° N.

These changes are directly associated with changes in the Hadley circulation (not shown; the major atmospheric circulation of air from the tropics into the mid-latitudes at altitude), including a reduction in the strength of the downward branch near the core of the Southern Hemisphere jet.

The thermal structure of the Southern Hemisphere atmosphere has also changed, with significant warming south of 30° S. Figure 3.3 illustrates this change by showing the vertically averaged temperature difference between the same two periods mentioned above. This warming has reduced the equator-to-pole temperature gradient, particularly in the Eastern Hemisphere. As well, other differences in the atmospheric circulation are associated with a change in the strength of the Southern Annular Mode (SAM; not shown), which is associated with weather systems and rainfall over southern Australia (see also Chapter 4).

These changes would be expected to have a marked impact on the stability of the atmosphere and the likelihood of formation of the weather systems that affect SWWA. During winter these weather systems are associated with the Southern Hemisphere storm tracks. These storms owe their formation to an unstable atmosphere, and this unstable state is reached when the vertical difference in zonal wind is large and exceeds a critical value. However, the reduced temperature gradient between higher and subtropical latitudes tends to reduce the vertical wind shear, stabilising the atmosphere and decreasing the likelihood that storms will form.

Changes in the atmospheric circulation and thermal structure have occurred not only in winter, but in other seasons as well. This has affected the likelihood in these seasons of the formation of storms that can bring rainfall to SWWA. These changes are illustrated in Figure 3.4. It shows, for all calendar months, the linear trends in atmospheric instability for the period 1948 to 2006 throughout the mid-latitudes of the Southern Hemisphere. Of note is that the trends that are shaded in this figure are highly statistically significant at the 95% level or greater, generally at the 99% level.

Highly significant negative trends occur upstream (again, roughly west) of Australia, in regions associated with storm formation. Further south, there are significant positive trends: an increase in atmospheric instability with maximum values near 60° S. There is a clear annual cycle in the position of the greatest negative trends. The areas of greatest reduction in atmospheric instability are generally located more equatorward (25 to 30° S) from May to October, and between 35 and 50° S from November to April. Positive trends occur between 50 and 70° S in all months. Thus, in all months, storm development tends to be reduced in the mid-latitudes but increases in likelihood at higher latitudes. The net result is fewer storms impacting on SWWA, and thus a reduction and continuing downward trend in rainfall.

How do these changes in atmospheric instability impact on the structure and growth rate of weather systems associated with the storm tracks? This question is addressed in Figure 3.5, which depicts the two types of weather (storm) modes that play a dominant role during July. In the early period (1949 to 1968), storm type 1 (Figure 3.5a) was the type of weather system most likely to form. This storm mode is shown at a particular phase (or time) and consists of a series of eastward propagating troughs (blue shading) and ridges (red shading) over southern Australia. As the troughs and ridges move eastward they amplify, reaching maximum amplitude – with a greater likelihood of rainfall – over SWWA. Thus, this mode had large impact on SWWA rainfall in the earlier period. However, in the latter period (1975 to 1994) and subsequently, the growth rate (and likelihood of storm formation) of this mode decreased by more than 30%. During the period 1997 to 2006 the growth rate has decreased even further to 37% of its value in the period 1949 to 1968. This is consistent with the negative July trends in instability shown in Figure 3.4(g) upstream of Australia. This explains why rainfall has decreased and continued in this downward trend.

At the same time, storm type 2 (Figure 3.5b) in the latter period has had a growth rate that is comparable to storm type 1. That is, both types are equally likely to occur. However, storm type 2 has a markedly different structure from storm type 1. It has very little amplitude over southern Australia, and its largest impact occurs in the South Pacific. This storm type originates south of Australia at about 60° S, and the observed increase in its likelihood of formation is consistent with the increase in atmospheric instability in that region (Figure 3.4g).

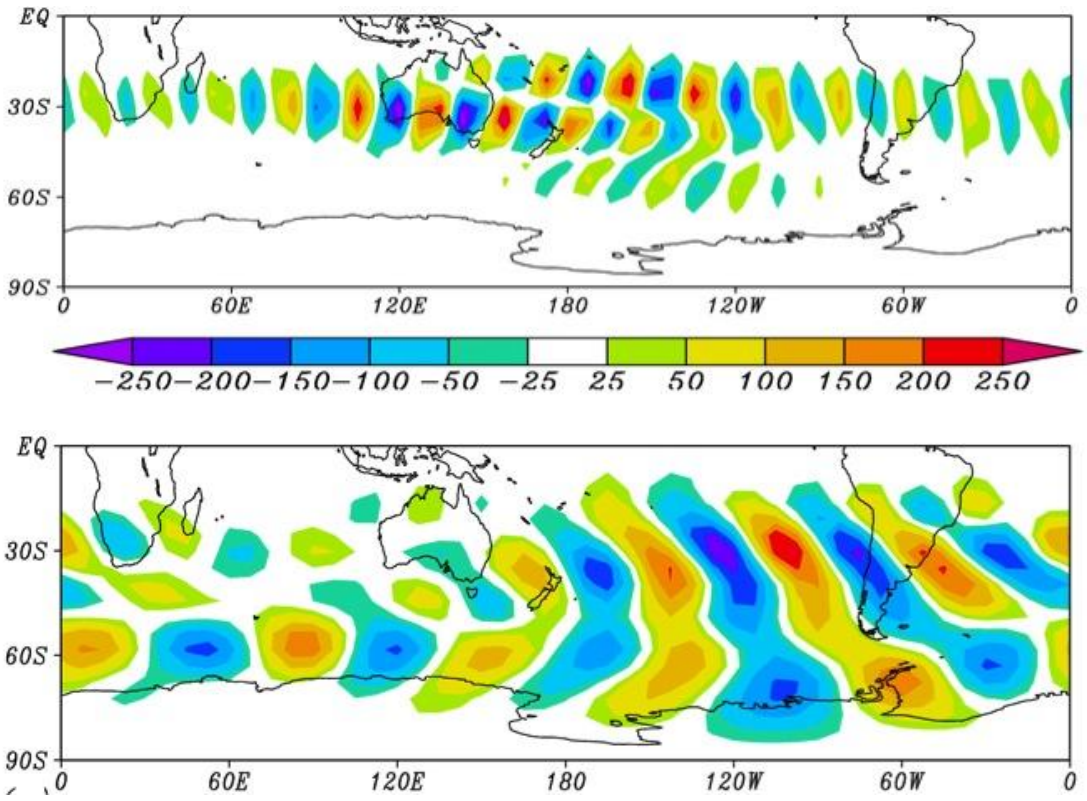

Figure 3.5 The 300-hectopascal streamfunction for (a) July storm type 1 and (b) July storm type 2.

Frederiksen et al. (2011a, b, c, d) provide a more comprehensive discussion of the relationship between changes in SWWA rainfall, the climate of the atmospheric circulation and thermal structure, and the Southern Hemisphere stormtracks in all months.

3.2 North-West Cloud Bands and Intraseasonal Oscillations

Not all of Western Australia has experienced reductions in winter rainfall. As Figure 3.1 illustrates, July rainfall has increased over central north-west and central Western Australia. This region is often affected by propagating cloud bands that originate off the north-west coast of Australia. Frederiksen and Frederiksen (2011) suggest that these positive trends in rainfall are attributable to the changing nature of two types of weather systems commonly associated with these regions: north-west cloud bands and intraseasonal oscillations.

North-west cloud bands: The first of these two types is associated with eastward propagating north-west cloud bands originating in the Indian Ocean off north-west Australia. They are characterised by an extensive layer of rain-bearing cloud and constitute an important weather feature of the subtropics to mid-latitudes in the Southern Hemisphere, providing rainfall across much of Australia. Over the last roughly fifty years, these north-west cloud band modes have increased their growth rates by approximately 25% or more for each of the 1975 to 1994 and 1997 to 2006 periods, compared with the 1949 to 1968 period. The increasing likelihood of development of these systems would be expected to have a positive impact on rainfall over central NWWA and can partly explain the changes observed.

The leading, or fastest-developing, north-west cloud band modes have periods of about eight days throughout. These modes consist of a series of high and low-pressure anomalies (or wave trains) that originate in the Indian Ocean and propagate eastward over Australia and into the South Pacific, and affect rainfall over central Western Australia. Figure 3.6a shows the 300-hPa streamfunction for the leading north-west cloud band mode for the 1975 to 1994 period. Figure 3.6b shows the corresponding divergence field, which is proportional to rainfall and indicates the location of the largest impact on rainfall associated with this type of weather system.

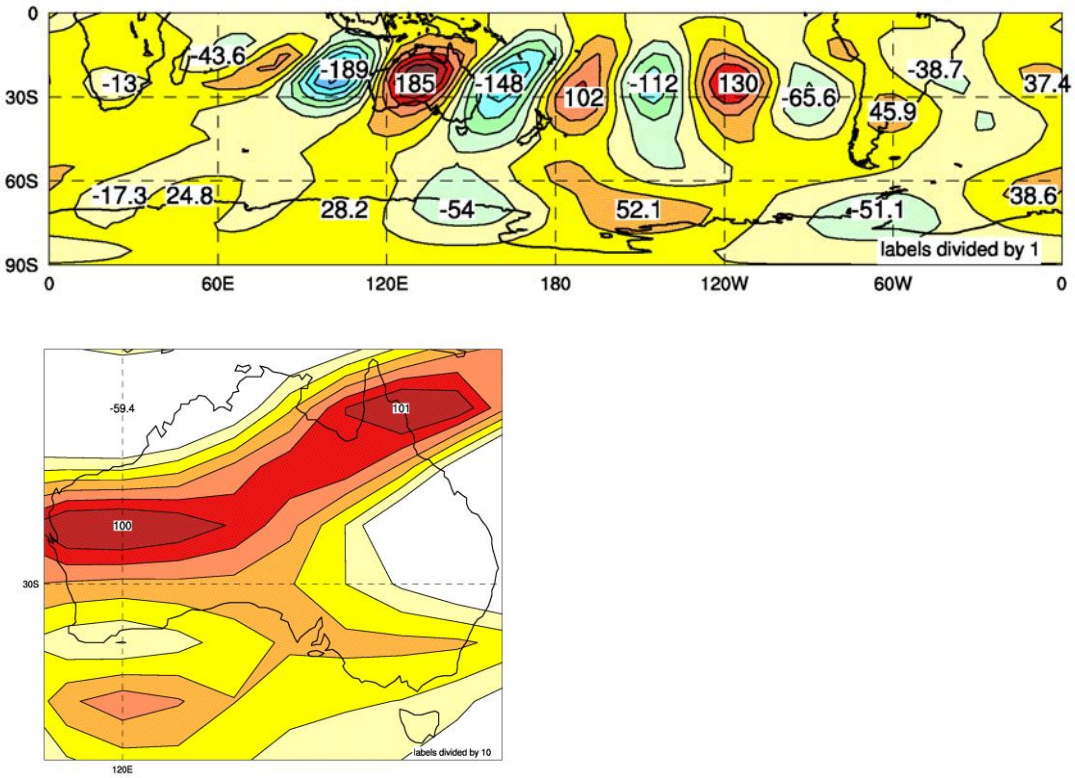

Figure 3.6 Leading north-west cloud band mode for 1975 to 1994. (a) shows 300-hectopascal streamfunction and (b) 300-hectopascal divergence. The orange to red areas in (b) indicate the location of rainfall associated with this weather pattern.

Intraseasonal oscillations: A second category of weather system that impacts rainfall over central NWWA is associated with variability at the intra-seasonal timescale of between 25 and 60 days. The leading intra-seasonal oscillation modes also consist of propagating wave trains of pressure anomalies extending again from the central Indian Ocean across central Western Australia. Compared to the period 1949 to 1969, the growth rates of these weather systems have also increased, by approximately 30% over each of the two periods 1975 to 94 and 1997 to 2006. Again, as with the north-west cloud bands, the increased growth rate of these modes in the latter periods is consistent with the increased rainfall over central NWWA.

3.3 Performance and Projections of Climate Models

To what extent can climate models replicate the observed changes described in the previous sections? This question is important when considering possible future changes under scenarios of increased GHG emissions. For SWWA, this would require climate models to reproduce the observed patterns for trends in atmospheric instability (Figure 3.4) and, as implied by these trends in instability, implicitly the changes in the properties of the storm track weather systems.

Figure 3.7 highlights the extent to which these models are able to capture the change in July atmospheric instability between the periods 1949 to 1968 and 1975 to 1994. Specifically, this figure demonstrates the results of observed anthropogenic forcing, including GHGs, from the pre-industrial period to the end of the 20th century. Shown are the results for 22 of the models used, which are from the IPCC Coupled Model Intercomparison Project Phase 3 (CMIP3; see Randall et al. 2007 and Meehl et al. 2007 for model nomenclature and description).

Figure 3.7 shows the extent to which the models are able to reproduce the pattern of observed changes in July atmospheric instability (Figure 3.4(g)) over the domain (longitude of 60 to 150° E, and latitude 45 to 15° S). This is the region of origin for storms that affect SWWA. The similarity in pattern between the models and observations is quantified by the use of the anomaly pattern correlation (APC). The APC indicates how much two patterns have in common. A value of 1.0 is a perfect match; a value of -1.0 is exactly the

opposite; and zero would represent an essentially random association. The APC was calculated in four different ways.

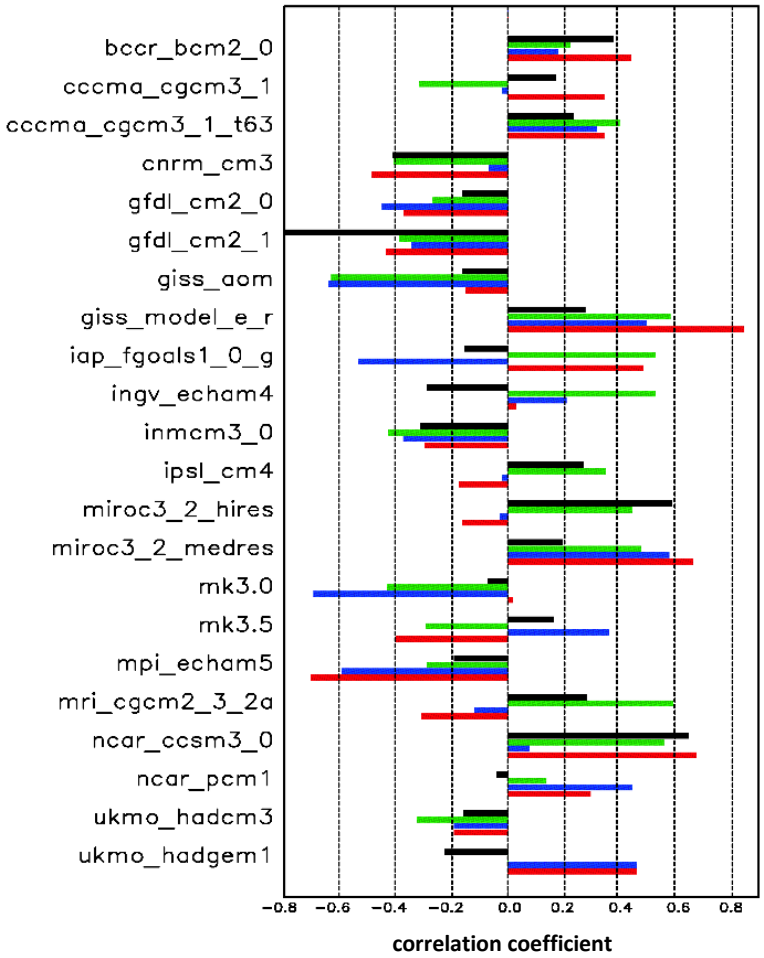

Figure 3.7 Climate models' ability to simulate atmospheric instability. Anomaly pattern correlation between the observed changes in atmospheric instability over the periods 1975 to 1994 and 1949 to 1968 and model changes for the periods: (i) 1975 to 1994 to 1949 to 1968 (black bars) and (ii) 1980 to 1999 and a pre-industrial control run (green, blue and red bars).

The black bars in Figure 3.7 represent the APCs of changes in atmospheric instability calculated for models using the same two 20-year periods described above (1949 to 68 and 1975 to 94). However, the timing of simulated changes in coupled models may not necessarily synchronise with the reanalysed observations. Therefore IOCI3 scientists have also considered whether the models can produce these changes taking into account all GHG forcing since pre-industrial times until the 1980 to 1999 period. This indicates the impact of all 20th century GHG forcing.

It is also important to understand the sensitivity of our results to the base period chosen in the pre-industrial model control runs, and how variability from one decade to another might influence the results. To explore this, IOCI3 scientists chose three adjoining 20-year periods at the end of the pre-industrial control runs, each separated by 20 years. These are designated, respectively, in Figure 3.7 by green, blue and red bars.

In Figure 3.7, the higher the models' score on the right-hand side of the figure (i.e., the closer the score is to a value of 1) the better the model captures the pattern of change in atmospheric instability. The results demonstrate that the models vary considerably in their ability to simulate the reanalysed observations. About a third of the models show a consistently negative APC in all four cases (e.g., *gfdl_cm2_1*, *giss_aom*, *mpi_echam5,* etc.). That is, these models actually indicate an increase in atmospheric instability that would lead to an increase in growth of the storm track modes; this is not consistent with observations. However, about a third of the models show a consistently positive APC (e.g. *miroc3_2_medres*, *giss_model_e_r*, *ncar_ccsm3_0,* etc.); this result is consistent with observations.

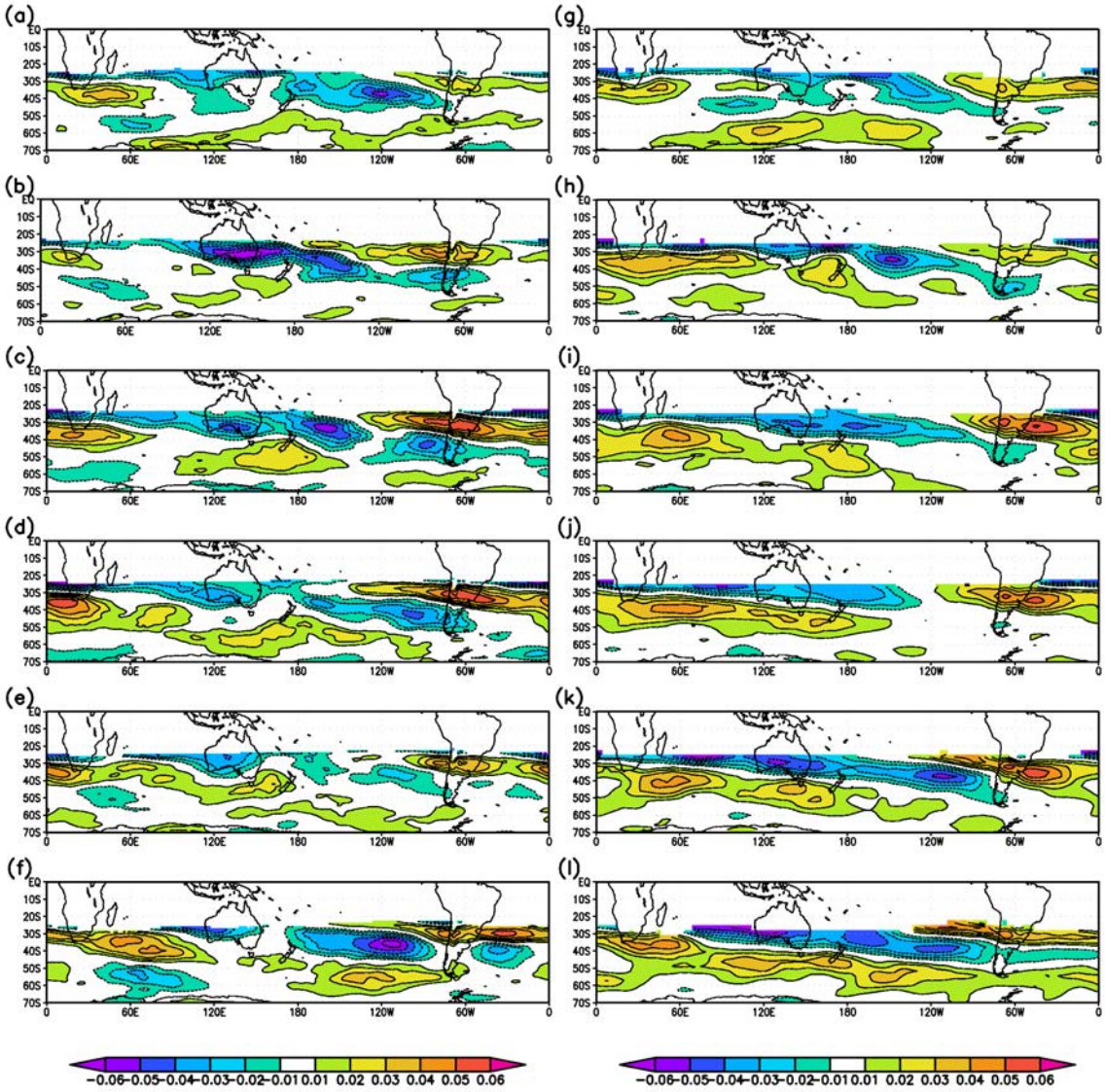

Figure 3.8 Trends in May to October atmospheric instability (2001 to 2100). (a) to (f) from the miroc3_3_hires model for SRES A1B emissions scenario; (g)-(L) from the miroc3_2_medres model for SRES A2 emissions scenario. Units are metres per second per year.

Many of the models fail to capture the necessary changes in the large-scale atmospheric circulation (e.g., in Figure 3.2) and the changes in the vertically-averaged temperature (Figure 3.3) needed to simulate the changes in atmospheric instability. Underlying these atmospheric changes in the Eastern Hemisphere are warm sea surface temperature anomalies (not shown) near 30° S, which many of the models are not able to simulate. Frederiksen et al. (2011a) showed that when natural and anthropogenic forcings are used in atmospheric-only model experiments forced by observed sea surface temperatures, all of the models they had access to produced the observed changes in the atmospheric instability between the periods 1949 to 1968 and 1975 to 1994 with similar magnitudes. This would suggest that there may be some problem with the ocean component or the coupling between the ocean and atmosphere in those coupled models that fail to produce the observed changes. Interestingly, Frederiksen et al. (2011a) also found that many of the models that did not simulate the 20th changes well showed similar patterns of changes in the atmospheric instability when forced with increasing carbon dioxide concentrations.

The *miroc3_2_medres* and *miroc3_2_hires* models capture the changes in atmospheric instability, storm track modes and rainfall particularly well. These two models were used to project future changes in atmospheric instability for the end of the 21st century. Figure 3.8a-f shows the projected trends in atmospheric instability over the period 2001 to 2100 for the months of May through October using the *miroc3_2_hires* model for the SRES (Special Report on Emissions Scenarios; see Box 3) A1B GHG emissions

scenario. Figure 3.8 g-l depict the same projections but using the *miroc3_2medires* model for the relatively high SRES A2 GHG emissions scenario.

Both simulations show negative trends for atmospheric instability near 30° S and positive trends further south. Thus they project a continuation of the patterns already observed (shown in Figure 3.4). The magnitude of the projected trends is about half that of the observed negative trend, but is similar to that modelled for the 20th century (see below for a discussion of this issue). This suggests that the trends seen in the 20th century are likely to continue into the 21st century. That is, these results imply a continuation of the downward trend in SWWA rainfall already observed, as the following results on the corresponding rainfall impact indicate.

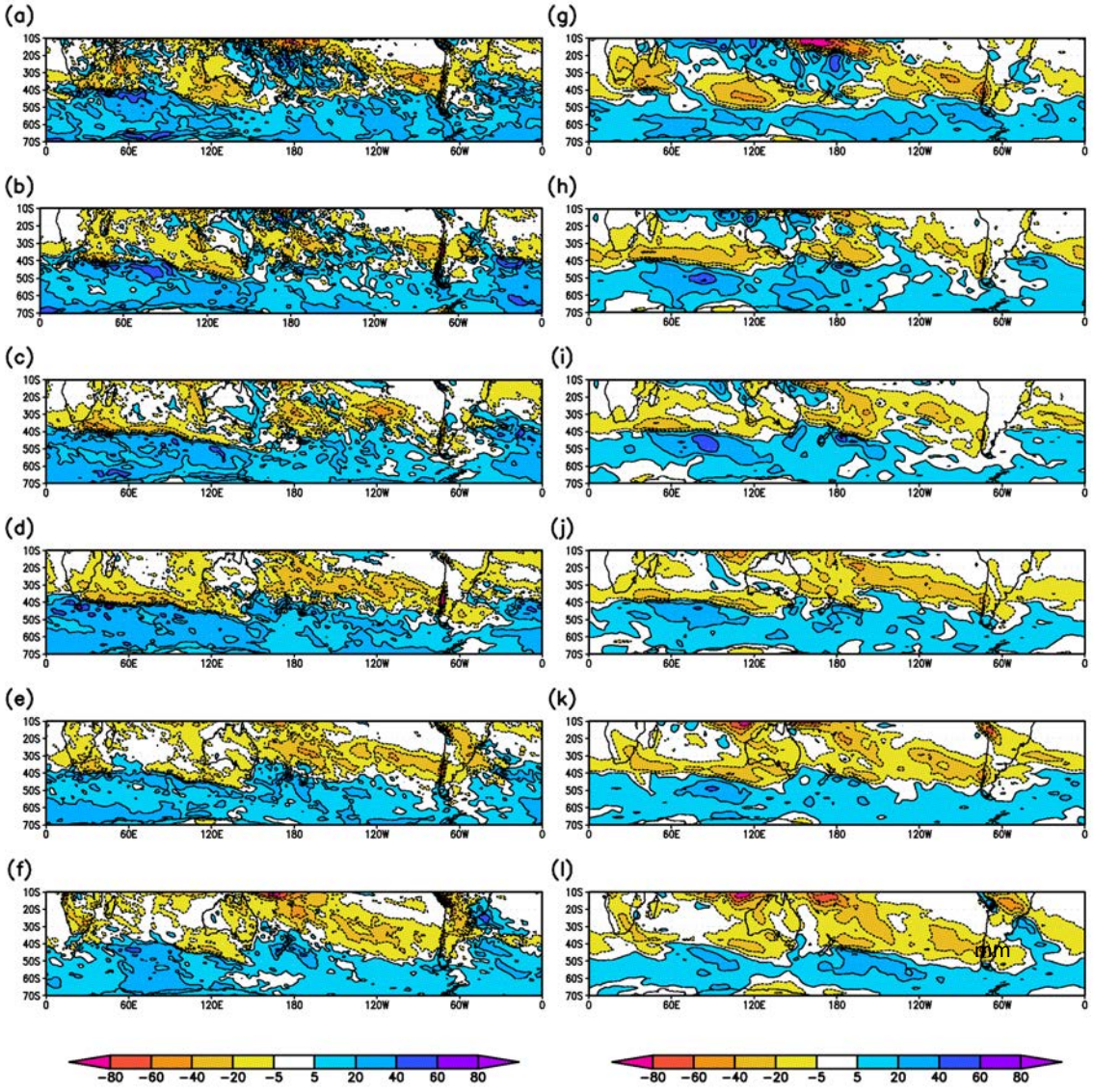

Figure 3.9 Projected changes in May to October rainfall between the two periods 2080 to 2099 and 1980 to 1999. Projections are made using: (a) to (f) the miroc3_2_hires model under the SRES A1B emissions scenario; and (g) to (l) the miroc3_2_medres model under the SRES A2 emissions scenario. Rainfall is given in millimetres, with yellow to red shading indicating a projected reduction, and blue to violet indicating a projected increase. SWWA is projected to undergo May to October rainfall reductions in every month over this half-year under both scenarios; some reductions could exceed 20 millimetres.

Figure 3.9 shows the results of the above two model projections for trends in May to October rainfall between the two periods 1980 to 1999 and 2080 to 2099. The results are consistent with trends in atmospheric instability. The projections show hemispheric reductions in rainfall in a zonal band north of 40° S, and increases in rainfall further south. Differences in rainfall between the periods 1980 to 1999 and 2080

to 2099 vary between -40 millimetres (mm) to +40 mm. Over SWWA, rainfall is projected to decrease in all months over this half of the year (Figure 3.10). In some months reductions exceed 20 mm, with these large reductions being especially prevalent in the SWWA region. Note, however, that the model results for the 20th century produce changes in rainfall which are about half those actually observed, and so may also be underestimating the projected changes.

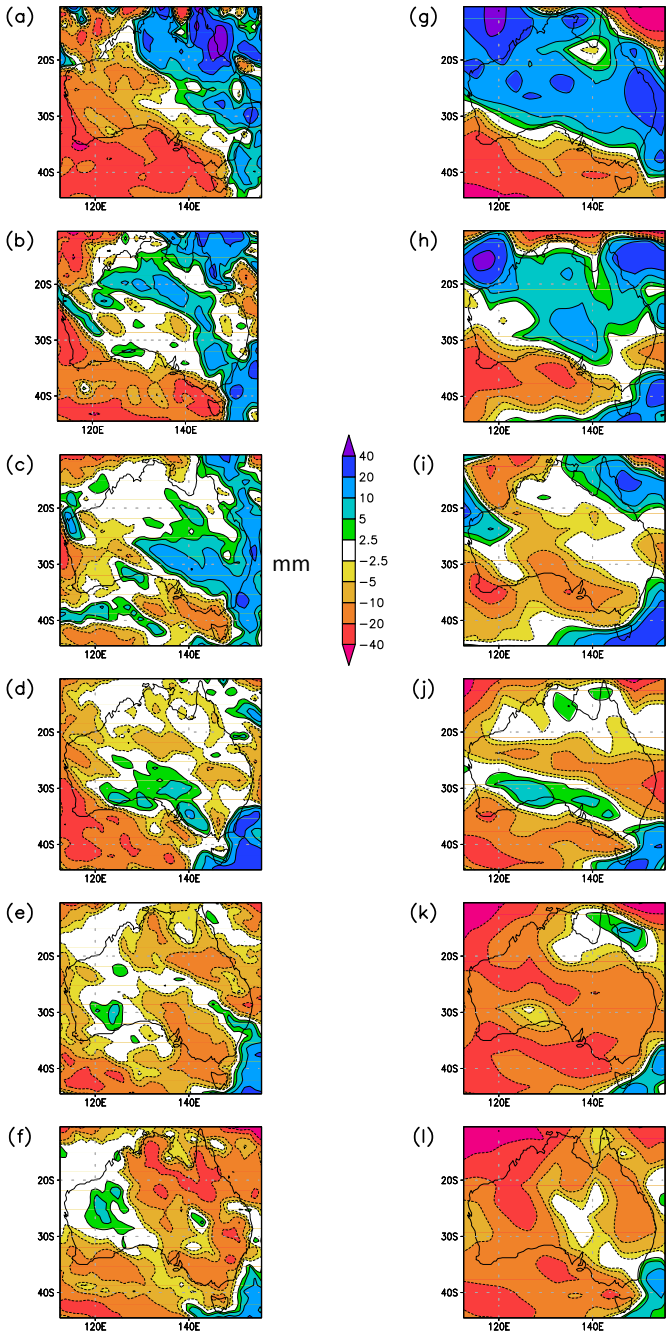

Figure 3.10. Projected changes in Australian May to October rainfall. As per Figure 3.9, but showing in more detail projected changes in Australian rainfall in millimetres. Yellow through red indicates areas of rainfall reduction, green through blue, areas of rainfall increase.

3.4 The Causes of Large-Scale Changes in Climate: Attribution

Determining the causes of the changing climate during the last half-century and the likely drivers of further change into the 21st century is of great importance for policy development. To attribute these causes one

must disentangle the anthropogenic component from natural internal variability across various time scales. Important driving forces for climate change, known as forcing agents, include GHGs, aerosols, changes in solar radiation and volcanic activity, and changes in surface albedo, roughness and evaporation due to land use.

Determining the impact of changes in external forcing on the climate is a very complex problem. This is because, as the climate changes in response to the forcing, this change influences the nature of the weather systems, which in turn feedback onto the climate. This feedback needs to be accounted for before the impact of the forcing agents can be determined for each climate variable, such as the circulation, temperature, or rainfall; this impact can be described by a forcing function. Zidikheri and Frederiksen (2011) have developed a methodology to estimate the feedback and directly calculate the forcing functions responsible for circulation and temperature changes. This provides a way to attribute this aspect of climate change. This method is the first capable of achieving this. The scheme was used to determine the anomalous temperature and circulation forcing functions responsible for the changes in the Southern Hemisphere circulation during the second half of the 20th century.

Figure 3.11 shows the anomalous temperature forcing function at an elevation equating to the 500-hPa pressure level. This is the forcing function associated with the changed temperature (Figure 3.3) and circulation (Figure 3.2) between the July periods 1949 to 68 and 1975 to 94. The figure demonstrates how the Southern Hemisphere circulation changes have been driven by a temperature forcing anomaly (change) that is largely zonally symmetric[9], i.e., is largely consistent across a given band of latitude. These temperature forcing anomalies have enhanced warming in the mid- to high latitudes while at the same time reducing warming in the tropics and subtropics. The effect is a reduction in the horizontal temperature gradients over mid-latitude regions such as those over southern Australia and SWWA in particular. In turn, this has: reduced the instability of the Southern Hemisphere atmosphere in the mid-latitude regions; reduced the intensity of storm formation; and reduced the resulting rainfall, as discussed earlier.

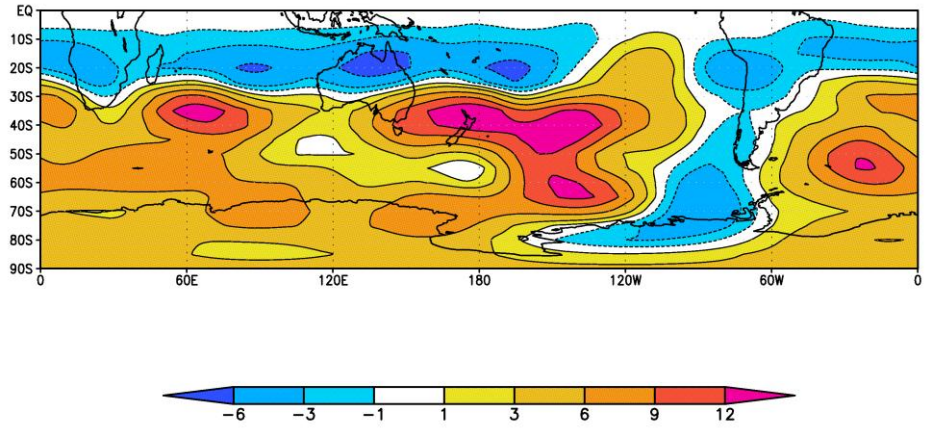

Figure 3.11 The anomalous forcing function at an elevation equivalent to 500 hectopascals associated with temperature and circulation changes between the periods 1975 to 1994 and 1949 to 1968. The yellow through magenta area illustrates temperature forcing anomalies – largely zonally symmetric – that have enhanced warming at mid- to high latitudes.

The largely zonally symmetric anomalous temperature forcing pattern shown in Figure 3.11 is consistent with anomalous forcing largely due to increasing GHGs. This pattern in Figure 3.11 is also consistent with the 20th and 21st century predictions of skilful climate models. Models such as the *miroc3_2_medres* and *miroc3_2_hires* coupled climate models, when forced by the radiative effects of increasing GHG concentrations, show very similar changes for Southern Hemisphere temperature and circulation. This includes changes in baroclinic instability (vertical shear instability) and southern Australian rainfall that are

[9] Zonally symmetric: the pattern seen at a given latitude tends to circle around the globe, across all longitudes.

very similar to those actually observed (Frederiksen et al. 2010, 2011a, b). Furthermore, the 21st century projections of these models, when forced by increasing anthropogenic gases under SRES B1, A1B and A2 scenarios, show a continuation of observed trends into the second half of the 21st century.

Knowledge gaps and future directions

The majority of the work described in this section focused primarily on SWWA and predominantly on the winter season. There is a great need to build on and expand existing methods of detection and attribution developed as part of IOCI3, and broaden their application to more phenomena affecting Western Australia, including over central and northern Western Australia, and in all seasons. There is also a need to provide confidence in understanding of the causes of observed changes and in projections.

An important aspect of future research should be to identify the physical processes and mechanisms responsible for these changes. In particular, one important objective is to disentangle the roles of anthropogenic forcing (e.g., GHGs, ozone, aerosols; see Chapter 5) and natural variability in the changing climate of Western Australia. An evaluation of the latest Coupled Model Intercomparison Project Phase 5 (CMIP5) climate simulations would help identify models that embody the correct physical processes and mechanisms, and are skilful in reproducing the observed climate and rainfall trends of the 20th century. Such an analysis would add confidence to future likely projections of Western Australian climate change into the 21st century, and provide guidance on which models are suitable for studies of climatic extremes, extreme weather and regional projections.

The impact of large-scale drivers on extremes of climate and weather is an important area that needs to be better understood. For example, possible causes of extreme events include low-frequency modes of variability such as the El Niño – Southern Oscillation (ENSO), the Indian Ocean Dipole, and weather systems such as Intra-seasonal Oscillations (e.g., the Madden-Julian Oscillation), north-west cloud band disturbances, monsoon, mid-latitude storms, TCs, and their interactions. Future research should focus on both dynamical and statistical techniques to elucidate the three-way interactions between systematic trends in climate change, low-frequency variability (teleconnections, or large-scale drivers) and weather systems in current and future climates under IPCC Fifth Assessment Report scenarios.

In particular, an area which should be studied is the future likelihood, risks and impacts of persistent severe weather events of prolonged heat waves and high or low rainfall, similar to those seen over east Australia during 2010/2011, where extremes in natural variability (e.g., ENSO) reinforce or act against climate change trends, and which can last from months to many seasons. Also, results from IOCI3 have shown that the rainfall deficit over SWWA is due to the decreased growth rate and southward shift in storms, and is associated with the observed expansion of the tropics. At the same time, there has been an increase in weather systems and rainfall associated with north-west cloud band disturbances and intraseasonal oscillation modes. This raises the issue of whether the continued expansion of the tropics under future climate change may cause these weather systems to intrude further south and make up the rainfall deficit caused by changes in the mid-latitude storms. This is something that needs to be explored.

The attribution of the causes of current and future climate change has major implications for policy development on climate adaptation. To solve the attribution problem, future research should use climate model simulations with different combinations of radiative forcing (e.g., GHGs, aerosols and ozone) and inverse modelling techniques developed in IOCI3. Novel dynamical and statistical methods developed by IOCI3 scientists could be used to analyse a wide range of weather systems and important large-scale modes of variability in the atmospheric circulation relevant to Western Australian climate and weather. These weather systems and modes of variability would include extra-tropical storms, blocking, north-west cloud band disturbances, intraseasonal oscillations (e.g., the Madden-Julian Oscillation), ENSO, SAM, Indian Ocean Dipole and modes related to trends in the large-scale Southern Hemisphere circulation.

4 South-West Western Australia's Changing Climate

Drafting Authors: Pandora Hope, Kevin Keay, Catherine J. Ganter, Yun Li, Steve Charles, Guobin Fu, Aloke Phatak and Mark Palmer

The climate of SWWA is characterised by dry, hot summers. This is due to the subtropical belt of high pressure that extends across this region, reaching its southernmost extension in January and February. During winter, this subtropical high-pressure belt lies to the north, almost completely outside the SWWA region. Winter weather in SWWA is characterised by moist unstable winds; 80% of rain falls between the months of April and October, most of it during the cooler winter months of June and July (Bates et al. 2008).

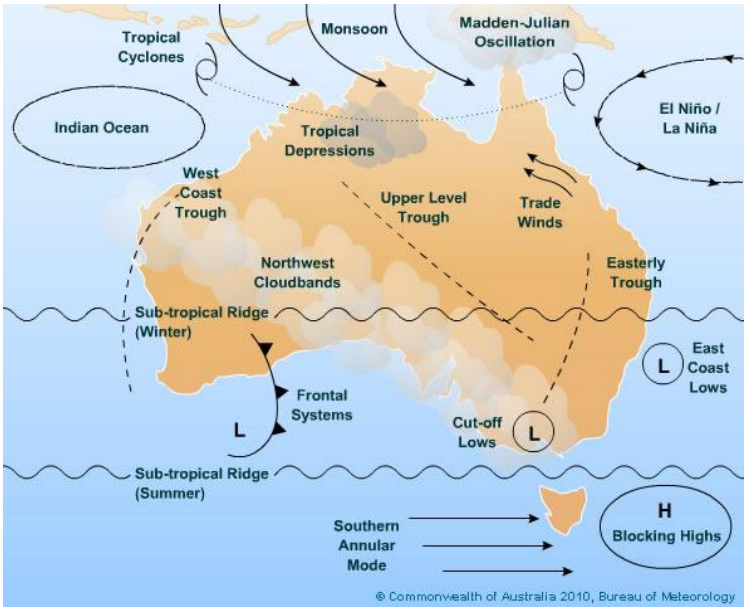

Figure 4.1 The main (but not all) influences upon the Australian Climate. These influences vary in their level of impact in different regions, depending on the time of the year. Note the upper-level winter jetstream is located at approximately 30¯ S, at the latitude of southern Australia.

This chapter describes IOCI3 work to improve the understanding of observed trends in SWWA climate and weather, in particular observed changes in rainfall and temperature. This includes insights on shifts in weather systems and other possible drivers of these changes. This chapter also reports on the results of downscaled model projections of future SWWA rainfall and temperature. The final section of this chapter focuses on present-day and possible future trends in SWWA extreme weather events: namely, intense rainfall and hot spells.

4.1 SWWA Rainfall: Observed Changes and their Causes

'Winter' (April to October) rainfall in SWWA is influenced by the upper level jetstream (Chapter 3), and the fronts, lows and high-pressure systems that cross the region (Figure 4.1). 'Summer' rainfall in SWWA is highly sporadic, and can be associated with the breakdown of TCs. This section further explores the recent declines in SWWA rainfall already noted in Chapter 3, and reports on estimates of future rainfall changes for the region.

4.1.1 INTENSIFIED AND EXPANDED SWWA DRYING AND ASSOCIATED MECHANISMS

Project Link: 1.2

Annual average rainfall across SWWA has continued the decline that began in the late 1960s (IOCI 2002; Hope et al. 2010; Chapter 3). These reductions have been particularly marked for early winter rainfall. Since 2000, rainfall totals have continued to be low, in many locations even lower than their 1969 to 1999 average (Figure 4.2). Moreover, this drying has expanded in geographic extent. Interannual variability of rainfall in the far south-west of Western Australia has declined along with total rainfall. This sub-section provides a more detailed understanding of the changes in the regional weather patterns behind these important rainfall reductions.

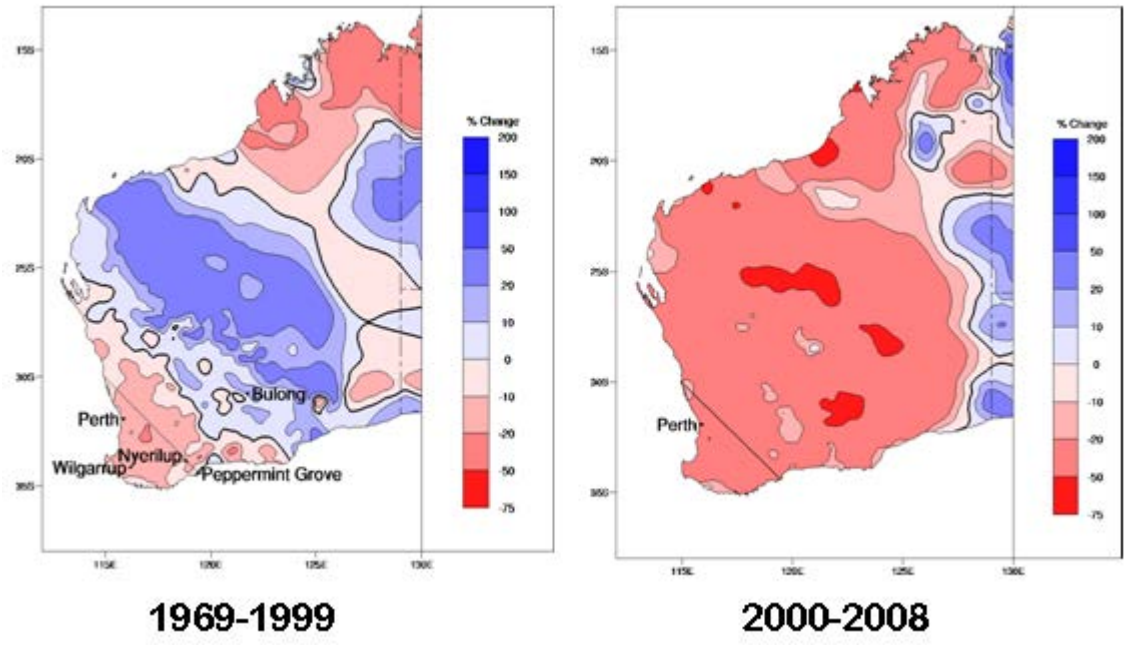

Figure 4.2 Early winter rainfall reductions in SWWA. Percentage change in May to July total rainfall (Australian Water Availability Project data; Jones et al., 2009) from the 1910 to 1968 mean to the stated periods. Drying was mainly centred on SWWA during the period 1969 to 1999, but this rainfall reduction has increased in intensity and expanded in area since 2000. Average rainfall in the SWWA region is south-west of the diagonal line.

To investigate regional weather patterns and their role in rainfall reductions, IOCI3 scientists employed a statistical method called a 'self-organising map' (Kohonen 2001; Hope et al. 2006; Sheridan and Lee 2011). The seasonal transition of the subtropical ridge is at its south-most extent in June and July, and thus these months were considered together. Since strong rainfall reductions have also been observed in May, autumn weather types are also explored below.

The self-organising map method allowed 20 patterns to be identified to form the continuum of weather types that influence SWWA in the months of June and July. Twenty weather types were identified as the smallest number that retained a small error between the observations and the types, but still captured all expected deep lows, intense highs and all weather patterns in between. These weather types are illustrated in Figure 4.3 together with the associated rainfall anomaly (Hope et al. 2006).

One key group of weather types is characterised by systems with a deep low across the region (see bottom row of Figure 4.3: types D4, A5, B5, C5 and D5). The presence of these low-pressure systems is associated with widespread rainfall across SWWA (i.e., these systems correlate at r=0.70 with SWWA rainfall). The number of days that these systems influence SWWA rainfall has decreased markedly since the 1970s. Compared to the period 1958 to 1975, the frequency of these types declined by 20% between 1976 and 1999 (Figure 4.4).

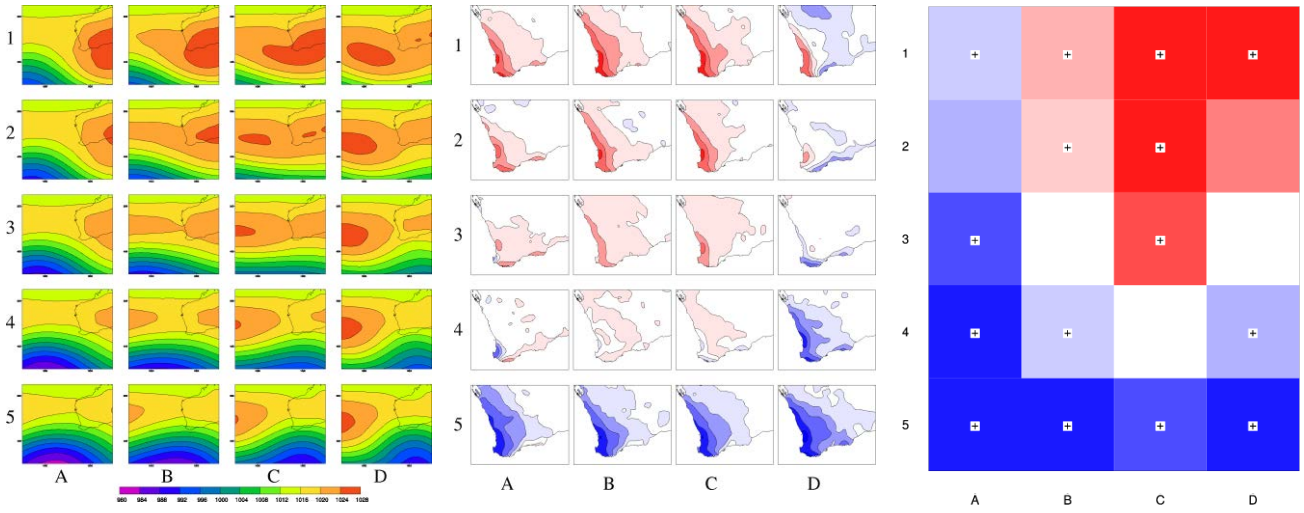

Figure 4.3 The self-organising map identifies the continuum of synoptic types across Western Australia in June and July. Left panel: synoptic types (mean sea-level pressure in hectopascals). Middle panel: rainfall anomalies (changes) corresponding to each synoptic type on the left. (Dark to pale shades of red, respectively, indicate greater to lesser rainfall reductions versus the average: -8,-4,-2,-1,-0.3 millimetres per day. Pale to dark blue indicates progressively more rainfall than average: 0.3,1,2,4,8 millimetres per day). The synoptic types in the left panel also correspond to the coloured squares in the right panel. Right panel: projected percentage change in occurrence of these synoptic types at the end of this century (2081 to 2100) versus the end of the last century (1961 to 2000). Red squares indicate synoptic types projected to become more common, blue those projected to decrease in future occurrence. 'Plus' signs indicate the significance of consensus across the models at the 5% level. All synoptic types with a deep low-pressure region south of SWWA during winter are projected to become less common in future.

However, since the year 2000 the incidence of systems with deep lows has changed little (Figure 4.4). Compared to the long-term (1958 to 1999) mean, these lows have declined in occurrence by just 0.8% since 2000; and compared to the shorter-term 1976 to 1999 mean, they have increased by 10%. Instead, the main weather system shift causing rainfall reductions since 2000 has been an increase (of 15% from the 1958 to 1999 mean) in the daily occurrence of synoptic types with high-pressure systems, as illustrated in Figure 4.5.[10] This group of weather types is identified in the left panel of Figure 4.3 as A1, B1, C1 and A2, B2. In summary, this finding indicates that recent rainfall reductions have more to do with the persistence of high-pressure systems over the region, and less to do with further decreases in the number of low-pressure systems. While the groups of synoptic types with extensive regions of high-pressure or deep lows have both increased in number since 2000, types in the top right of the self-organising map (Figure 4.3, types D1 and D2) have fallen to very low levels in recent years.

These recent shifts in synoptic systems can help explain the greater geographic extent of further decline in early winter rainfall in SWWA (as seen in Figure 4.2a). High-pressure systems exert their influence over a wider region than do low-pressure systems, and this might be expected to cause an expansion in the area experiencing a rainfall decline. Types D1 and D2 are associated with inland rainfall, and may also be indicative of the influence from cut-off lows, which are known to bring inland rainfall (Pook et al. 2012; Pook, pers. comm. 2012). Trends reveal that regions where May to July rainfall did not decline in the late 1960s (south coast and inland) are now seeing a decline in early winter. In regions that were already drying, the percentage change indicates a strengthening signal of rainfall decrease (in the far south-west and wheatbelt; see Table 4.1. These changes are described in detail in Hope and Ganter (2010).

As for the latter half of the cool season (August to October), rainfall trends in SWWA from 1950 to 2007 are weak. Whereas August and September rainfall has been increasing, October rainfall has been decreasing.

[10] The average count of these synoptic types in 2000 to 2008, minus the average of 1958 to 1999, and divided by the average of 1958 to 1999.

Improved understanding of the shifts in seasonal rainfall can help determine the management practices across a range of industries, for instance, the best timing for agricultural activities such as planting wheat.

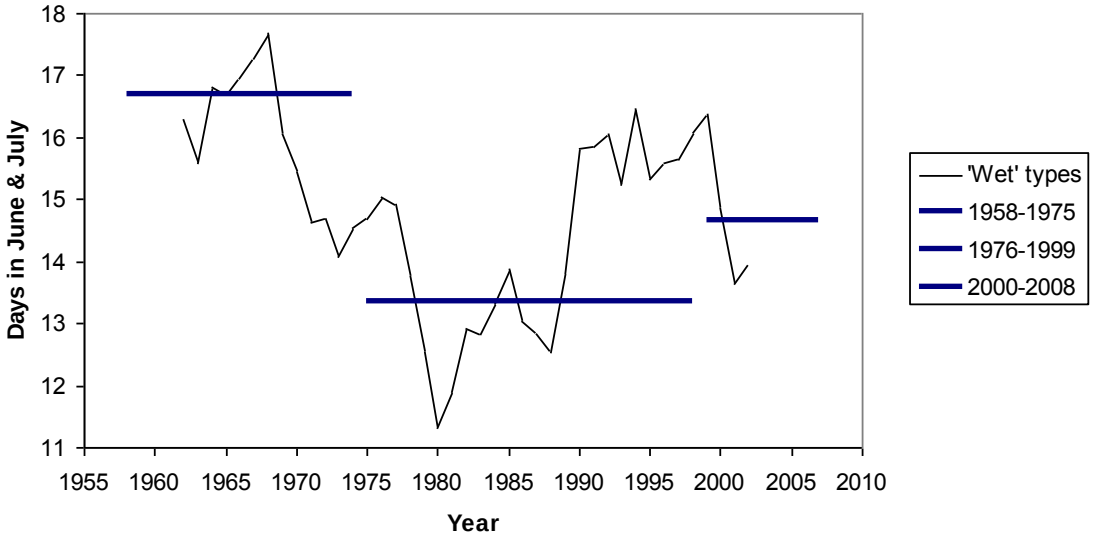

Figure 4.4 Smoothed series (11-year running mean*) of June and July synoptic types representing extensive wet conditions across SWWA. A marked decrease is shown in the number of days in June and July with these synoptic types after the 1970s, but no decrease associated with the recent rainfall declines since 2000. *N. B. The values of the 11 year averages are plotted at the middle year. The horizontal lines show the averages over the years stated in the key.

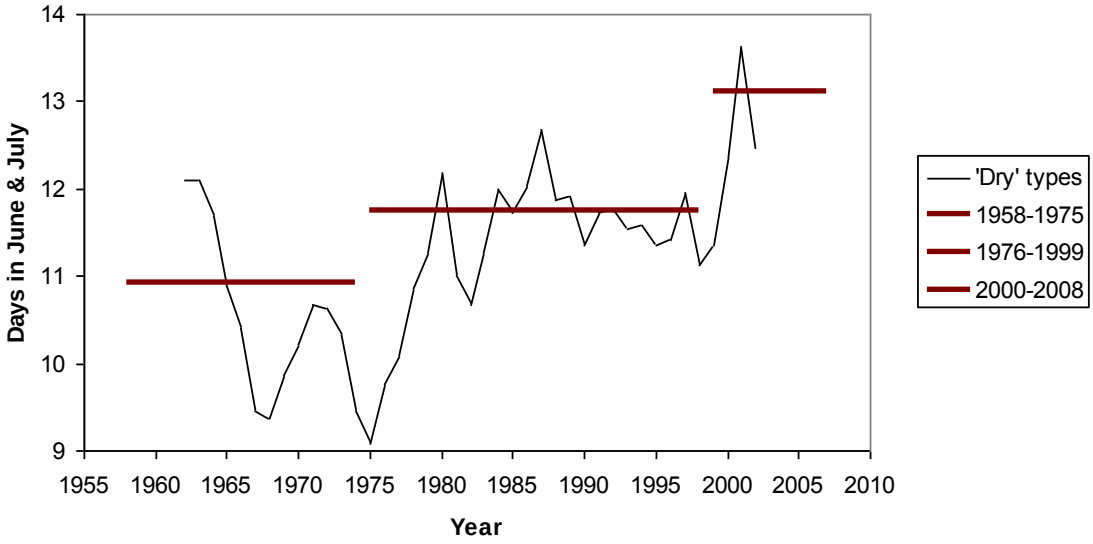

Figure 4.5 Smoothed series (11-year running mean*) of June and July synoptic types associated with dry conditions. Extensive high-pressure synoptic types are shown to have steadily increased in occurrence since the 1970s. Horizontal red lines indicate the average incidence of dry types over the periods indicated. N. B.: the values of the 11-year averages are plotted at the middle year. The horizontal lines show the averages over the years stated in the key.

For SWWA and the summer half-year, IOCI3 scientists found slight rainfall trends over the period from 1950 to present. Exceptions are inland areas and those along the south coast where increases were seen in both totals and, because summer rainfall is dominated by precipitation from extreme events, increases in rainfall extremes as well. Total November to April rainfall increased by 14 mm/decade at Bulong (inland) and 6.8 mm/decade at Peppermint Grove (south coast).

Table 4.1 The percentage change in May to July rainfall at representative stations for recent decades, compared to the 1910 to 1968 average. Note: the data used here end with the year 2009; Inclusion of later years would show still stronger declines. The location of each station is shown in Figure 4.2.

REGION	REPRESENTATIVE STATION	1969-1999	2000-2009
Far south-west	Wilgarrup (Manjimup)	-25%	-39%
South coast	Peppermint Grove	+7%	-13%
Inland	Bulong (near Kalgoorlie)	+22%	-35%

In autumn (March to May) SWWA has dried by 15% since the year 2000 compared to the 1900 to 2010 mean. May rainfall contributed an average of 58% to autumn SWWA rainfall over the period 1900 to 2010. April rainfall contributed 27% but March only 15% over this period. A self-organising map was developed to identify the continuum of weather types influencing the region in autumn. This showed that changes to May weather types are driving the overall autumn rainfall decline; May rainfall declined 25% post-2000 (2000 to 2010 average compared to the 1900 to 2010 long-term mean). As observed for the winter systems described above, the May rainfall decline is now largely being driven by an increase in high-pressure systems.

Conversely, April rainfall contributed a greater share to autumn rainfall during the period 2000 to 2010 compared to the 1900 to 2010 long-term mean. Its share of the total increased by 8%, while the contribution from May rainfall has dropped by the same amount. Mean SWWA rainfall during the period 2000 to 2010 was 20 mm for March, 44 mm for April and 67 mm for May. As amounts in May, June and July decrease, rainfall in months outside of this key, high rainfall period may become more important to this region.

Shifts in very intense rainfall events were also investigated by season using data from high-quality stations across SWWA. Over the period 1950 to 2007 trends will capture the late 1960s mean rainfall decline. Trends in the total rainfall above the 1961-to-1990[11] 95th percentile (the top 5% rainfall events in terms of intensity) generally followed the same direction as the rainfall mean. However, for stations in the far south-west (e.g., Wilgarrup), this was not true of the more recent 1970 to 2007 trend in early winter (May, June and July). Whereas the mean rainfall in this region declined by 21 mm/decade, total intense rainfall increased by 2 mm/decade. This demonstrates another feature associated with the above-mentioned increase in the daily occurrence of high-pressure systems that is driving recent declines in mean rainfall. That is, intense rainfall events are still occurring, but they are interspersed by ever-longer periods of dry conditions.

Overall, the above changes in the frequencies of weather systems are consistent with the changes in large-scale atmospheric circulation documented in Section 3.1. The subtropical jet steers cyclonic, mid-latitude storm systems and thunderstorms at lower levels in the atmosphere. A vigorous jetstream brings low- and high-pressure systems through in quick succession. A weakening of the jetstream leads to a stagnation of atmospheric patterns, and weaker surface low-pressure systems and cold fronts.

[11] 1961 to 1990 is a standard World Meteorological Organisation period.

Knowledge gaps and future directions

A long historical record of rainfall changes (i.e., paleoclimate information) would provide context for understanding the important recent (and future) changes in SWWA rainfall. This would aid efforts to determine the relative contribution to SWWA rainfall changes from anthropogenic climate change versus 'natural' interdecadal fluctuation. Drawing on the relevant literature, IOCI3 research and new datasets, IOCI3 scientists carried out initial scoping work to investigate whether examining isotopes in cave stalagmites in SWWA could provide proxy information on how the region's rainfall has varied over the last few centuries or longer. Isotopes from cave stalagmites generally correspond well to rainfall variability; however, shifts in the atmospheric circulation can confound this relationship (e.g., Fischer and Treble 2008). A combination of proxy measures and knowledge of circulation effects on SWWA (e.g., van Ommen and Morgan 2010) could provide a way forward by advancing understanding of the dominant circulation and rainfall changes through the last few hundred years.

4.1.1.1 The Southwest Australian circulation (SWAC) and its relationship with SWWA rainfall

In addition to the findings noted in Chapter 3 and those just above, IOCI3 scientists have done further work to investigate the variability and regional circulation features that influence SWWA rainfall. SWWA exhibits a regional atmospheric circulation feature which they have termed the Southwest Western Australian circulation (SWAC; Feng et al. 2010).

Preliminary work under IOCI3 examined the strength of the SWAC[12] and explored the impact of this circulation pattern of SWWA rainfall. Results indicate that the weakening trend in the SWAC may contribute to the long-term rainfall decrease over SWWA. In contrast to the large-scale atmospheric circulation described in Chapter 3, the SWAC defines *regional* atmospheric circulation over the wider SWWA region (35° to 25° S; 100° to 145° E).

The SWAC provides a new tool to better understand SWWA rainfall variability. It may offer a way of studying the attributes of rainfall variation, estimating the skill of climate models, and developing rainfall projections for SWWA. SWAC may be useful for both short-term forecasting capabilities and long-term trend projections.

Knowledge gaps and future directions

The development of the SWAC index is in its preliminary stages, and more work needs to be done, e.g., as to possible drivers of the variability described by the SWAC. These may include: (a) the shift of the planetary-scale thermal convection associated with a shift in the subtropical high (Zeng and Li 2002); and (b) the warming or cooling of sea surface temperatures west of SWWA over the Indian Ocean resulting, respectively, in a weak or strong SWAC, and negative or positive rainfall anomalies over SWWA.

4.1.2 RAINFALL PROJECTIONS FOR SWWA

Climate models suggest SWWA's drying trend will continue, as discussed in Sections 3.3 and 3.4. The extent to which drying may intensify and expand is an important question with relevance for policymakers. A brief discussion of prior work on SWWA rainfall projections provides some context for the new IOCI3 results reported in this sub-section.

Work under IOCI2 on SWWA rainfall (e.g., Bates et al. 2008) explored plausible futures using projections from nine climate models and three emissions scenarios.[13] All models and all scenarios projected winter rainfall decreases for the south-west corner of Western Australia by 2030, and a larger decrease by 2070. Downscaled projections produced results consistent with these findings, showing that wet synoptic types would decrease, and dry synoptic types would increase through this century (Bates et al. 2008). For May to

[12] As measured by the trend in the SWAC index, which is defined in Feng et al. 2010 (equation 1 and Figures 8 and 9).

[13] The SRES A2 (high), SRES B2 (low) and IS92a (intermediate) scenario.

October in SWWA, statistically downscaled results from ten CMIP3 models under the SRES A2 (high) GHG emissions scenario show a rainfall decrease of 8% to 30% at mid-century (2046 to 2065) compared to the end of last century (1981 to 2000; Timbal et al. 2008). At the end of the century (2081 to 2100) the decline ranges from 18% to 53%.

BoM and CSIRO (2007) provided projections of median annual rainfall change[14] under the six SRES GHG emissions scenarios. At 2030 decreases of up to 10% are seen in SWWA under all six scenarios; by 2050 decreases range from 10% under the B1 (low) GHG emissions scenario up to 20% under the A1F1 (highest) scenario; by 2070 decreases for part of all of SWWA range up to 20% in all scenarios.

In summary, this is a region of exceedingly robust projections in that climate models agree on the direction of change (Figure 4.6; IPCC 2007; BoM and CSIRO 2007).

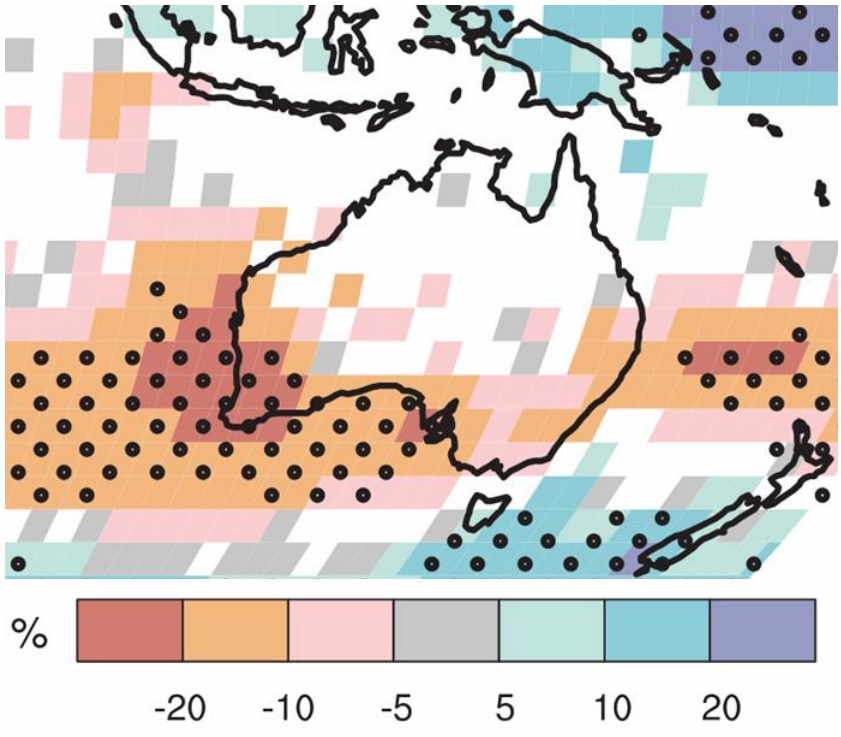

Figure 4.6 June to August rainfall is projected to decrease by more than 20% across SWWA at the end of this century (2080 to 2099) compared to the model mean value in 1980 to 1999, under the SRES A1B (intermediate) greenhouse gas emissions scenario. The black stippling indicates areas for which more than 90% of models agree on trends shown. From: IPCC Summary for Policy Makers (Figure 7).

4.1.2.1 Future shifts in synoptic types in SWWA

Project Link: 1.4

In addition to the work covered in Section 4.1.1 on observed weather system changes, IOCI3 scientists provided projections of future weather system changes in June and July. These projections suggest that, to the end of this century, the occurrence of synoptic types characterised by high pressure will increase (types C1, D1 and C2 on the top right of the June and July self-organising map; Figure 4.3, left panel) compared to 1961 to 2000, and that of low-pressure systems will decrease further (types A5, B5, C5, D5 and A4). Projections were made using the 13 CMIP3 climate models that had daily data available under SRES A2 (high) and B1 (low) GHG emissions scenarios. These simulations for the 2081 to 2100 period were compared to the 1961 to 2000 period, following the method of Hope (2006).

[14] Values are 'best estimates', i.e., based on ensemble average or multi-model mean; see p. 65 BoM and CSIRO, 2007.

The results from the A2 scenario at end of the century are shown in Figure 4.3 (right panel). The projected future changes differ a little from the changes that have been observed in recent years, with an increase in the occurrence of types (D1 and D2) that have recently seen a major decline. These sorts of synoptic systems may bring helpful rainfall to the wheatbelt and south coast (e.g., Pook et al. 2012). However, the projected future drop in the number of deep low-pressure systems is a feature consistent with observations over the last 50 years. This scenario would mean far less rainfall for the west coastal regions and far south-west. Individual models showed some quite emphatic results, with increases of more than 70% in the daily occurrences of some synoptic types associated with extensive high pressure, and almost as much decrease for types with deep low pressure (e.g., A4 and A5; see IOCI3 Milestone Report 4, Section 1.2 [appendix] for details). Thus the recent observed increase in the daily occurrence of synoptic types with extensive high pressure across the region may be expected to continue and possibly amplify.

Knowledge gaps and future directions

All models project that the mean pressure across southern Australian latitudes will increase at the end of this century. To explore whether the underlying increase in mean pressure across southern Australia is driving this shift in synoptic types seen in Figure 4.3 (right panel), the background mean trend could be removed. Thus we could explore whether patterns with the same gradients as a deep low would still occur, potentially bringing the same weather as a deep low seen in the present-day climate, but with higher central pressure. The overall increase in mean pressure will likely drive a further shift to a more settled weather regime for SWWA, with more highs persisting for longer.

BOX 2 ABOUT REANALYSIS DATA

A number of IOCI3 projects make use of reanalysis data. The Intergovernmental Panel on Climate Change (IPCC) provides the following description of reanalysis data:

> *Reanalyses are atmospheric and oceanic analyses of temperature, wind, current, and other meteorological and oceanographic quantities, created by processing past meteorological and oceanographic data using fixed state-of-the-art weather forecasting models and data assimilation techniques. Using fixed data assimilation avoids effects from the changing analysis system that occurs in operational analyses. Although continuity is improved, global reanalyses still suffer from changing coverage and biases in the observing systems.*[15]

Essentially these data provide climate researchers with a way to improve on the observed data used for climate modelling. Several different sources of reanalysis data are mentioned in this report, including those of the National Center for Environmental Protection (NCEP)/National Center for Atmospheric Research (NCAR) Reanalysis Project[16], and the European Centre for Medium-Range Weather Forecasts' (ECMWF) Interim Reanalysis Data (ERA Interim data). The various reanalysis datasets differ to some degree. This is because different physical and dynamical approaches and assumptions may be used to produce the different reanalysis datasets.

4.1.2.2 Station-scale rainfall projections for SWWA

Project Link: 3.1

Chapter 2 described how IOCI3 scientists have advanced a statistical downscaling technique to improve understanding of Western Australia's climate. This method was used to provide rainfall projections for a network of stations across SWWA relevant to the water supply and agricultural sectors.

Method: First the NHMM (Chapter 2) was calibrated to daily rainfall data from a network of 29 BoM gauges across SWWA. The 29 stations were selected by ranking them according to the completeness of their records and other data quality tests (e.g., minimising untagged accumulations as described in Viney and

[15] www.ipcc.ch/publications_and_data/ar4/wg1/en/annexessglossary-p-z.html

[16] www.esrl.noaa.gov/psd/data/reanalysis/reanalysis.shtml

Bates 2004). Stations were also selected for their relevance to the water and agriculture sectors. (See Appendix A for a complete list of stations.)

IOCI3 scientists then used the selected NHMMs to produce projections of future daily rainfall. (See Appendix A for details of this calibration, including combinations of weather states and predictor variables.) The calibrated NHMMs were driven with atmospheric predictors extracted from five CMIP3 GCMs for SRES B1 (low), A1B (intermediate) and A2 (high) GHG emissions scenarios for mid- and late-century time periods, as well as the 'present day'.[17,18] They chose five GCMs (CSIRO Mk3.5, GFDL 2.0, GFDL2.1, MIROC-medres and MPI-ECHAM5) based on their ability to reproduce the statistics of the predictor variables for current climate conditions. Although these five GCMs have been highly ranked (Smith and Chandler 2010) and used in other studies (Corney et al. 2010), they still exhibit biases in the statistics of the predictors used. Hence monthly bias-correction was applied to the predictor means and variances prior to their use in downscaling. Appendix B presents the mean NCEP/NCAR Reanalysis and GCM values for the SWWA predictors on a seasonal basis.

BOX 3 SRES SCENARIOS EXPLAINED

In the year 2000 the IPCC published a report describing GHG emissions scenarios, the Special Report on Emissions Scenarios (SRES). These SRES scenarios were used in the climate modelling that underpins the IPCC's third and fourth assessment reports. Greenhouse gas (GHG) emissions scenarios like these provide alternative assessments of how the future might unfold. Amongst other uses they are tools to assist in climate change analysis, including climate modelling, for the purpose of determining impacts, adaptation and mitigation. These scenarios have recently been revisited and revised for reporting in the Fifth Assessment Report in 2013.

The six SRES scenarios, in order of the highest to lowest emissions, are named: A1F1, A2, B2, A1B, B1, and A1T. The probability that any single emissions scenario will eventuate cannot be estimated, as future socioeconomic, technological and political conditions are uncertain. Currently emissions are tracking most closely to the A1F1 scenario (and higher than the path followed by the A2 scenario; Le Quere et al. 2009). Scenarios frequently used by IOCI3 research reported herein include the A2 (high), A1B (intermediate), and B1 (low) scenarios.

More information on SRES scenarios is available from the IPCC website:
www.ipcc.ch/ipccreports/sres/emission/index.php?idp=0

For each of the 29 stations, one hundred stochastic simulations of daily rainfall were generated for each GCM, SRES scenario and period combination (see above). The multiple simulations account for the range of possible rainfall sequences and intensities that can occur given the large-scale atmospheric sequences simulated by the GCMs.

Results: Because these analyses generated a large quantity of information, the results presented here include summaries averaged across all 29 SWWA stations. Readers seeking more detailed analyses of individual stations may find these in Appendix B and in the relevant IOCI3 Milestone Project Reports. The complete results are also available at: http://data.csiro.au/dap/

The results in Table 4.2 are given as mean annual projected changes as a proportion of present day (1962 to 1999) rainfall average, for a given scenario and time period. This table shows that the five GCMs produce a range of projections, and this leads to considerable uncertainty in the downscaled results. For example, at mid-century (2047 to 2064) projected rainfall under the B1 (low) scenario ranges from 90% of present-day levels under the Mk3.5 model to 79% of present under the GFDL2.1 model (i.e., declines of 10% and 21%, respectively, from present day levels). However, the range caused by using these five different GCMs is just one source of uncertainty. Other sources of unquantified uncertainty pertain to whether the statistical downscaling relationships of the historical period remain valid in the future; how the range of projections

[17] 'Present day' refers to the period 1962 to 1999, 'mid-century' to the period 2047 to 2064, and 'end of the century' to the period 2082 to 2099. These are the only periods for which daily predictor output is available from CMIP3 GCMs.

[18] These three SRES scenarios and two future periods were pre-determined by the availability of daily GCM output archived by the CMIP3 project.

would differ if a different downscaling technique or set of GCMs were used; and whether the newer CMIP5 models and scenarios would produce very different projections.

Nevertheless, consistent patterns emerge. Perhaps most important, all projections suggest that a drier future climate is in store for SWWA.[19] And by the end of century, the rainfall projections for the low, intermediate and high SRES scenarios all diverge. By this time, all five GCMs indicate greater rainfall reductions for the A1B (intermediate) and A2 (high) emissions scenarios compared to their respective B1 (low) scenario results. Four of the five models also indicate that the A2 scenario would produce the largest change (the single exception is the GFDL 2.1 model, which produces a larger change for the A1B scenario). The rainfall quantities projected by the NHMM using the GCMs for a particular SRES scenario and period are somewhat consistent, with the exception of the CSIRO Mk3.5 model. The NHMM downscaled CSIRO Mk3.5 model projects less drying than the other models for both future time periods. This is because, compared to the other four GCMs, for each scenario and period the CSIRO Mk3.5 GCM projects the least change in the selected predictors: mean sea level pressure, north-south mean sea level pressure gradient, and 700 hPa dew point temperature depression (DTD[20]), a measure of moisture content of the air. Global climate model predictor summaries are presented in Appendix B.

Averaged across all simulation years and stations, depending on the model, by mid-century mean annual rainfall is projected to decrease by 10 to 21% under the B1 scenario, 8 to 33% under the A1B scenario and 11 to 28% under the A2 scenario. By the end of the century the corresponding ranges are decreases of 6 to 28% (B1), 17 to 46% (A1B), and 20 to 43% (A2).

Table 4.2 Projected mean annual rainfall for SWWA. For mid-century (2047 to 2064) and end-of-century (2082 to 2099) periods using five global climate models and three SRES emissions scenarios. Projections are given as a proportion of 1962 to 1999 climatology.

	SCENARIO AND TIME PERIOD					
MODEL	**B1_MID**	**A1B_MID**	**A2_MID**	**B1_END**	**A1B_END**	**A2_END**
gfdl2.0	0.86	0.70	0.73	0.77	0.64	0.57
gfdl2.1	0.79	0.67	0.73	0.72	0.54	0.57
miroc	0.83	0.84	0.72	0.78	0.71	0.67
mk35	0.90	0.92	0.89	0.94	0.83	0.80
mpi	0.86	0.88	0.82	0.79	0.68	0.64

The results of these downscaled rainfall projections are also provided in Appendix B for each of the 29 stations, both as a proportion of present-day rainfall and as absolute values. Note also the caveats pertaining to the use of these results, as outlined above and in 'Knowledge gaps and future directions' below. For indicative purposes, a subset of these results from stations across SWWA is provided here (see Tables 4.3 and 4.4). Note that these mean annual rainfall results reflect long-term averages across the time periods simulated and hence 'average out' the year-to-year variability. For example, a simulated result of 330 mm of annual mean rainfall for mid-century reflects the average for the period 2047 to 2064. Future annual rainfall will continue to vary from one year to the next due to natural causes of variation; however, the size of these variations is projected to differ from those of the present day given the projected long-term drying of SWWA's climate. (Figure B-1, Appendix B reports probability distributions of projected annual rainfall, indicating possible changes to variability).

What causes these downscaled projections of a drier future for SWWA? These rainfall changes result from changes in the sequences of weather states simulated by the NHMMs, which in turn result from changes in

[19] That is, in Table 4.2 the proportions are less than 1.0 for all GCMs, SRES scenarios and periods.

[20] DTD equals air temperature minus dew point temperature.

the atmospheric predictors projected by the GCMs. Table 4.5 summarises the strength of the linear relationship between the weather state changes and atmospheric predictor changes. For the SWWA NHMMs, the relevant atmospheric predictors are measures of atmospheric circulation (i.e., those related to mean sea level pressure) and moisture content (DTD). See Appendix A, Figures A-1 and A-2 for illustrations of SWWA weather states as mean precipitation probability maps and corresponding composite atmospheric predictor fields.

Table 4.3 Projected changes in annual mean rainfall for selected stations across SWWA as a proportion of present-day values (1962 to 1999). Given for mid-century (2047 to 2064) and end-of-century (2082 to 2099) periods under three SRES emissions scenarios. The range of results in each cell reflects the range of downscaled projections produced by the five global climate models, illustrating one source of uncertainty in the results. A list of these results for all 29 stations is available in Appendix B.

STATION	PRESENT DAY	MID-CENTURY B1 (LOW)	MID-CENTURY A1B (MID-RANGE)	MID-CENTURY A2 (HIGH)	END OF CENTURY B1 (LOW)	END OF CENTURY A1B (MID-RANGE)	END OF CENTURY A2 (HIGH)
Dalwallinu	1	0.80–0.88	0.67–0.91	0.73–0.88	0.72–0.90	0.54–0.82	0.58–0.78
Perth Airport	1	0.77–0.90	0.64–0.93	0.69–0.88	0.70–0.94	0.51–0.82	0.53–0.79
Cape Leeuwin	1	0.84–0.93	0.75–0.95	0.77–0.92	0.79–0.97	0.64–0.88	0.65–0.87
Pemberton Forestry	1	0.82–0.92	0.72–0.95	0.74–0.91	0.77–0.96	0.60–0.87	0.61–0.84
Lake Grace	1	0.80–0.87	0.67–0.90	0.74–0.87	0.71–0.89	0.55–0.81	0.58–0.77
Wandering	1	0.77–0.89	0.64–0.91	0.70–0.88	0.69–0.92	0.50–0.81	0.53–0.78

Table 4.4 Present-day and projected annual mean rainfall for selected stations across SWWA. Values are given in millimetres for mid-century (2047 to 2064) and end-of-century (2082 to 2099) periods under three SRES emissions scenarios. The range of results in each cell reflects the range of downscaled projections produced by the five global climate models, illustrating one source of uncertainty in the results. A list of these results for all 29 stations is available in Appendix B.

STATION	PRESENT DAY	MID-CENTURY B1 (LOW)	MID-CENTURY A1B (MID-RANGE)	MID-CENTURY A2 (HIGH)	END OF CENTURY B1 (LOW)	END OF CENTURY A1B (MID-RANGE)	END OF CENTURY A2 (HIGH)
Dalwallinu	390–410	330–360	270–360	290–340	290–350	220–320	230–310
Perth Airport	770–800	610–690	510–720	550–680	560–730	400–630	420–610
Cape Leeuwin	990–1020	840–920	760–950	780–920	800–960	650–880	660–860
Pemberton Forestry	1160–1190	970–1060	850–1100	890–1050	910–1110	710–1000	720–970
Lake Grace	360–380	300–330	250–340	270–320	270–320	200–290	210–280
Wandering	570–600	460–510	380–520	410–500	410–530	300–460	310–440

For the summer half-year (November to April), changes in predictors of atmospheric moisture content are related to the projected future changes in weather states. In particular, a drier lower atmosphere (as indicated by increasing DTD at 850 hPa) is strongly related to a weather state (summer state 1) that occurs on 74% of days during the present period (1962 to 1999; Table 4.5) and is characterised by a dry pattern. All

GCMs project an increased drying of the lower atmosphere corresponding with an increase (of 3% by mid-century and 5% by the end of the century, on average) in this dry weather state.

Table 4.5 The strength of the relationship (R^2) between projected changes in SWWA weather state frequencies and atmospheric predictors. Global climate models project an increase in the frequency of the dry weather pattern 'summer state 1', and a corresponding increase in dew point temperature depression in the lower atmosphere (DTD850). During winter, they project a decrease in frequency of wet weather states ('winter states 1 to 5') and, correspondingly, a drier middle atmosphere (DTD700), an increase in mean sea level pressure (MSLP), and a reduced mean sea level pressure gradient (N-S MSLP) as shown in Appendix B. R^2 is the coefficient of determination between the mean frequency of each weather state and mean value of each atmospheric predictor for the changes from the five global climate models, three emissions scenarios and two projection periods.

STATION		MSLP	N-S MSLP	DTD700	DTD850
Summer state	1	0.09	0.02	0.27	0.67
	2	0.16	0.06	0.06	0.57
	3	0.19	0.01	0.27	0.56
	4	0.00	0.00	0.45	0.57
Winter state	1	0.85	0.95	0.86	
	2	0.46	0.82	0.89	
	3	0.83	0.96	0.90	
	4	0.83	0.79	0.69	
	5	0.72	0.93	0.89	
	6	0.82	0.96	0.90	

For the winter half-year (May to October) projected changes to both atmospheric circulation and moisture predictors are strongly related to projected changes in weather state frequency (Table 4.5). All wet states (winter states 1 to 5) are projected to decrease in frequency, and only the dry state (winter state 6) would increase in frequency in future. In nearly all cases, the GCMs project a corresponding increase in mean sea level pressure and a reduction in the mean sea level pressure gradient across SWWA. All projections indicate a drier middle atmosphere (i.e., an increase in DTD at 700 hPa).

Further details, including the extent of projected change to atmospheric predictors and all weather states, are reported in Appendix B, Tables B-3,4 (summer) and Tables B-5,6 (winter). Additional information is reported in the Project 3.1 Final Milestone Report.

Knowledge gaps and future directions

An important caution is that the level of uncertainty for rainfall projections is undoubtedly larger than that presented here, given that only five GCMs were used in conjunction with only one downscaling method. Furthermore, statistical downscaling does not necessarily reduce projection uncertainty, so whilst the results are suitable for scenario planning they should not be viewed as definitive predictions of the climate that will be experienced in the future. That is, these are projections of plausible future climates, not weather forecasts (see Summary Report, Box 4).

Note also that whereas NHMM simulations do a reasonable job of reproducing interannual variability and long-term trends, they are currently not well suited to the task of modelling daily rainfall extremes. Two factors may contribute to underestimation of daily rainfall extremes. Firstly – by definition – there are few extremes and so the calibrated NHMM parameters, being representative of the majority of the data, are not greatly influenced by the few extreme rainfalls in the records. Secondly, the atmospheric predictors are only used to define the transitions between weather states and not the intensity of rainfall within the

states. Further development of the NHMM to address this limitation is planned. A caveat is the strong possibility that the predictors on the reanalysis grid scale would inadequately represent the atmospheric conditions for extreme rainfalls caused by localised convective events (e.g., summer thunderstorms). This caveat obviously also applies to the inability of GCM predictors to represent such small-scale atmospheric conditions.

4.2 SWWA Temperature: Observed Changes and Future Projections

As in many other regions of Australia, SWWA's climate has undergone average warming over the past 50 years. This section covers IOCI3 work on trends and possible drivers of observed temperatures changes. It also reports on station-scale temperature projections for SWWA for the middle and end of the century.

4.2.1 SWWA MAXIMUM TEMPERATURE TRENDS AND ASSOCIATED CIRCULATION PATTERNS

Project Link: 1.2

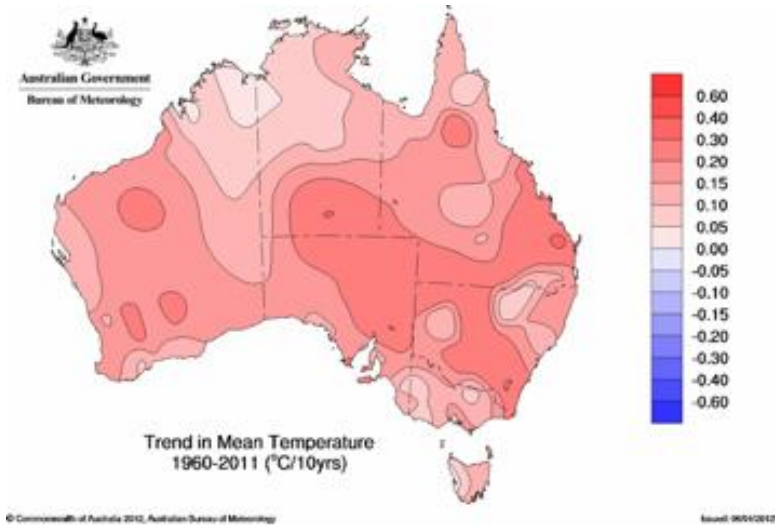

Figure 4.7 Mean temperature trends over the period 1960 to 2011 in degrees Celsius per decade. Source: Australian Bureau of Meteorology.

Annual mean temperatures across Western Australia have warmed over the last 50 years (Figure 4.7). Mean *maximum* summer temperatures have also warmed through the Pilbara and along the west coast in the south (Figure 4.8a). However, in the north of the state, the south coast, and the east of SWWA maximum temperatures have cooled (Figure 4.8a). In many areas within these regions the trends during the period 1961 to 2011 are significant at the 5% level (see stippling). Among the impacts of the cooling in the south of SWWA is a trend toward later ripening of wine grapes in Margaret River (Webb et al. 2012).[21] The possible causes and likely future progression of this cooling trend in the south-east of SWWA are explored here.

In the south of the state, rainfall is low and sporadic in summer, and in some years summer totals are less than 10 mm. Summer rainfall is often associated with cool maximum temperatures, and that is also the case in this region (Figure 4.8b). However, the low number of rainfall events suggests that the cooler maximum temperatures observed are more likely to be due to over-riding atmospheric circulation than to the cloud cover and rainfall on any given day.

[21] Note that whereas the ACORN-SAT data (which are more reliable) show a cooling trend in Margaret River, the cooling region in the AWAP data in Figure 4.8a does not extend this far west.

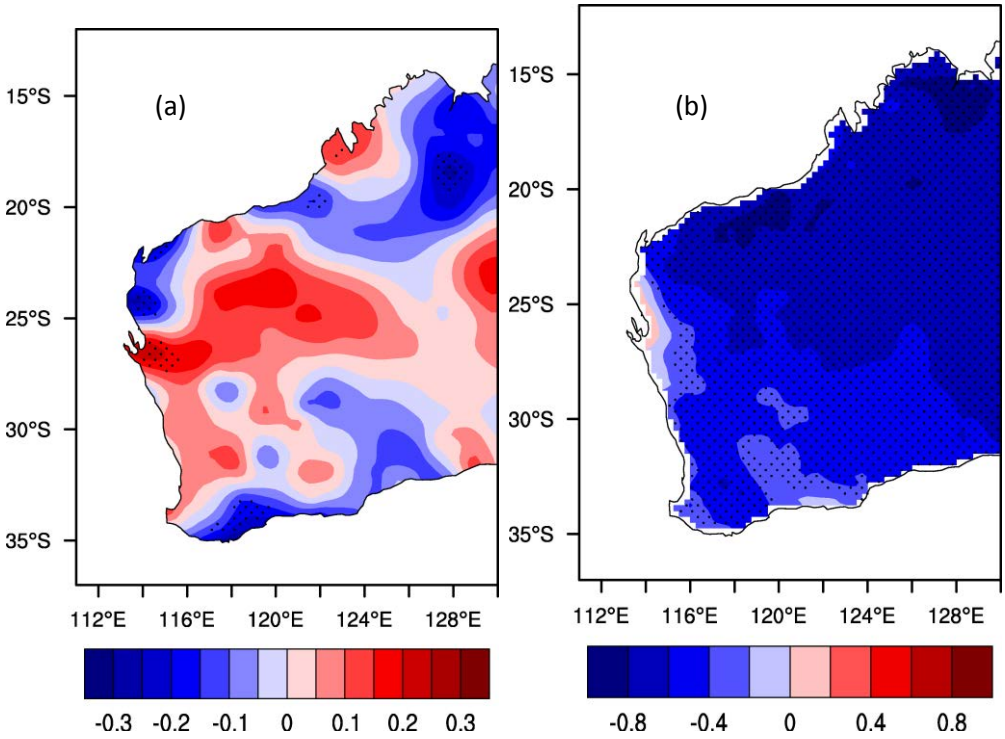

Figure 4.8 Trends in December to February maximum temperature, and relationship with rainfall in Western Australia. (a) Australian Water Availability Project gridded data in degrees Celsius per decade over the period 1961 to 2011. Locations with statistically significant (5%) trends are indicated by stippling. Note the cooling of maximum temperatures in the south-east of SWWA. (b) Summer (December to February) correlation is shown between mean maximum temperatures and rainfall at each grid-point (Australian Water Availability Project gridded data). The stippling indicates significant correlations at the 5% level.

Year by year the mean maximum temperatures in the region vary by about 4 °C. In 2010 the mean average summer temperatures in the east of SWWA were more than 33 °C, the warmest summer recorded, and rainfall was exceptionally low.

To explore the projected changes in temperature across this small region, IOCI3 scientists examined the associated circulation patterns (Hope and Keay, 2012). They used this approach because climate models should be able to capture these larger-scale features better than they capture local temperatures. Furthermore, improved understanding of the association between local temperatures and larger-scale circulation can help to build statistical downscaling models, such as discussed in the next section. The range of circulation patterns that influence SWWA in summer (December, January and February) was identified with a self-organising map (e.g., Hope et al. 2006) of 12 synoptic types (Figure 4.9).[22] The number of types chosen was relatively small compared to the winter analysis described in Section 4.1.1 because summer weather exhibits lower day-to-day variability. The 12 types identified represent the summer weather in SWWA well.

The composites of SWWA maximum temperature associated with these types (Figure 4.9, right panel) revealed distinct patterns of temperature across the region. Synoptic type A4 has a temperature anomaly pattern that resembles the observed trends in maximum temperature. The trends, associations and projected future changes of this synoptic type, and the closely related synoptic type A3, were explored to improve understanding of the synoptic conditions associated with the observed pattern of temperature change. Both synoptic type A4 and A3 had upward trends in occurrence from 1958 to 2011.

[22] Data used were daily (at about 14:00 hours) December to January mean sea-level pressure from the NCEP/NCAR reanalyses 1948 to 2011.

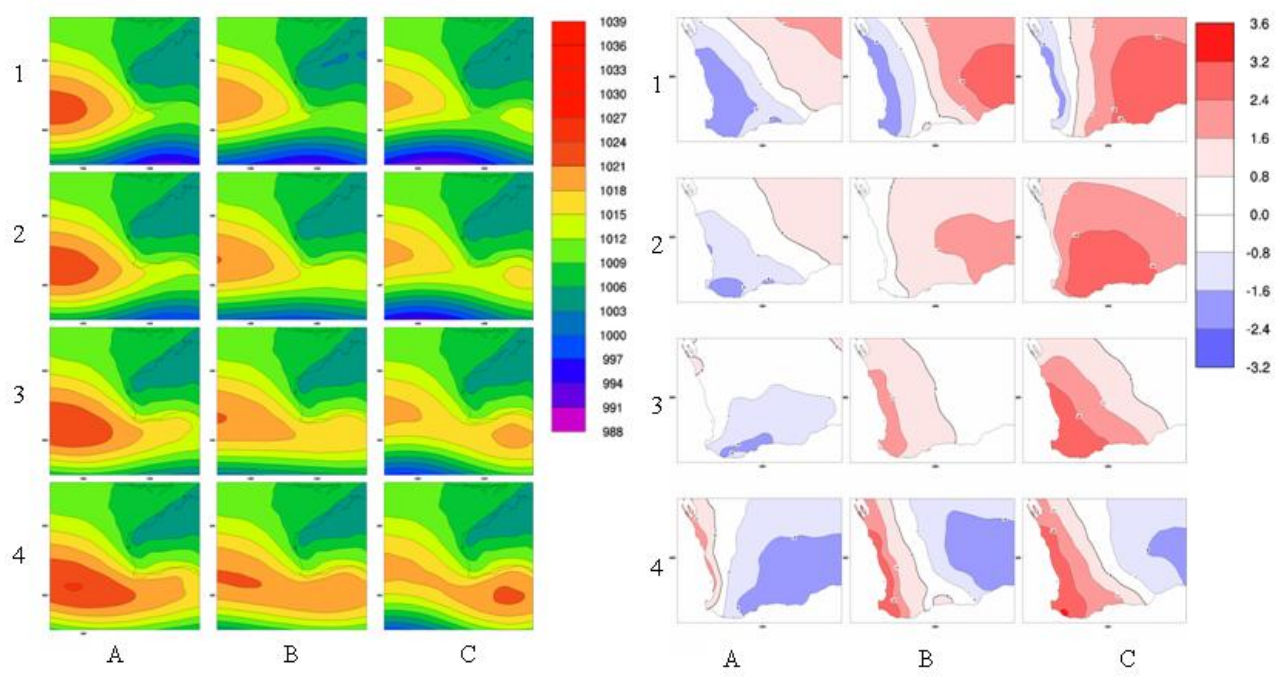

Figure 4.9 Self-organising map of synoptic types and associated temperature anomalies. Left panel: Self-organising map of summer (December, January, February) afternoon synoptic types (blue=low pressure, red=high pressure). Right panel: anomalous temperatures, in degrees Celsius, associated with each synoptic type.

To understand the wider drivers of changes to these synoptic types, their relationship with indices of large-scale variability was explored. Synoptic type A4 is associated with the highest pressure in the Indian Ocean of any identified synoptic type. To represent the strength of the Indian Ocean high, mean sea-level pressure data (HadSLP2r[23]) was averaged over the region of highest pressure. A strong correlation was found between this synoptic type and the Indian Ocean high (Table 4.6).

More pertinent still, the maximum temperature anomaly pattern of synoptic type A4 and the 1960 to 2011 trend resemble the temperature response caused by the easterly wind anomalies associated with the high phase of the SAM (Hendon et al. 2007). When SAM is in its high phase (i.e., when the SAM index is high), pressures at the latitude of southern Australia are high. Mean summer maximum temperatures and an index of the SAM[24] correlate negatively and significantly in the region of cooling in south-east SWWA (Figure 4.10). That is, a higher SAM index tends to be associated with cooler maximum temperatures in this region. Furthermore, there is a positive correlation between type A4 and A3 occurrence and the SAM index; more frequent occurrence of these types is associated with a higher SAM index (Table 4.6). Other types identified in the self-organising map are also associated with the SAM. For instance, synoptic types C1 and C2, which correspond with warm conditions over much of the region, correlated negatively with the SAM index (r=-0.39 and -0.31 respectively).

Given these associations, it is likely that the cooling of maximum temperatures in south-east SWWA is due to the increasing occurrence of synoptic type A4, and a decrease in the occurrence of patterns with the opposite anomalies, such as C1 and C2. These trends are likely to be linked to the observed intensifying Indian Ocean high and the rising SAM index. The precise drivers of the intensifying Indian Ocean high are unclear, as these drivers may have their origins in both the tropics and high latitudes. However, a plausible hypothesis is that the rising SAM index in summer is due in part to the growth of the Antarctic stratospheric ozone hole (Thompson and Solomon 2002).

[23] Mean sea level pressure was from the HadSLP2r dataset over the region: 57.5° E to 92.5° E, and 42.5° S to 32.5° S: www.metoffice.gov.uk/hadobs/hadslp2/ (Allan and Ansell, 2006).
[24] http://www.nerc-bas.ac.uk/icd/gjma/sam.html (Marshall 2003).

Table 4.6 Correlation between the daily occurrence of synoptic types A4 and A3, an index of Southern Annular Mode (SAM), and the strength of the Indian Ocean high. For summers in the period 1958 to 2011.

DECEMBER, JANUARY & FEBRUARY	TYPES A4+A3	SAM	INDIAN OCEAN HIGH
Types A4+A3	1	0.50	0.46
SAM		1	0.69

With the recovery of stratospheric ozone, the Antarctic ozone hole is projected to diminish in size over coming decades, and with it, this influence on the SAM may diminish too (Son et al. 2008; Arblaster et al. 2011). Thus this cooling pattern observed for maximum temperatures in south-east SWWA may reverse itself. Conversely, on the west coast of SWWA, observed warming may have been exacerbated by the response of the winds to the intensifying high-pressure band across southern Australia (and a rising SAM index). These trends would result in weaker-than-normal westerly winds, and a reduction of their associated cooling effect. Thus a future downward trend in the SAM index may mean this region would warm less quickly in future.

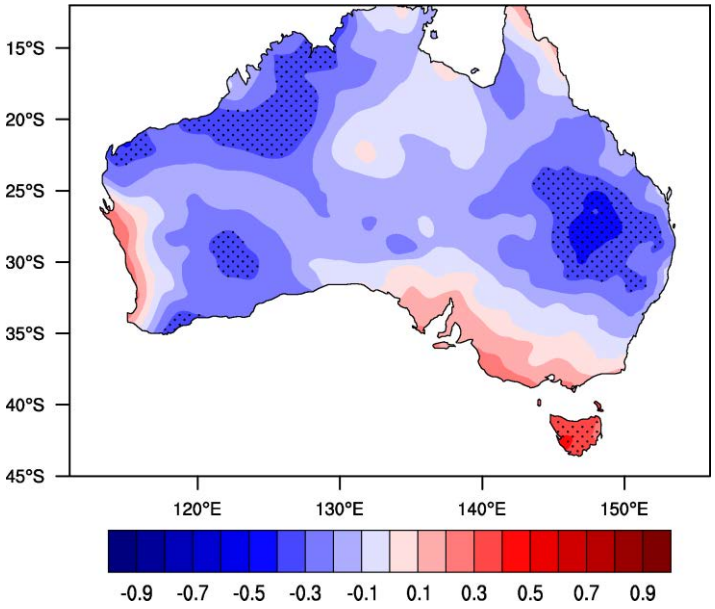

Figure 4.10 The relationship between summer maximum temperature and the Southern Annular Mode in Australia. Summer correlation is shown between maximum temperature and the Marshall index of the Southern Annular Mode at each grid-point. Stippling indicates significant correlations at the 5% level. The regions of significant negative correlation in the east of SWWA indicate that when the Southern Annular Mode index is high, maximum temperatures tend to be relatively cool in this region.

However, in contrast to the effect of ozone hole recovery, increasing levels of atmospheric GHGs are expected to push the SAM to its higher state, i.e., a state characterised by high pressure at the latitude of southern Australia. Through to the middle of this century these competing forces are expected to result in the SAM index persisting at approximately its current level. However, by the end of this century, all models[25] under SRES A2 (high) forcing scenario show a higher state of SAM, with higher pressures in the belt to the south of Australia in summer.

[25] See Section 4.1.2.1 for a description of models used.

Synoptic types A4 and A3 are projected to occur about 35% more often at the end of this century compared to the end of the last century. Types on the opposite end of the self-organising map are projected to occur about 35% less often. Types shown along the top of the self-organising map, which represent weather systems that bring cooler conditions to the west coast, are also projected to decrease (Figure 4.11).

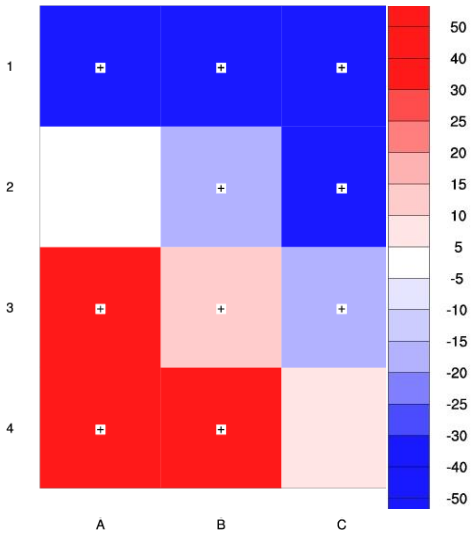

Figure 4.11 Projected changes in synoptic types associated with SWWA temperature anomalies. The projected percentage change in occurrence of the summer synoptic types in Figure 4.9 at the end of this century (2081 to 2100) compared the end of last century (1961 to 2000). Red squares indicate synoptic types projected to become more common, blue indicates those projected to decrease in future occurrence. 'Plus' signs indicate the significance of consensus across the models at the 5% level. Types A4 and A3, associated with high pressure in the Indian Ocean, are projected to become more common.

Knowledge gaps and future directions

Further investigation could explore whether the underlying increase in mean pressure across southern Australia projected for the end of the century is driving this shift in synoptic types, or whether systems with similar patterns to those along the top of the self-organising map will still occur, but with higher mean pressures.

4.2.2 STATION-SCALE TEMPERATURE PROJECTIONS FOR SWWA

Project Link: 3.1

In addition to rainfall projections (Section 4.1.2.2), the statistical downscaling advances described in Chapter 2 were used to provide projections of future daily maximum and minimum temperatures for SWWA for the 29 stations already noted. (See Appendix A for a complete list of stations)**.**

Method: The sequences of daily weather states and multi-site rainfall simulated by the NHMM (Appendix A) were used as input for a weather generator for daily temperatures to simulate a series of maximum and minimum temperatures for the SWWA station network. This model conditioned daily temperatures on the weather state and the wet/dry status of rainfall for each station on that day. It is important to condition the daily temperatures on the rainfall status because wet and dry days can have markedly different temperature characteristics. For example, on wet winter days minimum temperatures tend to be higher than on dry days, and maximum temperatures lower, due to cloudiness and rainfall.

The correlations between maximum and minimum temperatures at each station, and the spatial correlation between these variables across the stations, were taken into account. Output from the five GCMs named above (Section 4.1.2.2) for the SRES A2 (high) emissions scenario was downscaled dynamically to 65-km resolution using the CSIRO Conformal-Cubic Atmospheric Model (CCAM; see

glossary). This model's monthly projected changes in temperature (also calculated on a wet/dry day basis) were incorporated into the stochastic series of maximum and minimum daily temperatures. The ability to generate this *correlated* rainfall and temperature daily series has potential advantages over techniques that produce downscaled variables independently (e.g., Timbal et al. 2009). This is because it is more physically realistic to generate daily rainfall and temperature series correlated according to observed relationships so as to reproduce characteristics such as wet days with higher minimum and lower maximum temperatures than dry days.

Table 4.7 Downscaled projected mean annual maximum and minimum temperature changes for SWWA. In degrees Celsius for mid-century (2047 to 2064) and end-of-century (2082 to 2099) periods relative to the present day (1962 to 1999). Results presented here are an average of the values for all 29 stations studied.

	MAXIMUM TEMPERATURE		MINIMUM TEMPERATURE	
MODEL	A2_MID	A2_END	A2_MID	A2_END
gfdl2.0	2.1	3.5	1.7	3.0
gfdl2.1	1.7	3.4	1.7	3.2
miroc	1.5	2.6	2.0	3.5
mk35	2.4	4.2	2.2	4.1
mpi	1.7	3.5	1.6	3.3

Table 4.8 Downscaled projected mean annual maximum and minimum temperatures for selected SWWA stations. In degrees Celsius for mid-century (2047 to 2064) and end-of-century (2082 to 2099) periods. A list of these results for all 29 stations is available in Appendix B. *N. B.: because the daily temperature downscaling technique is based on a weather generator calibrated to observed data, the present-day simulations reproduce the observed values very closely and so a range is not shown. This is different to the NHMM rainfall simulations in Table 4.4, in which present-day differences between global climate model predictors produce a range of present-day rainfall.

	MINIMUM TEMPERATURE			MAXIMUM TEMPERATURE		
STATION	PRESENT DAY*	MID-CENTURY A2 (HIGH)	END OF CENTURY A2 (HIGH)	PRESENT DAY*	MID-CENTURY A2 (HIGH)	END OF CENTURY A2 (HIGH)
Dalwallinu	12.2	14.0–14.8	15.7–16.8	26.0	27.5–28.8	28.6–30.8
Perth Airport	12.6	14.1–14.7	15.5–16.5	24.5	26.0–26.8	27.3–28.6
Cape Leeuwin	14.1	15.3–15.8	16.5–17.1	20.1	21.3–21.7	22.5–22.9
Pemberton Forestry	10.3	11.6–12.1	12.8–13.6	20.5	22.0–22.4	23.3–23.9
Lake Grace	10.4	12.0–12.7	13.5–14.6	23.1	24.4–25.7	25.4–27.5
Wandering	9.1	10.8–11.4	12.3–13.4	23.3	24.8–25.8	26.0–27.8

Results: As with the downscaled rainfall projections described above, the large quantity of information generated is summarised here; full results are available in database form at: http://data.csiro.au/dap/. Table 4.7 reports the mean changes in annual daily maximum and minimum temperature projected by the coupled NHMM–weather generator. Averaged across all 29 stations for SWWA, daily maximum temperatures are projected to increase by 1.5 to 2.4 °C by mid-century and 2.6 to 4.2 °C by the end of the

century under the A2 (high) scenario. Daily minimum temperatures are projected to increase by 1.6 to 2.2 °C by mid-century and 3.0 to 4.1 °C by the end of the century (Table 4.7).

Downscaled CSIRO Mk3.5 projections give the greatest warming for SWWA. There is some inconsistency among the five GCMs in terms of whether the results project a greater increase in maximum or minimum temperatures. For both the mid- and end-of-century time periods, four of the five GCMs project maximum temperature increases of equal or greater magnitude than minimum temperature increases. The exception is the MIROC model; it projects the smallest maximum temperature increases but the second-largest minimum temperature increases. The temperature projections downscaled from the CSIRO Mk3.5 model show the greatest warming for maximum and minimum temperatures for both mid- and end-of-century periods.

For indicative purposes, Table 4.8 provides the downscaled maximum and minimum temperature results for a subset of the 29 stations; the results for the complete list of the 29 selected stations may be found in Appendix B.

4.3 Extreme Events in South-West Western Australia

Extremes of climate and weather have profound socio-economic and environmental consequences (e.g., Peng et al. 2011; Saunders et al. 2011). IOCI3 sought to provide information about rainfall and temperature extremes specific to the SWWA region for present-day and projected future climate conditions. Projecting future changes in the characteristics of extreme events is an emerging area of climate science. Thus IOCI3 work in this area focussed on developing new methods and techniques such as a statistical approach that integrates climate model output with observed data. This work has produced projections that appear plausible. However, future work is needed using additional climate models and more climate scenarios to provide more robust projections suitable for use in impact and vulnerability assessments.

4.3.1 OBSERVED AND PROJECTED RAINFALL EXTREMES

The SWWA winter (May to October) rainfall decline is partly due to reductions in the number and intensity of extreme events. It is important to understand these declines that have already negatively affected hydrological systems including rivers, wetlands, and shallow groundwater (IOCI 2002). Knowledge of extreme rainfall is also important for the engineering design of culverts, bridges, roads and dams.

4.3.1.1 The search for possible drivers of decreases in SWWA extreme rainfall events

Project Link: 3.2

Previous stages of IOCI reported that there has been a decline in the frequency and intensity of rainfall over SWWA for the winter half-year (Li et al. 2005; Smith et al. 2000; Nicholls et al. 1999). Analyses in Stage 3 showed that a similar pattern of decrease in rainfall extremes was evident when changes were examined nonparametrically, i.e., using techniques not reliant on assuming a particular functional form. This decrease was also apparent when examining the relationship with annual dam inflows, which have observably decreased in SWWA (Bates et al. 2010). These dam inflows serve as an integrated measure of rainfall over the study area.[26] The analysis concentrated on the winter yearly maximum rainfall.

In the analysis described below the distribution of the maximum value of extreme rainfall was modelled by a generalised extreme value distribution (see Box 4). Estimating the parameters of this distribution using observed extreme rainfall allowed IOCI3 scientists to characterise it. Changes in extreme rainfall should be manifested by changes in the parameters of this generalised extreme value distribution.

[26] Rainfall is the main influence on stream flow and catchment yields, but not the only influence. However, other potential causes of change were not investigated here.

BOX 4 MEANS TO EXTREMES: THE GENERALISED EXTREME VAVUE DISTRIBUTION

The generalised extreme value distribution is the basis for modelling and understanding the behaviour of climate *extremes*. By contrast, the more familiar normal distribution is used to describe the variability of *averages* of many climate variables. For example, the left-hand panel below shows a histogram of yearly average January and February temperatures at Perth Airport for a 65-year period ending in 2011. We can see that the histogram is roughly symmetric and bell-shaped. A normal distribution with mean, or location, (μ) and standard deviation, or scale (σ), calculated from these data has been superimposed (blue line).

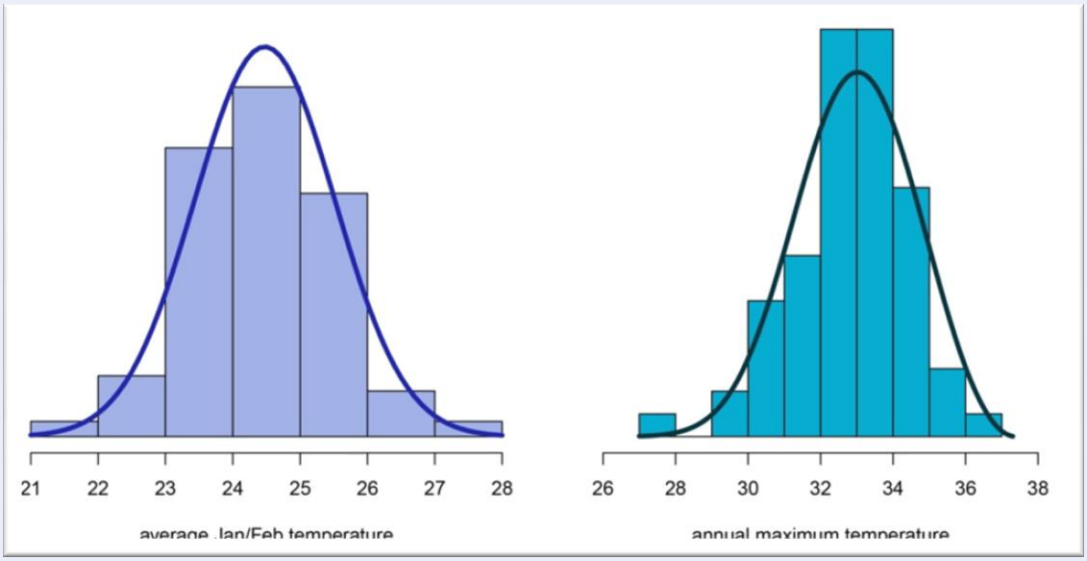

The right-hand panel shows a histogram of annual maximum temperatures over the same 65-year period. Note that the histogram is not symmetric but skewed. Superimposed on this histogram is a generalised extreme value distribution calculated from the data (the dark teal line). The generalised extreme value distribution often provides a good description of annual extreme temperature, rainfall, wind, and other climate variables. Because it is skewed, however, it requires three parameters to describe its appearance: a location (μ) and scale (σ) parameter as in the case of the normal distribution, and an additional one known as the shape parameter (ξ).

Broadly speaking, statistical modelling of extremes involves understanding how the three parameters of the generalised extreme value distribution might be changing over time, space, and under potential climate change. It can often be challenging because there is usually very little relevant data. For example, although we might have daily temperature records over, say, a 65-year period (more than 23,000 data points), we might have only 65 extreme data points if our interest is in modelling annual maximum temperature.

IOCI3 scientists conducted a literature review to identify possible factors that influence seasonal variation in extreme rainfall that could be used to model changes therein. Seven measures describing different aspects of the climate system – the Indian Ocean Dipole; ocean heat content (for the southern, northern and total Indian Ocean); the Southern Oscillation Index (as measured by Niño 3.4); the SAM; and SWAC – were used as covariates in the model. However, none of these relationships improved the statistical significance of the fitted model. Thus it appears that none of these measures of the state of the climate system are useful for seasonal forecasting of extreme rainfall.

IOCI3 scientists also used variable screening methods (Phatak et al. 2011) to try to identify atmospheric variables that might have an impact on extreme rainfall. Dew point temperature depression was selected as a measure of the moisture content of air and then used as a covariate for the fitting of the generalised extreme value for individual stations. The larger the value of DTD the drier the air, as might be expected. Use of DTD at 750 hPa proved to significantly improve the fit for a majority of the stations when it was used as a covariate for the scale parameter, but not for the location parameter. The sign of the corresponding covariate coefficient was negative, indicating that increasing dryness of the air led to decreasing extreme rainfall**.**

One possible reason for the lack of success in identifying large-scale seasonal factors that correlate with extreme rainfall may be explained by the work of Pook et al. (2012), who investigated synoptic

classifications of weather systems. Their synoptic analysis identified the change in synoptic systems associated with an observed downward trend in rainfall in SWWA since the mid-1990s. They showed that fronts are the dominant synoptic systems in the Central Wheatbelt, contributing 50% of rainfall, while cut-off lows contribute approximately 33%. Whereas frontal rain does not show a trend, rain from cut-off low type synoptic systems has declined in the past 30 years. However, the number of frontal and cutoff synoptic systems has not changed much during this period.

Knowledge gaps and future directions

Much work remains to be done on the possible reasons for reductions in extreme rainfall in SWWA. The above work by Pook et al. (2012) has implications for analysis of rainfall extremes. It suggests that the contribution of different synoptic systems to extreme rainfall should be examined, with the aim of analysing the different classifications separately. However, to do so would necessitate the classification of rainfall data according to the different synoptic systems. This classification was not available during the IOCI3 analyses.

4.3.1.2 Weather system shifts associated with extreme rainfall declines

As already observed, the significant winter rainfall decline in SWWA is partly a manifestation of a reduction in high-intensity extreme rainfall events. This decrease could be due to a combination of a natural drying trend and a greenhouse warming-induced drying trend (see Chapter 3).

High-intensity winter rainfall reductions since about 1965 coincided with the start of an upward trend in the SAM (Li et al. 2005). When this mode is at its high phase, the mid-latitude jetstream over the ocean shifts southward, and over land westerly winds decrease. At these mid-latitudes, weaker westerlies are associated with reduced SWWA winter rainfall (Cai et al. 2005). Analysis of both observations and modelling results (Cai and Watterson 2002)[27] indicated that SWWA winter rainfall tends to decrease as a result of decreased cloudiness and decreased westerly winds. Subsequent work by Bates et al. (2010) with the NCEP/NCAR reanalysis dataset showed that higher mean sea level pressure, lower north-south mean sea level pressure gradient (leading to weaker westerly winds) and lower moisture in the lower troposphere (decreased cloudiness) are implicated in the observed decline in May to July rainfall.

The possibility that SWWA winter rainfall reductions are due to multidecadal natural variability of the SAM was investigated in another modelling experiment (Cai et al. 2005).[28] The results suggested this drying trend could result from both natural multidecadal variability, and GHG forcing an induced upward trend in this mode. However, these results must be viewed as preliminary. The precise reason for the changes in the climatic state indicated by the SAM, and thus the drying trend in SWWA, remains uncertain and is still an area of ongoing research (Feng et al. 2010; Cai et al. 2011a).

4.3.1.3 Modelled projections of rainfall extremes

Project Link: 2.4

IOCI3 scientists have developed projections of extreme rainfall. These are high-resolution projections of the intensity-frequency-duration (IFD; Box 6) characteristics of rainfall under one climate change scenario. If climate change affects extremes, then the IFD curves would be expected to change too.

To make projections of extremes for the future, output from a climate model (CCAM) was integrated into a spatial extremes model. Other variables included in this model were location, height above sea level and distance from the coast. The fitted model was then used to derive projections of rainfall extremes for 2030 and 2070 by inserting the extreme value characteristics derived from the CCAM output for 2030 and 2070.

Results: Figure 4.12 shows projected spatial return levels of maximum 24-hour extreme rainfall events with 100-year return period at a 4-km spatial resolution.

---

[27] Using the CSIRO coupled GCM under increasing atmospheric carbon dioxide.

[28] Using the CSIRO Mark 3 GCM.

The IOCI3 study region for IFDs for SWWA is defined by Dalwallinu, Lake Grace and Pemberton, as delineated by the triangle in Figure 4.12c. It is clear that the projected change in these extreme rainfall events is not uniform across the study region. The projections suggest a decrease in the amount of rainfall associated with a 1-in-100 year rainfall event in the far south-west near Pemberton, but a slight increase to the north near Dalwallinu and in the region east of Lake Grace. For example, the 100-year return level of 24-hour rainfall at Pemberton changes from 115 mm under present-day conditions to 99 mm in 2070.

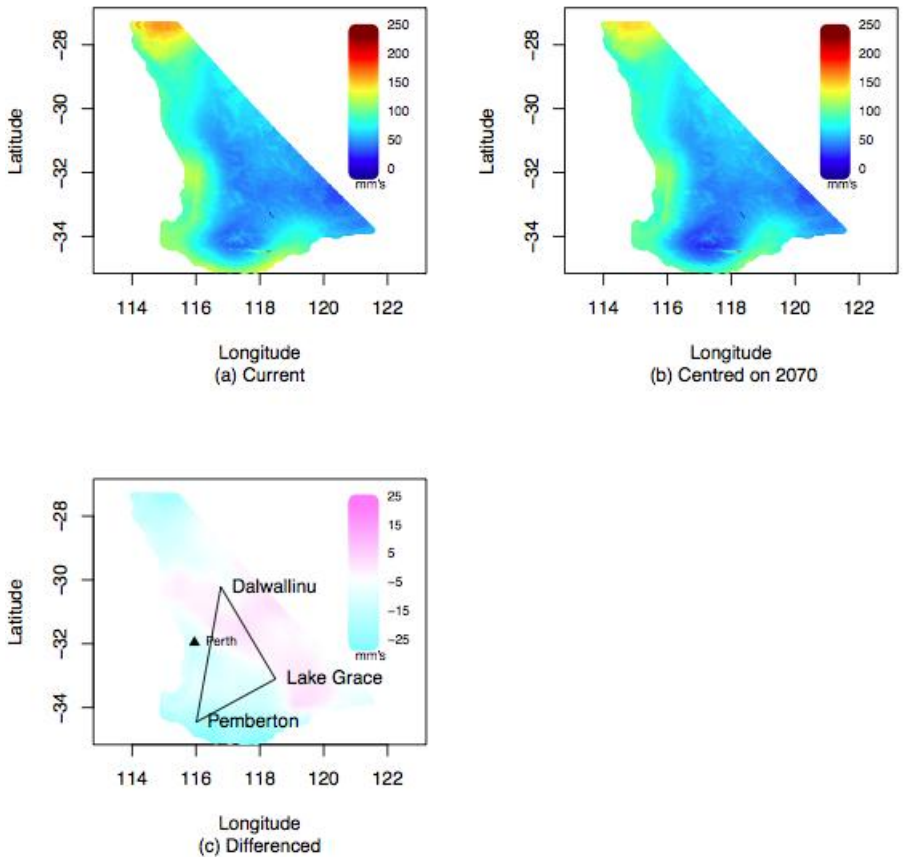

Figure 4.12 Spatial patterns and projected changes in extreme rainfall for SWWA. The 100-year return levels of maximum 24-hour rainfall are shown for the current climate (top left) and 2070 climate (top right). The bottom figure shows the differences between these two periods: pale blue areas indicate regions of decrease in 100-year extreme rainfall return levels, magenta areas represent an increase. The triangular area mapped is the IOCI3 study region for intensity-frequency-duration characteristics in SWWA, defined by Dalwallinu, Lake Grace and Pemberton.

From the statistical model it is possible to derive IFD curves. Figure 4.13 shows two sample IFD curves (for Perth and Pemberton) for current and projected (2070) conditions. The difference between the IFD curves for a 100-year return period is also shown in Figure 4.13.

BOX 5 RETURN PERIODS, RETURN LEVELS AND RECURRENCE INTERVALS EXPLAINED

Return period and return level are terms used to describe the probability (likelihood) of extreme events such as floods, storms or earthquakes. For example, the term '1-in-100 year storm' describes a major event of a magnitude or intensity (the return level) only likely to occur once every 100 years (the return period). The return period provides a statistical estimate of the interval of time (i.e. expected frequency) between the events specified. A return period is also known as a recurrence interval. The average recurrence interval (ARI) for rainfall is a statistical estimate of the average or expected period between occurrences of a particular rainfall amount being equalled or exceeded over a given duration. For example, in a location where the rainfall amount of 50 mm in one hour can be expected to be equalled or exceeded on average once in every 100 years, the average recurrence interval would be 100 years.

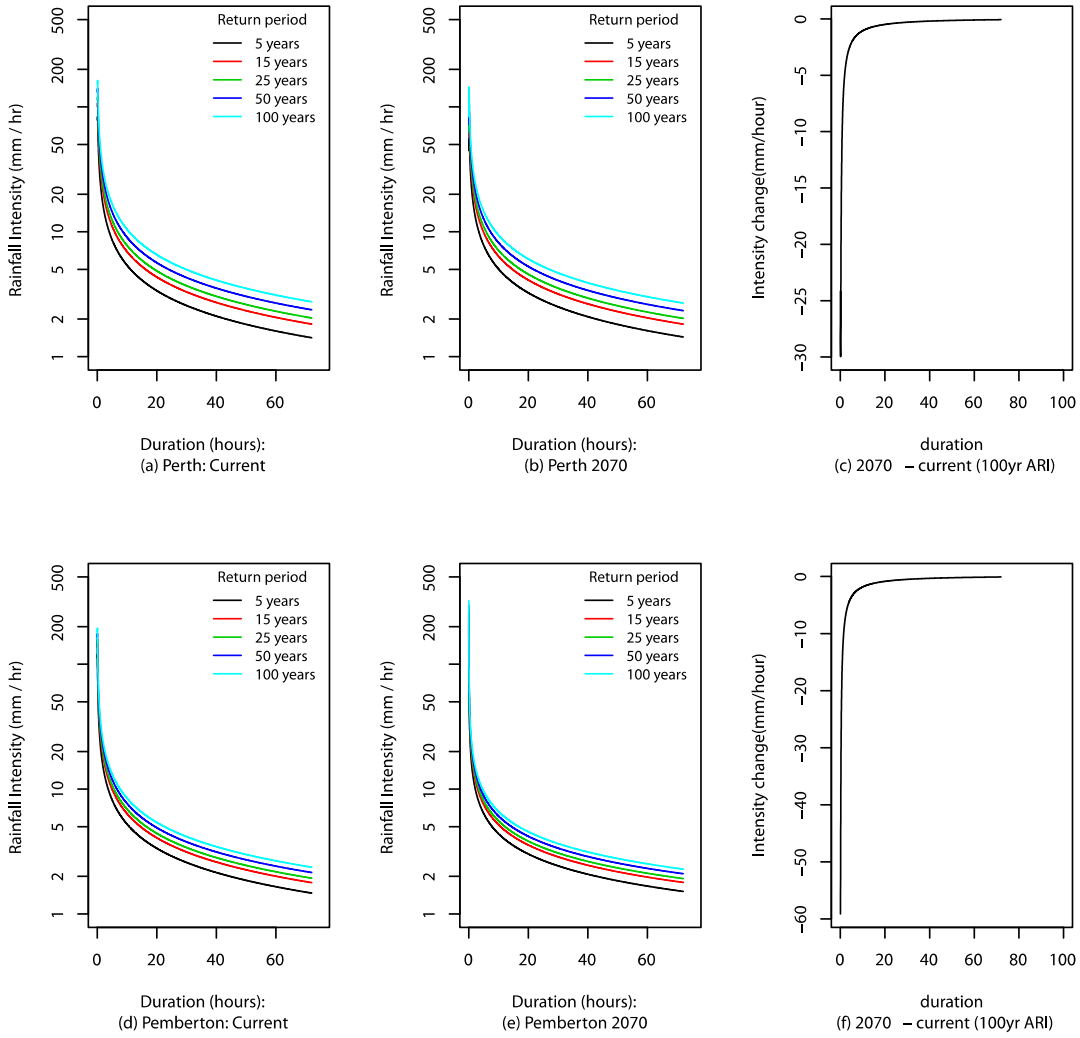

Figure 4.13 Perth and Pemberton intensity-frequency-duration curves for current and projected climates. Calculated for Perth (top) and Pemberton (bottom) for (a) current and (b) 2070 climate in millimetres per hour. (c) shows the difference in 100-year return levels of maximum 24-hour rainfall, a decrease.

The complete results for these projections may be obtained online at: http://data.csiro.au/dap/.

Knowledge gaps and future directions

These extreme rainfall projections should be seen as initial estimates only, and they should not be used for making impact, vulnerability and risk assessments. They were made using only one GCM/RCM combination (CSIRO Mk.3.0/CCAM) under a single (SRES A2) emissions scenario. Additional work using an ensemble of GCM and RCM results is required to provide more robust projections of climate extremes over SWWA.

Because extreme events are by definition rare, their analysis relies on small datasets. Furthermore, we are often interested in estimating the level of rainfall extremes associated with return periods larger than the length of the instrumental record. For example, we may only have 50 years of data but may be interested in how large a 1-in-200 year event might be. Consequently, the uncertainty associated with projections of extremes is large, especially when extrapolating from a small dataset.

Another limitation is that the model linking the outputs from the RCM and the spatial model is still being refined. Improved linkages would permit more accurate measures of variability. Using higher resolution RCMs might also improve projections because these models resolve atmospheric processes on a smaller scale.

BOX 6 INTENSITY-FREQUENCY-DURATION (IFD) CHARACTERISTICS AND CURVES

Intensity-frequency-duration (IFD) characteristics are statistics on rainfall. Rainfall is often thought of as being a certain depth (in millimetres) but it is also important to specify the duration, i.e., the time period over which rainfall is measured. This may be a year or month, but duration may also be measured in days, hours or minutes. One may also wish to know the frequency of a rainfall event, i.e., how often a given rainfall depth (e.g., 20 mm) occurring over a period (e.g., one hour) is exceeded, on average. Intensity is a measure of the rainfall rate (in mm/hour), essentially the heaviness of the rainfall. It is calculated by dividing the depth of the rainfall by its duration. These data are often used for engineering design (e.g., of stormwater systems or bridges and dams).

These characteristics of precipitation frequency may be combined to create IFD curves. Such curves are used to present the probabilistic relationship between average rainfall intensity, duration and frequency. IFD curves for Perth and Pemberton are shown in Figure 4.13.

4.3.2 STATISTICAL MODELLING OF TEMPERATURE EXTREMES: PAST CHANGES AND FUTURE PROJECTIONS FOR THE SOUTH WEST

Project Link: 2.4

Heat waves are meteorological events that have received much attention in recent years because they can be a major cause of weather-related fatalities (Gosling et al. 2009) and may increase in frequency, duration and intensity under global climate change (Meehl and Tebaldi 2004). Although inherently viewed as 'extreme' because they are severe and rare, heat waves are under-investigated compared to more widely studied catastrophic hazards such as TCs, floods and earthquakes.

Defining heat waves and hot spells: **the hot spell model**

There is no universally accepted definition of a heat wave; however, heat wave events are generally regarded as prolonged hot spells (Robinson 2001). A hot spell is often defined as consecutive days with daily maximum temperature exceeding a particular threshold of high temperature (e.g., 40 °C or the 95th percentile of daily maximum temperature in a summer season). Recently, Furrer et al. (2010) extended the point process approach in extreme value analysis to the modelling of hot spells. IOCI3 scientists used this approach and developed methods to identify the appropriate thresholds (Li et al. In prep).

In this report, the threshold was selected in such a way as to satisfy the assumptions made in fitting the statistical model for hot spell occurrence. Thresholds obtained in this manner may not coincide with temperature thresholds important to all stakeholders, but they are nevertheless realistic enough for the results of the hot spell model – especially estimated trends in intensity, frequency, and duration – to be broadly meaningful. The development of this hot spell model is an important first step. Additional work is required to refine this model in order to provide targeted information to suit wide-ranging stakeholder requirements – e.g., to inform health-sector studies on heat-related mortality or engineering design for heat-resistant infrastructure.

IOCI3 scientists used a chi-squared goodness-of-fit test for the Poisson-generalised Pareto model (Coles 2001) for both the hot spell frequency (number of hot spells per summer) and intensity (the maximum temperature of a hot spell). This approach allowed the occurrence of hot spells to be modelled by a Poisson process, and their intensity to be modelled by a generalised Pareto distribution. As for the hot spell duration, this was modelled through a geometric distribution (Furrer et al. 2010). IOCI3 scientists named this the hot spell model approach. Its constituents permit realistic modelling of hot spell characteristics, such as frequency, intensity and duration (Figure 4.14).

IOCI3 scientists used this hot spell model approach to model trends in hot spell intensity, frequency, and duration for SWWA. They considered the hot spell model parameters to be fixed over the summer within a given year, but allowed these parameters to shift from one year to another. Specifically, they used the generalised linear model framework to estimate the parameters in the hot spell model. This permitted them to evaluate the significance of trends in hot spell duration, frequency and intensity by fitting time (year) as a covariate.

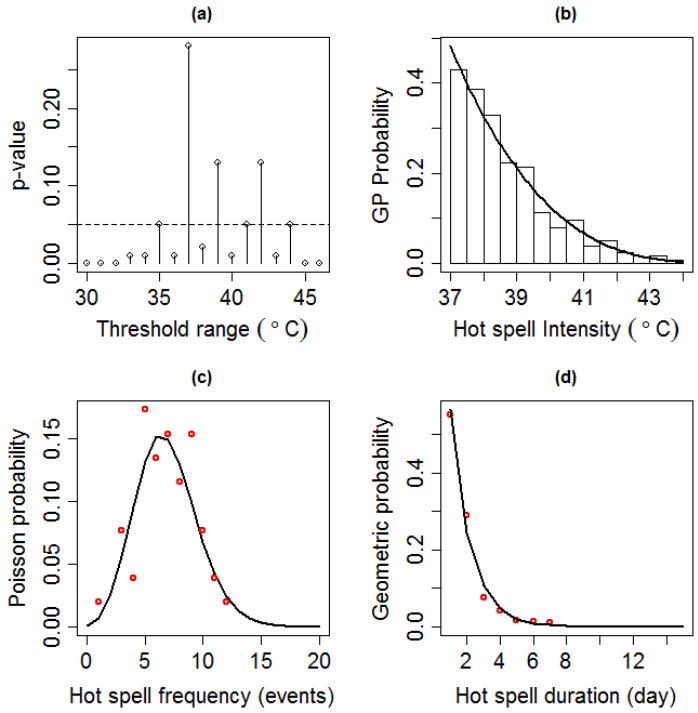

Figure 4.14 Summary of results from hot spell model for Perth Airport. Shown for summer (December, January and February) at Perth Airport for the period 1958 to 2011. (a) p-value of goodness of fit test for Poisson-generalised Pareto model for hot spells; (b) histogram and estimated generalised Pareto probability function (black curve) for hot spell intensity; (c) empirical probability ('o') and estimated Poisson probability function for the hot spell frequency; (d) empirical probability ('o') and estimated Poisson probability function for the hot spell duration. Note that the threshold of 37 °C is selected based on the maximum p-value. Accordingly, a hot spell for Perth Airport was defined as one or more (consecutive) days with maximum temperature over 37 °C.

For example, see Figure 4.15 for modelled trends at Perth Airport, where a hot spell was defined as one or more (consecutive) days with maximum temperatures exceeding 37 °C . The results for Perth Airport showed: (a) no trend in hot spell intensity; (b) a statistically significant increase in hot spell frequency from approximately six events in 1958 to eight events in 2011; and (c), a statistically significant downward trend in hot spell mean duration, from two days in 1958 to 1.5 days in 2011 (Figure 4.15).[29]

Use of Australian Water Availability Project (AWAP) data: A major challenge in the study of hot spells is the dearth of high-quality maximum daily temperature data. These data are available from only 11 stations sparsely distributed across SWWA, eight of which lie within the IOCI3 study region. To overcome this problem and to obtain good spatial-temporal coverage of hot spell characteristics across SWWA, IOCI3 scientists applied the hot spell model to both high-quality station data and the quarter-degree gridded (0.25° by 0.25° resolution) daily maximum temperature data from the Australian Bureau of Meteorology (Jones et al. 2009), generated as part of AWAP.[30] In this study AWAP data plus that from the 11 high-quality stations were taken as 'observed' data, referred to here as 'AWAP-station' data. Note that for this study, the AWAP-station data from the 1958 to 2010 summer season (December to February) is used, because this is the common period for which both AWAP and station maximum temperature data was available. AWAP station data is interpolated, and therefore not the same as observed station data. However, using it allowed IOCI3 scientists to compare the difference between AWAP data and output from CCAM in the

[29] The trends in hot spell frequency and duration are significant at the 5% level.

[30] The AWAP daily maximum temperature dataset uses the AWAP interpolation method on observed raw data; accordingly this dataset is considered an AWAP output. AWAP is run by the Bureau of Rural Sciences, CSIRO and BoM. See: www.eoc.csiro.au/awap/ and www.bom.gov.au/jsp/awap/).

present period (1981 to 2010) in order to justify initial projections of changes in hot spell behaviour using output from CCAM, despite having very little observed station data.

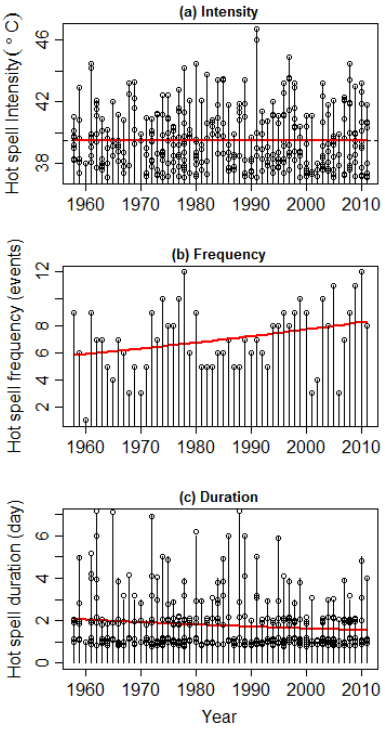

Figure 4.15 Summary of results from hot spell model for Perth Airport trends, 1958 to 2011. Summer hot spell characteristics shown are: (a) observed hot spell intensity ('o' points) and estimated trends (red curve) based on fitted generalised Pareto distribution to the maximum temperature of a hot spell; (b) observed hot spell frequency ('o' points) and estimated trends (red curve) based on the fitted Poisson distribution to the occurrences of hot spell; (c) observed hot spell duration ('o' points) and estimated trend (red curve) based on the fitted geometric distribution. The results indicate a statistically significant upward trend in hot spell frequency, and a statistically significant downward trend in hot spell duration at Perth Airport for the 1958 to 2011 period. There is no trend observed in hot spell intensity at Perth Airport since 1958.

Determining hot spell thresholds: IOCI3 scientists used the AWAP-station daily maximum temperature data to select thresholds for hot spells across south Western Australia for the period 1958 to 2010. Thresholds vary considerably from one location to another. Central and interior regions of SWWA have the highest thresholds, ranging from 40 to 45 °C; south parts of south Western Australia and coastal regions have lower thresholds of approximately 30 °C. The Perth Airport threshold is 37 °C.

Present-day hot spell characteristics and trends in south Western Australia

For this analysis, 'south Western Australia' refers to the area below the black horizontal line in Figure 4.16 (that is, south of 25° S).

Intensity: Spatial patterns of hot spell intensity for the period 1958 to 2010 resemble those of hot spell thresholds. That is, whereas central and inland regions of south Western Australia have high hot spell intensities (40 to 46 °C), south and coastal regions have lower intensity hot spells (30 to 35 °C; Figure 4.16). As to trends, it appears the intensity of hot spells increased over inland south Western Australia, but decreased over the south-west and the north-west of this region during the period 1958 to 2010 (Figure 4.16d). For example, hot spell intensity in the central inland region of south Western Australia increased by 1 °C to approximately 41 °C.

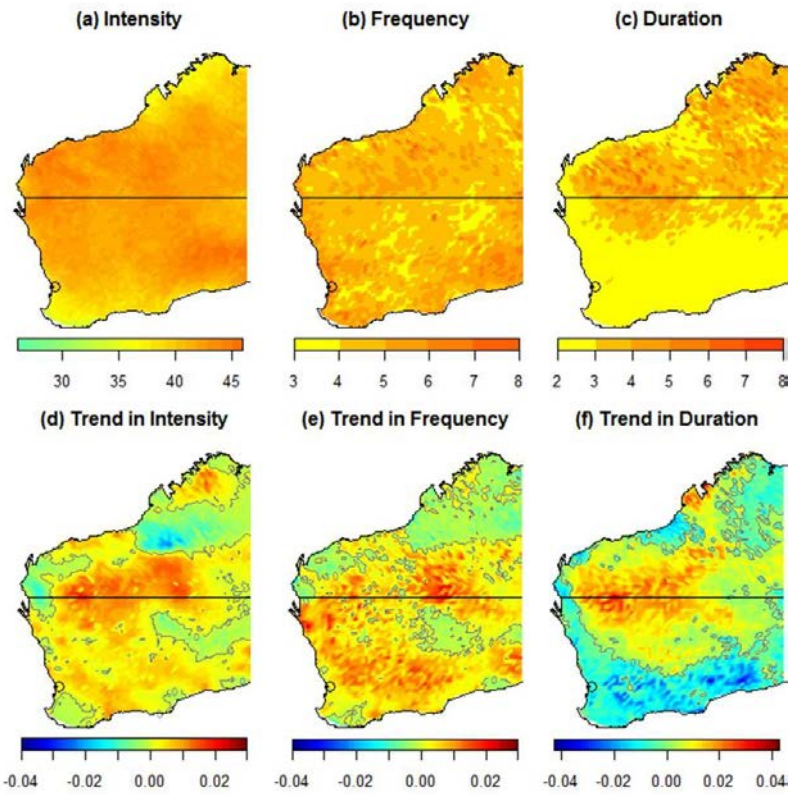

Figure 4.16 Spatial patterns and past changes in hot spell characteristics for Western Australia. (a) to (c): maps of mean hot spell intensity, frequency and duration during the period 1958 to 2010. (d) to (f): maps of trends (changes per year in exponential function of 'year') in hot spell intensity, frequency and duration for this period. All maps are estimated by the hot spell model, and based on data from 11 high-quality stations and Australia Water Availability Project daily maximum temperatures (1958 to 2010). Intensity is given in degrees Celsius, frequency in numbers of events, and duration in days. The black horizontal line at 25°S indicates the boundary between 'south Western Australia' (south of 25°S) and 'north Western Australia' (north of 25°S).

Frequency: The number of hot spell events per summer over south Western Australia ranged from three to eight. The area north of Perth and south-east inland areas have relatively high hot spell frequency (Figure 4.16b). Trends in hot spell frequency varied with location, with increases over much of south Western Australia during the period 1958 to 2010. As noted above, this includes Perth Airport, where hot spell frequency increased by 0.46 events per decade, equivalent to a 2.5-event increase over the 1958 to 2011 period[31] (Figure 4.15b). However, hot spell frequency decreased in north-east and south-west parts of the region over this period (Figure 4.16e).

Duration: This hot spell characteristic exhibited a fairly uniform pattern across south Western Australia, with events averaging two or three days in duration; an exception was a small, north inland part of the region, where duration averaged four to six days (Figure 4.16a). As for trends in hot spell duration, over the period 1958 to 2010 the length of hot spells increased over the north to central parts of south Western Australia, but decreased in the south-west. As noted above, this includes Perth Airport, where hot spells declined in mean duration from 2 days to 1.5 days over the period 1958 to 2011; this long-term trend of decline is statistically significant (at the 5% level). Most hot spells since the mid-1990s have had a shorter duration of one or two days (Figure 4.16f).

In summary, hot spell intensity varies across south Western Australia and has increased over inland areas. The frequency of hot spells ranges from three to eight events per summer, with frequency increasing in the central and north-west parts of the region, including Perth, over the period 1958 to 2010. Hot spell duration is fairly constant across most of south Western Australia, but durations have decreased in the

[31] Here the period 1958 to 2011 is used because this result is based on observed (station) data.

south-west, while increasing over the north to central parts of the region over the 1958 to 2010 study period.

Projections of future SWWA hot spells

Methods: IOCI3 scientists applied the hot spell model to daily maximum temperature data simulated from the CSIRO CCAM for both the present-day and a possible future climate. CCAM was driven by atmospheric fields from within the CSIRO Mk3.0 GCM host under the SRES A2 (high) GHG emissions scenario. It is important to demonstrate that the modelled (CCAM) outputs of daily maximum temperatures adequately simulate present-day hot spell characteristics over SWWA. Thus IOCI3 scientists compared the above-described AWAP-station maximum temperature data with the model data for calculations of hot spell thresholds, intensity, frequency and duration for the period 1981 to 2010.

The spatial pattern of thresholds estimated by the model's simulated data resembled that calculated using the AWAP-station data, despite some minor inconsistencies. This comparison is discussed in detail and illustrated in Appendix E. Since the daily maximum temperature simulations by CCAM were skilful enough to represent observed hot spell characteristics of the present-day (1981 to 2010) climate, IOCI3 scientists deemed these model simulations acceptable for producing projections of future SWWA hot spells.

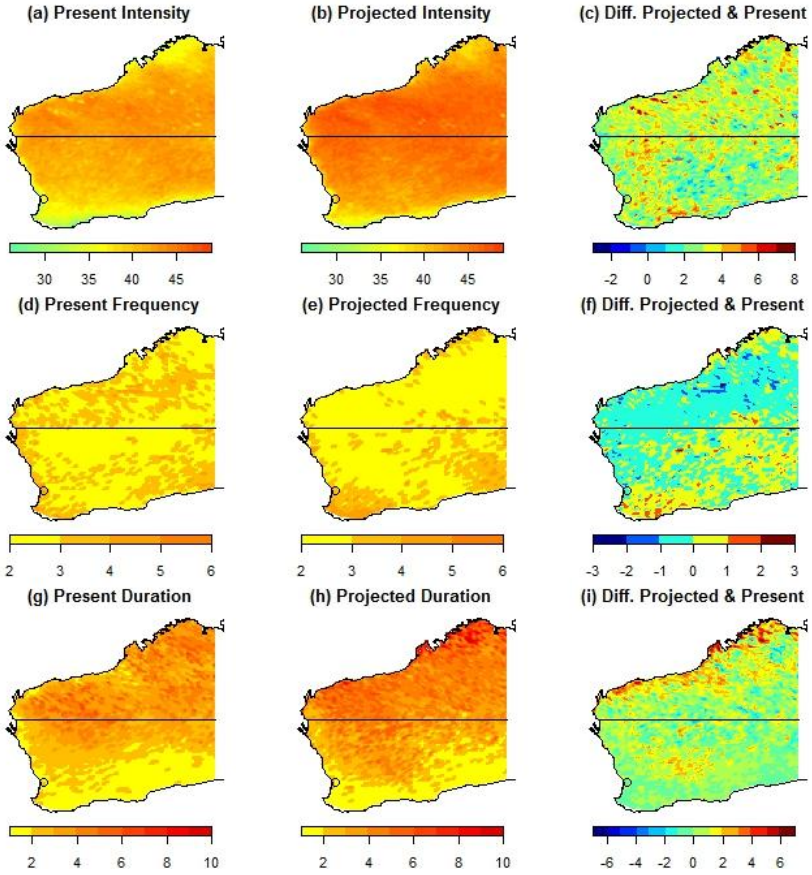

Figure 4.17 Projections of hot spell characteristics for Western Australia. Maps of mean hot spell intensity over SWWA and NWWA for (a) the present period, 1981-2010; (b) hot spell intensity for 2070 to 2099; and (c), their difference, as estimated by the hot spell model using projected maximum temperature under an SRES A2 (high) emissions scenario for the 2070 to 2099 period. Panels (d) to (f), same as (a) to (c) but for hot spell frequency; (g) to (i), same as (a) to (c) but for hot spell duration. Intensity is given in degrees Celsius, frequency in numbers of events, and duration in days. The black line demarcates the north/south Western Australia boundary as described above.

Results: Figure 4.17 compares the intensity, frequency and duration of hot spells estimated by applying the hot spell model to daily maximum temperatures simulated by the CCAM for both present-day (1981 to 2010) and end-of-century (2070 to 2099) conditions according to the SRES A2 (high) emissions scenario.

Intensity: For the present-day (1981 to 2010), the hot spell model estimates low-intensity hot spells over south-west and coastal areas of south Western Australia (about 30 °C), but further north to Perth and

beyond it estimates high-intensity hot spells (40 to 42 °C; Figure 4.17d). For the end of this century, the hot spell model projects an increase in hot spell intensity over all of south Western Australia (Figure 4.17e), with maximum increases over most western inland and northern areas, and less intense increases for coastal and central parts of the region (Figure 4.17f).

Frequency: For hot spell frequency in south Western Australia, CCAM simulated an average of two to four events each summer for the present-day climate (1981 to 2010). For most western inland locations, frequency was estimated at two hot spells per summer, and in central east parts of the region, at four to five hot spells per summer (Figure 4.17j). At the end of the century, hot spell frequency is projected to decrease in the central part of the region, but increase over the south-west (Figure 4.17i).

Duration: The hot spell model estimates hot spells of two to three days duration over most of south Western Australia for the present day (1981 to 2010), except north areas of south Western Australia where longer durations of five to six days were simulated. Projections for the end of the century suggest that the relatively long-lasting hot spells currently observed in the north of the region may also be experienced further south. Major increases in hot spell duration are projected for the central parts of south Western Australia (Figure 4.17l) for the end of the century.

In summary, compared to the present day (1981 to 2010), projections of hot spells for south Western Australia at the end of the century (2070 to 2099) suggest:

- Increases in hot spell intensity over south Western Australia, with a major increase over much of west inland and north parts of the region, and less intense increases in coastal and central areas.
- Decreases in hot spell frequency at the end of the century in north-west part of south Western Australia; but increases over the south-west.
- Marked increases in hot spell duration in the central areas of south Western Australia at the end of the century.

Knowledge gaps and future directions

These projections should be seen as initial estimates only and they should not be used for making impact, vulnerability and risk assessments. As with the rainfall projections described above, hot spell projections in this study were made using one climate model combination under one emissions scenario; further work using several GCMs would provide a better characterisation of the uncertainty of projections of future hot spells over SWWA.

As noted above, extreme events are by definition rare, and their analysis relies on partial (extreme) datasets (e.g., daily maximum temperatures higher than 35 °C). The caveats noted above for small datasets, and for extrapolating beyond relatively small observed records, also apply here to hot spells.

IOCI3 work on hot spells sought to overcome data shortages by using AWAP data. The AWAP methods used to construct the dataset (interpolation) may smooth out some extreme values; this may lead to an underestimation of extremes in some cases. To these uncertainties are added the uncertainties inherent in the use of climate models. As noted above, IOCI3 scientists have evaluated the over- and underestimation of hot spell characteristics, reported in detail in Appendix E.

Although IOCI3 scientists have demonstrated that the hot spell model can successfully model hot spell variations and trends, knowledge gaps remain about the physical processes that cause the observed variability and trends in hot spells. They have begun to explore the linkage between the SWAC (Section 4.1.1.1; Feng et al. 2010) and changes in hot spells over SWWA. The trend of decrease in the SWAC in recent decades may be linked to the decrease in hot spell duration observed in SWWA. A weaker SWAC also leads to strong north-easterly flows, which may contribute to the weak increase in hot spell frequency, while the decreased frequency of hot spells in SWWA is due to weakening south-easterlies.

Another approach would be to look at the meteorological conditions that lead to heat waves. Indices of atmospheric circulation patterns, such as blocking and SWAC, could be used as covariates instead of, or in addition to, a trend component of the hot spell model. Much more challenging would be to develop a hot spell model by including simultaneous treatment of both daily maximum and nightly minimum temperature, i.e., taking into account night-time weather conditions as well.

5 Improved Understanding of North-West Western Australia's Climate

Drafting authors: Steve Charles, Guobin Fu, Janice Wormworth, John McBride, Richard Dare, Sally Lavender, Debbie Abbs, Leon Rotstayn, Yun Li, Tony Rafter, Aloke Phatak, Mark Palmer and Tony Rafter

An important goal of IOCI3 was to further the understanding of NWWA's climate systems. Relatively little is known about the climate of the North West and even basic weather data are much sparser than in the South West. Research undertaken in IOCI3 improved knowledge of the causes of rainfall variability and extreme events in NWWA, along with the tools (e.g., climate models) to explore these. However, much work remains to be done in this area

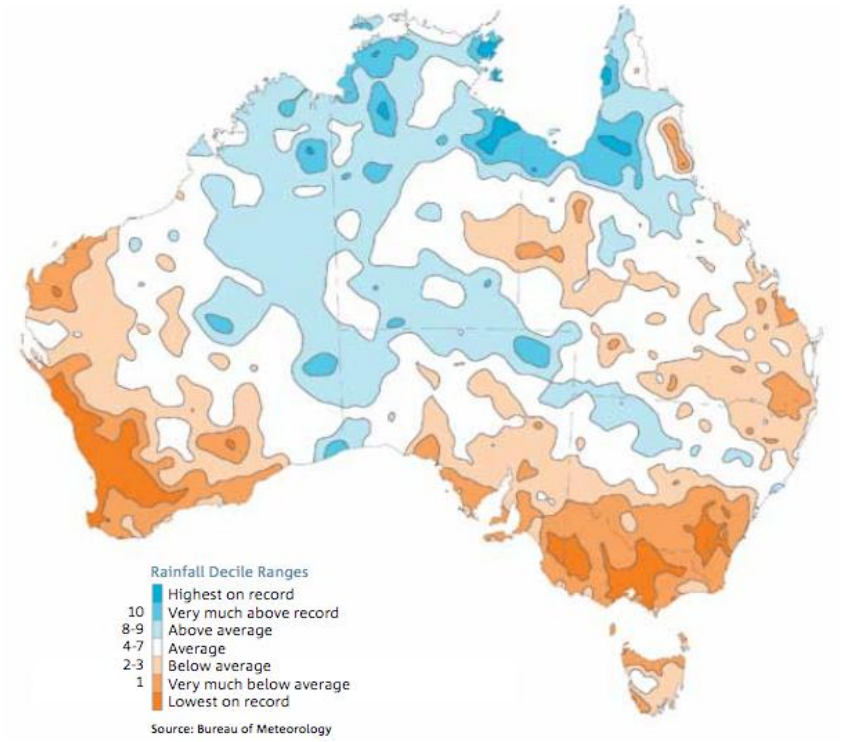

Figure 5.1 Australian rainfall decile ranges, showing an increase in rainfall in NWWA; CSIRO and BoM 2012. AWAP data.

This chapter covers IOCI3 findings on NWWA's observed climate and weather, namely rainfall, temperature and extreme events. It discusses the possible causes of these changes, including the hypothesised effect of aerosols on rainfall trends. This chapter also reports on IOCI3 projections of future changes in NWWA climate and weather, including station-scale projections of annual mean temperature and rainfall, and projections of extreme events. In addition, it presents analyses of regional TC behaviour and trends, and projections of future changes to the characteristics of TCs that affect Western Australia.

5.1 North-West Western Australia Rainfall

As noted in Chapter 1, NWWA has undergone a marked increase in total annual rainfall since 1950 (Figure 5.1; BoM and CSIRO 2007; CSIRO and BoM 2012). This section examines changes to weather patterns

associated with NWWA rainfall, and provides results of station-scale projections of NWWA rainfall under future climate conditions.

5.1.1 OBSERVED CHANGES IN NWWA WEATHER PATTERNS

Project Link: 2.3

Rainfall in the Kimberley is highly seasonal, with a large proportion of the annual total falling during the December to March period. IOCI3 scientists examined the weather associated with wet and dry conditions for nine stations over the summer half-year (November to April). They found that of the four dominant rainfall patterns (as defined by the NHMM; Section 2.2) the two wettest weather patterns associated with very wet and moderately wet conditions throughout the Kimberley have become more common over the past 50 years. Conversely, the two patterns associated with mostly dry and very dry conditions have decreased in occurrence over this period. Overall, the two wet patterns increased in frequency from about 30% to 40% of days between the 1960s and 2000s. The rate of increase in the wettest pattern (and corresponding rate of decrease in the driest pattern) was greatest from 1960 to 1980, tapering off after 1980. These shifts in weather pattern occurrence concur with the wider body of research regarding rainfall trends in this region.

The Pilbara region's dry season is also extensive, but less distinct than that of the Kimberley. Since 1980 the frequency of the NHMM weather pattern associated with dry conditions across ten Pilbara stations in the summer half-year has decreased, as has a pattern associated with rainfall in the southern Pilbara. The two wetter weather states have increased in frequency. One of these, a pattern associated with rainfall in the north-east Pilbara, has steadily become more frequent since the 1960s. The other, associated with wet conditions across all ten stations, has increased slightly in frequency since 1960.

These changes could indicate longer tropical wet seasons for both the Kimberley and eastern Pilbara. The ability to simulate the weather patterns associated with trends in rainfall in the Kimberley and Pilbara regions is incorporated in the NHMM downscaling models that produce more realistic, station-scale model rainfall projections for these regions (see below).

5.1.2 STATION-SCALE RAINFALL PROJECTIONS FOR NWWA

Project Link: 2.3

The method used to produce downscaled rainfall projections for SWWA (Chapter 4) was also applied to NWWA's Kimberley and Pilbara regions. The NHMM model was calibrated to networks of nine Kimberley stations and ten Pilbara stations. These stations were chosen for the completeness of their daily rainfall records (i.e., selected stations had less than 5% of days missing for each decade from the 1960s to present) and based on testing for untagged accumulations (Viney and Bates 2004). Because this was the first time the NHMM had been applied to tropical and subtropical regions, it was important to assess the validity of the weather states and predictor variables selected to calibrate the model. This calibration process is described in full in Appendix C.

Whereas the calibration showed that the NHMM simulations do reproduce much of the observed interannual variability and long-term trends in rainfall, it also indicated how extreme wet years can be underestimated. This is predominantly a result of the inability to generate extreme daily rainfalls that are sufficiently intense. This is related to the aforementioned limitation of the current version of the NHMM, given (i) the atmospheric predictors are only used to define the transitions between weather states and not the intensity of rainfall within the states and (ii) the inability of reanalysis (and GCM) predictors to represent the atmospheric conditions that produce these localised (small spatial extent and short life) events.

IOCI3 scientists produced downscaled projections using the same GCMs, SRES scenarios and periods already described.[32] This generated 100 stochastic time series, for which only summaries of key statistics are provided here. The full results are available online at: http://data.csiro.au/dap/. Note there is uncertainty in the future aerosol trends used by these GCMs. Given the hypothesised influence of aerosol trends on observed rainfall trends (increases) in NWWA (see Section 5.1.4), there is a caveat on how well the projected trends relate to observed trends.

Table 5.1 presents the projected changes in mean annual rainfall for the two regions. The majority of projections indicate a future decrease in rainfall (i.e., proportions of less than 1.0). Averaged across all simulation years and stations, with the range depending on the downscaled GCM, by mid-century mean annual Kimberley rainfall is projected to decrease by 1 to 26% under the B1 (low) scenario; 2 to 24% under the A1B (intermediate) scenario; and range from a 5% increase to a 26% decrease under the A2 (high) scenario. Corresponding end-of-century projections for mean annual Kimberley rainfall are decreases (relative to the present day) of 3 to 29% (B1 scenario); 6 to 29% (A1B); and 3 to 33% (A2).

For the Pilbara, again with the GCM-dependent range averaged across simulation years and stations, the corresponding projections for mid-century mean annual rainfall changes relative to present day are: a 1 to 15% decrease (B1 scenario); 1 to 24% decrease (A1B); and a 5% increase to a 14% decrease (A2). Corresponding end-of-century projections for mean annual Pilbara rainfall changes are: a 0 to 21% decrease (B1 scenario); 9 to 24% decrease (A1B); and 9 to 28% decrease (A2).

The CSIRO Mk3.5 GCM produced significantly drier projections than the other GCMs, with most of this projected change having occurred by mid-century. There is a fairly consistent signal of increased drying from mid- to late century, but this depends to some extent on both the GCM and SRES scenario used. In most cases projections from both the A1B and A2 scenarios are drier than those from the B1 scenario for the end of the century.

For several GCMs, the A1B (intermediate) GHG emissions scenario results indicate a drier climate than those for the A2 (high) scenario. This indicates the significant role that model differences play, emphasising that changes projected by GCMs are not solely dominated by responses to enhanced GHG forcing, but also reflect the difference in the way each model represents both physical and dynamic properties of the climate system.

The results of the downscaled rainfall projections are also provided for the individual Kimberley and Pilbara stations in Appendix D, both as a proportion of present-day rainfall and as absolute values. For indicative purposes, subsets of these Kimberley and Pilbara results are provided here (Tables 5.2 to 5.5). As noted in Chapter 4, these mean annual rainfall results reflect long-term averages across the time periods simulated; hence they 'average out' the year-to-year variability. (Figures D-1 and 2 in Appendix D provide the probability distributions of projected annual rainfall, showing expected changes to interannual variability).

What causes most of these modelling results to project a drier future for the Kimberley and Pilbara regions? As noted in Section 4.1.2.2, these projected rainfall changes result from changes in the sequences of weather states simulated by the NHMM due to changes in the atmospheric predictors projected by the GCMs. (See Appendix C for illustrations of Kimberley and Pilbara weather states as mean precipitation probability maps and corresponding composite atmospheric predictor plots.)

For the summer half-year in the Kimberley, the NHMM defines four summer weather states that graduate from the wettest (state 1) to the driest (state 4). There are moderate to strong relationships between the projected changes in frequencies of summer states 1, 2 and 4 and changes in wind speed and moisture in the lower atmosphere (i.e., both at the 850 hPa level; Table 5.6). For summer state 1, which is characterised by wet conditions everywhere in the Kimberley, decreases or no change are projected for mid-century (from a mean present-day frequency of 9%). However, by the end of the century almost all

[32] Five CMIP3 GCMs; the SRES B1, A1B and A2 GHG emissions scenarios; and the 1962 to 1999 (present day), 2047 to 2064 (mid-century) and 2082 to 2099 (end-of-century) time periods.

projections indicate summer state 1 will decrease in frequency. Projections for the driest weather pattern (summer state 4) suggest increases or no change in frequency by mid-century (from a mean present-day frequency of 31%). However, all projections indicate this dry state will occur about 3% more often by the end of the century. Most GCM projections indicate a decrease in moisture content in the lower atmosphere, and some indicate an increase in wind speed in the lower atmosphere, corresponding with these changes to weather state frequencies.

Table 5.1 Downscaled projections of mean annual rainfall for the Kimberley and Pilbara regions as a proportion of 1962 to 1999 climatology. Averaged across nine Kimberly stations and ten Pilbara stations for five global climate models, three SRES scenarios and two future time periods: mid-century (2047 to 2064) and end of century (2082 to 2099).

GCM	B1_MID	A1B_MID	A2_MID	B1_END	A1B_END	A2_END
			Kimberley			
gfdl2.0	0.91	0.88	1.05	0.96	0.87	0.97
gfdl2.1	0.96	0.90	0.99	0.96	0.84	0.89
miroc	0.95	0.96	1.03	0.97	0.94	0.79
mk35	0.74	0.76	0.74	0.71	0.71	0.67
mpi	0.99	0.98	0.97	0.94	0.85	0.92
			Pilbara			
gfdl2.0	0.91	0.83	0.96	1.00	0.88	0.90
gfdl2.1	0.96	0.89	1.05	0.90	0.81	0.87
miroc	0.95	0.93	0.95	0.97	0.91	0.84
mk35	0.85	0.76	0.86	0.79	0.76	0.72
mpi	0.99	0.99	0.96	0.90	0.87	0.91

Table 5.2 Projected changes in annual mean rainfall for selected Kimberley stations as a proportion of present-day values (1962 to 1999). Values are given for mid-century (2047 to 2064) and end-of-century (2082 to 2099) periods under three climate scenarios. The range of results in each cell reflects the range of downscaled projections produced by the five global climate models, illustrating some of the uncertainty in the results. These results for all ten selected stations are available in Appendix D.

STATION	PRESENT DAY	MID-CENTURY B1 (LOW)	MID-CENTURY A1B (MID-RANGE)	MID-CENTURY A2 (HIGH)	END OF CENTURY B1 (LOW)	END OF CENTURY A1B (MID-RANGE)	END OF CENTURY A2 (HIGH)
Kalumburu Mission	1	0.80–0.99	0.83–0.99	0.81–1.03	0.79–0.99	0.79–0.97	0.78–0.99
Margaret River Station	1	0.71–0.99	0.74–0.99	0.71–1.06	0.69–0.98	0.69–0.93	0.64–0.97
Broome Airport	1	0.72–0.98	0.73–0.97	0.69–1.06	0.68–0.95	0.68–0.93	0.61–0.96

Table 5.3 Present-day and projected annual mean rainfall for selected Kimberley stations. Values are given in millimetres for mid-century (2047 to 2064) and end-of-century (2082 to 2099) periods under three climate scenarios. The range of results in each cell reflects the range of downscaled projections produced by the five global climate models, illustrating some of the uncertainty in the results. These results for all nine selected stations are available in Appendix D.

STATION	PRESENT DAY	MID-CENTURY B1 (LOW)	MID-CENTURY A1B (MID-RANGE)	MID-CENTURY A2 (HIGH)	END OF CENTURY B1 (LOW)	END OF CENTURY A1B (MID-RANGE)	END OF CENTURY A2 (HIGH)
Kalumburu Mission	1260–1280	1030–1250	1070–1260	1030–1320	1010–1260	1010–1240	990–1260
Margaret River Station	530–550	390–530	400–520	380–560	380–530	370–500	340–520
Broome Airport	640–660	480–630	480–630	460–680	450–630	450–600	410–620

Table 5.4 Projected changes in annual mean rainfall for selected Pilbara stations as a proportion of present-day values (1962 to 1999). As per the description in Table 5.2 above.

STATION	PRESENT DAY	MID-CENTURY B1 (LOW)	MID-CENTURY A1B (MID-RANGE)	MID-CENTURY A2 (HIGH)	END OF CENTURY B1 (LOW)	END OF CENTURY A1B (MID-RANGE)	END OF CENTURY A2 (HIGH)
Port Hedland Airport	1	0.82–1.00	0.72–0.98	0.84–1.05	0.75–0.99	0.72–0.88	0.67–0.89
Learmonth Airport	1	0.87–1.00	0.78–1.00	0.88–1.06	0.81–1.00	0.78–0.94	0.73–0.93
Mount Vernon	1	0.85–0.99	0.79–0.98	0.84–1.02	0.80–1.01	0.78–0.92	0.75–0.95

Table 5.5 Present-day and projected annual mean rainfall for selected Pilbara stations. In millimetres, as per the description in Table 5.3 above.

STATION	PRESENT DAY	MID-CENTURY B1 (LOW)	MID-CENTURY A1B (MID-RANGE)	MID-CENTURY A2 (HIGH)	END OF CENTURY B1 (LOW)	END OF CENTURY A1B (MID-RANGE)	END OF CENTURY A2 (HIGH)
Port Hedland Airport	300–360	250–340	220–340	260–380	230–340	220–300	210–310
Learmonth Airport	240–280	210–280	190–270	220–290	200–270	190–240	180–250
Mount Vernon	300–320	250–310	230–310	250–330	240–320	230–290	220–300

For the Kimberley winter, nearly all NHMM projections indicate a small increase (of approximately 1%) in the frequency of the 'dry everywhere' weather pattern, winter state 1, from its present-day frequency of 86%. They also project a corresponding decrease in winter state 2, characterised by minor inland rainfall, from its present-day frequency of 10%. These changes correlate with projected increases in mean sea level pressure (Table 5.6).

For the Pilbara summer half-year, most models project a slight decrease in occurrence of summer state 1 for the middle and the end of the century (relative to its present-day frequency of 11%). This weather pattern is characterised by slightly wet conditions for all stations. The GCMs project a corresponding drying

of the middle atmosphere (i.e., mean increases DTD at the 700 hPa level). Conversely, for the mid- and end-of-century period, most projections indicate an increase (of 4%) in the frequency of summer state 3, the 'dry everywhere' weather pattern that predominates on 73% of days in the present day. Correspondingly, models project a decrease in the mean east-west sea level pressure gradient and in the wind speed of the lower atmosphere (i.e., at the 850 hPa level) for both periods, with larger decreases projected for the end of century.

For the Pilbara winter half-year, projected changes in weather state frequencies are correlated with changes to the east-west mean sea-level pressure gradient for all weather states (Table 5.6). About half of projections indicate that winter state 3, the predominant 'dry everywhere' weather pattern, will decrease (by 1% from its present-day frequency of 67%) by mid-century, with little further change by end of century.

Table 5.6 The strength of the relationship (R^2) between projected changes in weather state frequencies and atmospheric predictors for the Kimberley and Pilbara. See Table 4.5 for a definition of R^2.

STATIONS		KIMBERLEY			PILBARA		
		N-S MSLP	V850	DTD850	E-W MSLP	U850	DTD700
Summer state	1	0.00	0.71	0.74	0.37	0.43	0.78
	2	0.03	0.62	0.89	0.80	0.75	0.42
	3	0.00	0.11	0.26	0.73	0.72	0.59
	4	0.02	0.74	0.86	0.63	0.55	0.10
		MSLP	E-W MSLP	DTD700	E-W MSLP	U700	DTD700
Winter state	1	0.97	0.06	0.09	0.80	0.01	0.43
	2	0.86	0.00	0.01	0.91	0.00	0.33
	3	0.28	0.77	0.44	0.92	0.00	0.30
	4	0.38	0.57	0.50	0.96	0.00	0.18

More detailed information on these changes to Kimberley and Pilbara weather states and atmospheric predictors is reported in Appendix D, Tables D-5 though D-8 (Kimberley) and Tables D-9 through D-12 (Pilbara). Further information is also provided in the Project 2.3 Final Milestone Report.

Knowledge gaps and future directions

The same caveats regarding uncertainty in rainfall projections noted in Chapter 4 for downscaled projections for SWWA also apply here. Furthermore, as noted there is an additional source of uncertainty for NWWA given that observed rainfall records indicate a current increasing rainfall trend in the Kimberley and east Pilbara, whereas the majority of downscaled projections indicate future decreases (Table 5.1). Possible reasons for this inconsistency, including the influence of aerosols generated from human activity, are discussed in detail in Section 5.1.4. However, statistical downscaling should account for historical aerosol effects, as these effects influence the predictors used.

Also as noted above, whereas NHMM simulations reproduce interannual variability and long-term trends reasonably well, they are not well suited to the task of modelling daily rainfall extremes. Thus extremes-based methods (Section 5.3.1) will produce more robust projections for the modelling of daily rainfall extremes in NWWA. These caveats should be considered when these NHMM simulations are used for any climate impacts assessment for the NWWA region.

5.1.3 TROPICAL CYCLONES' MAJOR CONTRIBUTION TO WET SEASON RAINFALL

Project link: 2.2

Landfalling tropical cyclones (TCs) can bring torrential rainfall and cause flooding. However, TC rainfall may also contribute significantly to fresh water supplies for settlements, agriculture and ecosystem health. This illustrates the importance of understanding the contribution of TCs to mean seasonal rainfall, how it varies over months and years, and from one location to another (Dare et al. 2012). Past research has shown that TCs contribute as much as 40 to 55% of seasonal rainfall near the coast of Western Australia (Jiang and Zipser 2010). In Broome this figure was found to be 26% (using data for the 1974/5 through 1978/9 TC seasons; McBride 1983).

IOIC3 scientists studied rainfall associated with TCs using a high-quality 0.05° by 0.05° gridded rainfall dataset (Jones et al. 2009) covering the Australian continent, and a reanalysed TC track dataset provided by the BoM National Climate Centre. Of the 216 TCs observed in the Western Australia region (longitudes 105° E to 129° E) over the 41 TC seasons studied (the period from 1969/1970 to 2009/2010), 167 storms crossed or grazed the coastline. Rainfall observed over the continent within 500 km of the centre of each of these 167 TCs was deemed to be 'TC rainfall'.[33]

They found that TC rainfall makes up a substantial proportion of mean rainfall over the November-April TC season in the areas affected by these storms (Figure 5.2). For areas west of 125° E (the west-central Pilbara, Gascoyne and Mid-West regions of Western Australia), TCs supplied 20 to 40% of rainfall within 150 km of the coast, and approximately 20% further inland.

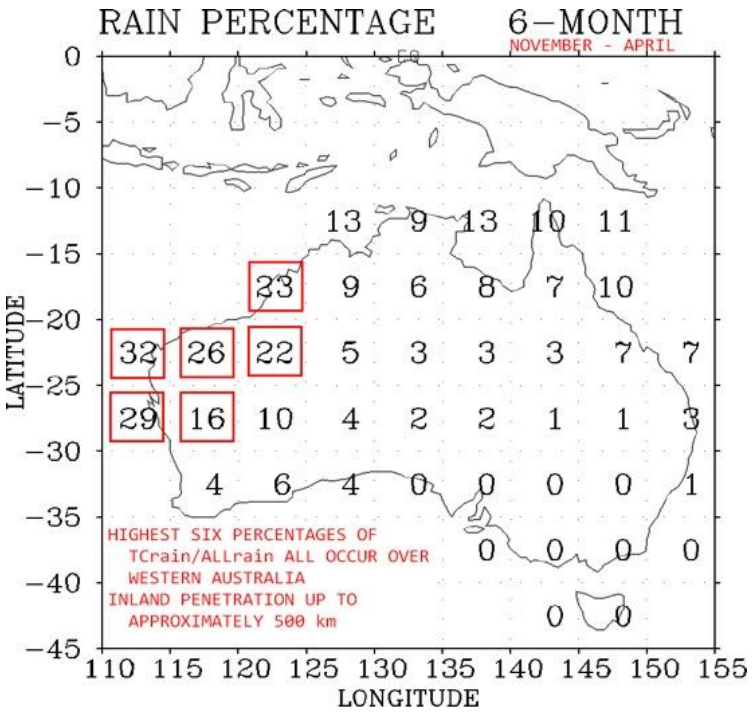

Figure 5.2 The percentage of the 'all rain' amount that is due to tropical cyclones, for each 5° by 5° box over the six-month November to April period.

[33] The methods used were considered likely to result in a conservative estimate of TC-associated rainfall rather than an overestimate. See Dare et al. (2012) for a description of the methods.

Looking at the TC contribution to total rainfall specifically during the peak TC season (January to March; when the largest numbers of TCs either cross or graze the coast), this reaches 40% in coastal regions west of 120° E. During December, prior to the wet season, this proportion is much higher, approximately 60 to 70% of rainfall totals for the region west of 115° E, i.e., the coastal regions of the Pilbara and Gascoyne.

Looking specifically at the coast, the percentage contributions by TCs are greatest west of 125° E, with mean coastal values of 20 to 40% (versus inland values of approximately 20% for this region). The 120 to 125° E longitude band experiences the highest coastal (0 to 50 km) TC-influenced rainfall rate (the mean amount of rainfall in mm per month, November to April).

TC rainfall generally decreases with distance inland from the coast; however, the western region of the continent experiences the greatest inland penetration of TC track in Australia: up to 500 km inland. Associated with this greater inland penetration of TC tracks is the greater inland penetration of TC rainfall in the western region. In particular, in the Pilbara, the percentage of rainfall due to TCs is approximately 20% of the relatively low total rainfall.

Although TCs make a valuable contribution to rainfall in the western region of Australia, this varies greatly from one TC season to the next. This is unsurprising considering the small number of TCs affecting a given coastal area each season. Some sections along the Western Australian coast may receive no TC rainfall during some seasons. In the Gascoyne, the TC rainfall contribution is highly inconsistent, varying interannually from 0-86%. In this region 17 of the 41 TC seasons analysed received mean monthly rainfall amounts of less than 1 mm.

This interannual variation strongly affects the reliability of this rainfall as a source for water supplies in NWWA. For example, at the Harding Dam (a drinking water supply for 20,000 people), capacity fell to 20% in 2010 before being recharged by TC rainfall (Western Australia Water Corporation 2011).

5.1.3.1 Tropical cyclone contributions to changes in NWWA rainfall

Project Link: 2.4

As noted above, northern Australia receives the majority of its annual rainfall during the summer monsoon season, which coincides with the TC season. The rainfall increases observed in this region over recent decades raise the question: are these changes associated with observed changes in TC frequency or intensity? This question is of particular relevance given the expected decrease in TC numbers under future climates (Section 5.3.3.2; Abbs 2012; Lavender and Walsh 2011).

To investigate the contribution of TCs to Australian region rainfall and to quantify trends in these systems, IOCI3 scientists analysed two datasets. The first, rainfall data for 1970 to 2009, was obtained from the AWAP database (Raupach et al. 2009). These data were interpolated onto a 1° by 1° grid. Extreme precipitation events were taken as the events above the 99th percentile (of daily accumulation), as calculated for each one-degree grid-box. The second dataset, a TC best-track dataset, was obtained from the National Oceanic and Atmospheric Administration's International Best Track Archive for Climate Stewardship (IBTrACS) dataset (Knapp et al. 2009) for the period 1970 to 2009. These data were interpolated to a 1° by 1° grid and the region of influence of each TC was calculated using an effective radius of 5° longitude/latitude. Here IOCI3 scientists analysed the number of TC-days[34] per grid-box, rather than actual numbers of TCs. The precipitation efficiency of TCs was calculated based on the amount of rainfall per TC-day per grid-box.

As described above, tropical cyclones influence Australia's north and north-west, with the largest annual totals in TC rainfall over north-west Australia. Figure 5.3 shows that TC-days account for 20 to 30% of the annual rainfall to parts of the north-west Australian coastline around Port Hedland. The contribution of TCs to rainfall calculated in this analysis is lower than in analyses that consider individual stations (e.g., Ng 2010) due to the coarser resolution of the dataset used here. However, the results reported here are

[34] 'TC-days' refers to days on which tropical cyclones occurred within a 5° by 5° grid box.

consistent with those above (Section 5.1.3). North of Broome, the majority of annual rainfall is provided by the monsoon and the contribution assigned to TCs decreases to around 10%. However, when IOCI3 scientists restricted this analysis to TC contributions to extreme rainfall alone – i.e., to those events above the 99th percentile in terms of daily accumulation – they found that TCs are the source of more than 35% of extreme rainfall over north-west Australia (Figure 5.3b).

Section 5.3.3.1 reports that thus far no significant trends can be detected in the frequency of TCs (Kuleshov et al. 2010a). However, over much of north-west Australia, between Broome and Carnarvon, the percent contribution of TCs to annual rainfall has decreased (not significantly). Further north, close to Darwin, a much smaller percentage of rainfall is attributable to TCs. However, over the 40 years of the analysis (1970 to 2009) there has been a statistically significant increase in TC-related rainfall in this area (Figure 5.3c). When narrowing this analysis to the percentage of extreme precipitation (again, greater than 99th percentile) influenced by TCs (Figure 5.3d), these results are even more pronounced. However, when averaged over the continent's entire north-west, no overall change in the percentage of TC rainfall is evident. This would suggest that the positive rainfall trend over this region results from synoptic systems other than TCs.

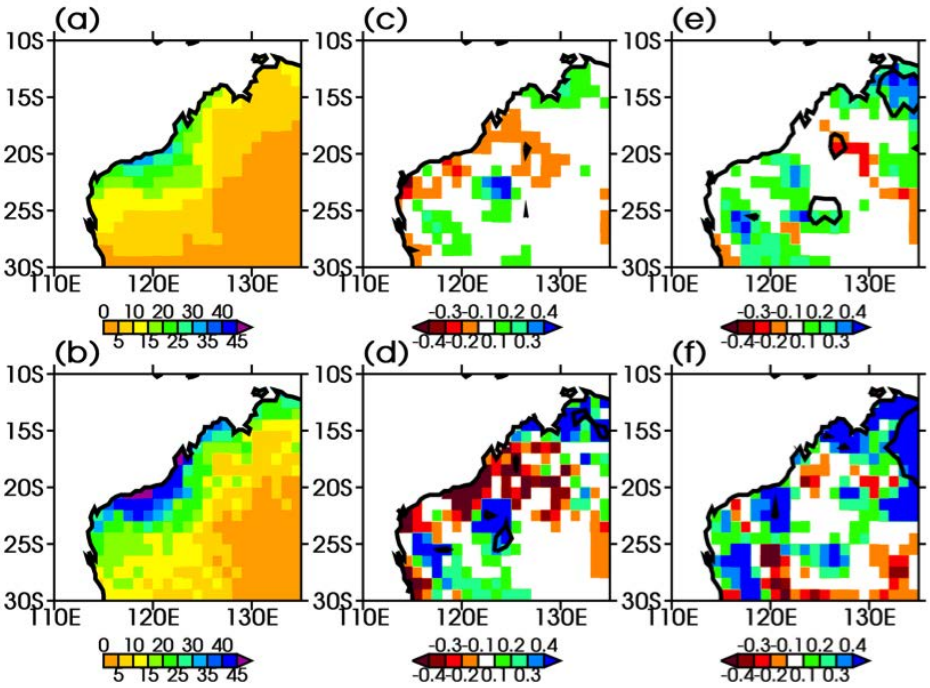

Figure 5.3 Climatologies of rainfall and rainfall change, including tropical cyclones for north-west Australia. Shown are climatologies (for the period 1970 to 2009) of the percentage of (a) annual precipitation; and (b) extreme precipitation influenced by tropical cyclones. Tropical cyclones provide 20 to 30% of the annual rainfall to the area around Port Hedland, and provide about 35% of the total *extreme* rainfall to a still greater portion of north-western Australia. Also shown are trends in the percentage of: (c) annual precipitation; and (d) extreme precipitation influenced by tropical cyclones over the period 1970 to 2009. Figures (e) and (f) show the trend in the amount of precipitation (in millimetres) per tropical cyclone day per year over the period (e) 1970 to 2009 and (f) 1989 to 2009. Black lines in (c) to (f) highlight values significant at the 90% level.

Projections of tropical cyclones in the region point to a future increase in the intensity of the strongest storms (Section 5.3.3.2). But has the amount of precipitation associated with each TC (i.e., the precipitation efficiency) already increased? IOCI3 scientists analysed trends in the precipitation efficiency of Australian

region TCs and closed lows[35] over the past 21 (1989 to 2009) and 40 years (1970 to 2009) to look for any changes in associated rainfall amounts. They found an acceleration in the rate of increase in rainfall associated with TCs. When they considered the full 40-year period (Figure 5.3e) they found that small, statistically significant increases in precipitation associated with these events are evident to the north and west of the continent. However, when they restricted this analysis to the more recent 21-year period (Figure 5.3f), much larger trends were evident. These results are consistent with the projected increase in TC rainfall described in Section 5.3.3.2. Section 5.3.1.1 also discusses these weather systems' contribution to NWWA rainfall within the context of extreme rainfall events.

5.1.4 AEROSOLS' POSSIBLE ROLE IN NORTH-WEST AUSTRALIA'S RAINFALL INCREASE

Project Link: 2.1

As noted above, rainfall has increased significantly over north-west Australia in recent decades (Figure 5.4).[36] The majority of climate models simulate decreasing rainfall in this region when forced by increasing concentrations of long-lived GHGs (Watterson 2012); this raises questions about alternative causes of this trend of rainfall increase. An exploratory study with a low-resolution version of the CSIRO climate model (CSIRO Mk3A) suggested that this rainfall increase might be caused by the large Asian aerosol haze, which consists mainly of fine particles generated by human activity (Rotstayn et al. 2007; see this reference and Shi et al. (2008) for the model's limitations). Aerosols tend to exert a cooling effect on climate, effectively 'masking' the effects of increasing GHG concentrations. Human activities that generate aerosols include industry, motor vehicle use and vegetation burning.

IOCI3 scientists further evaluated this possibility using an improved climate model (CSIRO Mk3.6; Rotstayn et al. 2012); compared to Mk3A, Mk3.6 has much finer resolution and provides a better simulation of processes that are important for Australian climate. They also considered other possible causes of increased rainfall in north-west Australia, such as changes in the atmospheric concentrations of GHGs and ozone, or natural climate variability.

Few other studies have systematically attempted to attribute the cause of the north-west Australian rainfall increase; see Rotstayn et al. (2012) for an overview. Cai et al. (2011b) analysed model output[37] and grouped models according to whether they included aerosol effects, but were unable to detect a clear aerosol influence. This may reflect the very crude aerosol treatments of these earlier models, or the fact that models differ in the way they simulate changes to rainfall patterns over north-west Australia in response to an applied forcing. An interesting hypothesis suggested by Lin and Li (2012), discussed below, links the north-west Australian rainfall increase to ascending motion induced by an increase in sea surface temperatures in the tropical Atlantic. Note that, if found to be correct, this also raises the question of what has ultimately caused tropical Atlantic sea surface temperatures to increase.

Why is it important to understand the cause of rainfall changes in north-west Australia? A reduction in aerosols from Asia is expected to take place over the next few decades, in response to concerns about human health and other adverse effects of aerosol pollution. If aerosols have substantially caused the observed rainfall increase, then this rainfall trend would be expected to reverse. Other possible causes of the observed rainfall increase, such as Antarctic ozone depletion or natural variability, are also potential relatively short-term influences, whereas increasing long-lived GHGs are a much longer-term influence. The required policy response may differ, depending on whether the cause is long-term or short-term.

[35] The closed lows defined here are weather systems with a distinct pressure or geopotential height minimum at one or more of the following levels: at the surface, and at elevations corresponding to the 850, 700, 500 or 300 hPa levels. They are associated with a closed circulation of the wind at that given level and have a lifetime of two days or longer.

[36] In this section, 'north-west Australia' refers to the land area defined by the black lines in Figure 5.4. This encompasses the NWWA study area of IOCI3 illustrated in Figure 1.1, as well as an additional area to its south-east.

[37] From CMIP3 models.

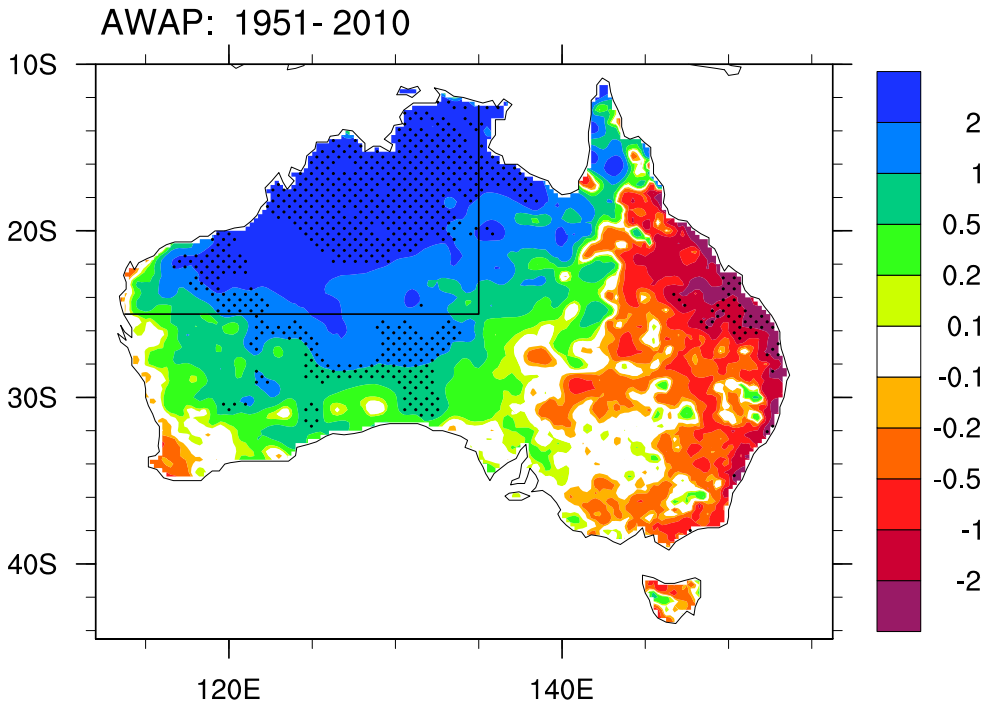

Figure 5.4 December to March rainfall trends as shown by observations from the Australian Water Availability Project (Jones et al. 2009), given in millimetres per day per century for 1951 to 2010. Stippled trends are significant at 5%, meaning there is only a 5% probability of obtaining that result by chance. The land area enclosed by the black lines denotes the region referred to as north-west Australia in the text.

Australia has relatively low levels of aerosols but is just across the equator from the planet's highest concentration of aerosols from human activity. Figure 5.5 shows a calculation of the radiative forcing due to aerosols from human activity, with negative numbers denoting a cooling effect. The strongest such effects are in the South-East Asian Region. Figure 5.5 also shows that aerosol forcing is highly variable in space, implying that aerosols have a strong ability to induce changes in wind patterns (Rotstayn and Lohmann 2002); this may include the monsoonal winds that carry moisture towards north-west Australia in summer.

Modelling results: aerosols and greenhouse gases

IOCI3 scientists collaborated with the Queensland Climate Change Centre of Excellence to carry out modelling simulations with the CSIRO Mk3.6 climate model.[38] They carried out experiments with different forcing assumptions for the historical period (1850 to 2010), and projections for the 21st century (2011 to 2100). Each experiment consisted of 10 runs (or 'members') with identical assumptions about changes in forcing; the 10 runs differed only with respect to the atmospheric and oceanic state used to initialise the run in 1850. The reason they used 10 runs for each experiment is that the average of the 10 runs (the 'ensemble average') gives a more reliable estimate of the effects of the forcing agent being considered. In contrast, each individual run within an experiment shows a strong influence of natural decadal variability, which is a ubiquitous feature of the Australian climate. IOCI3 scientists focussed mainly on the 10-member experiments listed in Table 5.7. Further details of the simulations are given by Rotstayn et al. (2012).

[38] These simulations are a subset of more than 150 simulations that comprise an Australian submission to CMIP5 (Taylor et al. 2012). This project will provide the climate modelling input to the Fifth Assessment Report of the IPCC. A special focus of the Australian submission (described by Collier et al. 2011) was the inclusion of a large number of 'single-forcing' simulations, which enable separation of the effects of increasing long-lived GHGs from those of aerosols and other forcing agents.

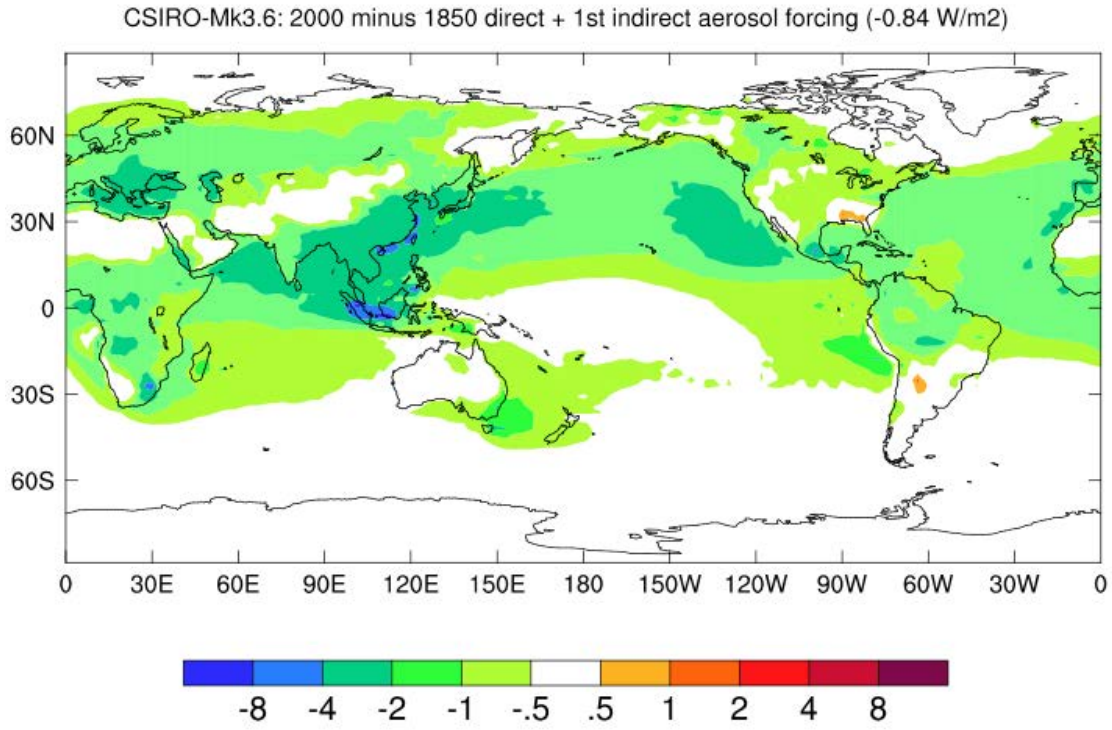

Figure 5.5 The cooling influence of aerosols. Note that this cooling influence (shown as green through blue areas) on solar radiation intensities (in Watts per square metre) at the top of the atmosphere is most pronounced in the South-East Asian Region, just across the equator from Australia. These estimates were calculated using the CSIRO Mark3.6 global climate model.

Table 5.7 Forcing assumptions of the ten-member experiments used in IOCI3 to separate the effects of different forcing agents: greenhouse gases, aerosols from human activity, ozone and natural forcing.

FORCING	DESCRIPTION
HIST	Standard historical experiment for 1850 to 2010 influenced by 'all forcings', namely, long-lived GHGs, ozone, aerosols from human activity, and natural forcing. • *Purpose: Simulation of past climate change in response to all potential influences.*
NO_AA	Same as HIST, but with aerosols from human activity fixed at 1850 levels. • *Purpose: The difference of HIST minus NO_AA gives the simulated past climate change in response to aerosols from human activity in a warming climate.*
GHGAS	Same as HIST, but influenced only by changes in long-lived GHGs. • *Purpose: Simulation of past climate change due only to increasing long-lived GHGs.*
RCP4.5	Projection for 2011 to 2100 based on Representative Concentration Pathway (RCP) 4.5, in which total radiative forcing is stabilised before 2100 at roughly 4.5 Watts per square meter (Clarke et al. 2007). • *Purpose: Projections to estimate possible future climate change in a 'mid-range' scenario for increasing concentrations of long-lived GHGs, reinforced by the effects of decreasing aerosols.*

Figure 5.6 compares ensemble-average summer rainfall trends for the historical climate simulated by HIST (1951 to 2010) and projected future climate simulated by RCP4.5 (2011 to 2100). HIST, which includes increases in aerosols from human activity, shows modest increases over some areas, but these are mostly

not significant. In contrast, RCP4.5 shows substantial, statistically significant decreases in rainfall over most of Australia, especially the North West.

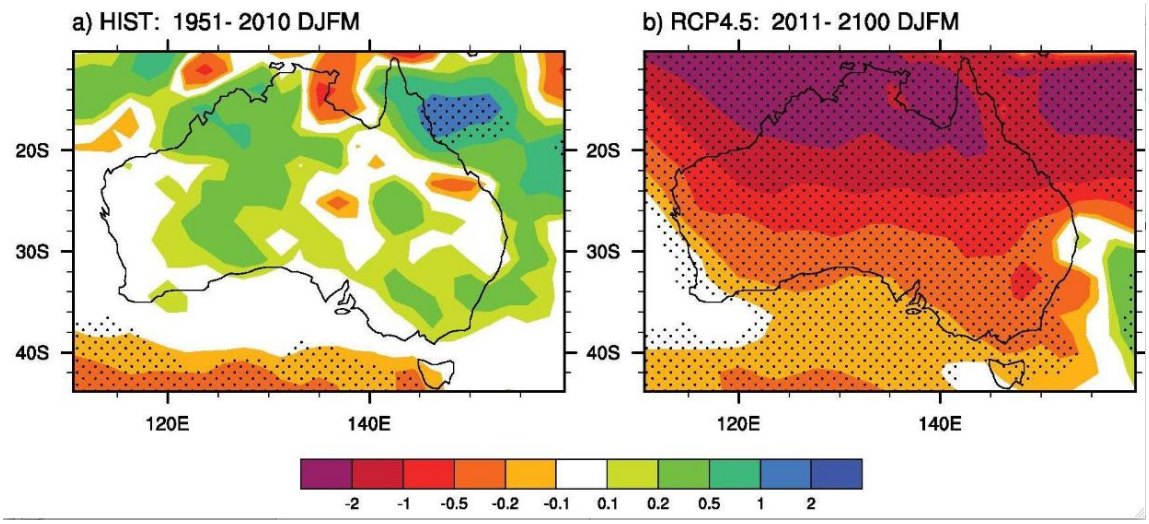

Figure 5.6 Climate modelling of past and future December to March rainfall change for the Australian region. In (a) the historical (1951 to 2010) effects of all forcings including aerosols are simulated under the set of assumptions referred to as HIST (see Table 5.7). Here the effects of rising greenhouse gas concentrations are masked by aerosol-induced increases in rainfall (green through blue areas). In (b), the simulation of 21st century (2011 to 2100) rainfall is strongly influenced by increasing greenhouse gas forcing, reinforced by decreasing aerosols, under the set of assumptions referred to as RCP4.5. The result is drying (yellow to red areas). Rainfall change is given in millimetres per day per century; stippled trends are significant at the 5% level.

How do we reconcile the fact that projected future rainfall changes in RCP4.5 differ so dramatically from historical rainfall changes simulated by runs such as HIST? Figure 5.7 sheds some light on this question. When the model is used to simulate historical rainfall trends influenced only by changes in long-lived GHGs (Figure 5.7a), the result resembles a weaker version of 21st century projected trends (Figure 5.6b) in runs such as RCP4.5, which are strongly driven by increasing long-lived GHGs. That is, the model simulates rainfall decreases over north-west Australia. However, in the simulation of historical rainfall changes from HIST (Figure 5.6a), the effects of increasing long-lived GHGs are substantially masked by an aerosol-induced increase of rainfall, which is largest over north-west Australia (Figure 5.7b).

Simulations also showed a similar, but less pronounced masking effect due to changes in ozone (Rotstayn et al. 2012). This is broadly consistent with another recent modelling study, which indicated that Antarctic ozone depletion has caused an increase in summer rainfall across the low latitudes of the Southern Hemisphere (Kang et al. 2011).

Possible mechanism for aerosol effect on Western Australia rainfall

To gain scientific confidence in such results, it is necessary to: (1) explain the physical mechanism in the model and in observations; and (2) compare results across a range of GCMs. Rotstayn et al. (2012) discussed the mechanism in the CSIRO Mk3.6 model by which aerosols from human activity contribute to increasing rainfall in north-west Australia. The key associated feature is a cyclonic (clockwise) circulation trend off the coast, which strengthens the monsoonal winds, and carries more moisture towards north-west Australia from the Indian Ocean. This mechanism is seen in both the model and in data from reanalyses (Box 2). Under IOCI3, scientists have also proposed specific processes that may explain the connection between aerosol forcing and the cyclonic circulation trend. Further work is needed to establish the veracity of the proposed mechanism, and the extent to which these findings are model-dependent.

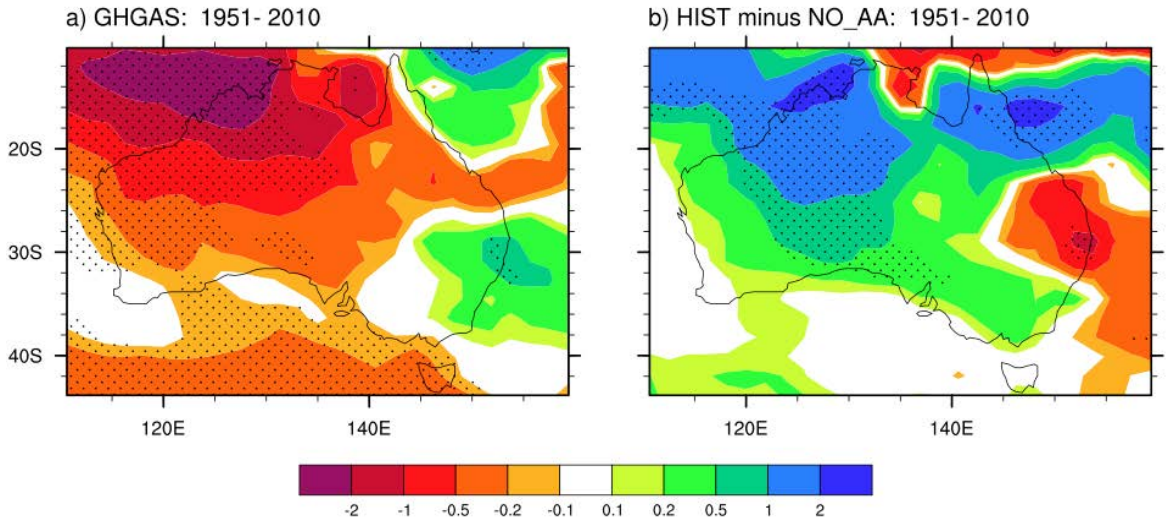

Figure 5.7 Contrasting the influence of aerosols and greenhouse gases using simulations of historical (1951 to 2010) December to March rainfall change for the Australian region. In (a) historical December to March rainfall trends are simulated only under the influence of increases in long-lived greenhouse gases (experiment GHGAS; see Table 5.6). These simulations produce rainfall decreases over north-west Australia. In (b), simulations illustrate the historical effects of aerosols (as calculated from the difference of experiments HIST and NO_AA; see Table 5.7). The drying influence of increasing greenhouse gas concentrations (panel a) is masked by the aerosol-induced increase in rainfall (panel b). Rainfall change is given in millimetres per day per century; stippled trends are significant at the 5% level.

Can the model attribute the observed rainfall changes?

The ten-member ensemble averages in each experiment were designed to capture the forced response to changes in aerosols, ozone or long-lived GHGs by averaging out the effects of decadal variability. However, these ensemble averages were unable to capture the large magnitude of the observed trend of rainfall increase over north-west Australia (see Figure 5.4). The observed rainfall increase is 2.72 mm per day per century, whereas the ensemble-average increase in HIST minus NO_AA is 0.95 mm per day per century. Two of the individual runs in HIST minus NO_AA simulate rainfall increases that are larger than the observed trend value. In other words, the aerosol-induced effect (in isolation) plus natural variability could explain the observed rainfall trend. However, given that the real climate system includes forcing from both aerosols and long-lived GHGs, this does not amount to an attribution of the rainfall trend. Further, the model does not simulate the observed rainfall increase in the 'all forcings' experiment (HIST), even in a single run. This indicates that the model is unable to explain the full extent of rainfall increase in the experiment that attempts to most realistically simulate historical climate change.

Also puzzling is that the model's simulation of decadal variability appears to be realistic, but the model cannot explain the large observed rainfall trend solely by natural decadal variability (Rotstayn et al. 2012). This apparent paradox is discussed by Rotstayn et al. (2012); they concluded that the observed trend most likely includes a forced component, and also a component associated with natural variability. The paradox can be resolved by noting that, because the simulated forcing and response for each forcing agent are presumably inaccurate to varying degrees, the simulated rainfall response to the total forcing will also be inaccurate.

Knowledge gaps and future directions

The results from CSIRO Mk3.6 suggest that aerosols from human activity have contributed to the observed rainfall increase over north-west Australia. They also suggest that future rainfall trends may look very different from recent trends: future trends will be driven by increasing concentrations of long-lived GHGs, and an unmasking of the effects of GHGs, if aerosol levels decrease as expected. However, this is a complex research question, and the discussion above alludes to some of the many uncertainties.

Results based on one climate model, like those presented here, should be treated as a hypothesis. Going forward, CMIP5 will provide a valuable opportunity to compare results from a range of models. These models are currently receiving intense scrutiny from climate scientists, so that their strengths and limitations can be assessed. Although it is currently uncertain how many modelling groups will contribute single-forcing simulations to the CMIP5 database, a recent and concerted effort to encourage other groups to submit similar simulations will enable modellers to isolate the effects of aerosols from human activity (Boucher et al. 2011). This could include downscaling from these simulations, in the manner of the IOCI3 project described in Section 5.1.2 (above).

When comparing these results from those in Section 5.1.2, the following should be noted: (1) the approach in Section 5.1.2 uses downscaling from several GCMs to simulate changes in rainfall over the study area, whereas this project uses new simulations with one GCM (CSIRO-Mk3.6); (2) the GCMs and emissions scenarios used in Section 5.1.2 are from the earlier CMIP3 project, whereas this current project uses one of the new CMIP5 scenarios, and teases apart the roles of different forcing agents in historical 'single-forcing' runs; (3) aerosol decreases in the 21st century are much stronger in the new CMIP5 scenarios than in CMIP3, and this probably adds to the rainfall decreases simulated by Mk3.6; (4) the projected changes (of rainfall decrease) are of the same sign (direction) in both Section 5.1.2 and 5.1.4. Section 5.1.2 notes that CSIRO-Mk3.5 (the immediate predecessor to CSIRO-Mk3.6) simulates relatively strong rainfall decreases, as does CSIRO-Mk3.6. In this sense, the results are broadly consistent between the two projects.

This IOCI3 investigation focussed on mean rainfall, however, much of the rainfall in north-west Australia is associated with TCs or other extreme rainfall events (Section 5.1.3). The connection between different forcing agents, mean rainfall and such high-impact events is an important topic for future research. Another area of further investigation is the possible underlying mechanism, discussed above, by which aerosols may influence rainfall in north-west Australia (Rotstayn et al. 2012).

5.1.5 LINKING NORTH-WEST AUSTRALIAN RAINFALL VARIABILITY AND WETTING TREND TO THE REMOTE INFLUENCE OF THE TROPICAL ATLANTIC

Changes in the tropical Atlantic Ocean may exert a remote influence on rainfall in north-west Australia. IOCI3 scientists (in collaboration with the Chinese Academy of Sciences) have investigated whether north-west Australia's summer (December-March) rainfall variability and wetting trend are influenced by a mid-latitude teleconnection pattern associated with enhanced atmospheric ascending motion in the tropical Atlantic (Lin and Li 2012).

Results show that the ascending motion induced by warming of sea surface temperatures in the tropical Atlantic may lead to a Rossby wave train, which emanates from the west coast of subtropical South America and extends south-eastward to mid-latitudes of the South Atlantic Ocean. This wave train then travels eastward, embedded in the westerly jet waveguide, over the South Atlantic and South Indian Oceans. The Rossby wave is thought to induce an anticyclonic anomaly in the upper troposphere over Australia, at the exit of the westerly jet waveguide. It then enhances in-situ ascending motion and the associated increased rainfall in NWWA.

A significant correlation (r=0.62 at the 0.01 level) was found between north-west Australian summer rainfall and the tropical Atlantic vertical velocity. This suggests that a remote mechanism, i.e., the trend of enhanced upward motion in the atmosphere induced by tropical Atlantic Ocean warming, could partially explain NWWA's observed rainfall trends.

5.2 Station-Scale Temperature Projections for NWWA

Project Link: 2.3

Although some parts of NWWA have followed the general warming trend observed over most of the Australian continent, much of NWWA underwent minimal warming or even slight cooling over the 1960 to

2011 period (CSIRO and BoM 2012). Will these trends continue in future? This question is addressed in this section, which reports on IOCI3 results of station-scale temperature projections for NWWA.

The statistical downscaling techniques used to provide projections of daily temperatures for SWWA (Section 4.1.2) were also applied to the Kimberley and Pilbara regions of NWWA. The downscaled projections for an SRES A2 (high) emissions scenario for annual average maximum and minimum daily temperature for these station networks are shown in Table 5.8.

As might be expected, projected temperature increases are larger at the end of the century than at mid-century under this scenario. The results downscaled from the CSIRO Mk3.5 model project the largest increases in warming in all cases. In contrast to the somewhat inconsistent results for SWWA (Table 4.2), the projections for the Kimberley suggest that minimum temperatures will warm as much or more than the corresponding maximum temperatures, regardless of the time period or GCM used. For the Pilbara, results are mixed: four of the downscaled GCMs project greater increases for maximum temperatures than for minimum temperatures for mid-century; but at the end of the century all five GCMs project a greater (or equal) increase in minimum temperature compared to maximum temperature for this region as well.

Averaged across all simulation years and all nine Kimberley stations, the annual average maximum daily temperatures are projected to increase by 1.8 to 2.7 °C by mid-century; and 3.6 to 4.6 °C by the end of the century. Annual average daily minimum temperatures are projected to increase by 2.0 to 2.7 °C by mid-century and 4.2 to 4.9 °C by the end of the century (Table 5.8).

The corresponding projections for the Pilbara, averaged across all simulation years and all ten selected stations are: an increase in annual average maximum daily temperatures of 2.0 to 3.2 °C by mid-century; and of 3.8 to 4.6 °C by the end of the century. Annual average daily minimum temperatures are projected to increase by 1.9 to 2.4 °C by mid-century and 4.1 to 4.6 °C by the end of the century (Table 5.8).

For indicative purposes, Table 5.9 and 5.10 provide the downscaled maximum and minimum temperature results for a subset of three Kimberley and three Pilbara stations; these results for the full list of stations are reported in Appendix D.

Table 5.8 Projected mean annual temperature changes for the Kimberley and Pilbara. In degrees Celsius, relative to the period 1962 to 1999, averaged across nine Kimberley and 10 Pilbara stations, for mid- (2047 to 2064) and end-of-century (2082 to 2099) periods, downscaled from five global climate models using an A2 (high) greenhouse gas emissions scenario.

	MAXIMUM TEMPERATURE		MINIMUM TEMPERATURE	
GCM	A2_MID	A2_END	A2_MID	A2_END
		Kimberley		
gfdl2.0	2.5	4.2	2.5	4.7
gfdl2.1	2.1	3.8	2.2	4.2
miroc	1.8	3.6	2.4	4.8
mk35	2.7	4.6	2.7	4.9
mpi	1.8	4.2	2.0	4.7
		Pilbara		
gfdl2.0	2.9	3.9	2.2	4.1
gfdl2.1	2.2	3.9	2.1	4.2
miroc	2.0	3.8	2.3	4.5
mk35	3.2	4.6	2.4	4.6
mpi	2.1	4.1	1.9	4.4

Coastal stations are influenced by the cooling effects of the seabreeze. Thus it is instructive to compare projections for coastal and inland stations, to gauge whether the relative coolness of coastal locations is reflected in the results. For the Kimberley stations, average coastal station maximum temperatures are projected to increase by 1.9 °C by mid-century and 3.7 °C at the end of the century, compared to 2.3°C and 4.3°C, respectively, for inland stations. Average coastal station minimum temperatures are projected to increase by 2.1 °C by mid-century and 4.2 °C by the end of the century, compared to 2.5 °C and 4.9 °C, respectively, for inland stations.

For the Pilbara stations, average coastal station maximum temperatures are projected to increase by 1.8 °C for mid-century, and 3.6 °C end of century, compared to 2.5 °C and 4.6 °C, respectively, for inland stations. Projected average coastal station minimum temperature increases are 2.0 °C by mid-century and 3.9 °C by the end of the century, compared to 2.4 °C and 4.8 °C, respectively, for inland stations. The projected differences between inland and coastal stations are greatest for the Pilbara by the end of century, when inland increases are projected to be about 1 °C greater. Thus it is evident that a coastal effect is incorporated in the projected changes.

Table 5.9 Projected mean annual maximum and minimum temperatures for selected Kimberley stations. In degrees Celsius for mid-century (2047 to 2064) and end-of-century (2082 to 2099) periods, downscaled from five global climate models downscaled using an A2 (high) scenario.

	MINIMUM TEMPERATURE			MAXIMUM TEMPERATURE		
STATION	PRESENT DAY	MID-CENTURY A2 (HIGH)	END OF CENTURY A2 (HIGH)	PRESENT DAY	MID-CENTURY A2 (HIGH)	END OF CENTURY A2 (HIGH)
Kalumburu Mission	21.0	23.0–23.6	25.0–25.7	34.4	36.0–37.2	37.5–38.8
Margaret River Station	20.5	22.6–23.4	24.9–25.8	34.6	36.6–37.5	38.5–39.7
Broome Airport	21.2	22.8–23.2	24.5–25.2	32.3	33.6–33.9	35.2–35.8

Table 5.10 Projected mean annual maximum and minimum temperatures for selected Pilbara stations. In degrees Celsius for mid-century (2047 to 2064) and end-of-century (2082 to 2099) periods, downscaled from five global climate models using an A2 (high) scenario.

	MINIMUM TEMPERATURE			MAXIMUM TEMPERATURE		
STATION	PRESENT DAY	MID-CENTURY A2 (HIGH)	END OF CENTURY A2 (HIGH)	PRESENT DAY	MID-CENTURY A2 (HIGH)	END OF CENTURY A2 (HIGH)
Port Hedland Airport	19.7	21.7–22.5	24.3–24.8	33.3	35.2–36.2	37.3–38.4
Learmonth Airport	17.7	19.0–19.5	20.4–21.3	31.6	32.9–33.3	34.2–35.0
Mount Vernon	17.3	19.4–20.2	22.1–22.7	32.1	34.1–35.3	36.0–37.6

Knowledge gaps and limitations of current approach

The weather generator approach used here is based on a multivariate normal distribution. By virtue of this approach, extreme values may not be adequately represented in the tails of the distributions (e.g., see Ruff and Neelin 2012). Thus this approach may be less well suited to the task of modelling extreme temperatures than the approach used to model hot spell projections (Section 5.3.2).

The weather generator approach is potentially extendable to additional daily weather variables as required by impacts models (e.g., solar radiation), again within the limitations of the multivariate normal assumptions of the technique. Ongoing research by overseas collaborators is addressing this challenge using generalised linear models; this is a more advanced approach than that used here, and one that should be tested for future application to Western Australia.

5.3 Extreme Events in North-West Western Australia

IOCI3 sought to provide information about rainfall and temperature extremes that affect the NWWA region, for present day and projected climate conditions. In addition, because tropical cyclones are the most regular major meteorological disaster affecting northern Western Australia, IOCI3 also advanced the science of climate change impacts on TCs, and provided projections of possible future changes to TC characteristics including their frequency, intensity and associated rainfall.

5.2.1 OBSERVED AND PROJECTED RAINFALL EXTREMES FOR NWWA

Drivers and projections of NWWA extreme rainfall

Project Link: 2.4

Chapter 4 described some IOCI3 advances in the use of methods to examine extreme climate events on local and regional scales. It described how IOCI3 scientists have applied and/or developed existing or new statistical, physical and physical-statistical methods. This statistical approach was also used to develop multi-site models for rainfall extremes for NWWA for present-day and projected climatic conditions. A challenge to conducting this research in NWWA is the sparsity of rainfall stations, a problem that has been alleviated to some extent by the use of covariates and modelled data.

Following the procedure described in Section 4.3.1.1, a range of atmospheric drivers was investigated. Two of them, relative humidity at 700 hPa and the v-wind[39] component at 700 hPa, were selected for further examination by inclusion in the fitting of the generalised extreme value distribution to individual stations. However, they did not significantly improve individual fits.

Section 4.3.1.3 described how the CSIRO CCAM model was incorporated in a physical-statistical approach to develop projections of extreme rainfall. The output from CCAM has been used to produce climate change scenarios of extreme rainfall for NWWA for the periods centred on 2030 and 2070 under an SRES A2 (high) GHG emissions scenario. These projections provide very-high resolution scenarios of the IFD characteristics of seasonal rainfall under climate change. The modelled data are also valuable in complementing other covariates such as distance from the coast and height above sea level. This can be used to 'infill' regions of the NWWA that have few rainfall monitoring stations.

Figure 5.8 illustrates the estimated return levels for extreme 24-hour rainfall events with a 100-year return period under current and projected 2070 climate conditions; it also shows the difference in rainfall intensity

[39] Wind speed and direction can be broken into two components: v-wind represents the south/north component, and u-wind the west/east component.

between these two periods. These results suggest that change in extreme rainfall amounts will not be consistent across NWWA. Instead, whereas extreme rainfall is projected to increase in some regions, it could decrease in others. Roughly speaking the Pilbara shows a decrease while the Kimberley around Broome shows an increase. The climate model used to drive this modelling does not include aerosol forcing; as discussed in Section 5.1.4, it is not surprising that decreases in extreme rainfall are projected for some regions.

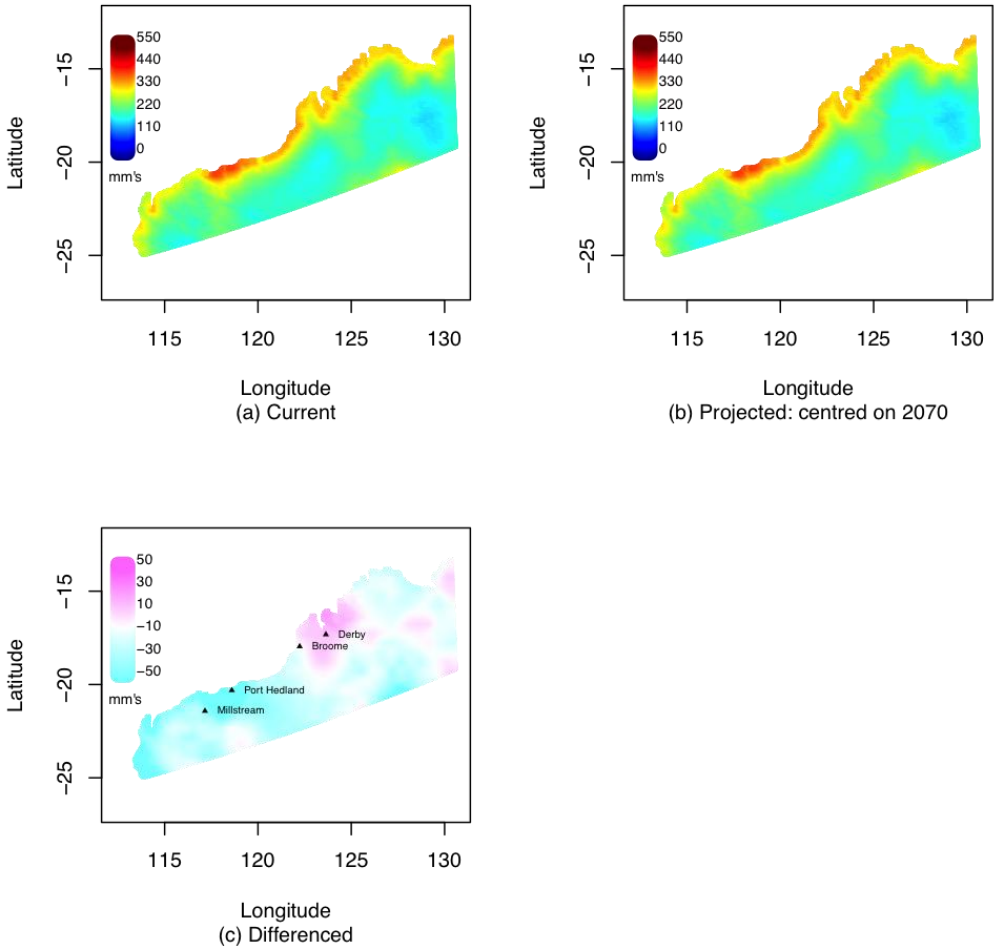

Figure 5.8 Extreme rainfall with a 100-year return period under the current climate (a), projected climate at 2070 under an SRES A2 emissions scenario (b), and the difference between these two periods (c). Figures 5.8(a) and (b) show 24-hour return levels in millimetres; yellow to red areas indicate higher extreme 24-hour rainfall, green to blue areas lower. In (c) the magenta areas indicate regions where projected extreme 24-hour rainfall amounts are expected to increase by 2070; pale blue indicates areas of projected decrease.

These techniques can also be used to model IFD curves for both gauged and ungauged locations, under the current climate and for projected climates at 2030 and 2070. This has been done for a range of gauged stations, shown in Figure 5.9. This includes stations for which extreme rainfall is projected to decrease (Port Hedland), increase (Derby) and undergo little change (Millstream and Broome).

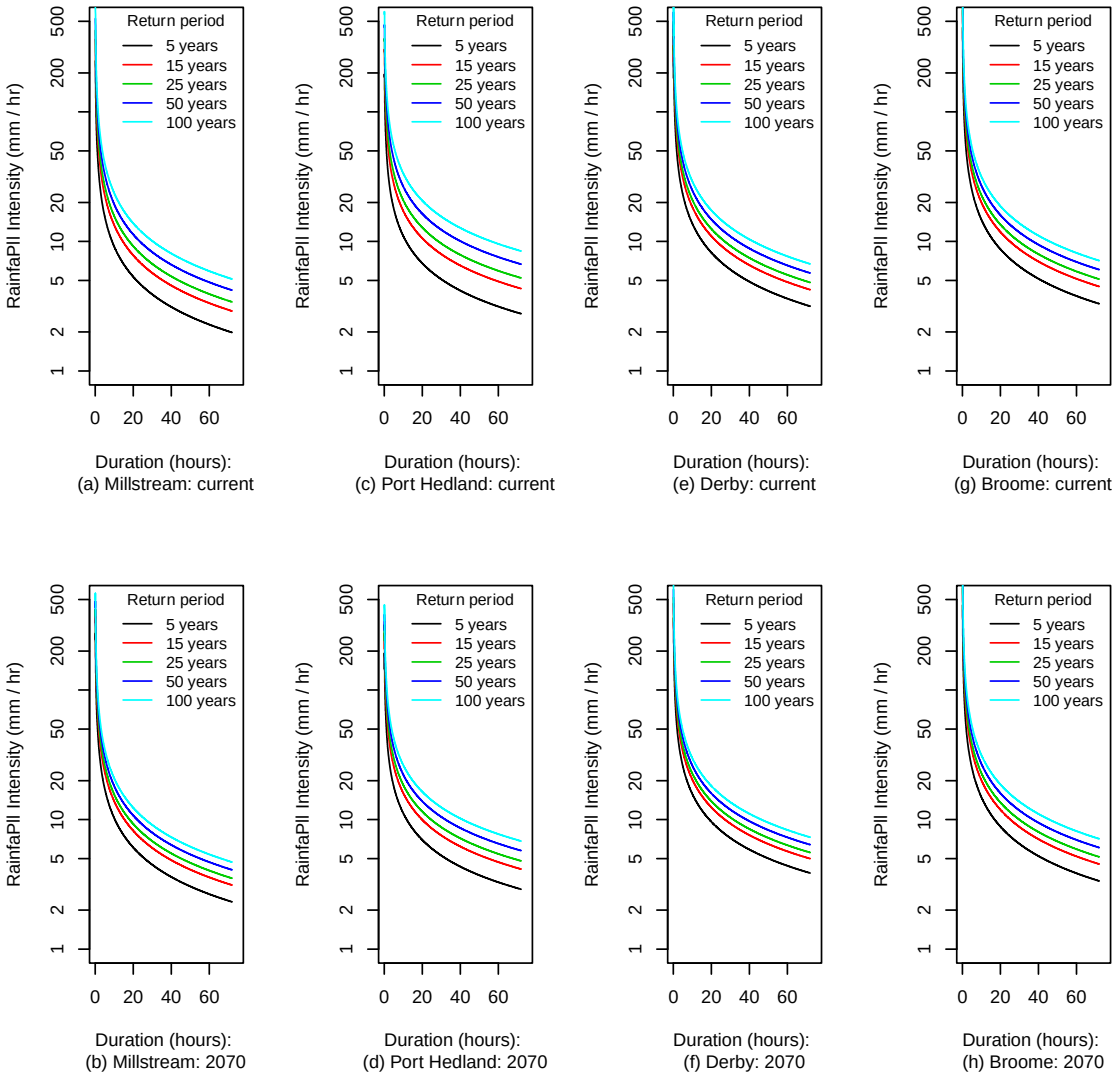

Figure 5.9 Intensity-frequency-duration curves for Millstream, Port Hedland, Derby and Broome for current and projected climates. Considering 100-year return periods, this shows little change in the intensity of rainfall events (in millimetres per hour) at Millstream and Broome; a decrease at Port Hedland; and an increase at Derby for a projected future climate at 2070 under an SRES A2 (high) emissions scenario.

Knowledge gaps and future directions

For reasons already noted in Chapter 4 (use of a single climate model combination and a single emissions scenario; small datasets for extreme events; and the need to further refine the linkage between the RCM output and the spatial model), these projections should be seen as initial estimates only, and should not be used for making impacts, vulnerability and risk assessments.

5.3.1.1 Differentiating between tropical cyclone and other sources of extreme rainfall

Project Link: 2.4

Where the influence of TCs is not large, other synoptic low-pressure systems are known to contribute to rainfall and produce extreme rainfall events. Across tropical Australia a large proportion of rainfall can be attributed to the monsoon and, in particular, monsoon lows or depressions (Figure 4.1).

To assess the relative extreme rainfall contribution of monsoon lows and TCs (both a form of closed low), IOCI3 scientists applied a detection scheme to ERA Interim data[40] (Simmons et al. 2006) that identified closed low-pressure systems. This allowed them to detect any closed low-pressure systems at multiple atmospheric levels: at the surface, and at elevations corresponding to the 850, 700, 500 and 300 hPa atmospheric pressure levels. A closed low was deemed to exist where the mean sea level pressure or the geopotential height was lower than the surrounding 24 grid-points. The detections were combined into tracks and discarded if the closed low existed for less than two days. As with the TC rainfall analysis described in Section 5.1.3.1, these data were interpolated to a 1° by 1° grid and assumed to influence a radius of 5° longitude/latitude.

An analysis of the 21 years (1989 to 2009) over which ERA Interim data are available revealed that closed lows account for approximately 40 to 60% of annual rainfall over north-west Australia. If extreme precipitation events alone are considered, the closed-low contribution is more than 60%.

Annual rainfall has significantly increased over northern Australia over the period 1989 to 2009: 15 to 25% per decade for the region north of Broome (Figure 5.10a). Over the same period the number of days influenced by closed lows has increased by a small amount (Figure 5.10b), with a much larger increase in closed-low related rainfall (Figure 5.10d) than non-low rainfall (Figure 5.10c). IOCI3 scientists found that these long-lived closed lows are able to explain a very high proportion of the rainfall trend over north-west Australia (Figure 5.10e). For these lows to explain such a large proportion of the increased rainfall with only a small increase in occurrence suggests an increase in their precipitation efficiency. As with the TC rainfall reported in Section 5.1.3.1, IOCI3 scientists found an increase in the precipitation efficiency of closed lows, that is, an increase in the amount of rainfall per closed low day over the 21-year period, in the same region as the observed rainfall increase (Figure 5.10f).

This result will include changes in TC-associated rainfall, related to the increase in precipitation efficiency of TCs described in Section 5.1.3.1. To ascertain the effect of including TCs in these results, IOCI3 scientists separated TCs from other closed-low systems and again analysed the data. They found that closed low systems (excluding TCs) explained more than 50% of the rainfall trend over north-west Australia over the 21-year period.

[40] Obtained from the ECMWF on a 1.5° by 1.5° grid for the period 1989 to 2009 (Simmons et al. 2006); see Box 2 for an explanation of reanalysis data.

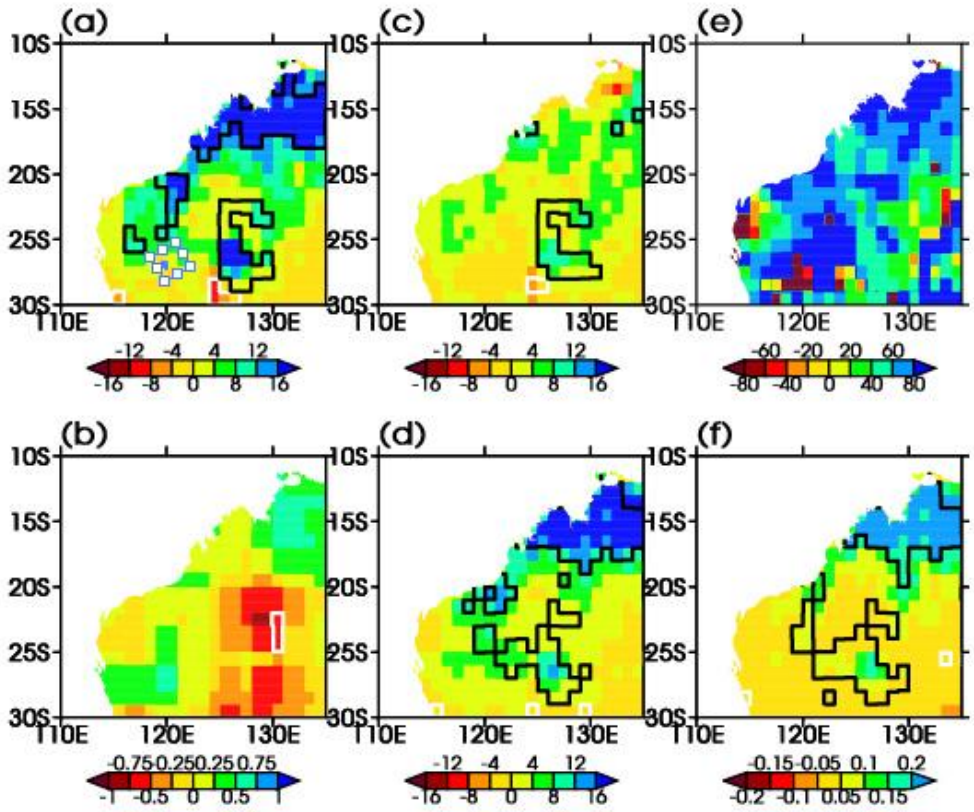

Figure 5.10 Rainfall and closed-low pressure systems in north-west Australia. Trends in (a) total rainfall (millimetres), (b) number of days influenced by closed lows, (c) non-closed-low related rainfall (millimetres) and (d) closed-low related rainfall (millimetres). (e) Percentage of the total rainfall trend that can be attributed to closed lows. (f) Trend in the amount of precipitation (millimetres) per closed low day. All trends over the period 1989 to 2009. Black (white) lines highlight positive (negative) values significant at the 90% level.

5.2.2 OBSERVED AND PROJECTED TEMPERATURE EXTREMES FOR THE NORTH WEST

Project Link: 2.4

This section describes the results of IOCI3 research on observed and future temperature extremes (i.e., hot spells as defined in Section 4.3.2) in north Western Australia. For this analysis, 'north Western Australia' refers to the area above the black horizontal line in Figure 4.16 (that is, north of 25° S). IOCI3 scientists applied the same hot spell model used to examine these events in south Western Australia. However, they first evaluated the hot spell model's ability to estimate hot spell characteristics (intensity, frequency and duration) in north Western Australia. This was done by comparing the model's outputs for hot spell characteristics with those of observed 1958 to 2011 summer (December through February) data from two stations: Port Hedland and Meekatharra airports. The results of this evaluation, detailed in Appendix F, demonstrated that the hot spell model performed very well, estimating with sufficient skill the hot spell characteristics of observed data.

Having demonstrated the hot spell model's validity for application to north Western Australia station data, IOCI3 scientists used it to calculate trends in hot spell characteristics using 1958 to 2011 summer station data. In Figure 5.11, the left panel and right panel, respectively, illustrate changes in the observed intensity, frequency and duration of hot spells at Port Hedland and Meekatharra airports. In some cases (e.g., Figure 5.11b, right panel), trends appear to be non-linear. At both Port Hedland and Meekatharra, there is no significant trend in hot spell intensity or duration. At Port Hedland there is no significant trend in hot spell frequency, but at Meekatharra the number of hot spells has increased non-linearly and significantly (at the 0.001 probability level) from three events per season in 1958 to six events per season in 2011.

IOCI3 scientists used the hot spell model to estimate north Western Australia hot spell characteristics and trends from summer-season (December through February) AWAP-station data for the 1958 to 2010 period (see Section 4.3.2 for explanation of AWAP-station data). This permitted them to examine how hot spell characteristics, including thresholds, vary spatially across north Western Australia. Figure 4.16 (a to c) shows the spatial patterns of the averaged hot spell characteristics (intensity, frequency and duration) and of their trend coefficients over the period 1958 to 2010 (Figure 4.16d-f), as generated by the hot spell model.

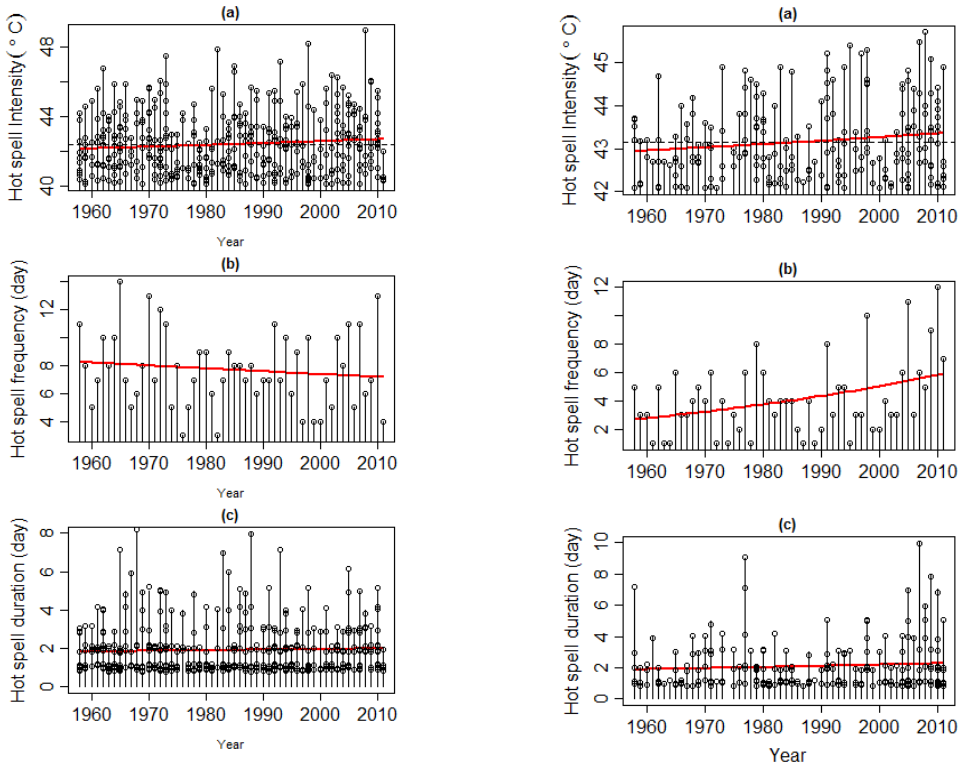

Figure 5.11 Changes to Port Hedland and Meekatharra hot spell characteristics, 1958 to 2011. Left panel for Port Hedland: (a) Observed hot spell intensity ('o' points) and estimated trends (red curve) based on fitted generalised Pareto distribution to the maximum temperature of a hot spell; (b) observed hot spell frequency ('o' points) and estimated trends (red curve) based on the fitted Poisson distribution to the occurrences of hot spell; (c) observed hot spell duration ('o' points) and estimated trend (red curve) based on the fitted geometric distribution. The results indicate a non-significant decrease in hot spell frequency (with p-value 0.36), but no observed trend in hot spell intensity or duration at Port Hedland Airport since 1958. Right panel for Meekatharra: description of each diagram is as per left panel. At Meekatharra Airport both the intensity and frequency of hot spells increased over the period 1958 to 2011 (a-b). While the increase in intensity was weak and non-significant, hot spell frequency showed a significant (at the 0.001 level) non-linear trend of increase, from three events in 1958 to six events in 2011. Almost no change in duration (c) was observed over the study period.

Hot spell thresholds for most parts of north Western Australia exceed 40 °C. This includes the Pilbara coast, where thresholds range from 33 to 46 °C, and inland areas, where most thresholds approach 45 °C. However, thresholds are considerably lower along the Kimberley coast, where they range from the low to mid-30s (°C).

The spatial pattern for intensity of hot spells roughly resembles that for thresholds. Lower hot spell intensities along the Kimberly coast range from the mid- to high 30s (°C). For the rest of north Western Australia, hot spell intensities range from 40 to 45 °C. As for hot spell frequency (Figure 4.16b), in coastal areas the number of events ranged from four to seven per summer over the period 1958 to 2010. Lower frequencies are seen in the south-west Kimberley region, about three to four events per summer. Some parts of inland north Western Australia experience higher hot spell frequencies than coastal areas, between three and eight events per summer. The duration of hot spells is generally of shorter in coastal areas than

inland areas (Figure 4.16c). Durations of two to three days were found for the Pilbara coast to the south-west part of north Western Australia, versus three to seven days for south inland areas.

Turning to observed trends in hot spell characteristics over the period 1958 to 2010 (Figure 4.16d-f), most inland (particularly south inland) areas of north Western Australia experienced increases in the intensity, frequency and duration of these events. However, along coastal areas and the south part of the Kimberley region hot spell intensity has tended to decrease. Hot spell frequency also decreased, in the south and north part of the Kimberley, and in the south-west corner of north Western Australia. Duration of hot spells also decreased in the south-west and east Kimberley, and the south-west corner of the region.

Projections of future hot spells in the North West

To provide projections of possible future changes to north Western Australia hot spells, IOCI3 scientists applied the same method used for SWWA hot spell projections (Section 4.3.2). However, they first tested the suitability of these model outputs by comparing the AWAP-station and CCAM (modelled) data. This comparison indicated how well this method simulates north Western Australia hot spell characteristics for the present-day climate (i.e., the period 1981 to 2010). They found hot spell characteristics estimated from CCAM output to be generally consistent with those seen in AWAP-station data for the present climate. Frequency was the hot spell characteristic estimated with the greatest consistency by AWAP-station and CCAM data. However, compared to AWAP-station data, simulations using CCAM data tended to overestimate or underestimate hot spell characteristics in some parts of north Western Australia. Appendix G provides a detailed discussion of this evaluation.

Apart from these deficiencies, estimates of hot spell characteristics based on the hot spell model using the CCAM-simulated data were deemed sufficient to provide projections for north Western Australia hot spells characteristics under a future climate. Figure 4.17 compares the intensity, frequency and duration of hot spells estimated by applying the hot spell model to daily maximum temperatures simulated by the CCAM for both present-day (1981 to 2010) and end-of-century (2070 to 2099) conditions according to the SRES A2 (high) GHG emissions scenario.

Intensity: The results suggest that hot spells will become more intense in north Western Australia by the end of the century (Figure 4.17a-c). Among the largest increases are those projected for some Pilbara coastal areas, particularly around Karratha. In general, moderate intensity increases are projected for the Kimberly region; however, in some areas of the Kimberley hot spell intensity could decrease in future.

Frequency: The hot spell model suggests that compared to the present day, hot spell frequency in north Western Australia would not differ much at the end of the century under an A2 emissions scenario (Figures 4.17d-f). In most inland areas of north Western Australia (except the south-east corner), a future decrease in hot spell frequency is projected, with larger deceases in some central inland areas.

Duration: Hot spell model projections indicate that hot spell duration could decrease in some coastal Pilbara and north-coastal Kimberly areas by the end of the century under the A2 emissions scenario. However, near Karratha and south of Broome hot spell duration is projected to increase. In many inland areas of NWWA hot spell duration is projected to increase (Figures 4.17g-i).

Knowledge gaps and future directions

The same limitations and caveats already discussed in Section 4.3.2 in relation to SWWA hot spells also apply here: the use of a single GCM; the uncertainties inherent in the use of AWAP data; and a need to better understand the possible drivers of hot spells. As already noted, a comparison of the observed and modelled data and an evaluation of the modelled data shortcomings are provided in the Appendix. Again, these projections should be seen as initial estimates only, and they should not be used for making impact, vulnerability and risk assessments.

5.2.3 TROPICAL CYCLONE OBSERVATIONS AND PROJECTIONS

Tropical cyclones produce fierce winds, extreme rainfall, storm surge, lightning and shoreline erosion, and along with floods they can threaten life, property, businesses, and the environment. The Western

Australian coastline between Broome and Exmouth has the highest frequency of coastal crossings of the entire Australian coastline. The potential impact of climate change on tropical cyclone activity affecting the state is therefore a question with relevance for policymakers in Western Australia.

5.3.3.1 Advancing the science of climate change impacts on tropical cyclones

Project Link: 2.2

To this end IOCI3 scientists participated in a major international collaboration to synthesise the state of the science of climate change impacts on TCs. This was carried out through an Expert Team of the World Meteorological Organization, and resulted in a Nature Geoscience paper (Knutson et al. 2010)[41] that summarises what is known – and what is not yet understood – about TCs and climate change. Because the results of this international collaboration provide valuable context for this section's discussion of IOCI3 research on TCs, they are summarised in the seven points below.

The challenges of detecting change:

- Whether the characteristics of TCs have changed or will change in a warming climate – and if so, how – has been the subject of considerable investigation, often with conflicting results.
- Large fluctuations in the frequency and intensity of TCs greatly complicate efforts to both detect their long-term trends and to determine whether these changes are driven by rising levels of atmospheric GHGs.
- The availability and quality of global historical records of TCs is quite limited, and this further impedes efforts to detect trends in TC characteristics. As a result, it is not yet possible to ascertain whether past changes in TC activity have exceeded the variability expected from natural causes.

Projections for the future:

- However, future projections based on theory and high-resolution dynamical models consistently indicate that greenhouse warming will cause the globally-averaged intensity of TCs to shift towards stronger storms, with intensity increases of 2 to 11% by 2100.
- Existing modelling studies also consistently project decreases of 6 to 34% in the globally averaged frequency of TCs.
- Balanced against this, higher resolution modelling studies typically project substantial increases in the frequency of the most intense cyclones, and increases of the order of 20% in the precipitation rate within 100 km of the storm centre.
- For all cyclone parameters (frequency, intensity and rainfall), projected changes for individual basins show large variations between different modelling studies.

The last of these findings is particularly significant for the Western Australia. It makes the point that the international modelling groups are not obtaining consistent results on TCs for individual cyclone basins, such as the South Indian Ocean. This is explored further below under, 'Tropical cyclone projections'.

The second of the above findings refers to the fact that a trend in cyclone numbers can be very difficult to determine if that trend is small compared to the year-to-year variations (i.e., internannual variability). Sophisticated statistical techniques are required to determine whether any observed trend is 'statistically significant', i.e., it must be demonstrated the trend is unlikely to have occurred by chance. The normal way to determine this is to create a very large number of artificial time series, i.e., by randomly shuffling the years to produce artificial time series of cyclone numbers or cyclone intensity. Comparing the distribution of artificial trends to that of the observed trend indicates the statistical significance of the latter.

IOCI3 scientists collaborated with the BoM National Climate Centre to investigate the quality of the west Australian (or South Indian Ocean) TC dataset, and report on the history of methods used to determine Southern Hemisphere TC intensity and numbers (Kuleshov et al. 2010b; see also Chapter 2). They explained that cyclone intensity is estimated primarily from the patterns of infrared temperature of TC cloud systems,

[41] The paper explicitly mentions the contribution of IOCI in funding the Australian participation.

as observed by meteorological satellites. They also documented changes in data availability and satellite interpretation procedures over the period of record.

IOCI3 scientists also developed a number of statistical tests to determine whether any trends exist in Australian TC numbers (Kuleshov et al. 2010a). Figure 5.12 shows the time series of the number of severe TCs (as defined by central pressures of less than 950 hPa). The figure has time series for the entire Southern Hemisphere (top curve) plus three sub-regions. It shows an upward trend in the number of severe TCs observed for the Southern Hemisphere and also for the South Indian Ocean. These trends do satisfy the statistical significance tests described above. However, IOCI3 scientists also carried out a 'break-point analysis' to examine the time series for discontinuities or step changes. This revealed a step-change in the data around the year 1991, corresponding to the time when the availability of infrared satellite imagery improved. Since the data do not form a continuous series, the best way to model these data was to account for this step change (Kuleshov et al. 2010a).

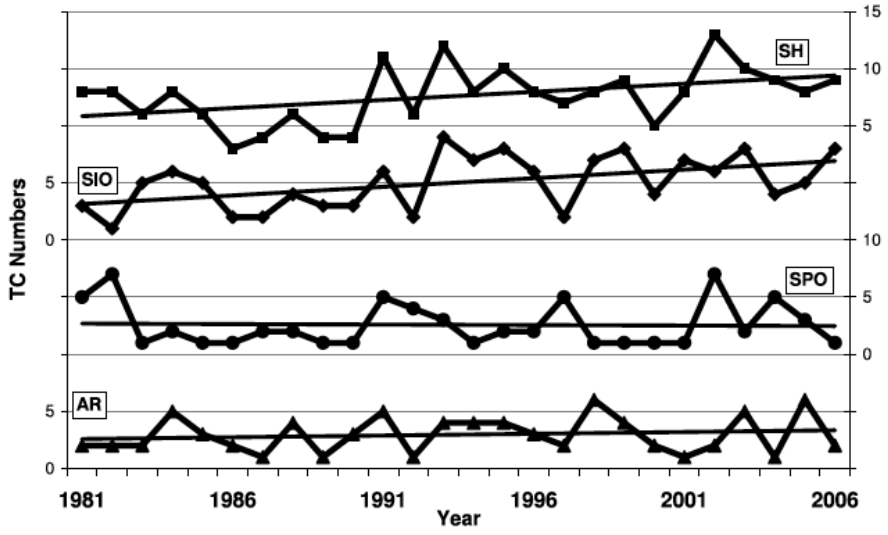

Figure 5.12 Observed tropical cyclone frequency in the Southern Hemisphere. Annual numbers of severe tropical cyclones (TCs) with central pressures less than 950 hectopascals in the Southern Hemisphere (SH), Southern Indian Ocean (SIO), South Pacific Ocean (SPO), and the Australian region (AR) (triangles, left axis), 1981/1982 to 2006/2007 tropical cyclone seasons, with linear trends. (Note: the right axis has counts for SH and SPO; the left axis for SIO and AR).

Based on their analysis they concluded that, for the 1981/2 to 2006/7 time period, there are no apparent trends in the total numbers of TCs in the five regions of the Southern Hemisphere examined. For the Australian region there were also no significant trends in the number of severe cyclones. However, looking specifically at the South Indian Ocean, there are statistically significant positive trends in the number of severe TCs (and consequently the Southern Hemisphere; Figure 5.12). The break-point analysis and the qualitative discussion of changes in data availability and in operational procedures would suggest that changes in data quality influence these apparent trends to some extent. However, given the theoretical expectation that the response to the warming oceans will be an increase in the number of most intense cyclones, it is also possible that these trends indicate this physical effect. Trends over the period for which the data are most reliable (approximately 1993/4 onward) are for the most part not significant.

Efforts to consolidate historical data from various regions are currently limited by the inhomogeneity of TC observation and analysis practice. Evidently there is a considerable need for reanalysis of historical TC data to obtain globally homogeneous records. These homogeneity issues place limits on our present ability to answer the important question, 'how is TC activity changing?' and, more generally, the possible relationship of any such trends to global climate change.

Tropical cyclones and sea surface temperatures

Tropical cyclones generally form only over the tropical oceans where sea temperatures exceed 26.5 °C. This is because the energy source for a TC is the heat stored in the ocean; this energy is transferred to the

atmosphere through evaporation and subsequently released into the atmosphere through latent heat release in the cyclone rain clouds. Climate models project that tropical ocean temperatures will continue to increase under climate change. Thus changes to TC activity are expected.

To understand how cyclones will respond to the projected temperature changes, it is important to understand the details of the relationship between ocean temperature and TCs. Hence IOCI3 scientists carried out a number of investigations on this relationship, as described below.

Correlations with ocean temperature: They examined how the presence of TCs correlates with sea surface temperatures, for both *in-situ* sea surface temperatures and for sea surface temperatures across the wider tropics. Positive *in-situ* correlations during the beginning of the cyclone season were found. That is, the presence of warmer seas corresponds to more TCs from October through December (Figure 5.13). Conversely, in mid-season (January to March), the correlations are negative, i.e., warmer sea surface temperatures are associated with fewer cyclones.

The proposed explanation is that their separate associations with ENSO dominate the variability of both TCs and sea surface temperatures off Western Australia. Thus the major finding is that *in-situ* statistical relationships (i.e., linear correlations such as these) between indices of cyclone activity and sea surface temperature are dominated by large-scale patterns, reflecting the large-scale structure of ENSO or ENSO-related phenomena. This makes the challenge of determining TC responses to changing sea surface temperatures more difficult; the TC response to sea surface temperatures is not simply local, but instead must be interpreted in terms of sea surface temperature effects on the larger-scale dynamical circulation systems that foster the formation of TCs.

Ocean temperature and tropical cyclone formation: One well recognised necessary condition for TC formation is the presence of ocean temperatures of at least (approximately) 26.5 °C. However, ocean temperatures have warmed and are likely to continue to do so, so that the region at or above this threshold sea-surface temperature may be expected to expand in extent. It is therefore important to ask, 'How robust is this 26.5 °C formation threshold'?

IOCI3 scientists examined the sea surface temperatures at which TCs form using a local database and information within an international database on TCs and cyclone tracks for the years 1981 to 2003 (Dare and McBride 2011a). This revealed that although 26.5 °C is not an absolute threshold, more than 98% of TCs form above this sea surface temperature value. This threshold is most apparent over the 48 hours preceding TC development. This is presumably due to the fact that, as the cyclone develops, it cools the underlying sea surface (Dare and McBride 2011b). The data demonstrate that TCs occur at higher sea surface temperatures at the early stage of their life cycle, and then tend to move to lower sea surface temperatures after they develop.

IOCI3 scientists also examined the response of the sea surface temperature threshold to global warming. They observed that, globally, TCs are forming at sea surface temperatures warmer than 26.5 °C, i.e, a shift of 0.2 °C has occurred in the mean temperature of TC formation. However, no shift can be detected in the threshold temperature towards a higher value (Dare and McBride 2011a). Thus as oceans warm, it cannot be assumed that the region of cyclone formation will correspondingly expand. Sea surface temperature is just one factor affecting TC formation; therefore changes in sea surface temperature alone do not imply a larger area conducive to TC formation.

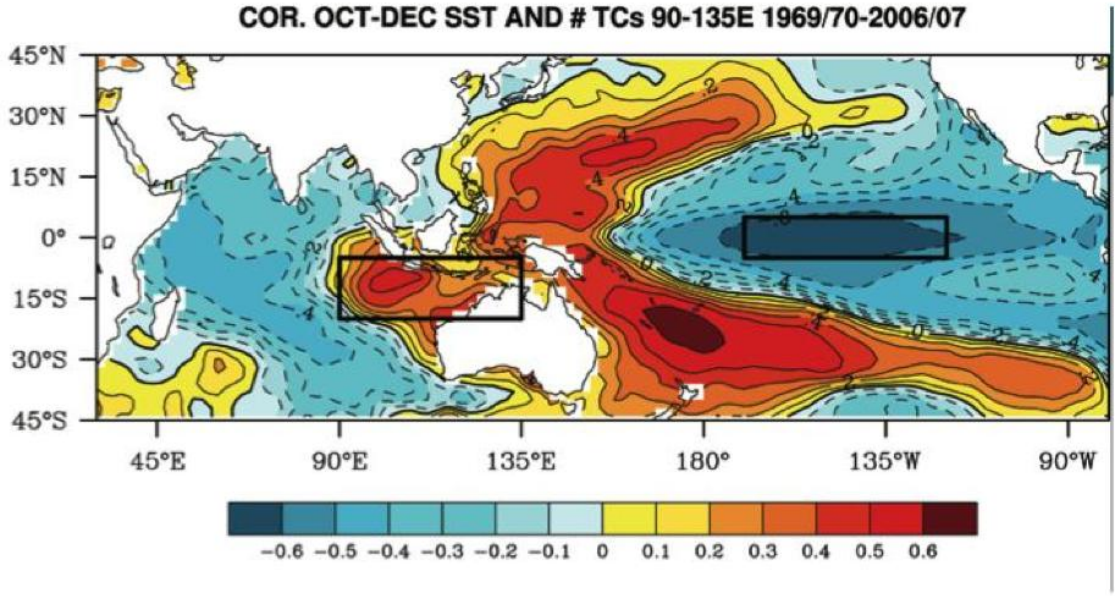

Figure 5.13 Tropical cyclone correlations with sea surface temperature. Patterns of linear correlation coefficient between the number of tropical cyclones in the boxed area north-west of Australia versus sea surface temperature at each point in the Indian and Pacific Oceans during the October to December period. The boxed area in the Central Pacific (right-hand side of the figure) denotes the region of the Nino-3.4 ENSO index. During the October-December period warmer seas correspond to higher numbers of tropical cyclones.

How tropical cyclones affect ocean temperature: There is a complex relationship between TCs and sea surface temperatures. Not only should sea surface temperature influence a TC's development and final intensity, but TCs should also be expected to influence sea surface temperatures as they pass over. This is because TCs extract energy from the underlying sea surface, and also cause dynamical upwelling of the sea, bringing deep, colder water to the surface. Improved understanding of these effects is important for climate change studies, and to understand the influence of TCs on Indian Ocean circulation.

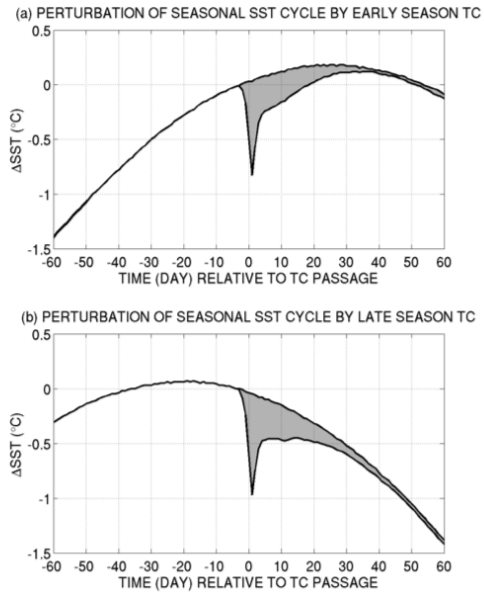

Figure 5.14 Tropical cyclone influence on ocean temperature. Perturbation of seasonal sea surface temperature cycle by (a) early season tropical cyclone, and (b) late season tropical cyclone.

To quantify these effects on underlying ocean temperature, IOCI3 scientists examined the reduction in sea surface temperature with the passage of a TC, as well as the ensuing temperature recovery time (Figure 5.14). In general, it was found that the greater the temperature reduction as the cyclone passes over, the

longer the time taken for the sea surface temperature to recover. However, the error bars (standard deviation) for sea surface temperature anomalies are so large that the relationship between the two variables (temperature reduction and recovery time) can be considered to be insignificant. Further analysis showed that both rapid and slow recoveries can occur across the range of cyclone intensity classes and the range of storm translation speeds.

Nonetheless, this work demonstrated that TCs can greatly influence the heat balance of the underlying ocean. It also demonstrated TCs' sometimes-large impact on the seasonal cycle of ocean surface temperature, as follows. When cyclones occur in the first half of the cyclone season, they disrupt the seasonal warming trend, which does not resume until 30 days after cyclone passage. Furthermore, cyclones that occur in the late half of the season bring an approximately 0.5 °C temperature drop, from which the ocean temperature does not recover, due to the seasonal cooling cycle.

Knowledge gaps and Future Directions

The impact of TCs on climate is still not well understood. Important first steps under IOCI3 documented the impact of cyclones on sea surface temperature, but further work should incorporate sub-surface temperature data and should involve case studies of individual cyclone and cyclone seasons.

The study of the sea surface temperature at which cyclone development occurs should be extended to study cyclone intensification, particularly rapid intensification. The lack of a discernible trend in the value of the threshold temperature reported above is at odds with reports in the literature. In the international literature changes have been reported in the threshold for large-scale organised convection in the atmosphere associated with TC formation. These differences need to be resolved.

Changes in satellite detection methods and limitations in the historic data have made it difficult to detect trends in cyclone behaviour. More work on the observed records of TCs is needed to understand what conditions lead to years with more intense cyclones, and to years with cyclones making landfall further southwards. More work on historical TC data, including landfall observations, is needed to obtain a longer, consistent cyclone record suitable for trend detection.

5.3.3.2 Tropical cyclone projections for the west Australian region

Project Link: 2.4

As noted above, IOCI3 research on tropical cyclone observations indicates that no significant trends in TC intensity or frequency are detectable thus far. However, a number of studies on a range of different ocean basins suggest that TC intensity could increase in future, even as the number of TCs is expected to decline (Knutson et al. 2008).

IOCI3 scientists sought to examine how climate change may influence TCs in the region of the Indian Ocean where they affect NWWA. They used outputs from simulations made with CCAM to assess its ability to simulate the climate of TCs in the region and to provide projections of changes in TC characteristics. These simulations used a 65-km grid spacing and were initialised with either NCEP reanalysis data or outputs from GCMs.[42] The NCEP reanalysis, or GCMs, also provided large-scale climate information to the boundaries of the region of interest throughout the simulation. Six GCMs, sourced from the IPCC CMIP3 archive, were considered. The results showed that the model is able to simulate the spatial characteristics of TC occurrence in the Australian region, and that it can differentiate between changes in TC occurrence in El Niño and La Niña events. However, the frequency of TCs simulated by the model is less than the frequency actually observed; on average, only approximately 60% of the observed number of TCs was simulated by CCAM.

Climate change projections using this modelling system suggest a future decrease in TC numbers in the west Australian region, especially in the region of current preferred occurrence. On average, for the period

[42] Some simulations were forced with bias-corrected sea surface temperatures only while others were forced using sea surface temperatures and large-scale atmospheric conditions from the parent GCM.

2051 to 2090 relative to 1971 to 2000, the simulations show an approximately 50% decrease in occurrence for the region. The modelling also projects a small decrease (0.6 days) in the duration of a given TC, and a 100-km southward movement in the genesis and decay[43] regions over this period (Abbs 2012).

The modelling system just described cannot resolve important TC structures such as the eyewall; thus TCs identified in CCAM are referred to as tropical cyclone-like vortices. The eyewall is where the strongest winds and heaviest rainfall occur. It is the most dangerous and destructive part of a TC and is characterised by deep convective clouds rising to a height of 15,000 metres. Resolving these structures is necessary to provide projections of changes in TC intensity and rainfall. This requires further downscaling of individual tropical cyclone-like vortices at a spatial scale of 5 km or higher.

To provide these fine-scale projections of changes in TC intensity and rainfall, IOCI3 scientists used the Regional Atmospheric Modelling System to downscale tropical cyclone-like vortices from one of the 65-km CCAM simulations to a grid spacing of 5 km. This was done for the climates of the late 20th century (1961 to 2000) and late 21st century (2051 to 2090), with one hundred and twenty tropical cyclone-like vortices downscaled for each climate period.

An analysis of storm characteristics for the 12 hours of model time centred on the time of minimum pressure (the period of maximum TC intensity) shows a tendency towards larger, more intense TCs in future. This finding is illustrated in Figure 5.15, which shows changes in the storm maximum wind speed and the storm maximum integrated kinetic energy, both measures of intensity.

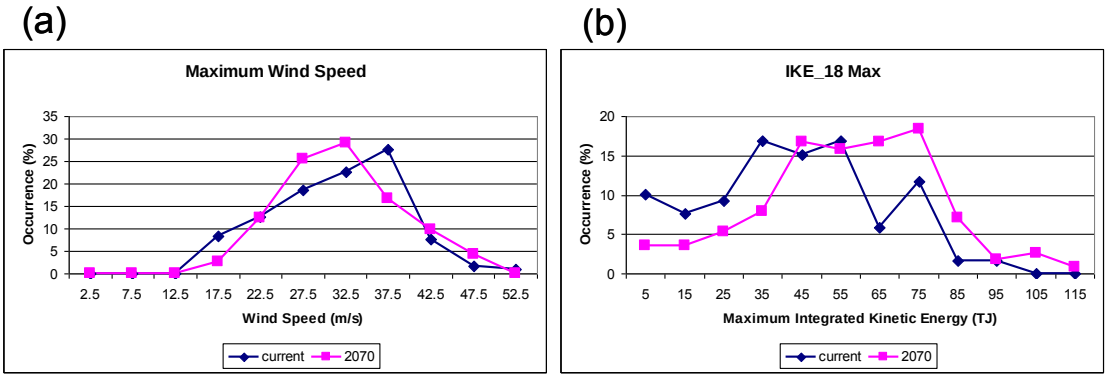

Figure 5.15 Projected changes in measures of tropical cyclone wind speed and intensity. Probability density functions of (a) storm maximum wind speed and (b) integrated kinetic energy (IKE) for the late 20th and late 21st century based on the outputs from the 5-km Regional Atmospheric Modelling System. In (a), the fuchsia plot indicates that storm intensity will increase for the proportion of storms with a maximum wind speed greater than 40 metres per second.ms $^{-1}$ (i.e., those points on the far right of the graph). Since wind speed alone does not fully explain a tropical cyclone's potential to cause damage, IOCI3 scientists used the additional measure, integrated kinetic energy, which contains information related to both strong winds and TC size. Importantly, in (b) integrated kinetic energy also shows a possible tendency of increase in future

The storm maximum wind speed (Figure 5.15a) is the maximum wind speed simulated throughout the lifetime of the TC. The downscaled projections indicate that the likelihood of occurrence will increase for that proportion of storms with a maximum wind speed greater than 40 m/s (approximately Category 3 to 5 cyclones).

However, Powell and Reinhold (2007) point out that a better measure of a TC's destructive potential, particularly that due to waves and storm surge, is the integrated kinetic energy. This is calculated by integrating (summing) the kinetic energy produced over that part of the TC where wind speed exceeds 18 m/s for each time step. Thus the integrated kinetic energy contains information related to both strong winds and TC size. As Figure 5.15b illustrates, there is a tendency for a future increase in integrated kinetic

[43] Genesis defines the location and time at which a tropical closed low reaches TC wind speed of approximately 18m/s. Decay occurs when the system is no longer at TC strength.

energy. When IOCI3 scientists used separate measures of TC size, such as the radius of maximum winds and radius to gale-force winds, they found these measures also project an increase in the size of late 21st century TCs, yielding results consistent with those obtained from the above integrated kinetic energy calculations.

IOCI3 scientists also investigated possible changes in the intensity of rainfall associated with TCs. They analysed precipitation outputs (i.e., of the above-mentioned Regional Atmospheric Modelling System downscaling to a 5-km resolution) from these simulations for the 12 hours of maximum storm intensity, over an 800 by 800 km box centred on the storm centre. These results show large expected increases in rainfall intensity in the area surrounding the TC. Intensity increases of 23% are projected for rainfall occurring within 200 km from the storm centre, and of 33% for rainfall with 300 km from the storm centre. These projected increases in rainfall intensity are larger than the values described by Knutson et al. (2008) for Atlantic hurricanes. This discrepancy could be due to a number of factors related to the methods used here, including (a) use of a higher resolution model for the simulations; and (b) performing the analysis for the 12 hours during which the storm was most intense.

Knowledge gaps and future directions

These tropical cyclone projections were produced by downscaling outputs from a single RCM (CCAM). It should be cautioned that this model simulates fewer TCs than were actually recorded in observed data. To provide more robust projections, this study must be replicated using additional climate models. As noted above, this modelling study projected an increase in the intensity of the most severe TCs, consistent with the results of international modelling studies focusing on the North Atlantic.

5.3.3.3 Cost analysis of tropical cyclone impacts on Western Australia

Project Link: 2.2

A cost analysis of the impacts of tropical cyclones on Western Australia was carried out under IOCI3 by an experienced meteorologist who has worked with cyclone forecasters and disaster experts around the world (McBride 2012). This analysis was based on information from the relevant literature, government websites, and discussions with forecasters and mining company representatives.

Economic losses to private property and public infrastructure in Western Australia due to *direct damage* from TCs are estimated to be on the order of $40 million to $100 million per year, depending on the data source and the method used to extrapolate from insurance payout to total cost. However, this analysis proposes that direct property damage is not the major economic impact to the State. Rather the major impact is the cost to the mining (minerals and energy) sector, which conducts exploration, extraction and export in a cyclone-prone area.

The ongoing costs to the mining sector include: carrying out exports subject to port closures during cyclone events; flooding of mines; transport closures due to flooding and road damage; and the ongoing adaptation and preventive measures that underpin the activities of this sector. In general, these costs to mining are not publicly documented and are not reflected in insurance industry records. This analysis acquired evidence of these costs through discussions with industry, from mining company quarterly reports, and by examining cases of cyclone-related port closures that have affected Australia's trade balance.

Analysis of insurance industry disaster payouts indicated that the cost of direct damage ($40 million to $100 million per year) from TCs in Western Australian is not large compared to other Australian disasters such as those caused by flooding, bushfire and hailstorms in major cities. The study presents the concept of 'economic-extreme disasters' such as Tropical Cyclone Tracy, the 2011 Queensland floods, and the Black Saturday Victorian fires. It is contended that the cost of these major events is several multiples of that of a normal TC (or other natural disaster) event. For example the time series of (inflation-adjusted) TC losses for Australia is dominated by one very large event, Tropical Cyclone Tracy. Any figures on mean annual losses or comparisons of cyclones with other hazards are greatly altered depending on whether or not this one event is included in such analyses.

Both in Australia and globally the increase in insurance payouts for disasters over recent decades is believed to be dominated by increasing vulnerability due to population growth and infrastructure

development in coastal regions. There is no clear evidence of any climate change signal in disaster costs. Consistent with this, in Western Australia the annual cost to private property, government infrastructure and the mining sector should rise in coming decades for the same reasons: higher infrastructure and construction costs and increasing vulnerability due to larger populations and intensified infrastructure development on the coast. If changes in TC activity prove to be consistent with climate scientists' projections (see section above), this signal will be difficult to detect in the regular TC insurance loss statistics.

A potential major impact of climate change would be an increase in the frequency of economic-extreme disasters (e.g., Tropical Cyclone Tracy in Australia and Hurricane Anita in the USA). There is no scientific evidence to suggest that this is likely to happen, however, any change in the frequency of such events remains a major potential impact of climate change and should be further studied. A second major impact of climate change would be the possibility of an acceleration in the time-series of costs associated with TCs due to coastal inundation against a background of higher sea levels (e.g., see Walsh et al. 2012).

We note that rainfall associated with these storms (Dare et al. 2012) can constitute an important source of urban water supply and rainfall for agriculture (Section 5.1.3). This is likely to have a positive economic impact in Western Australia.

Knowledge gaps and future directions

Although this IOCI3 work proposed that the economic impact of TCs on Western Australia's mining sector is *the* major impact, this contention is difficult to substantiate without obtaining cost documentation from within this industry.

The lack of publically available documentation of this cost to industry is a concern. If Australian economists were to address this issue, along with the issue of the wider economic costs due to TCs in Western Australia, this would be of considerable value to this industrial sector and to the wider community. Toward this end we propose a framework that groups TC-related costs into three categories: (i) damage costs; (ii) ongoing operating costs to industry; and (iii) extreme disaster costs.

It has been proposed that the economic impact of climate-change related shifts in TC activity would be difficult to detect in normal damage losses against a background of increasing population, infrastructure and construction costs. However, any increase in the probability of economically-extreme disaster events (e.g., Tropical Cyclone Tracy), or a non-linear increase in inundation due to rising sea levels, could have a large impact. It is recommended that Western Australia's vulnerability to changes in the frequency of extreme cyclone-related disasters be studied in a climate change context.

6 Forecasting and Seasonal Predictability

Drafting authors: Carsten Frederiksen, Janice Wormworth and John McBride

6.1 Quantifying the Limits of Seasonal Predictability of Western Australia Rainfall and Surface Temperature

Project Link: 1.3

Climate variability has a major influence on the Western Australian economy, primarily through its direct impact on agriculture. Skilful seasonal forecasts can help society manage its response to climate variability to some extent. However, prior to IOCI3, no attempt had been made to systematically estimate the upper limits of skill of such forecasts through the use of observational datasets. Yet if an estimate like this was performed, it could identify the regions and seasons for which skilful forecasts might be expected.

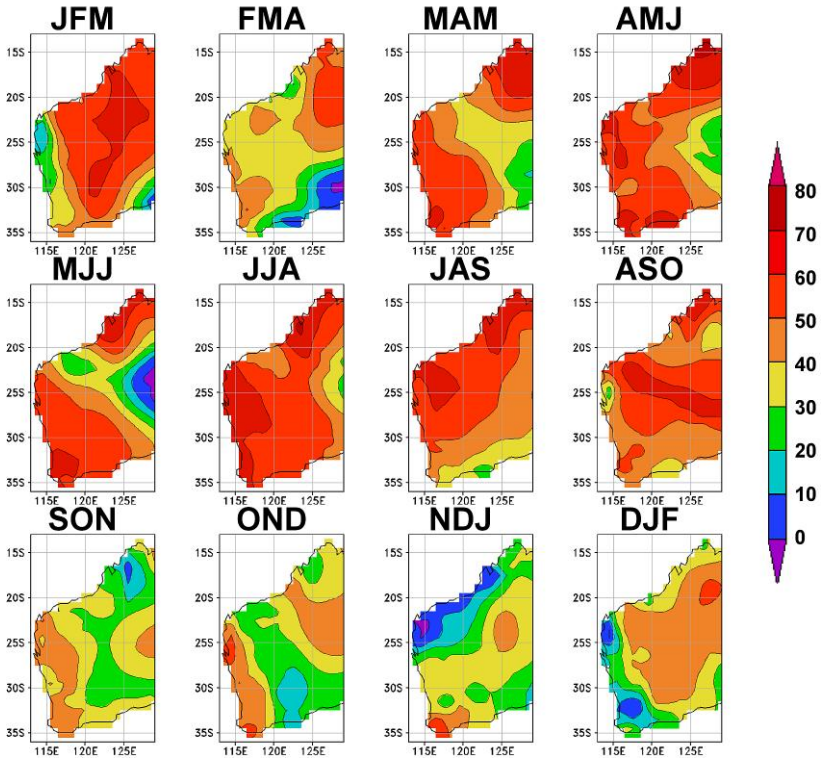

Figure 6.1 Potential predictability (%) of Western Australia maximum temperatures. Results indicate that the potential for skilful prediction (>20-30%) is possible in much of the state over most of the year (as indicated by green, yellow, orange and red areas).

Toward this goal, IOCI3 scientists developed two new techniques. These were used to estimate the predictive characteristics of Western Australia surface temperature and rainfall in all seasons. Their methodologies were guided by an underlying goal: to identify two components of year-to-year climate variability. The first of these two components relates to variability *within* the season. This 'intraseasonal' component is generally considered to be unpredictable a season or more before the forecast period. The second component has two parts: it is associated with slowly varying external influences on the atmosphere (e.g., sea surface temperature or GHG forcing); and slowly varying internal atmospheric variability (e.g., associated with the Southern Annular Mode).

Unlike the first component, the second is often referred to as the 'potentially' predictable component, because these slowly varying external influences or internal dynamics may themselves be predictable. Therefore the proportion of the second component in the total year-to-year variability gives a measure of the potential predictability of the climate variable. Detailed descriptions of these methods appear in Frederiksen et al. (2008) and Grainger et al. (2008, 2009). Frederiksen and Zheng (2007) provide an overview of the general framework for these methods.

The methods were applied to monthly means of Western Australian surface maximum and minimum temperature, and daily rainfall obtained from BoM (see Frederiksen et al. 2008; Grainger et al. 2008 for details). Estimates of the potential predictability of Western Australian surface maximum temperature, minimum temperature and rainfall are shown in Figures 6.1, 6.2 and 6.3, respectively. Note that seasonal forecasts by BoM are given each month for the following three-month average (i.e., season). This is why the results presented here are for each of the twelve 'three-month seasons'. The potential predictability is expressed as a percentage of the total year-to-year variability. Past experience suggests that a value of 20-30% is likely to provide some benefit and reasonably skilful prediction.

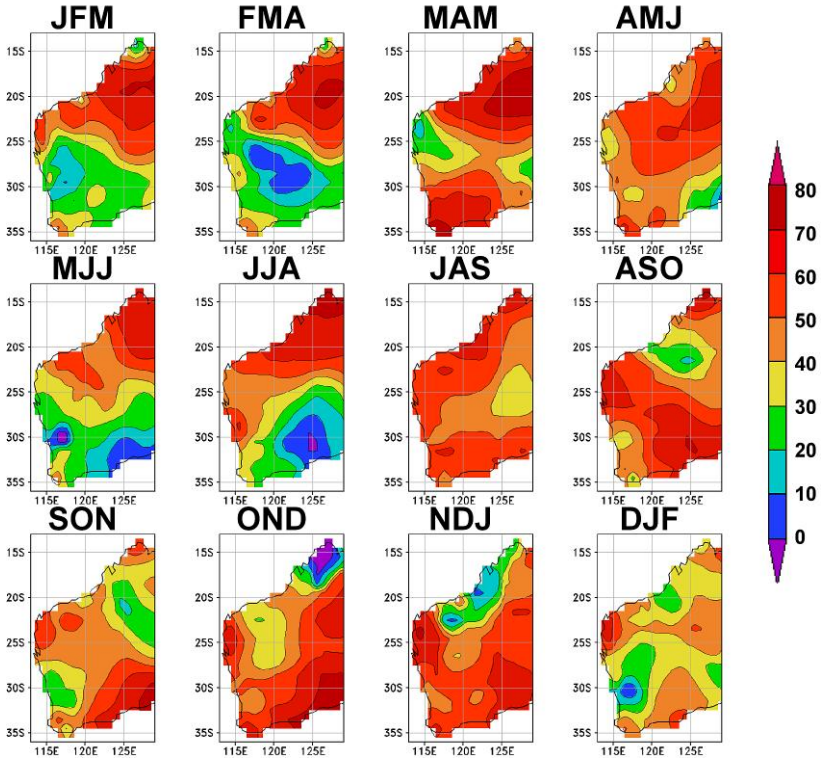

Figure 6.2 Potential predictability (%) of Western Australia minimum temperatures. Again, the potential for skilful predictions (>20-30%) is possible in much of the state (green, yellow, orange and red areas), although the spatial pattern differs from that of maximum temperature (Figure 6.1).

The predictability of both maximum and minimum temperatures shows a distinct annual cycle. In all seasons, however, large areas of the state generally have very high potential predictability. As to spatial structure, the predictability for maximum temperature differs greatly in its spatial pattern compared to predictability for minimum temperature. This difference is seen in all seasons. These differing patterns of variability have been attributed to the different physical processes that determine daily surface maximum and minimum temperatures, processes which can be considered in terms of the diurnal cycle of the surface energy budget (see Grainger et al. 2009 for discussion and references).

Regarding surface maximum temperature, potential predictability is generally high (at least 50%) north of 20° S throughout most of the year, except during SON, OND and NDJ. Statewide, the predictability is lowest during the seasons SON to DJF. The lowest predictability occurs along the west coast during DJF and JFM; along the north-west coast during NDJ; the south of the state during FMA; and over the central east of the state during MJJ. In SWWA, the predictability is generally greater than 30% and can exceed 60% in all seasons except during DJF.

Regarding surface minimum temperature, potential predictability is also generally high north of 20° S (with some regions exceeding 70%), although it is much lower in OND. The lowest potential predictability tends to occur over a large area south of 25° S during JFM, FMA, MJJ and JJA. In most other seasons there is generally good predictability for minimum temperature (greater than 40%) over much of the state. As is the case with maximum temperature, predictability for minimum temperature in SWWA is generally greater than 30% in all seasons and can exceed 60%.

The picture for rainfall is quite different. The (unpredictable) intraseasonal component clearly plays a much larger role in the year-to-year variability of mean seasonal rainfall, compared with the surface temperature. Consequently, rainfall is much less predictable than temperature at the long range.

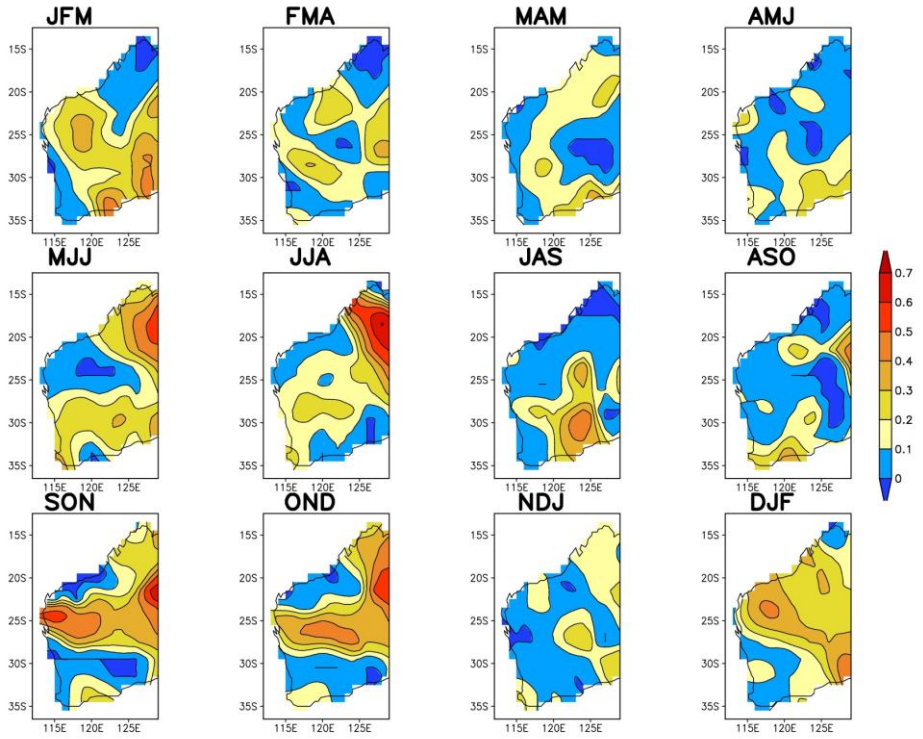

Figure 6.3 Potential predictability (%) of Western Australia mean seasonal rainfall. Though much less predictable than surface temperature, rainfall also exhibits a distinct annual cycle in its pattern of potential predictability.

As with temperature, rainfall exhibits a distinct annual cycle in its pattern of potential predictability. From NDJ to AMJ, the potential predictability is very low north of 20° S, indicating that intraseasonal processes dominate. This is the period when much of the weather over the North is governed by the Madden-Julian Oscillation. This weather fluctuation is a major source of intraseasonal variability in the tropics that would account for this low predictability. South of 20° S, during these seasons, predictability varies between 20 to 40% over large areas of the state, especially during DJF and JFM. The highest level of predictability (as high as 70%) occurs over northern Western Australia during MJJ, JJA, SON and OND. During spring (SON and OND) there is also substantial predictability over central Western Australia including near the coast. Over SWWA, predictability during MJJ and JJA ranges from 20 to 30%, indicating that there is some potential for skilful long-range seasonal prediction during these seasons. During the rest of the year there is very low predictability over the SWWA.

6.2 Tropical Cyclone Forecasts

Project Link: 2.2

IOCI3 scientists collaborated with the Centre for Australian Weather and Climate Research and MeteoFrance to develop a statistical forecast model for tropical cyclone activity along the Western

Australian coastline. This model provides an online real-time forecast system for TC activity for one week, two weeks and three weeks ahead.

The model builds upon an earlier one by Leroy and Wheeler (2008) by adding new predictors that represent the state of the large-scale climate system, in particular, the influence of ENSO, the Indian Ocean Dipole and the Modoki structure[44] of ENSO events. Another enhancement is the model's capacity to represent the forecasts in the form of spatial maps for the Southern Hemisphere, whereas the prior scheme forecast only a single number for the probability of a cyclone anywhere in the South-east Indian Ocean. The new scheme presents the forecast probabilities as maps based on forecasts at grid-points located 7.5 degrees latitude and 10 degrees longitude apart across the South Indian and South Pacific oceans.

The model is a statistical (logistical regression) model, whereby the large-scale parameters as used as 'predictors' to determine the probability of a cyclone occurring in the coming seven days, 8 to 14 days and 15 to 21 days ahead. Six large-scale variables are used as predictors. Two measure the state of the Madden-Julian Oscillation. Three are indices of the state of large-scale tropical interannual variability.[45] The final predictor measures the climatological seasonal cycle of TC activity.

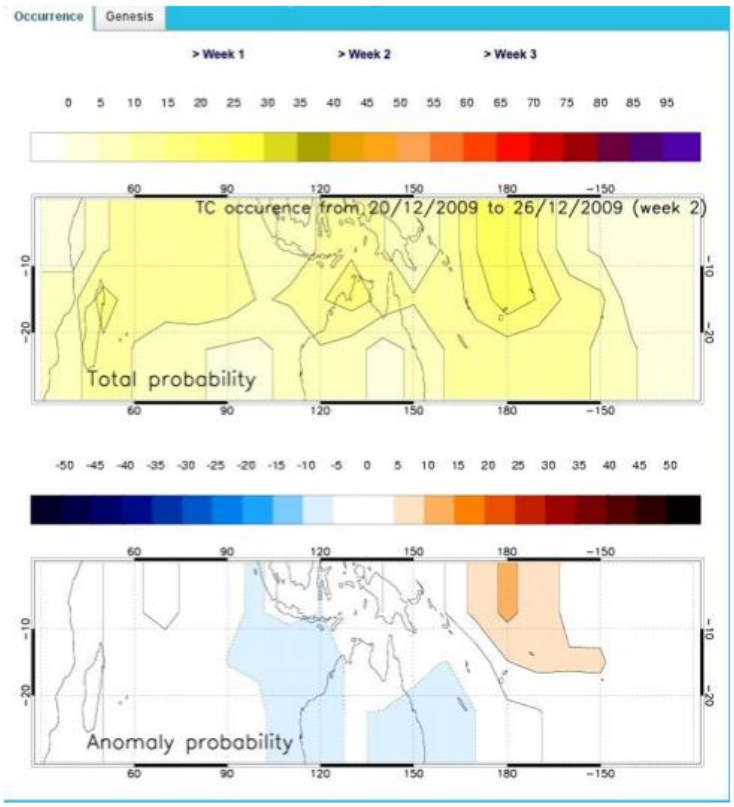

Figure 6.4 Sample forecast for tropical cyclone activity screen captured from the MeteoFrance website. Upper panel is the forecast probability of occurrence for a period from eight to 14 days into the future from the time the forecast was issued. Lower panel shows the deviation of the forecast from one obtained simply by use of the primary predictor: daily climatology. The coloured shading represents different probability levels as denoted by the keys.

The maps (Figure 6.4) show the forecasted probability of at least one TC occurring. Forecasts are presented in terms of the probability of a TC occurring at that location. A lower separate panel shows how the forecast is different from climatology as measured by the output of a simpler model, which uses only the climatological seasonal cycle as a predictor.

[44] See glossary for an explanation of Modoki structure.

[45] NINO3.4, the Trans-Nino index and the Indian Dipole Mode index.

In the example given, the yellow shading shows that for most of the region the probability that a TC will occur at each location in the next eight to 14 days from the issuing of the forecast is between 5% and 30%. The contours show higher probabilities (near 30 %) around the vicinity of the dateline (the Fiji region) in the South Pacific. Looking at the lower panel, the probabilities are increased relative to climatology in that region (the brown shading). This is due to the phase of the Madden-Julian Oscillation.

The forecasts from this new model are operational on the webpage of MeteoFrance at:

www.meteo.nc/espro/previcycl/cyclA.php

Skill scores and reliability diagrams for the forecast model are available at that site and verification for the forecasts each season is ongoing. Vitart et al. (2010) compared the forecast skill with that of the European Centre for Medium-Range Weather Prediction operational Numerical Weather Prediction model. They found the statistical model (developed for IOCI3) has superior skill to the numerical forecasts for the second and third weeks of the forecast. Thus, the new IOCI statistical model represents the current 'state of the science' for a two-week TC forecast.

7 Implications of IOCI3 Research for Adaptation and Decision-Making

Drafting authors: Doerte Jakob, Agata Imielska, Pandora Hope and Kevin Keay

This chapter elaborates on the use of IOCI research to inform policymaking, a topic briefly touched upon in Chapter 1. It reports some examples of how IOCI3 scientists have applied their research to areas with relevance for policymaking and management. It also provides specific examples on the use of IOCI climate science information for management decisions in a range of Western Australian Government sectors.

7.1 Applied Research within IOCI3

This section provides examples of how IOCI3 scientists have carried out applied research to address issues related to climate risk and climate change adaptation.

7.1.1 SECTOR-RELEVANT CLIMATOLOGIES

Project Link: 1.4

IOCI3 scientists sought to develop climatologies of fire danger and heat stress. Analyses of fire danger focused on the Grassland Fire Danger Index, which combines meteorological information about temperature, wind speed and relative humidity whilst making assumptions about fuel load and curing. The challenges IOCI3 scientists face regarding wind speed calculations are discussed further below.

As for climatologies of heat stress, these were developed on the basis of gridded temperature data and compared to analyses of station data. Two measures are used: the first describes the human capability to adjust to heat (acclimatisation index); the second describes how unusual the heat experienced is, from a climatological perspective (Nairn et al. 2009). These measures were combined to form the Integrated Excess Heat Factor. The annual climatologies of this factor show regional and strong interannual variability.

A climatology of heat stress (1961 to 1990) is provided in Figure 7.1. It shows that the west coast and south parts of Western Australia experience higher Integrated Excess Heat Factor values, while tropical areas tend to experience lower values (i.e., lower heat stress). A comparison of a strong El Niño and strong La Niña event (1997/98 and 1999/00 respectively – Figure 7.1) shows high Integrated Excess Heat Factor values during the El Niño event and low heat stress during the La Niña event across much of Western Australia. Heat stress during the 1974/75 strong La Niña has a different pattern from the 1999/00 event, with high Integrated Excess Heat Factor values across the west coast and southern Western Australia.

Knowledge gap and future directions

Regarding the Grassland Fire Danger Index, IOCI3 scientists identified that the inherent sensitivity of this index to estimates of wind speed was a major challenge to producing meaningful climatologies. Establishing local wind speeds with the required degree of accuracy poses a major challenge (Lucas 2010, Jakob 2010). Further work is proposed to develop techniques to optimally combine surface observations and model data.

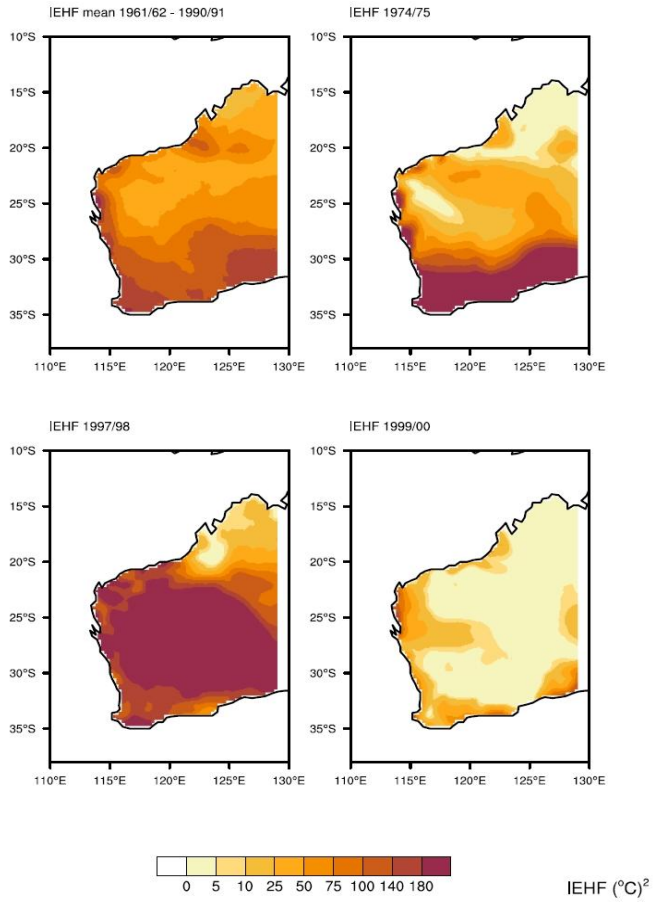

Figure 7.1 Integrated Excess Heat Factor (in $°C^2$) for Western Australia. The total annual value (based on a 30-year reference period) is shown in the top left panel. Examples for the pattern of annual Integrated Excess Heat Factor are shown for two strong La Niña events (right column; top refers to the 1974/75 event and bottom to 1999/00) and a strong El Niño (1997/8) event (bottom left). The calculation of annual values is based on the 12-month period from July to June.

7.1.2 APPLICATION OF SELF-ORGANISING MAPS TO LOW PUERULUS RETURNS

Project Link: 2.1

IOCI3 scientists applied the self-organising map method to examine potential climate-related causes of low returns of puerulus (the larvae of western rocklobster, *Panulirus cygnus*). These low return rates lead, in turn, to low recruitment of rock lobsters for this economically valuable fishery, making this an important natural resource management issue for Western Australia.

IOCI3 scientists collaborated with those from the Western Australian Marine Science Institution (Ming Feng, Evan Weller and Nick Caputi) in order to apply their analysis and results in the most informed and informative way. The shared goal was to understand the association between particular weather systems and variability in the number of late larval-stage lobsters settling on inshore reefs along Western Australia's west coast each year.

The 'puerulus settlement index' (i.e., the abundance of settling puerulus) correlates strongly with lobster catches three and four years later. The puerulus settlement during the 2008/09 West Coast Rock Lobster season was the lowest in the 40-year time series of puerulus collections at Dongara and Jurien. Higher strength of the Leeuwin Current is conducive to a good settlement rate, as are strong onshore winds; other factors such as water temperatures are also important (Caputi et al. 2001). However, during the record low settlement year of 2008/09 the Leeuwin Current was relatively strong. Were weather conditions unusual that year, and have such weather conditions been present in other years with poor settlement rates?

Western Australian Fisheries staff are exploring these questions from many angles. They were keen to apply IOCI3 results to address these questions. They provided guidance to IOCI3 scientists on the optimum time of year to focus their inquiry. This led IOCI3 scientists to re-apply their methods to try to determine whether certain weather states have dominated during these low-return years.

A self-organising map was constructed to identify the dominant synoptic types throughout the key months of interest: July to December. Reanalysis data for mean sea-level pressure (1948 to 2010) at 14:00 hours. Each day was used to define a continuum of 35 map types (Figure 7.2). A relatively high number of types is included in this self-organising map (i.e., compared to that for the June and July season described in Section 4.1) because it covers six months, and encompasses weather systems indicative of winter, spring and summer.

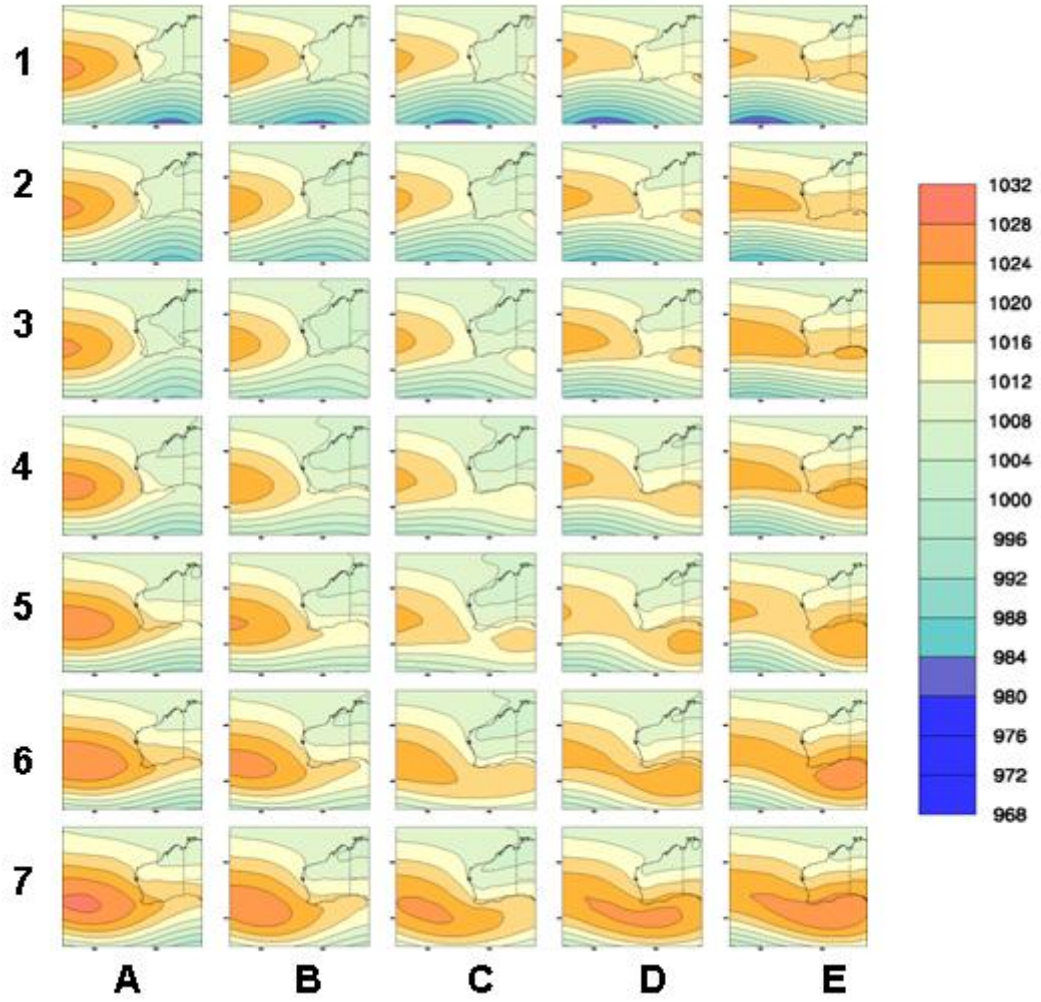

Figure 7.2 Self-organising map of 14:00 hours (WST) mean sea level pressure for the synoptic (weather) types during the July to December half-year over the period 1948 to 2010. Blue shades indicate low pressure, while orange shades indicate high pressure.

The self-organising map in Figure 7.2 shows that a full range of synoptic types occur over this half of the year. These range from deep low-pressure systems (most evident in the top two rows of the figure) to bands of very high pressure (bottom rows). Maps illustrating the composite of winds associated with each weather type were also produced. The vectors in the region of the southern west coast are predominantly onshore, except for the weather types in the bottom right corner of the self-organising map (Figure 7.2). The latter are types with offshore flow (e.g., types D7 and E7). These types with offshore wind flows were the most numerous, relative to other types, in 2008, and again in 2010. The wind anomaly for type E7 is

shown in Figure 7.3, illustrating an offshore flow that is clearly evident along the west coast. This type occurred predominantly in August in 2008.

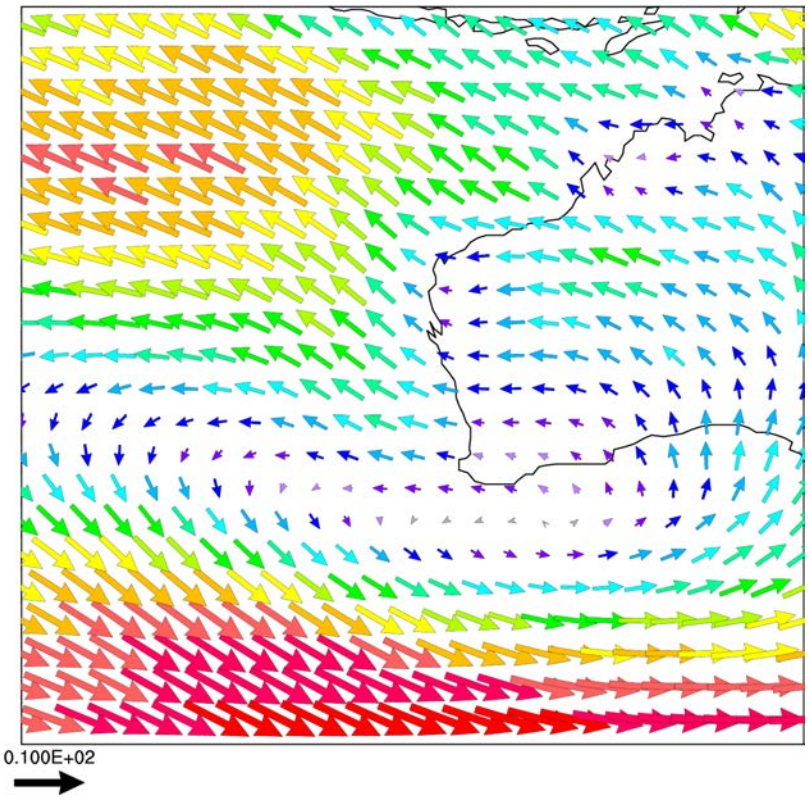

Figure 7.3 Wind anomaly associated with lower puerulus settlements. Arrows indicate wind direction and strength (larger red arrows = stronger winds). This figure illustrates the composite winds for synoptic type E7 from the bottom right of the SOM, for which an offshore flow along the west coast is clearly evident.

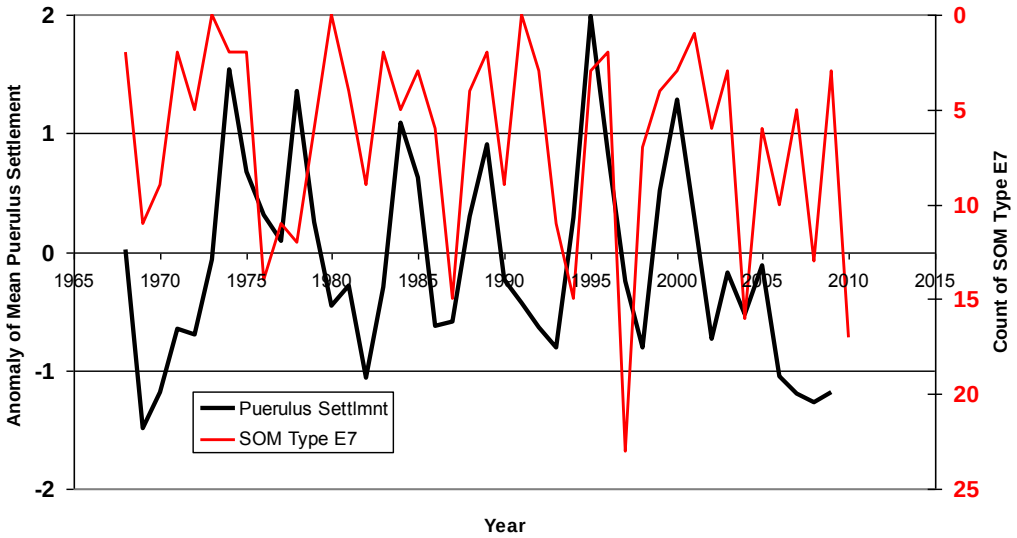

Figure 7.4 Puerulus settlement anomaly and wind anomaly type E7 over time. Standardized annual puerulus settlement from Evan Weller, CSIRO (in black, scale on left axis); number of occurrences of synoptic type E7 (in red, reversed scale on right axis).

Data on standardised annual puerulus settlement was then compared with the weather types of the self-organising map to test for associations. The series for type E7 correlated negatively with settlement (at r=-

0.25, significant at the 90% level). That is, a greater occurrence of this weather type tended to be associated with lower puerulus settlement. The offshore winds represented by synoptic type E7 are thought to create weather conditions that make it more difficult for pueruli to return. Figure 7.4 shows that type E7 had a high occurrence in 2008 (note that the scale is reversed) and this likely contributed to the low settlement rates in that year; however, Figure 7.4 also shows this synoptic type did not have a high occurrence in 2009. Thus the association is not a simple one, and depends on the months throughout the season when these systems dominate and a host of oceanic and population factors as well.

IOCI3 scientists are collaborating with Western Australian Department of Fisheries staff to examine the weather regimes in other years – those with both poor and excellent puerulus settlement rates – to explore more fully the range of possible weather drivers behind low settlement rates in recent years.

7.2 How IOCI research is used in policy and management

Many fields of policy must plan for future action that is based on fundamental assumptions about the climate. The best available climate science information can help inform such policy and thereby facilitate the efficient use of resources.

This section provides specific examples of how IOCI research has been taken up to guide climate adaptation. As noted in Section 1.2.2, IOCI has informed policy in areas related to water, fisheries, agriculture, health and emergency services, and IOCI3 work on NWWA is expected to have relevance for decision making in the mining and petroleum sectors. Many of these examples are drawn from a recent report on IOCI by the independent consultants ACIL Tasman (2011). Although it is impossible to ascertain the total policy uptake of IOCI science, this report found that evidence collected from stakeholders pointed to 'significant uptake'.

IOCI has influenced crucial decisions to secure alternative water sources for Perth in response to SWWA's drying trend. IOCI 1 and 2 showed that the drying was not temporary or cyclical – hastening and strengthening the case for a desalination plant. It also informed the decision by the Western Australian Government in July 2011 to approve a $450 million expansion of SWWA's second desalination plant to meet the region's urgent need for a new water source.

The Department of Water also uses IOCI data extensively when de-rating[46] water sources based upon rainfall projections for SWWA. As noted in Section 2.2, statistical downscaling techniques developed under IOCI have been used by the Department of Water to assess water supply vulnerability to climate change (Bates et al. 2010 and Charles et al. 2007) and to help quantify the uncertainties in climate change projections of groundwater recharge (Crosbie et al. 2011). More recently, the Department of Water has used IOCI data to inform its recommendations on aspects of forestry-related to catchment management (i.e., how dense forest cover should be on lands rehabilitated after mining activities).

In the agriculture sector, IOCI has assisted the Department of Agriculture and Food to understand, under future climate scenarios, which land uses would best suit different parts of Western Australia. The Department passes this advice onto farmers to inform their investment decisions. Information from IOCI has also indicated that some areas in SWWA will, in future, no longer be too wet for crops. Knowing that these areas will be just dry enough in future has been a factor behind the Department of Agriculture and Food's research on crops that can be sustained in relatively wet areas.

The Department of Mines and Petroleum uses IOCI research to inform mine safety and environmental regulation. This Department has been involved with the IOCI since its first stage. However, IOCI3 work in NWWA, where major mining and energy infrastructure is located, is expected to provide information with particular relevance to this sector. For example, local rainfall information helps determine the best location for mine tailings dams by helping to gauge whether they could be breached (and thereby release

[46] Downgrading expected long-term average inflow.

pollutants). Rainfall information from IOCI can indicate whether mines would have sufficient drainage, and whether infrastructure for power, water, gas and transport (roads, rail and ports) may withstand likely weather scenarios.

The Department of Health needs to know how future temperature and rainfall changes may influence public health through the rise of new disease vectors (e.g., Ross River virus) or by causing bushfires or other emergencies to become more frequent. Along with the Fire and Emergency Services Authority**,** this Department relies on IOCI climate scenarios to allow it to develop appropriate strategies and policies for the future. For example, baseline climate information from IOCI underpinned the development of the Department's 2007 publication, Health Impacts from Climate Change.

Glossary

Aerosols - A collection of airborne solid or liquid particles, with a typical size between 0.01 and 10 micrometer (a millionth of a meter) that reside in the atmosphere for at least several hours. Aerosols may be of either natural or anthropogenic origin. Aerosols may influence climate in several ways: directly through scattering and absorbing radiation, and indirectly through acting as cloud condensation nuclei or modifying the optical properties and lifetime of clouds. (Source: IPCC 4th Assessment Report, WG 1 Glossary.)

Anomaly - In the field of meteorology, an anomaly refers to the departure of an element, such as monthly maximum temperature, from its long-period average value at the location concerned. For example, if Perth's maximum temperature for June was 1 ˚C higher than the long-term average for this month, this would be an anomaly +1 ˚C.

Antarctic Oscillation (AAO) - See Southern Annular Mode.

Anthropogenic - Resulting from or produced by humans.

Coupled Model Intercomparison Project (CMIP) - A standard experimental protocol, established under the World Climate Research Programme, for studying the output of global climate models. Since 1995 CMIP has provided the scientific community with infrastructure to systematically analyse these models, thereby facilitating their improvement. CMIP5 will provide model simulations for the IPCC's Fifth Assessment Report; CMIP3 facilitated the modelling that fed into the IPCC's (2007) Fourth Assessment Report. See: cmip-pcmdi.llnl.gov

Closed low (weather system): A low-pressure region with a distinct centre of cyclonic circulation and completely encircled by one or more isobars. Closed lows aloft may be partially or completely disconnected from the primary westerly current, and thus progress eastward more slowly.

CSIRO - Conformal-Cubic Atmospheric Model (CCAM) - A variable resolution global climate model developed by CSIRO. An advantage of CCAM is that while it can perform broad-scale modelling, its grid can be 'stretched' or 'nudged' to provide simulations at finer scales (down to ten kilometres or less) to focus on small regions of interest and provide local-scale climate projections. CCAM can also be used to dynamically downscale global climate models to higher resolutions. It also has the ability correct some of the biases (in sea surface temperatures) from the GCMs before downscaling. Output from CCAM simulations for other projects were used as inputs to projects under IOCI3.

El-Niño Southern Oscillation (ENSO) - ENSO is the oscillation between El Niño and La Niña conditions. El Niño refers to the extensive warming of the central and eastern tropical Pacific Ocean that leads to a major shift in weather patterns across the Pacific every three to eight years. El Niño conditions generally result in below-average rainfall over much of eastern Australia. La Niña, the opposite phase, is associated with cooler than average sea surface temperatures in the central and eastern tropical Pacific Ocean, conditions that generally result in above-average rainfall over much of Australia.

Forcing - More accurately, 'radiative forcing', denotes 'an externally imposed perturbation in the radiative energy budget of the Earth's climate system,' according to the IPCC, and 'radiative forcing is a simple measure for both quantifying and ranking the many different influences on climate change...' Forcing agents – the driving forces for climate change – include greenhouse gases, aerosols, and changes in solar radiation, volcanic activity as well as changes in surface albedo, roughness and evaporation due to land use.

Generalised linear models - A widely-used class of statistical models that relate responses to linear combinations of predictor variables. They allow models to be fit to data that follow probability distributions other than the normal distribution, such as the Poisson distribution. This is an attractive approach because it provides a general theoretical framework and unified approach for many commonly encountered statistical models and procedures.

Generalised extreme value - see Box 5, Technical Report.

Homogenised / homogenisation - The degree of consistency in a record over time is often referred to as 'data homogeneity'. Several factors can introduce changes in the data (as a function of time) that are not related to physical changes in climate. Such changes are referred to as 'inhomogeneities'. The detection and correction for these artificial changes is termed 'homogenisation'.

Hadley circulation - Also called Hadley cell circulation; essentially a large-scale north-south (meridional) atmospheric circulation. Warm air rises at the equator, then travels in the upper atmosphere toward the poles, where it descends. Some of the descending air travels along the surface toward the equator as part of the trade winds, closing the loop.

High-Latitude Mode - See Southern Annular Mode.

Indian Ocean Dipole (IOD) - A couple ocean-atmosphere phenomenon in the equatorial Indian Ocean that affects the climate of Australia. It is commonly measured by an index that is the difference between sea surface temperature in the western and eastern equatorial Indian Ocean. Positive IOD periods are characterised by cooler than normal tropical eastern Indian Ocean water, and warmer than normal tropical western Indian Ocean water. This pattern is associated with a decrease in rainfall over parts of central and southern Australia. The opposite pattern prevails during negative IOD periods, which are associated with increased rainfall over parts of southern Australia. (Source: Australian Bureau of Meteorology.)

Intergovernmental Panel on Climate Change (IPCC) - Established by the United Nations Environment Programme and the World Meteorological Organization, the IPCC is the leading international body for the assessment of the scientific, technical and socio-economic information relevant for the understanding of the risk of human-induced climate change. See: www.ipcc.ch.

Jetstream - A flat, tubular current of air located in the tropopause, the area in the Earth's atmosphere located between the troposphere and the stratosphere. These powerful winds are generated by strong pressure gradients which reflect the great temperature differences at high altitudes. (Source: Australian Bureau of Meteorology.)

Madden-Julian Oscillation (MJO) - The major fluctuation in tropical weather on weekly to monthly timescales. The MJO can be characterized as an eastward moving 'pulse' of cloud and rainfall near the equator that typically recurs every 30 to 60 days. (Source: Australian Bureau of Meteorology.)

Modoki structure (of ENSO events) - The traditional El Niño event has become less frequent and a different kind of El Niño (the El Niño Modoki) more common during the late twentieth century. The El Niño Modoki is associated with warm sea surface temperatures in the central Pacific, straddled on the east and west by cooler sea surface temperatures. The regional climate impacts of El Niño Modoki episodes are distinct from the traditional El Niño events.

Monsoon - A seasonal wind. The northern Australian monsoon season generally lasts from December to March. It is associated with the inflow of moist west to north-westerly winds into the monsoon trough, producing convective cloud and heavy rainfall over northern Australia. These moisture-laden winds originate from the Indian Ocean and southern Asian waters. The north Australian wet season encompasses the monsoon months but can extend several months on either side. (Source: Australian Bureau of Meteorology.)

Poisson distribution - In probability theory or statistics, the Poisson distribution is used to establish the distribution of rare events (events with small numbers). It specifies the likelihood of a given count, such as the likely number of hot spell occurrences, during one period of observation, predicting the degree of spread around a known average rate of occurrence.

Generalised Pareto distribution - The generalised Pareto distribution is used to provide a good fit to extremes of complicated data, and is often used to model the tails of another distribution. This makes it useful for the modelling of extreme events such as hot spells.

Regional climate model (RCM) - Regional planning often requires information at much finer spatial scales than provided by the coarse resolution of global climate models. One possible solution is to embed a regional climate model in the global climate model. Regional climate models work to increase the resolution of the global climate model in a small area of interest, down to scales of 50 or 25 km. (See also spatial downscaling, Box 1, Technical Report). The global climate model is used to determine the large-scale effects on global climate. Its outputs (e.g., for temperature or wind) are used as inputs for the regional climate model, which can resolve the local impacts because it contains small-scale information, such land height and land use.

Southern Annular Mode (SAM) - Also known as the Southern Hemisphere Annular Mode or Antarctic Oscillation. This mode of climate variability can affect rainfall in southern Australia. It refers to the north/south movement of a belt of strong westerly winds associated with storm systems. During a 'positive' SAM event, this belt of strong westerly winds contracts toward the south pole; during a 'negative' SAM event the strong westerly winds expand toward the equator, resulting in more storm systems over southern Australia. (Source: Australian Bureau of Meteorology.)

Special Report on Emissions Scenarios (SRES) - see Box 3, Technical Report.

Synoptic scale meteorology - That primarily concerned with the observation of large-scale weather systems, generally on the scale of 1000 km or more.

Synoptic Typing - The classification of synoptic weather systems (i.e., large-scale features of the lower atmosphere such as the highs and lows over mid-latitude regions).

Return level & **Return period** - Terms used to describe the probability (likelihood) of extreme events such as floods, storms or earthquakes. For example, the term '1-in-100 year storm' describes a major event of a magnitude or intensity (the return level) only likely to occur once every 100 years (the return period). See also Box 5, Technical Report.

Projection: A projection is a statement about the response of the climate system to emission or concentration scenarios of greenhouse gases and aerosols, or radiative forcing scenarios, often based upon simulations by climate models. Climate projections depend upon the scenarios used, which are based on assumptions concerning, for example, future socioeconomic and technological developments. These assumptions may or may not be realized and are therefore subject to substantial uncertainty. (Source: IPCC 4th Assessment Report, WG 1 Glossary.)

Teleconnection - In atmospheric science, a teleconnection refers to the linkages over great distance of seemingly disconnected climate anomalies.

References

Abbs D., 2012: The impact of climate change on the climatology of tropical cyclones in the Australian region. CSIRO Climate Adaptation Flagship Working Paper No. 11. Available from http://www.csiro.au/en/Organisation-Structure/Flagships/Climate-Adaptation-Flagship/CAF-working-papers.aspx

ACIL Tasman, 2011: An Assessment of the Indian Ocean Climate Initiative. Final Report to the Department of Environment and Conservation, June 2011.

Allan, R., and T. J. Ansell, 2006: A new globally complete monthly historical gridded mean sea level pressure dataset (HadSLP2): 1850-2004. Journal of Climate, 19, 5816-5842.

Arblaster, J. M., G. A. Meehl, and D. J. Karoly, 2011: Future climate change in the Southern Hemisphere: Competing effects of ozone and greenhouse gases. Geophysical Research Letters, 38, L02701, doi:10.1029/2010GL045384.

Bates, B. C., P. Hope, B. Ryan, I. Smith, and S. Charles, 2008: Key findings from the Indian Ocean Climate Initiative. Climatic Change, 89, 339-354.

Bates, B. C., R. E. Chandler, S. P. Charles, and E. P. Campbell, 2010: Assessment of apparent non-stationarity in time series of annual inflow, daily precipitation and atmospheric circulation indices: A case study from southwest Western Australia. Water Resources Research, doi:10.1029/2010WR009509.

Boucher, O., M. Collier, J. -L. Dufresne, P. Forster, J. Haywood, S. Jeffrey, A. Jones, U. Lohmann, P. Rasch, L. Rotstayn, B. Stevens, K. Taylor, and K. von Salzen, 2011: Climate response to aerosol forcings in CMIP5, CLIVAR Exchanges, 56, 25–27.

Bureau of Meteorology and CSIRO, 2007: Climate Change in Australia. Technical Report, Commonwealth Scientific and Industrial Research Organisation, 148. (http://www.climatechangeinaustralia.gov.au)

Cai, W. J., and I. G. Watterson, 2002: Modes of interannual variability of the southern hemisphere circulation simulated by the CSIRO climate model. Journal of Climate, 15, 1159-1174.

Cai, W. J., G. Shi, and Y. Li, 2005: Multidecadal fluctuations of winter rainfall over southwest Western Australia simulated in the CSIRO Mark 3 coupled model. Geophysical Research Letters, 32, L12701.

Cai, W., P. vav Rensch, S. Borlace, and T. Cowan, 2011a: Does the Southern Annular Mode contribute to the persistence of the multidecade-long drought over southwest Western Australia? Geophysical Research Letters, 38, doi:10.1029/2011GL047943

Cai, W., T. Cowan, A. Sullivan, J. Ribbe, and G. Shi, 2011b: Are anthropogenic aerosols responsible for the northwest Australia summer rainfall increase? A CMIP3 perspective and implications, Journal of Climate, 24, 2556–2564, doi:10.1175/2010JCLI3832.1.

Caputi, N., C. Chubb, and A. Pearce, 2001: Environmental effects on recruitment of the western rock lobster, Panulirus cygnus. Australian Marine and Freshwater Research, 52, 1167-1174.

Charles, S. P., B. C. Bates, P. H. Whetton, and J. P. Hughes, 1999a: Validation of a downscaling model for changed climate conditions in southwestern Australia. Climate Research, 12(1), 1-14.

Charles, S. P., B. C. Bates, and J. P. Hughes, 1999b: A spatio-temporal model for downscaling precipitation occurrence and amounts. Journal of Geophysical Research, 104, 31657-31669.

Charles, S. P., M. A. Bari, A. Kitsios, and B. C. Bates, 2007: Effect of GCM bias on downscaled precipitation and runoff projections for the Serpentine catchment, Western Australia. International Journal of Climatology, 27, 1673-1690.

Clarke, L., J. Edmonds, H. Jacoby, H. Pitcher, J. Reilly, and R. Richels, 2007: Scenarios of Greenhouse Gas Emissions and Atmospheric Concentrations, Sub-report 2.1A of Synthesis and Assessment Product 2.1, Department of Energy, Washington, DC., USA, 154 pp.

Collier, M. A., S. J. Jeffrey, and L. D. Rotstayn, 2011: The latest Australian CMIP climate model submission, Bulletin of the Australian Meteorological and Oceanographic Society, 24, 104-108

Coles, S. G., 2001: An Introduction to Statistical Modelling of Extreme Values. Springer-Verlag, London Limited.

Corney S. P., J. J. Katzfey, J. L. McGregor, M. R. Grose, J. C. Bennett, C. J. White, G. K. Holz, S. M. Gaynor, and N. L. Bindoff, 2010: Climate Futures for Tasmania: Climate Modelling Technical Report. Antarctic Climate & Ecosystems Cooperative Research Centre, Hobart, Tasmania. Available online: www.dpac.tas.gov.au/divisions/climatechange/adapting/climate_futures/climate_futures_for_tasmania_reports.

Crosbie, R. S., W. R. Dawes, S. P. Charles, F. S. Mpelasoka, S. Aryal, O. Barron, and G. K. Summerell, 2011: Differences in future recharge estimates due to GCMs, downscaling methods and hydrological models. Geophysical Research Letters, 38, L11406.

CSIRO & BoM, 2012: State of the Climate 2012. Available at: http://www.bom.gov.au/announcements/media_releases/ho/stateClimate2012.pdfs

Dare, R.A., and J. L. McBride, 2011a: The threshold sea surface temperature condition for tropical cyclogenesis. Journal of Climate, 24, 4570-4576.

Dare, R. A., and J. L. McBride, 2011b: Sea surface temperature response to tropical cyclones. Monthly Weather Review, 139, 3798–3808.

Dare, R.A., N. E. Davidson, and J. L. McBride, 2012: Tropical cyclone contribution to rainfall over Australia. Monthly Weather Review. http://dx.doi.org/10.1175/MWR-D-11-00340.1

Farre, I., and I. Foster, 2009: Wheat yields and future climate in Western Australia, Climate 21 Workshop Paper, Perth, Australia, 5pp. www.agric.wa.gov.au/PC_94107.html?s=1226046262

Feng J, L. Li, and Y. Li, 2010: A monsoon-like Southwest Australian circulation and its relation with rainfall in Southwest Western Australia. Journal of Climate, 23, 1334-1353.

Feng, J., J. P. Li, and Y. Li, 2010: Is there a relationship between the SAM and southwest Western Australian winter rainfall? Journal of Climate, 23, 6082-6089.

Fischer, M. J., and P. C. Treble, 2008: Calibrating climate-δ18O regression models for the interpretation of high-resolution speleothem δ18O time series. Journal of Geophyscial Research, 113, D17103.

Fowler, H. J., S. Blenkinsop, and C. Tebaldi, 2007: Linking climate change modelling to impacts studies: recent advances in downscaling techniques for hydrological modelling. International Journal of Climatology, 27, 1547-1578.

Frederiksen, J. S., and C .S. Frederiksen, 2005: Decadal Changes in Southern Hemisphere Winter Cyclogenesis. CSIRO Marine and Atmospheric Research Paper No. 002, 35pps.

Frederiksen, J. S., and C. S. Frederiksen, 2007: Inter-decadal changes in Southern Hemisphere winter storm track modes. Tellus, 59 A, 559-617.

Frederiksen, C. S., and X. Zheng, 2007: Coherent Structures of Interannual Variability of the Atmospheric Circulation: The Role of Intraseasonal Variability. Frontiers in Turbulence and Coherent Structures, World Scientific Lecture Notes in Complex Systems, Vol. 6, Eds Jim Denier and Jorgen Frederiksen, World Scientific Publications, 87-120.

Frederiksen, C. S., S. Grainger, and X. Zheng, 2008: A Method for Estimating the Potential Long-range Predictability of Precipitation over Western Australia. ANZIAM Journal, 50, C569-C583. http://anziamj.austms.org.au/ojs/index.php/ANZIAMJ/article/view/1411

Frederiksen, C. S., J. S. Frederiksen, and S. L. Osbrough, 2009a: Simulations of twentieth century atmospheric circulation changes over Australia. MODSIM, 9, 2555-2561. (http://mssanz.org.au/modsim2009/frederiksen_c.pdf)

Frederiksen, J. S., C. S. Frederiksen, and S. L. Osbrough, 2009b: Modelling of changes in Southern Hemisphere weather systems during the 20th century. MODSIM, 9, 2562-2568. (http://mssanz.org.au/modsim2009/frederiksen_j.pdf)

Frederiksen, J. S., C. S. Frederiksen, S. L. Osbrough, and J. M. Sisson, 2010: Causes of changing Southern Hemispheric weather systems. Chapter 8, Managing Climate Change, Eds. I. Jupp, P. Holper and W. Cai, CSIRO publishing, pp 85-98.

Frederiksen, J. S., and C. S. Frederiksen, 2011: Twentieth century winter changes in Southern Hemisphere synoptic weather modes. Advances in Meteorology, Article ID 353829, 16pp, doi:10.1155/2011/353829.

Frederiksen, C. S., J. S. Frederiksen, J. M. Sisson, and S. L. Osbrough, 2011a: Changes and projections in Australian winter rainfall: Anthropogenic forcing and internal variability. International Journal of Climate Change: Impacts and Responses, 2, 143-162.

Frederiksen, C. S., J. S. Frederiksen, J. M. Sisson, and S. L. Osbrough, 2011b: Australian winter circulation and rainfall changes and projections. International Journal of Climate Change Strategies and Management, 3, 170-188.

Frederiksen, C. S., J. S. Frederiksen, J. M. Sisson, and S. L. Osbrough, 2011c: Observed and projected changes in the annual cycle of Southern Hemisphere storm formation. MODSIM, 11, 2719-2725. (http://mssanz.org.au/modsim2011/frederiksen2.pdf)

Frederiksen, J. S., C. S. Frederiksen, J. M. Sisson, and S. L. Osbrough, and J. M. Sisson 2011d: Changes in Southern Hemisphere rainfall, circulation and weather systems. MODSIM, 11, 2712-2718. (http://mssanz.org.au/modsim2011/frederiksen.pdf).

Furrer, E. M., R. W. Katz, M. D. Walter, and R. Furrer, 2010: Statistical modeling of hot spells and heat waves. Climate Research, 43, 191-205.

Gosling, S. N., J. A. Lowe, G. R. McGregor, M. Pelling, and B. D. Malamud, 2009: Associations between elevated atmospheric temperature and human mortality: A critical review of the literature. Climatic Change, 92, 299-341, doi 10.1007/s10584-008-9441-x.

Grainger, S., Frederiksen C. S., and Zheng X., 2008: Estimating the Potential Predictability of Western Australian Surface Temperature using Monthly Data. ANZIAM Journal, 50, C598-C609. http://anziamj.austms.org.au/ojs/index.php/ANZIAMJ/article/view/1414

Grainger, S., C.S. Frederiksen, X. and Zheng, 2009: Estimating the Potential Predictability of Australian Surface Maximum and Minimum Temperature. Climate Dynamics, 32, 443-455, doi 10.1007/s00382-008-0506-3.

Hendon, H., D. W. J. Thompson, and M. C. Wheeler, 2007: Australian rainfall and surface temperature variations associated with the Southern Hemisphere Annular Mode. Journal of Climate, 20, 2452-2467.

Hope, P. K., 2006: Projected future changes in synoptic systems influencing southwest Western Australia. Climate Dynamics, 26, 765-780.

Hope, P. K., W. Drosdowsky, and N. Nicholls, 2006: Shifts in synoptic systems influencing south west Western Australia. Climate Dynamics, 26, 751-764.

Hope, P., and C. J. Ganter, 2010: Recent and projected rainfall trends in south-west Australia and the associated shifts in weather systems. Chapter 5, Managing Climate Change, Eds. I. Jupp, P. Holper and W. Cai, CSIRO Publishing, pp 53-63.

Hope, P., and K. Keay, 2012: Circulation drivers of cooling in southwest Australia. Submitted to Climate Dynamics

IOCI Report, 2002: Climate Variability and Change in South West Western Australia. Indian Ocean Climate Initiative Panel, Perth, November, 2002, 34pp.

IPCC, 2007: Summary for Policy Makers. In: Climate Change 2007: The Physical Science Basis. Contribution of Working Group I to the Fourth Assessment Report of the Intergovernmental Panel on Climate Change, S. Solomon, D. Qin, M. Manning, Z. Chen,

Jiang, H., and E. J. Zipser, 2010: Contribution of tropical cyclones to the global precipitation from eight seasons of TRMM data: Regional, seasonal, and interannual variations. Journal of Climate, 23, 1526-1543.

Jones, D. A., W. Wang, and R. Fawcett, 2009: High-quality spatial climate data-sets for Australia. Australian Meteorological and Oceanographic Journal, 58, 233-248.

Jakob, D., 2010: Challenges in developing a high-quality surface wind-speed data-set for Australia. Australian Meteorological and Oceanographic Journal, 60, 227-236.

Jovanovic, B., D. Collins, K. Braganza, D. Jakob, and D. Jones, 2010: A high-quality monthly total cloud amount dataset for Australia, Climatic Change, 108, 485-517.

Kang, S. M., L. M. Polvani, J. C. Fyfe, and M. Sigmond, 2011: Impact of polar ozone depletion on subtropical precipitation, Science, 332, 951–954, doi:10.1126/science.1202131.

Kirshner, S., 2005: Modeling of multivariate time series using hidden Markov models, PhD Thesis, University of California, 202pp.

Knapp K. R., M. C. Kruk, D. H. Levinson, and E. J. Gibney, 2009: Archive compiles new resource for global tropical cyclone research. EOS, Transactions AGU, 90, 46, doi:10.1029/2009EO060,002.

Knutson, T. R., J. J. Sirutis, S. T. Garner, G. A. Vecchi. and I. M. Held, 2008: Simulated reduction in Atlantic hurricane frequency under twenty-first-century warming conditions. Nature Geoscience, 1, 359-364.

Knutson, T. R., J. McBride, J. Chan, K. A. Emanuel, G. Holland, C. Landsea, I. Held, J. Kossin, A. K. Srivastava, and M. Sugi, 2010: Tropical cyclones and climate change. Nature Geoscience, 3, 157-163. doi:10.1038/ngeo779.

Kohonen, T., 2001: Self-Organising Maps. 3rd ed., Springer-Verlag, Berlin-Heidelberg.

Kuleshov, Y., R. Fawcett, L. Qi, B. Trewin, D. Jones, J. McBride, and H. Ramsay, 2010a: Trends in tropical cyclones in the South Indian Ocean and the South Pacific Ocean, Journal of Geophysical Research, 115, D01101, doi:10.1029/2009JD012372.

Kuleshov, Y., L. Qi, D. Jones, R. Fawcett, F. Chane-Ming, J. McBride, and H. Ramsay, 2010b: On Developing a Tropical Cyclone Archive and Climatology for the South Indian and South Pacific Oceans. In: Indian Ocean Tropical Cyclones and Climate Change, 4, 189-197, doi:10.1007/978-90-481-3109-9_23 Springer, Netherlands.

Lavender, S. L., and K. J. E. Walsh, 2011: Dynamically downscaled simulations of Australian region tropical cyclones in current and future climates. Geophysical Research Letters, 38, L10705, doi:10.1029/2011GL047,499.

Lavery B., A. Kariko, and N. Nicholls, 1992: A historical rainfall data set for Australia. Australian Meteorological Magazine, 40, 33–39.

Le Quere, C., M. R., Raupach, J. G. Canadell, G. Marland, L. Bopp, P. Ciais, T. J. Conway, S. C. Doney, R. A. Feely, P. Foster, P. Friedlingstein, K. Gurney; R. A. Houghton, J. I. House, C. Huntingford, P. E. Levy, M. R. Lomas, J. Majkut, N. Metzl, J. P. Ometto, G. P. Peters, I. C. Prentice, J. T. Randerson, S. W. Running, J. L. Sarmiento, U. Schuster, W. Sitch, T. Takahashi, N. Viovy, G. R. Van Der Werf, and F. I. Woodward, 2009: Trends in the sources and sinks of carbon dioxide. Nature Geoscience, 2, 831-836

Leroy, A., and M. C. Wheeler, 2008: Statistical Prediction of Weekly Tropical Cyclone Activity in the Southern Hemisphere. Monthly Weather Review, 136, 3637–3654.

Li, Y., W. Cai, and E. P. Campbell, 2005: Statistical modeling of extreme rainfall in southwest Western Australia. Journal of Climate, 18, 852-863.

Li, Y., R. W. Katz, and R. Lau, In Preparation: Statistical modelling of hot spells in Western Australia, for Journal of Climate.

Lin, Z., and Y. Li, 2012: Remote influence of the tropical Atlantic on the variability and trend in North West Australia summer rainfall. Journal of Climate, 25, 2408-2420.

Lucas, C., 2010: On developing a historical fire weather data-set for Australia. Australian Meteorological and Oceanographic Journal, 60, 1-14.

Maraun, D., and Co-authors, 2010: Precipitation downscaling under climate change: Recent developments to bridge the gap between dynamical models and the end user. Reviews of Geophysics, 48, RG3003.

Marinelli, M., K. Braganza, D. Collins, D. Jones, S. Maguire, and G. Cook, 2012: Defining a high-quality daily rainfall candidate network for Western Australia. Australian Meteorological and Oceanographic Journal. Accepted for publication.

Marshall, G. J., 2003: Trends in the Southern Annular Mode from observations and reanalyses. Journal of Climate, 16, 4134-4143.

McBride, J. L., 1983: Australian tropical weather systems. In: Australian Conference on Tropical Meteorology, Melbourne, 24-25 March 1983, 7-9.

McBride, J. L., 2012: The Estimated Costs of Tropical Cyclone Impacts in Western Australia. An IOCI3 Technical Report. Available at: www.ioci.org.au/publications/ioci-stage-3/doc_download/120-the-estimated-cost-of-tropical-cyclone-impacts-in-western-australia.html

McBride, J. L., 2012: The Cost Impact of Tropical Cyclones on Western Australia. A Technical Report for the Indian Ocean Climate Initiative (IOCI) Stage 3.

McBride, J. L, H. A. Ramsay, and M. B. Richman, Submitted: Trend Analyses of Globally Consistent satellite-based estimates of tropical cyclone intensity. Geophysical Research Letters.

Meehl, G. A, and C. Tebaldi, 2004: More intense, more frequent, and longer lasting heat waves in the 21st century. Science, 305, 994–997.

Meehl, G. A., C. Covey, T. Delworth, M. Latif, B. McAvaney, J. F. B. Mitchell, R. J. Stouffer, and K. E. Taylor, 2007: The WCRP CMIP3 multimodel dataset: A new era in climate change research. Bulletin of the American Meteorological Society, 88, 1383-1394, doi:10.1175/BAMS-88-9-1383.

Nairn, J., R. Fawcett, and D. Ray, 2009: Defining and predicting excessive heat events, a national system. Understanding High Impact Weather, CAWCR Modelling Workshop, 30 Nov to 2 Dec, 2009.

Ng, B., 2010: Tropical Cyclones and Northwestern Australian Rainfall. Honours thesis. School of Earth Sciences, University of Melbourne

Nicholls, N., L. Chambers, M. Haylock, C. Frederiksen, D. Jones, and W. Drosdowsky, 1999: Climate Variability and Predictability for South-West Western Australia. Indian Ocean Climate Initiative. Research Report, 1-52.

Peng, B., S. Williams, M. Loughnan, G. Lloyd, A. Hansen, T. Kjellstrom, K. Dear, and A. Saniotis, 2011: The effects of extreme heat on human mortality and morbidity in Australia: Implications for public health. Asia Pacific Journal of Public Health, 23, 27S-36S.

Phatak, A., C. Chan, and H. Kiiveri, 2010: Fast variable selection for extreme values. Proceedings of 2010 International Congress on Environmental Modelling and Software, Ottawa, Canada, July, 2010.

Pook M. J., J. S. Risbey, and P. C. McIntosh, 2012: The synoptic climatology of cool-season rainfall in the central wheatbelt of Western Australia. Monthly Weather Review, 140, 28-43.

Powell, M. D., and T. A. Reinhold, 2007: Tropical cyclone destructive potential by integrated kinetic energy. Bulletin of the American Meteorological Society, 88, 513–526.

Randall, D.A., R. A. Wood, S. Bony, R. Colman, T. Fichefet, J. Fyfe, V. Kattsov, A. Pitman, J. Shukla, J. Srinivasan, R. J. Stouffer, A. Sumi, and K. E. Taylor, 2007: Climate models and their evaluation, in Climate Change 2007: The Physical Science Basis, in Solomon, S. et al. (Eds.) Contribution of Working Group I to the Fourth Assessment Report of the Intergovernmental Panel on Climate Change, Cambridge Univ. Press, Cambridge, U. K., pp. 589-662.

Raupach, M. R., P. R. Briggs, V. Haverd, E. A. King, M. Paget, and C. M.Trudinger, 2009; Australian Water Availability Project (AWAP): CSIRO Marine and Atmospheric Research Component: Final report for phase 3. Technical Report 013, Centre for Australian Weather and Climate Research.

Robinson, P., 2001: On the definition of a heat wave. Journal of Applied Meteorology, 40, 762-775.

Rotstayn, L. D., and U. Lohmann, 2002: Tropical rainfall trends and the indirect aerosol effect. Journal of Climate, 15, 2103–2116.

Rotstayn, L. D., W. Cai, M. R. Dix, G. D. Farquhar, Y. Feng, P. Ginoux, M. Herzog, A. Ito, J. E. Penner, M. L. Roderick, and M. Wang, 2007: Have Australian rainfall and cloudiness increased due to the remote effects of Asian anthropogenic aerosols? Journal of Geophysical Research, 112, D09202, doi:10.1029/2006JD007712.

Rotstayn, L. D., S. J. Jeffrey, M. A. Collier, S. M. Dravitzki, A. C. Hirst, J. I. Syktus, and K. K. Wong, 2012: Aerosol- and greenhouse gas induced changes in summer rainfall and circulation in the Australasian region: a study using single-forcing climate simulations. Atmospheric Chemistry and Physics, In press.

Ruff, T. W., and J. D. Neelin, 2012: Long tails in regional surface temperature probability distributions with implications for extremes under global warming. Geophysical Research Letters, 39, L04704, doi:10.1029/2011GL050610.

Saunders, D. A., P. Mawsaon, and R. Dawson, 2011: The impact of two extreme weather events and other causes of death on Carnaby's Black Cockatoo: a promise of things to come for a threatened species? Pacific Conservation Biology, 17, 141-148.

Sheridan, S. C., and C. C. Lee, 2011: The self-organizing map in synoptic climatological research. Progress in Physical Geography, 35, 109-119, doi:10.1177/0309133310397582.

Shi, G., W. Cai, T. Cowan, J. Ribbe, L. Rotstayn, and M. Dix, 2008: Variability and trend of the North West Australia rainfall: observations and coupled climate modeling. Journal of Climate, 21, 2938–2959.

Simmons, A., S. Uppala, D. Dee, and S. Kobayashi, 2006: ERA-interim: New ECMWF reanalysis products from 1989 onwards. ECMWF Newsletter, 110, 26–35.

Siriwardena, L., and A. Seed, 2010: Extension and fixing errors of quality coded daily rain gauge data (disaggregation of flagged and unflagged accumulated data, infilling missing data and correcting some date shifted data), FORTRAN Program Manual, Program – Stage 2.

Smith, I. N., B. C. Bates, E. P. Campbell, and N. Nicholls, 2000: Cause and predictability of decadal variations. Indian Ocean Climate Initiative Research Report, 9–13.

Smith., I., and E. Chandler, 2010: Refining rainfall projections for the Murray Darling Basin of south-east Australia—the effect of sampling model results based on performance. Climatic Change 102(3), 377-393. Doi: 10.1007/s10584-009-9757-1.

Son, S.-W., L. M. Polvani, D. W. Waugh, H. Akiyoshi, R. Garcia, D. Kinnison, S. Pawson, E. Rozanov, T. G. Shepherd, and K. Shibata, 2008: The impact of stratospheric ozone recovery on the Southern Hemisphere westerly jet. Science, 320, 1486-1489.

Taylor, K., R. Stouffer, and G. Meehl, 2012: An Overview of CMIP5 and the Experiment Design. Bulletin of the American Meteorological Society., doi:10.1175/BAMS-D-11-00094.1, in press.

Thompson, D. W. J., and S. Solomon, 2002: Interpretation of recent Southern Hemisphere climate change. Science, 296, 895-899.

Timbal, B., P. Hope, and S. Charles, 2008: Evaluating the consistency between statistically downscaled and global dynamical model climate change projections, Journal of Climate, 21, 6052-6059, doi:10.1175/2008JCLI2379.1.

Timbal, B., E. Fernandez, and Z. Li, 2009: Generalization of a statistical downscaling model to provide local climate change projections for Australia, Environmental Modelling and Software, 24, 341-358.

Trewin, B. C., 2012a: A daily homogenised temperature data set for Australia. International Journal of Climatology. Published online 13 June 2012, doi:10.1002/joc.3530.

Trewin, B. C., 2012b: Techniques involved in developing the Australian Climate Observations Reference Network – Surface Air Temperature (ACORN-SAT) dataset, CAWCR Technical Report No. 49, Centre for Australian Weather and Climate Research.

van Ommen, T. D., and V. Morgan, 2010: Snowfall increase in coastal East Antarctica linked with southwest Western Australian drought. Nature Geoscience, 3, 267-272, doi:10.1038/NGEO761.

Viney, N. R., and B.C. Bates, 2004: It never rains on Sunday: the prevalence and implications of untagged multi-day rainfall accumulations in the Australian high quality data set. International Journal of Climatology, 24, 1171-1192.

Vitart, F., A. Leroy, and M. C. Wheeler, 2010: A comparison of dynamical and statistical predictions of weekly tropical cyclone activity in the Southern Hemisphere. Monthly Weather Review, 138, 3671-3682.

Walsh, K. J. E., K. L. McInnes, and J. L. McBride, 2012: Climate change impacts on tropical cyclones and extreme sea levels in the South Pacific–a regional assessment. Global and Planetary Change, 80-81, 149-164.

Watterson, I. G., 2012: Understanding and partitioning future climates for Australian regions from CMIP3 using ocean warming indices. Climatic Change, 111, 903-922, doi:10.1007/s10584-011-0166-x.

Webb, L. B., P. H. Whetton, J. Bhend, R. Darbyshire, P. R. Briggs, and E. W. R. Barlow, 2012: Earlier wine-grape ripening driven by climatic warming and drying and management practices. Nature Climate Change, 2, 259-264, doi:10.1038/nclimate1417.

Western Australia Water Corporation, 2011: Annual Report 2011. http://www.watercorporation.com.au/P/publications_annual_reports.cfm.

Zeng, Q., and J. Li, 2002: On the Interaction between Northern and Southern Hemispheric Atmospheres and the Essence of Tropical Monsoon, Chinese Journal of Atmospheric Sciences, 26, 207-226. (English version available at: web.lasg.ac.cn/staff/ljp/Epublication.html.)

Zidikheri, M. J., and J. S. Frederiksen, 2011: Inverse method for attribution of climate change. ANZIAM Journal, 52, C823-C836.

APPENDICES

Appendices

Appendix A – Calibration of NHMM to SWWA Station Network

The non-homogeneous hidden Markov model (NHMM) was calibrated to a network of 29 Australian Bureau of Meteorology daily rainfall gauges across SWWA (Table A-1). These stations were selected on the basis of their relatively high data quality and their relevance to the water and agriculture sectors. NHMM selection involved determining the optimum combination of the number of weather states and the set of atmospheric predictor variables (derived from NCEP/NCAR Reanalysis). Calibration was undertaken for two seasons, the May-October 'winter' half-year and the November-April 'summer' half-year. The selected combinations are summarised in Table A-2. The weather states are best visualised by mean precipitation occurrence patterns and composite plots of their associated synoptic patterns (Figures A-1 and A-2).

Table A-1 South-west Western Australia stations selected for non-homogeneous Markov model calibration.

1	8039	Dalwallinu P.O.	31.35	116.66
2	8138	Wongan Hills Research Station	31.94	116.72
3	9007	Chidlow P.O.	32.34	116.26
4	9018	Gingin P.O.	31.96	115.90
5	9021	Perth Airport MO	32.36	115.97
6	9023	Jarrahdale	32.20	116.06
7	9031	Mundaring Weir	31.56	116.16
8	9039	Serpentine	31.73	116.00
9	9044	Wungong Dam	33.96	116.06
10	9045	Yanchep Park	34.37	115.67
11	9105	Wanneroo	33.54	115.79
12	9510	Bridgetown P.O.	33.57	116.14
13	9518	Cape Leeuwin	32.71	115.13
14	9519	Cape Naturaliste	32.50	115.02
15	9534	Donnybrook P.O.	34.45	115.82
16	9538	Dwellingup Forestry	33.36	116.06
17	9572	Mandurah Composite	33.13	115.77
18	9592	Pemberton Forestry	30.81	116.04
19	9628	Collie	31.66	116.16
20	9642	Wokalup Research Station	31.64	115.88
21	10007	Bencubbin	31.50	117.86
22	10035	Cunderdin P.O.	32.33	117.25
23	10073	Kellerberrin Composite	33.34	117.72
24	10093	Merredin Research Station	33.69	118.22
25	10536	Corrigin P.O.	33.10	117.87
26	10542	Darkan P.O.	32.68	116.74
27	10579	Katanning P.O.	31.35	117.56
28	10592	Lake Grace P.O.	31.94	118.46
29	10648	Wandering P.O.	32.34	116.67

Table A-2 Numbers of weather states and sets of atmospheric predictors of selected for non-homogeneous Markov models (NHMMs) for SWWA. The summer half-year is November through to April; the winter half-year is May though to October.

SEASON	FITTED NHMM*
Summer	4 weather states
	MSLP
	North - South MSLP gradient
	DTD @ 700 hPa
	DTD @ 850 hPa
Winter	6 weather states
	MSLP
	North - South MSLP gradient
	DTD @ 700 hPa

* MSLP = mean sea level pressure; DTD = dew point temperature depression (air temperature minus dew point temperature).

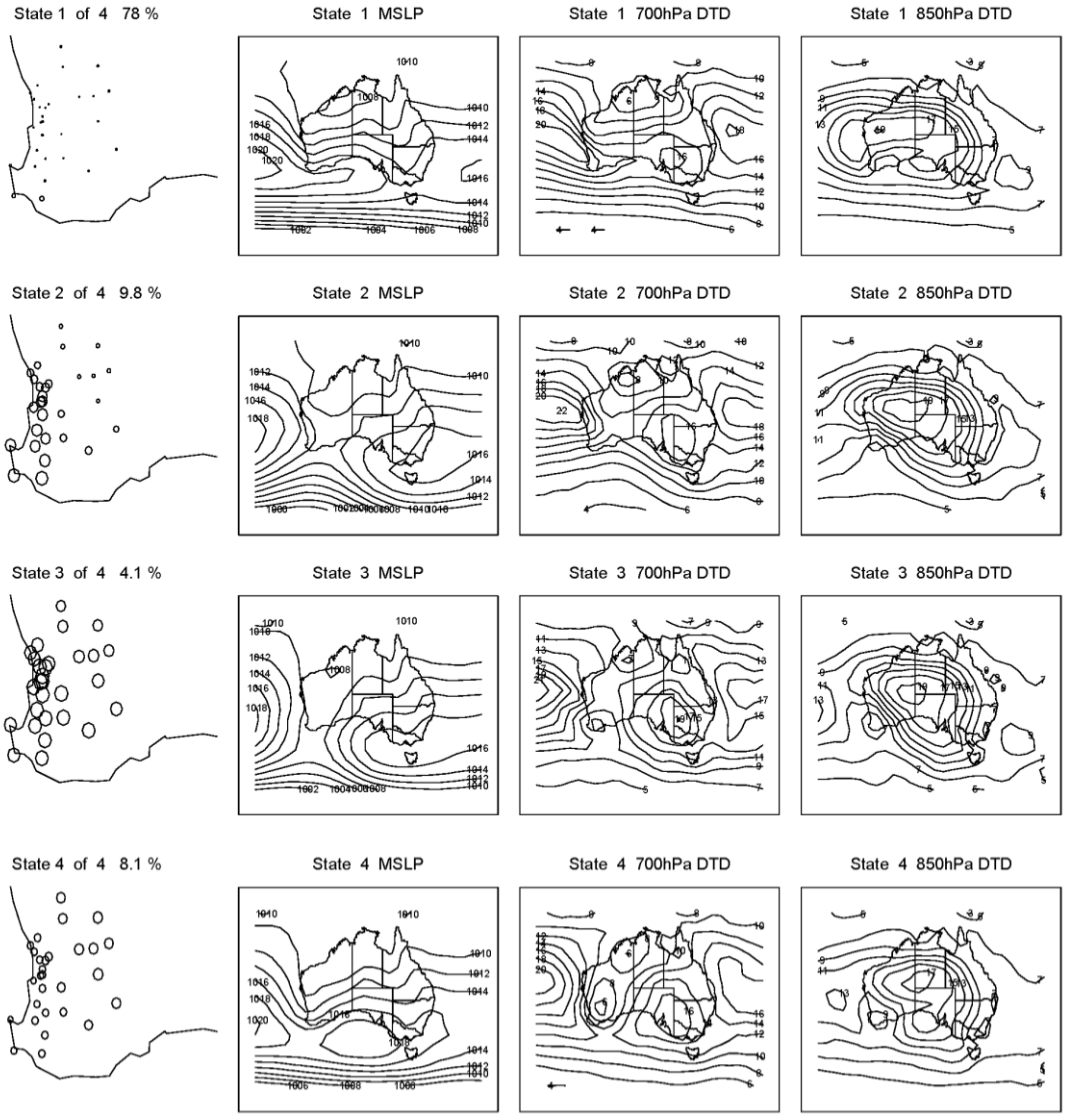

Figure A-1 Summer weather states as mean precipitation probability maps and corresponding composite atmospheric predictor fields for SWWA.

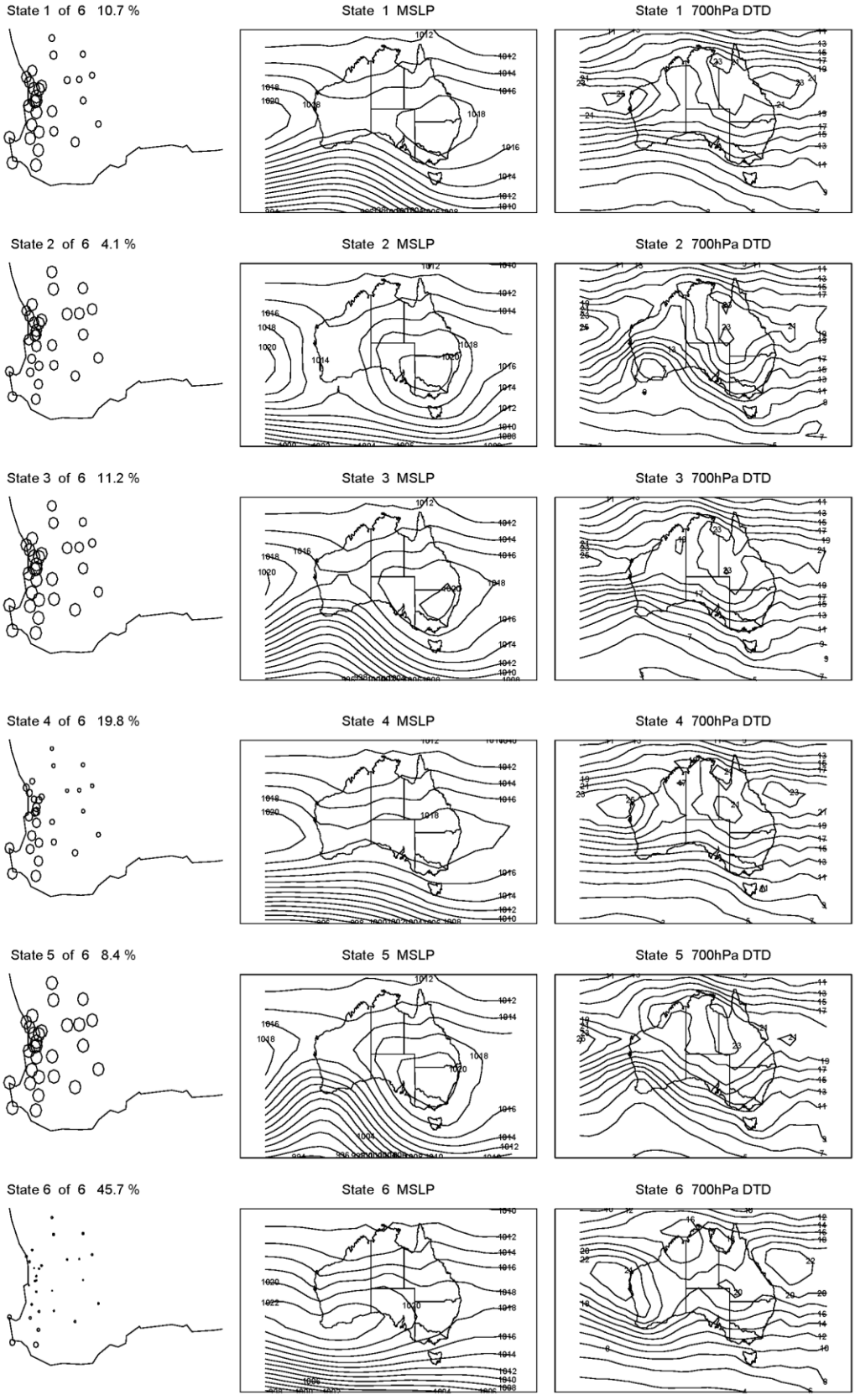

Figure A-2 Winter weather states as mean precipitation probability maps and corresponding composite atmospheric predictor fields for SWWA.

Appendix B – Downscaled SWWA Rainfall and Temperature Projections

Table B-1 Projected change in annual mean rainfall for 29 stations across SWWA, as a proportion of present-day values (1962-1999). Values are given for mid-century (2047-2064) and end-of-century (2082-2099) periods under three SRES (B1, A1B & A2) GHG emissions scenarios. The range of results in each cell reflects the range of downscaled projections produced by five global climate models, illustrating one source of uncertainty in the results.

Dalwallinu	1	0.80–0.88	0.67–0.91	0.73–0.88	0.72–0.90	0.54–0.82	0.58–0.78
Wongan Hills R. S.	1	0.79–0.88	0.65–0.91	0.72–0.87	0.70–0.91	0.52–0.81	0.56–0.78
Chidlow	1	0.76–0.90	0.64–0.93	0.69–0.89	0.70–0.95	0.51–0.83	0.53–0.80
Gingin	1	0.77–0.90	0.65–0.92	0.70–0.88	0.70–0.94	0.51–0.82	0.54–0.80
Perth Airport	1	0.77–0.90	0.64–0.93	0.69–0.88	0.70–0.94	0.51–0.82	0.53–0.79
Jarrahdale	1	0.78–0.90	0.66–0.93	0.70–0.89	0.71–0.95	0.52–0.83	0.54–0.80
Mundaring Weir	1	0.77–0.90	0.64–0.93	0.69–0.88	0.70–0.94	0.51–0.82	0.53–0.80
Serpentine	1	0.78–0.90	0.66–0.93	0.70–0.89	0.71–0.95	0.52–0.84	0.55–0.81
Wungong Dam	1	0.78–0.90	0.66–0.93	0.70–0.89	0.71–0.95	0.52–0.83	0.54–0.80
Yanchep Park	1	0.79–0.91	0.68–0.93	0.72–0.89	0.73–0.95	0.55–0.85	0.57–0.83
Wanneroo	1	0.79–0.90	0.67–0.94	0.72–0.89	0.73–0.95	0.54–0.84	0.57–0.81
Bridgetown	1	0.80–0.91	0.68–0.93	0.72–0.90	0.73–0.95	0.55–0.84	0.58–0.81
Cape Leeuwin	1	0.84–0.93	0.75–0.95	0.77–0.92	0.79–0.97	0.64–0.88	0.65–0.87
Cape Naturaliste	1	0.81–0.92	0.71–0.95	0.74–0.92	0.76–0.97	0.59–0.87	0.60–0.85
Donnybrook	1	0.79–0.91	0.68–0.94	0.72–0.90	0.74–0.96	0.55–0.85	0.57–0.82
Dwellingup Forestry	1	0.78–0.90	0.66–0.93	0.70–0.89	0.72–0.95	0.53–0.83	0.55–0.80
Mandurah Composite	1	0.78–0.90	0.67–0.93	0.70–0.89	0.71–0.95	0.52–0.84	0.55–0.81
Pemberton Forestry	1	0.82–0.92	0.72–0.95	0.74–0.91	0.77–0.96	0.60–0.87	0.61–0.84
Collie	1	0.78–0.91	0.67–0.94	0.71–0.89	0.72–0.95	0.54–0.84	0.56–0.81
Wokalup R. S.	1	0.79–0.91	0.68–0.94	0.71–0.90	0.73–0.95	0.54–0.84	0.56–0.82
Bencubbin	1	0.81–0.87	0.68–0.90	0.74–0.87	0.71–0.90	0.55–0.82	0.59–0.78
Cunderdin	1	0.79–0.88	0.65–0.90	0.71–0.87	0.70–0.91	0.51–0.80	0.55–0.77
Kellerberrin Composite	1	0.79–0.87	0.65–0.90	0.72–0.87	0.69–0.90	0.52–0.80	0.56–0.77
Merredin R.S.	1	0.81–0.88	0.68–0.90	0.74–0.87	0.71–0.91	0.55–0.82	0.58–0.78
Corrigin	1	0.79–0.87	0.66–0.90	0.71–0.87	0.70–0.90	0.51–0.80	0.56–0.77
Darkan	1	0.77–0.89	0.66–0.92	0.71–0.88	0.71–0.93	0.52–0.82	0.55–0.78
Katanning	1	0.79–0.88	0.67–0.91	0.72–0.88	0.72–0.92	0.54–0.82	0.57–0.78
Lake Grace	1	0.80–0.87	0.67–0.90	0.74–0.87	0.71–0.89	0.55–0.81	0.58–0.77
Wandering	1	0.77–0.89	0.64–0.91	0.70–0.88	0.69–0.92	0.50–0.81	0.53–0.78

Table B-2 Present-day and projected annual mean rainfall (in millimetres) for 29 stations across SWWA. Values are given for mid-century (2047-2064) and end-of-century (2082-2099) periods under three SRES emissions scenarios (B1, A1B & A2). The range of results in each cell reflects the range of downscaled projections produced by the five global climate models, illustrating one source of uncertainty in the results.

Dalwallinu	390–410	330–360	270–360	290–340	290–350	220–320	230–310
Wongan Hills	410–420	330–360	270–370	300–350	290–370	220–330	230–320
R. S. Chidlow	850–890	670–770	560–790	610–750	610–800	450–700	460–680
Gingin	680–710	540–610	450–620	490–600	490–640	360–560	370–540
Perth Airport	770–800	610–690	510–720	550–680	560–730	400–630	420–610
Jarrahdale	1130–1180	910–1020	770–1050	820–1010	830–1070	610–940	630–910
Mundaring Weir	970–1010	770–870	640–900	700–850	700–910	510–800	530–770
Serpentine	890–930	720–810	610–830	650–790	660–850	480–750	500–720
Wungong Dam	1090–1140	870–980	740–1020	790–970	800–1040	590–910	610–880
Yanchep Park	740–770	600–680	520–700	550–670	560–710	420–630	430–620
Wanneroo	780–820	640–710	540–730	590–700	580–740	440–660	450–640
Bridgetown	790–820	640–710	550–730	590–710	590–750	450–660	470–640
Cape Leeuwin	990–1020	840–920	760–950	780–920	800–960	650–880	660–860
Cape Naturaliste	820–850	680–760	600–780	630–750	640–790	490–710	510–690
Donnybrook	940–980	770–860	660–890	700–850	710–900	530–800	550–780
Dwellingup Forestry	1250–1310	1010–1130	860–1170	910–1120	920–1190	680–1040	710–1010
Mandurah Composite	870–910	710–780	600–820	640–780	640–830	470–730	490–700
Pemberton Forestry	1160–1190	970–1060	850–1100	890–1050	910–1110	710–1000	720–970
Collie	870–910	700–790	600–810	640–780	650–830	480–730	500–710
Wokalup R. S.	960–990	780–870	670–900	700–860	720–910	530–810	550–780
Bencubbin	340–360	280–310	240–310	250–300	250–310	190–280	200–260
Cunderdin	390–410	320–350	260–360	280–340	280–360	210–310	220–300
Kellerberrin	330–350	270–300	220–300	240–290	240–300	180–260	190–250
Composite Merredin R.S.	340–360	290–310	240–320	260–300	250–310	190–280	200–270
Corrigin	380–400	310–340	260–350	270–330	270–340	200–300	210–290
Darkan	510–540	410–460	350–470	380–450	380–480	280–420	290–400
Katanning	470–490	390–420	330–440	350–420	350–430	260–390	270–370
Lake Grace	360–380	300–330	250–340	270–320	270–320	200–290	210–280
Wandering	570–600	460–510	380–520	410–500	410–530	300–460	310–440

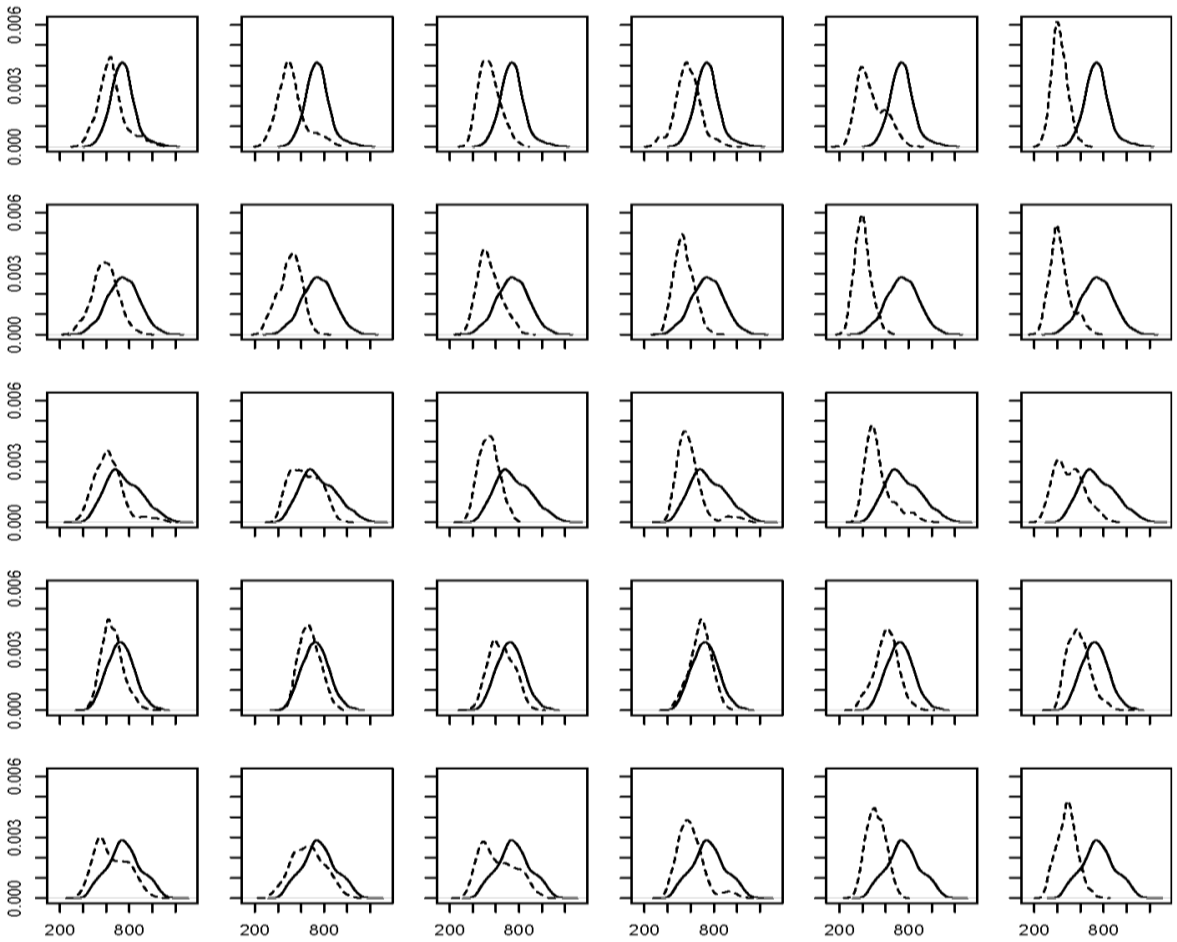

Figure B-1 The probability of realising a given level of annual rainfall under the present day and future climate. The probability distribution under the current climate run (solid lines) is compared to the projected climate (dashed lines). Downscaled results are averaged across the 29 SWWA stations. Note all projections shift to the left, implying reduced rainfall in future. Rows from top to bottom represent the five global climate models (GFDL2.0, GFDL2.1, MIROC-medres, CSIRO Mk3.5 and MPI-ECHAM5) for six SRES-scenario and period combinations (columns left to right: B1 mid-century, A1B mid-century, A2 mid-century, B1 end-century, A1B end-century and A2 end-century). The uncertainty in these results is highlighted by the differences in results across the five global climate models.

Table B-3 South-west Western Australia summer weather state means and changes. The first four data columns list the mean frequency of respective weather states. The next four columns are the changes in weather state frequencies relative to the present climate (downscaled values [203CM] for the present day [1961-2000] relative to NCEP/NCAR Reanalysis [NNR] data; and global climate model projections for mid-century and end-of-century periods relative to downscaled present-day values).

PERIOD	DATA/GCM	STATE 1	STATE 2	STATE 3	STATE 4				
Full	NNR	0.74	0.11	0.06	0.09				
1st half	NNR	0.74	0.11	0.06	0.09				
2nd half	NNR	0.74	0.11	0.06	0.09				
20C3M	GFDL2.0	0.75	0.11	0.05	0.09	0.01	0.00	-0.01	0.00
20C3M	GFDL2.1	0.75	0.10	0.06	0.09	0.01	-0.01	0.00	0.00
20C3M	MIROC	0.74	0.11	0.06	0.10	-0.01	0.00	0.00	0.01
20C3M	MK35	0.75	0.11	0.05	0.09	0.01	0.00	0.00	0.00
20C3M	ECHAM5	0.74	0.11	0.06	0.09	0.00	-0.01	0.00	0.00
B1_mid	GFDL2.0	0.79	0.10	0.04	0.07	0.04	-0.01	-0.01	-0.02
B1_mid	GFDL2.1	0.77	0.10	0.05	0.08	0.02	0.00	-0.01	-0.01
B1_mid	MIROC	0.75	0.11	0.05	0.09	0.02	0.00	-0.01	-0.01
B1_mid	MK35	0.81	0.09	0.04	0.07	0.05	-0.02	-0.01	-0.02
B1_mid	ECHAM5	0.76	0.11	0.05	0.09	0.01	0.00	0.00	-0.01
A1B_mid	GFDL2.0	0.79	0.10	0.04	0.07	0.03	-0.01	-0.01	-0.02
A1B_mid	GFDL2.1	0.81	0.09	0.04	0.07	0.06	-0.01	-0.02	-0.03
A1B_mid	MIROC	0.77	0.10	0.05	0.08	0.04	-0.01	-0.01	-0.02
A1B_mid	MK35	0.79	0.10	0.04	0.07	0.04	-0.01	-0.01	-0.02
A1B_mid	ECHAM5	0.75	0.11	0.06	0.09	0.00	0.00	0.00	-0.01
A2_mid	GFDL2.0	0.79	0.10	0.04	0.07	0.04	-0.01	-0.01	-0.02
A2_mid	GFDL2.1	0.78	0.10	0.04	0.08	0.03	0.00	-0.01	-0.02
A2_mid	MIROC	0.78	0.10	0.04	0.08	0.04	-0.01	-0.01	-0.01
A2_mid	MK35	0.79	0.10	0.04	0.07	0.04	-0.01	-0.01	-0.02
A2_mid	ECHAM5	0.76	0.10	0.05	0.08	0.02	0.00	0.00	-0.01
B1_end	GFDL2.0	0.77	0.11	0.05	0.08	0.01	0.00	0.00	-0.01
B1_end	GFDL2.1	0.80	0.09	0.04	0.06	0.05	-0.01	-0.01	-0.03
B1_end	MIROC	0.79	0.09	0.04	0.08	0.05	-0.02	-0.01	-0.02
B1_end	MK35	0.79	0.10	0.04	0.07	0.04	-0.01	-0.01	-0.02
B1_end	ECHAM5	0.79	0.10	0.04	0.07	0.04	-0.01	-0.01	-0.02
A1B_end	GFDL2.0	0.80	0.09	0.04	0.07	0.05	-0.01	-0.01	-0.02
A1B_end	GFDL2.1	0.83	0.09	0.03	0.05	0.08	-0.02	-0.02	-0.04
A1B_end	MIROC	0.78	0.10	0.04	0.08	0.05	-0.01	-0.01	-0.02
A1B_end	MK35	0.81	0.09	0.04	0.06	0.06	-0.02	-0.02	-0.02
A1B_end	ECHAM5	0.79	0.10	0.04	0.07	0.05	-0.01	-0.01	-0.02
A2_end	GFDL2.0	0.82	0.09	0.03	0.06	0.06	-0.02	-0.02	-0.03
A2_end	GFDL2.1	0.79	0.09	0.04	0.07	0.04	-0.01	-0.01	-0.02
A2_end	MIROC	0.80	0.09	0.04	0.08	0.06	-0.02	-0.02	-0.02
A2_end	MK35	0.83	0.08	0.03	0.06	0.08	-0.03	-0.02	-0.03
A2_end	ECHAM5	0.79	0.09	0.04	0.07	0.05	-0.01	-0.01	-0.02

Table B-4 South-west Western Australia summer atmospheric predictor means and changes. The first four data columns are the mean values of the respective atmospheric predictors. The next four columns are the changes in predictor values; downscaled values for the present day [1961-2000] relative to NCEP/NCAR Reanalysis [NNR] data; and projections for mid-century and end-of-century periods relative to downscaled present-day values.

PERIOD		MSLP	N-S MSLP	DTD 700	DTD 850				
Full	NNR	1016.00	-3.38	15.53	15.30				
1st half	NNR	1015.90	-3.34	14.90	15.39	-0.10	0.04	-0.63	0.09
2nd half	NNR	1016.02	-3.38	16.70	15.23	0.02	0.00	1.17	-0.07
20C3M	GFDL2.0	1016.66	-4.02	16.97	16.58	0.66	-0.64	1.44	1.28
20C3M	GFDL2.1	1016.06	-4.63	16.89	14.24	0.06	-1.25	1.36	-1.06
20C3M	MIROC	1015.97	-4.13	17.20	12.70	-0.03	-0.75	1.67	-2.60
20C3M	MK35	1016.89	-2.66	15.51	10.45	0.89	0.72	-0.02	-4.85
20C3M	ECHAM5	1016.19	-4.13	16.31	14.42	0.19	-0.75	0.78	-0.88
B1_mid	GFDL2.0	1016.74	-4.03	18.01	17.85	0.08	-0.01	1.04	1.27
B1_mid	GFDL2.1	1016.26	-4.63	17.74	14.80	0.20	0.00	0.85	0.56
B1_mid	MIROC	1016.56	-4.12	17.60	13.09	0.59	0.01	0.40	0.39
B1_mid	MK35	1017.21	-2.36	15.73	12.42	0.32	0.30	0.23	1.97
B1_mid	ECHAM5	1016.33	-4.03	16.69	14.89	0.13	0.11	0.38	0.47
A1B_mid	GFDL2.0	1016.68	-4.04	18.08	17.57	0.03	-0.02	1.11	0.99
A1B_mid	GFDL2.1	1016.54	-4.63	18.66	15.84	0.48	0.00	1.77	1.61
A1B_mid	MIROC	1016.57	-4.13	17.94	13.55	0.60	0.01	0.74	0.85
A1B_mid	MK35	1016.89	-2.28	15.85	12.53	-0.01	0.38	0.34	2.08
A1B_mid	ECHAM5	1016.31	-3.99	16.66	14.74	0.12	0.14	0.35	0.32
A2_mid	GFDL2.0	1016.86	-4.11	18.28	17.42	0.20	-0.09	1.32	0.84
A2_mid	GFDL2.1	1016.31	-4.65	18.26	14.87	0.25	-0.01	1.37	0.63
A2_mid	MIROC	1016.71	-4.24	17.96	13.11	0.74	-0.11	0.76	0.41
A2_mid	MK35	1017.01	-2.29	15.74	12.06	0.11	0.37	0.23	1.61
A2_mid	ECHAM5	1016.33	-3.95	16.83	15.27	0.13	0.19	0.52	0.85
B1_end	GFDL2.0	1016.47	-4.07	17.90	16.94	-0.18	-0.04	0.93	0.36
B1_end	GFDL2.1	1016.33	-4.68	18.57	15.64	0.27	-0.05	1.68	1.41
B1_end	MIROC	1016.85	-4.26	18.03	13.54	0.88	-0.13	0.84	0.84
B1_end	MK35	1017.08	-2.22	16.02	12.64	0.18	0.44	0.52	2.18
B1_end	ECHAM5	1016.23	-4.01	17.40	16.25	0.04	0.12	1.09	1.83
A1B_end	GFDL2.0	1016.82	-4.03	18.80	18.36	0.16	-0.01	1.83	1.78
A1B_end	GFDL2.1	1016.66	-4.66	19.21	16.73	0.60	-0.03	2.32	2.50
A1B_end	MIROC	1017.08	-4.22	18.26	13.85	1.11	-0.08	1.07	1.15
A1B_end	MK35	1016.99	-2.14	16.08	13.16	0.09	0.52	0.57	2.71
A1B_end	ECHAM5	1016.28	-3.97	17.65	16.40	0.08	0.16	1.34	1.98
A2_end	GFDL2.0	1016.88	-4.06	18.83	18.39	0.23	-0.04	1.87	1.81
A2_end	GFDL2.1	1016.28	-4.58	18.91	15.62	0.23	0.05	2.02	1.38
A2_end	MIROC	1017.49	-4.07	18.40	14.43	1.52	0.06	1.21	1.72
A2_end	MK35	1017.09	-2.22	16.29	13.79	0.20	0.44	0.78	3.33
A2_end	ECHAM5	1016.25	-4.04	17.83	16.51	0.06	0.10	1.52	2.09

Table B-5 South-west Western Australia winter weather state means and changes. First six data columns are mean frequency of respective weather state. Next six columns are the changes in weather state frequencies relative to the present climate (downscaled values [203CM] for the present day [1961-2000] relative to NCEP/NCAR Reanalysis [NNR] data; and global climate model projections for mid-century and end-of-century periods relative to downscaled present-day values).

PERIOD	DATA/GCM	STATE 1	STATE 2	STATE 3	STATE 4	STATE 5	STATE 6						
Full	NNR	0.10	0.04	0.12	0.20	0.09	0.44						
1st half	NNR	0.11	0.04	0.12	0.21	0.09	0.43	0.01	0.00	0.00	0.01	0.00	-0.01
2nd half	NNR	0.09	0.04	0.11	0.19	0.08	0.48	0.01	0.00	-0.01	-0.01	-0.01	0.04
20C3M	GFDL2.0	0.10	0.04	0.12	0.19	0.09	0.45	0.00	0.00	0.00	-0.01	0.00	0.01
20C3M	GFDL2.1	0.10	0.04	0.12	0.19	0.09	0.46	0.00	0.00	0.00	-0.01	0.00	0.02
20C3M	MIROC	0.10	0.04	0.12	0.19	0.09	0.46	0.00	0.00	0.00	-0.01	0.00	0.02
20C3M	MK35	0.10	0.05	0.11	0.20	0.09	0.46	0.00	0.01	-0.01	0.00	0.00	0.02
20C3M	ECHAM5	0.10	0.04	0.12	0.19	0.09	0.46	0.00	0.00	0.00	-0.01	0.00	0.02
B1_mid	GFDL2.0	0.09	0.03	0.11	0.19	0.07	0.51	0.01	-0.01	-0.01	-0.01	-0.01	0.05
B1_mid	GFDL2.1	0.08	0.03	0.09	0.18	0.06	0.55	0.01	-0.01	-0.03	-0.01	-0.03	0.09
B1_mid	MIROC	0.08	0.03	0.09	0.17	0.07	0.54	0.02	-0.01	-0.02	-0.02	-0.02	0.08
B1_mid	MK35	0.09	0.04	0.10	0.19	0.08	0.49	0.01	0.00	-0.01	0.00	-0.01	0.03
B1_mid	ECHAM5	0.09	0.04	0.10	0.18	0.07	0.52	0.01	-0.01	-0.02	0.00	-0.02	0.06
A1B_mid	GFDL2.0	0.07	0.03	0.08	0.18	0.05	0.59	0.03	-0.02	-0.04	-0.02	-0.04	0.14
A1B_mid	GFDL2.1	0.07	0.03	0.08	0.18	0.05	0.59	0.02	-0.02	-0.04	-0.02	-0.04	0.13
A1B_mid	MIROC	0.08	0.03	0.09	0.18	0.08	0.55	0.02	-0.01	-0.03	-0.02	-0.02	0.09
A1B_mid	MK35	0.10	0.04	0.11	0.21	0.08	0.46	0.00	0.00	0.00	0.01	0.00	0.00
A1B_mid	ECHAM5	0.08	0.03	0.10	0.18	0.07	0.53	0.01	-0.01	-0.02	-0.01	-0.02	0.07
A2_mid	GFDL2.0	0.08	0.03	0.09	0.19	0.06	0.56	0.02	-0.02	-0.03	-0.01	-0.03	0.11
A2_mid	GFDL2.1	0.08	0.03	0.08	0.18	0.05	0.58	0.02	-0.01	-0.03	-0.02	-0.04	0.12
A2_mid	MIROC	0.07	0.03	0.08	0.17	0.06	0.59	0.03	-0.01	-0.04	-0.02	-0.03	0.13
A2_mid	MK35	0.09	0.04	0.10	0.19	0.08	0.50	0.01	-0.01	-0.01	-0.01	-0.01	0.04
A2_mid	ECHAM5	0.08	0.03	0.09	0.18	0.07	0.54	0.01	-0.01	-0.02	-0.01	-0.02	0.08
B1_end	GFDL2.0	0.08	0.03	0.09	0.19	0.06	0.55	0.02	-0.02	-0.03	-0.01	-0.03	0.10
B1_end	GFDL2.1	0.08	0.03	0.09	0.18	0.06	0.57	0.02	-0.01	-0.03	-0.02	-0.03	0.11
B1_end	MIROC	0.08	0.03	0.09	0.18	0.07	0.56	0.02	-0.01	-0.03	-0.01	-0.03	0.10
B1_end	MK35	0.10	0.04	0.11	0.21	0.08	0.46	0.00	0.00	0.00	0.01	0.00	0.00
B1_end	ECHAM5	0.08	0.03	0.09	0.18	0.07	0.54	0.01	-0.01	-0.03	-0.01	-0.02	0.08
A1B_end	GFDL2.0	0.07	0.02	0.07	0.17	0.05	0.62	0.03	-0.02	-0.05	-0.03	-0.04	0.17
A1B_end	GFDL2.1	0.06	0.02	0.06	0.16	0.04	0.66	0.04	-0.02	-0.06	-0.04	-0.05	0.21
A1B_end	MIROC	0.07	0.03	0.08	0.16	0.06	0.60	0.03	-0.01	-0.04	-0.03	-0.03	0.14
A1B_end	MK35	0.09	0.04	0.10	0.21	0.07	0.49	0.00	0.00	-0.02	0.01	-0.02	0.03
A1B_end	ECHAM5	0.07	0.03	0.07	0.17	0.05	0.61	0.03	-0.02	-0.04	-0.02	-0.04	0.15
A2_end	GFDL2.0	0.06	0.02	0.06	0.16	0.04	0.66	0.04	-0.03	-0.06	-0.04	-0.05	0.21
A2_end	GFDL2.1	0.06	0.02	0.06	0.15	0.04	0.67	0.04	-0.02	-0.06	-0.04	-0.05	0.21
A2_end	MIROC	0.07	0.03	0.07	0.17	0.05	0.61	0.03	-0.01	-0.04	-0.03	-0.04	0.15
A2_end	MK35	0.09	0.04	0.10	0.20	0.07	0.51	0.01	-0.01	-0.02	0.01	-0.02	0.05
A2_end	ECHAM5	0.07	0.02	0.07	0.17	0.05	0.62	0.03	-0.02	-0.05	-0.02	-0.04	0.16

Table B-6 South-west Western Australia winter atmospheric predictor means and changes. The first three data columns are the mean values of the respective atmospheric predictors. The next three columns are the changes in predictor values; downscaled values for the present day [1961-2000] relative to NCEP/NCAR Reanalysis [NNR] data; and projections for mid-century and end-of-century periods relative to downscaled present-day values).

PERIOD	DATA/GCM	MSLP	N-S MSLP	DTD 700			
Full	NNR	1017.58	-1.46	15.25			
1st half	NNR	1017.47	-1.47	14.63	-0.11	-0.01	-0.62
2nd half	NNR	1017.93	-1.59	16.70	0.35	-0.13	1.45
20C3M	GFDL2.0	1015.69	-1.23	13.82	-1.89	0.23	-1.43
20C3M	GFDL2.1	1017.92	-2.28	15.38	0.34	-0.82	0.13
20C3M	MIROC	1016.58	-1.40	17.09	-1.00	0.06	1.84
20C3M	MK35	1021.09	-1.82	17.49	3.51	-0.36	2.24
20C3M	ECHAM5	1017.56	-1.45	15.50	-0.02	0.01	0.25
B1_mid	GFDL2.0	1015.97	-1.45	15.32	0.28	-0.22	1.49
B1_mid	GFDL2.1	1019.12	-2.77	17.18	1.20	-0.50	1.80
B1_mid	MIROC	1018.12	-1.86	18.67	1.54	-0.46	1.58
B1_mid	MK35	1021.72	-1.82	18.40	0.63	-0.01	0.90
B1_mid	ECHAM5	1018.42	-1.66	17.45	0.86	-0.21	1.96
A1B_mid	GFDL2.0	1017.41	-1.95	16.64	1.72	-0.72	2.82
A1B_mid	GFDL2.1	1019.67	-2.87	18.46	1.75	-0.59	3.08
A1B_mid	MIROC	1018.20	-1.75	18.65	1.63	-0.36	1.56
A1B_mid	MK35	1021.14	-1.75	18.18	0.05	0.07	0.68
A1B_mid	ECHAM5	1018.50	-1.75	17.14	0.94	-0.30	1.64
A2_mid	GFDL2.0	1016.83	-1.86	16.05	1.14	-0.63	2.23
A2_mid	GFDL2.1	1019.45	-2.86	17.99	1.53	-0.58	2.61
A2_mid	MIROC	1019.08	-2.23	19.07	2.50	-0.84	1.98
A2_mid	MK35	1021.50	-1.86	18.74	0.42	-0.04	1.25
A2_mid	ECHAM5	1018.82	-1.88	17.47	1.27	-0.43	1.97
B1_end	GFDL2.0	1016.57	-1.72	16.12	0.88	-0.48	2.30
B1_end	GFDL2.1	1019.45	-2.83	17.73	1.53	-0.55	2.34
B1_end	MIROC	1018.50	-1.84	18.99	1.92	-0.44	1.90
B1_end	MK35	1021.08	-1.64	18.49	-0.01	0.18	1.00
B1_end	ECHAM5	1018.61	-1.80	18.02	1.05	-0.35	2.52
A1B_end	GFDL2.0	1017.59	-2.11	17.51	1.90	-0.88	3.69
A1B_end	GFDL2.1	1020.68	-3.28	19.61	2.76	-1.00	4.23
A1B_end	MIROC	1019.28	-2.04	20.01	2.70	-0.64	2.92
A1B_end	MK35	1021.81	-1.92	18.74	0.73	-0.10	1.24
A1B_end	ECHAM5	1019.72	-2.30	19.02	2.16	-0.85	3.52
A2_end	GFDL2.0	1018.18	-2.45	18.10	2.48	-1.22	4.28
A2_end	GFDL2.1	1020.66	-3.31	20.03	2.74	-1.03	4.65
A2_end	MIROC	1019.64	-2.10	19.92	3.07	-0.71	2.83
A2_end	MK35	1021.79	-1.99	19.34	0.70	-0.17	1.85
A2_end	ECHAM5	1019.77	-2.33	19.51	2.21	-0.88	4.01

Table B-7 Downscaled projected mean annual maximum and minimum temperatures in °C for mid-century (2047-2064) and end-of-century (2082-2099) periods relative to the present day (1962-1999) for selected sites across SWWA under the SRES A2 emissions scenario.

	MINIMUM TEMPERATURE			MAXIMUM TEMPERATURE		
STATION	PRESENT DAY	MID-CENTURY A2 (HIGH)	END OF CENTURY A2 (HIGH)	PRESENT DAY	MID-CENTURY A2 (HIGH)	END OF CENTURY A2 (HIGH)
Dalwallinu	12.2	14.0–14.8	15.7–16.8	26.0	27.5–28.8	28.6–30.8
Wongan Hills R. S.	11.9	13.6–14.4	15.3–16.4	25.0	26.5–27.7	27.5–29.7
Chidlow	11.1	12.8–13.4	14.4–15.4	23.4	24.8–26.0	26.0–28.0
Gingin	12.4	14.1–14.8	15.7–16.7	24.3	25.8–26.8	26.9–28.7
Perth Airport	12.6	14.1–14.7	15.5–16.5	24.5	26.0–26.8	27.3–28.6
Jarrahdale	10.9	12.4–13.0	13.7–14.8	22.8	24.4–25.1	25.7–26.9
Mundaring Weir	11.9	13.4–14.0	14.8–15.8	24.2	25.7–26.4	26.9–28.2
Serpentine	12.2	13.7–14.2	15.0–16.0	23.9	25.4–26.1	26.7–27.9
Wungong Dam	11.6	13.1–13.7	14.5–15.6	23.3	24.9–25.6	26.1–27.4
Yanchep Park	13.6	15.1–15.7	16.5–17.5	24.0	25.6–26.2	26.8–28.0
Wanneroo	13.1	14.8–15.5	16.5–17.4	23.9	25.4–26.4	26.5–28.3
Bridgetown	8.8	10.3–10.8	11.5–12.5	22.2	23.8–24.5	25.0–26.3
Cape Leeuwin	14.1	15.3–15.8	16.5–17.1	20.1	21.3–21.7	22.5–22.9
Cape Naturaliste	13.0	14.2–14.7	15.4–16.1	21.2	22.5–22.8	23.6–24.3
Donnybrook	10.1	11.7–12.1	12.9–13.9	23.2	24.8–25.5	26.0–27.4
Dwellingup Forestry	10.0	11.4–12.0	12.7–13.8	21.9	23.5–24.2	24.8–26.0
Mandurah Composite	13.1	14.6–15.1	15.9–16.9	23.6	25.1–25.8	26.4–27.6
Pemberton Forestry	10.3	11.6–12.1	12.8–13.6	20.5	22.0–22.4	23.3–23.9
Collie	9.9	11.4–11.9	12.7–13.7	22.4	24.0–24.7	25.2–26.6
Wokalup R. S.	11.7	13.2–13.7	14.5–15.5	23.2	24.7–25.4	26.0–27.2
Bencubbin	11.8	13.7–14.5	15.5–16.7	25.6	27.0–28.5	27.9–30.5
Cunderdin	11.4	13.2–13.9	14.9–16.0	25.3	26.7–28.1	27.6–30.1
Kellerberrin Composite	11.1	12.9–13.6	14.5–15.7	25.0	26.4–27.8	27.4–29.8
Merredin R.S.	11.4	13.2–14.0	14.8–16.1	25.0	26.4–27.9	27.3–29.8
Corrigin	10.1	11.7–12.4	13.2–14.4	23.6	24.9–26.2	25.8–28.2
Darkan	9.1	10.7–11.2	12.1–13.1	21.9	23.3–24.2	24.5–26.1
Katanning	9.5	11.1–11.6	12.5–13.5	22.2	23.5–24.5	24.7–26.4
Lake Grace	10.4	12.0–12.7	13.5–14.6	23.1	24.4–25.7	25.4–27.5
Wandering	9.1	10.8–11.4	12.3–13.4	23.3	24.8–25.8	26.0–27.8

Appendix C – Calibration of NHMM to NWWA Station Network

The new version of the NHMM stochastic downscaling model (Kirshner 2005) developed under IOCI3 was calibrated to two regions in NWWA: a nine-station network in the Kimberley and a ten-station network in the Pilbara (Table C-1, Figure C-1). Of the stations available in the region, those selected had relatively high-quality historical weather records. The NHMM was calibrated for two seasons: a May-October 'winter' half-year and a November-April 'summer' half-year. Calibration involved determining an optimum combination of the number of weather states and set of predictor variables (derived from NCEP/NCAR reanalysis). These predictors represent the key atmospheric processes influencing the rainfall variability for the stations and seasons of interest, such as the position and strength of pressure systems and the degree of saturation of the lower atmosphere. The selected combinations are listed in Table C-2 and the weather states are illustrated in Figures C-2 to C-5.

Table C-1. North-west Western Australia stations selected for NHMM calibration.

		Kimberley		
1	1021	Kalumburu Mission	14.30	126.64
2	2012	Halls Creek Airport	18.23	127.66
3	2016	Lissadell	16.67	128.55
4	2019	Margaret River Station	18.62	126.86
5	3003	Broome Airport	17.95	122.23
6	3017	Mount House Station	17.05	125.70
7	3024	Udialla	17.95	123.74
8	3027	Fossil Downs	18.14	125.78
9	3030	Bidyadanga	18.68	121.78
		Pilbara		
1	4020	Marble Bar Comp	21.18	119.75
2	4032	Port Hedland Airport	20.37	118.63
3	5001	Coolawanyah	21.80	117.81
4	5007	Learmonth Airport	22.24	114.10
5	5008	Mardie	21.19	115.98
6	5052	Karratha Station	20.88	116.68
7	6011	Carnarvon Airport	24.89	113.67
8	6050	Wandagee	23.76	114.55
9	6072	Nyang Station	23.03	115.04
10	7059	Mount Vernon	24.23	118.24

Although the NHMM had been previously applied to SWWA, this was its first use for tropical and subtropical regions. The atmospheric processes influencing rainfall variability may differ between these regions. Thus it was important to assess the validity of the weather states and atmospheric predictor variables that were selected to calibrate the model. Figures C-5 and C-6 illustrate the results of this assessment for sample stations from the two regions for the wet season (i.e, the summer half-year). On the one hand, the figures show that the NHMM simulations *do* reproduce much of the observed interannual variability and long-term trends. On the other hand, they illustrate how extreme wet years can be underestimated.

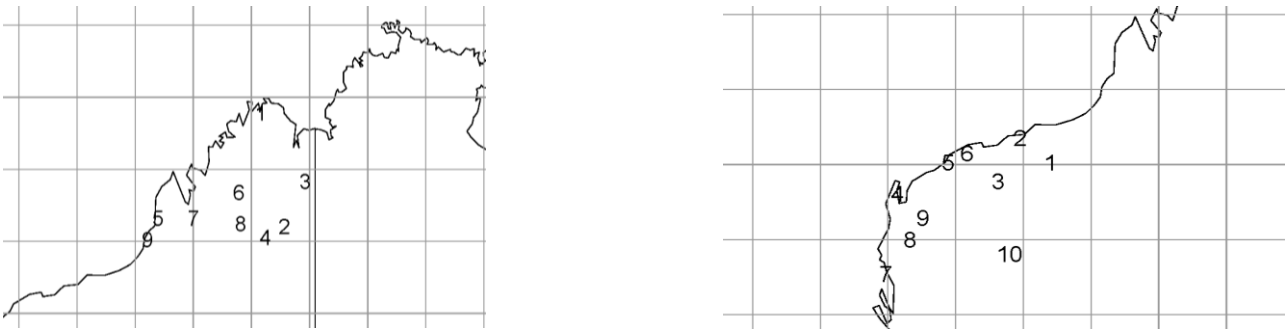

Figure C-1. Location of Kimberley and Pilbara stations used to calibrate a new version of the NHMM downscaling model (grid is the NCEP/NCAR Reanalysis predictor data grid).

For example, consider Kalumburu Mission. Here the NHMM under-estimates wet season rainfall for the summers of 1959/60, 1960/61, 1961/62, 1963/64, 1978/79, 1990/91, 1996/97, and 2001/2002 (Figure C-6). For Carnarvon Airport, rainfall is under-estimated for the several summers including 1962/63, 1966/67, 1969/70 and 1974/75 (Figure C-7). These results are not unexpected given the NHMM is not designed to model extreme daily rainfall.

Table C-2. Number of weather states and predictors of selected NHMMs for North-west Western Australia. Summer is November through April; winter is May through October.

SEASON	KIMBERLEY NHMM*	PILBARA NHMM*
Summer	4 States	4 States
	North - South MSLP gradient	East - West MSLP gradient
	Northerly wind speed @ 850 hPa	Easterley wind speed @ 850 hPa
	DTD @ 850 hPa	DTD @ 700 hPa
Winter	4 States	4 States
	MSLP	East - West MSLP gradient
	East - West MSLP gradient	Easterley wind speed @ 700 hPa
	DTD @ 700 hPa	DTD @ 700 hPa

* MSLP = mean sea level pressure; DTD = dew point temperature depression (air temperature minus dew point temperature).

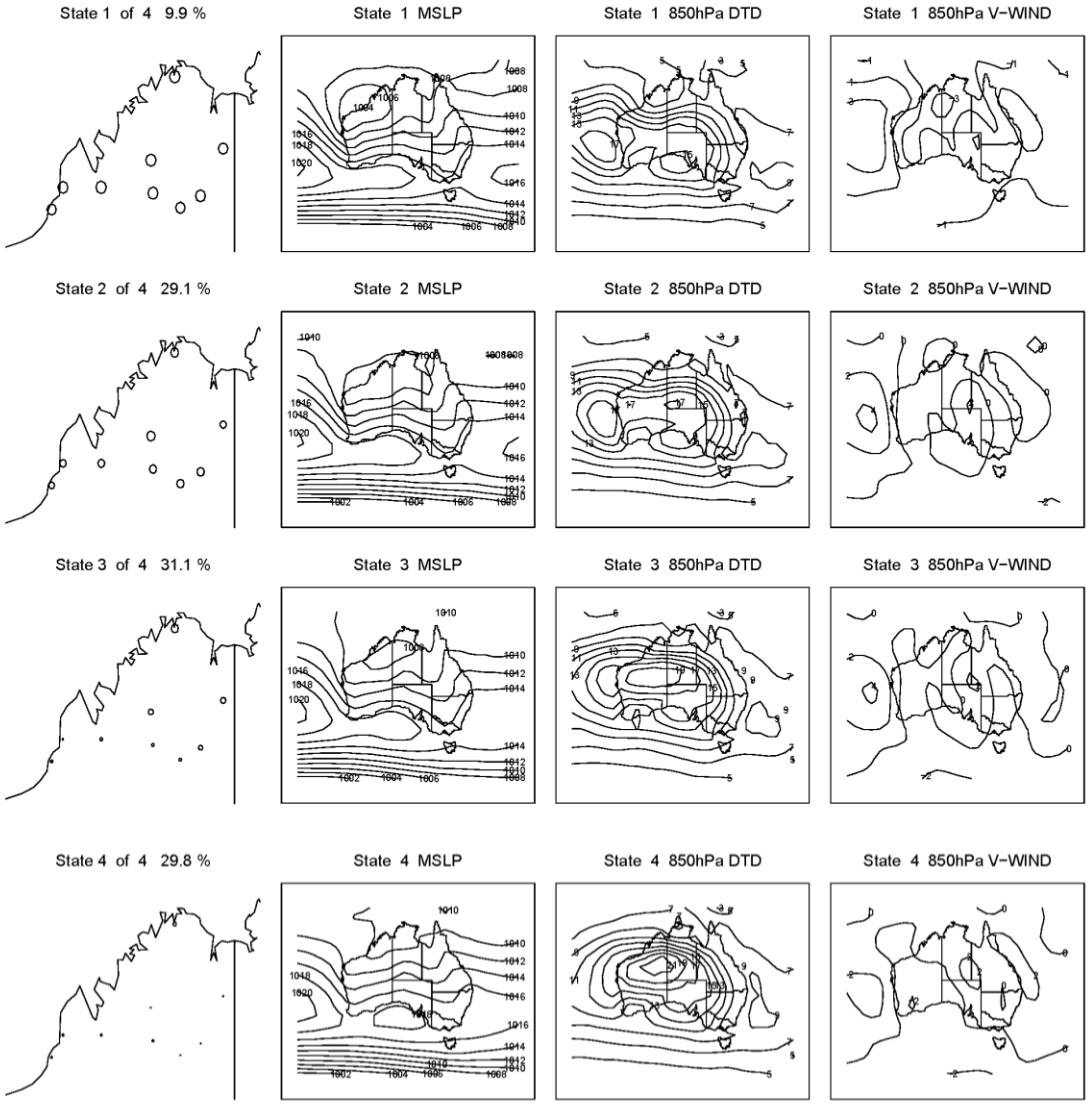

Figure C-2 Kimberley summer weather states as mean precipitation probability maps and corresponding composite atmospheric predictor plots.

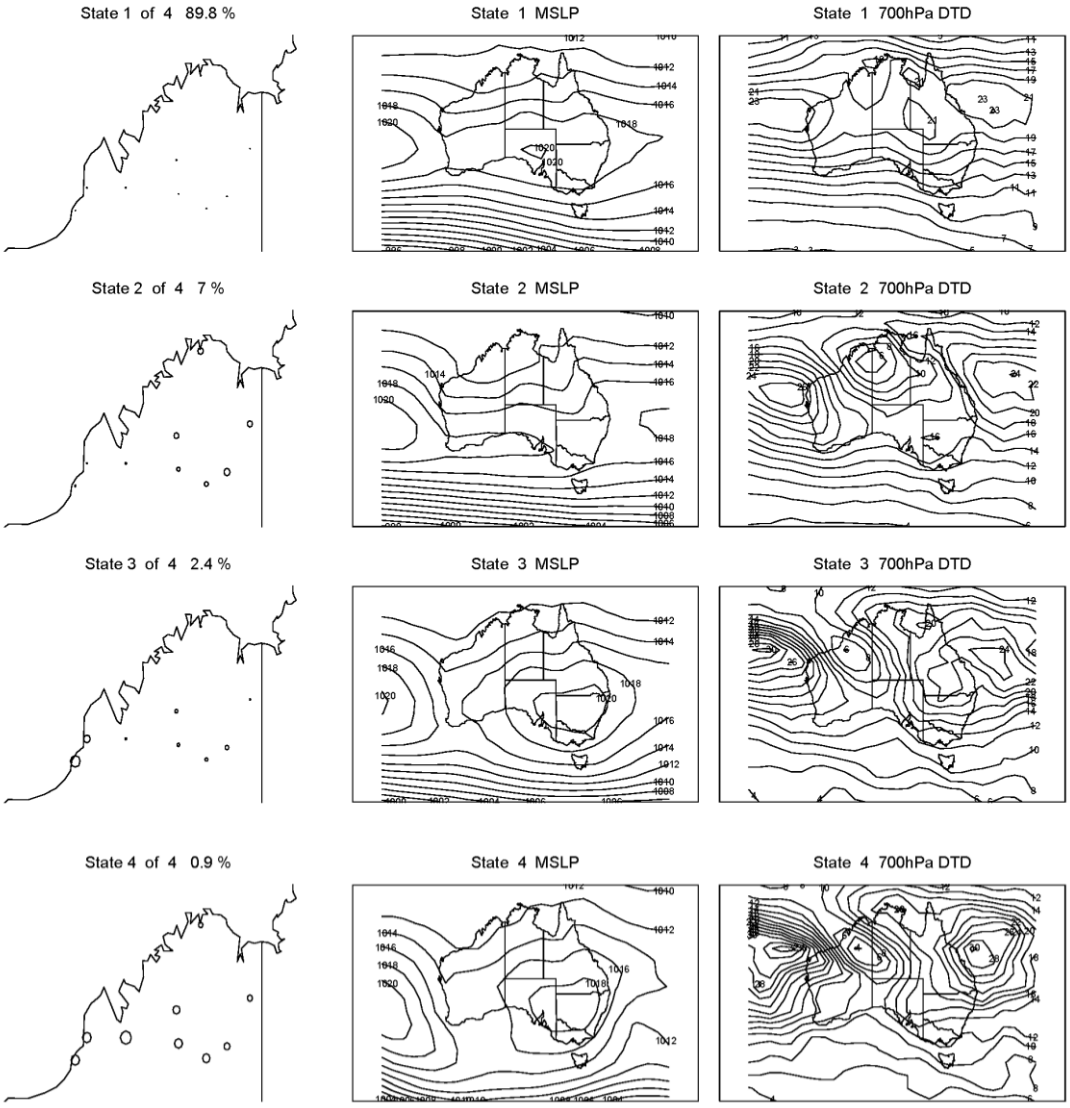

Figure C-3 Kimberley winter weather states as mean precipitation probability maps and corresponding composite atmospheric predictor plots.

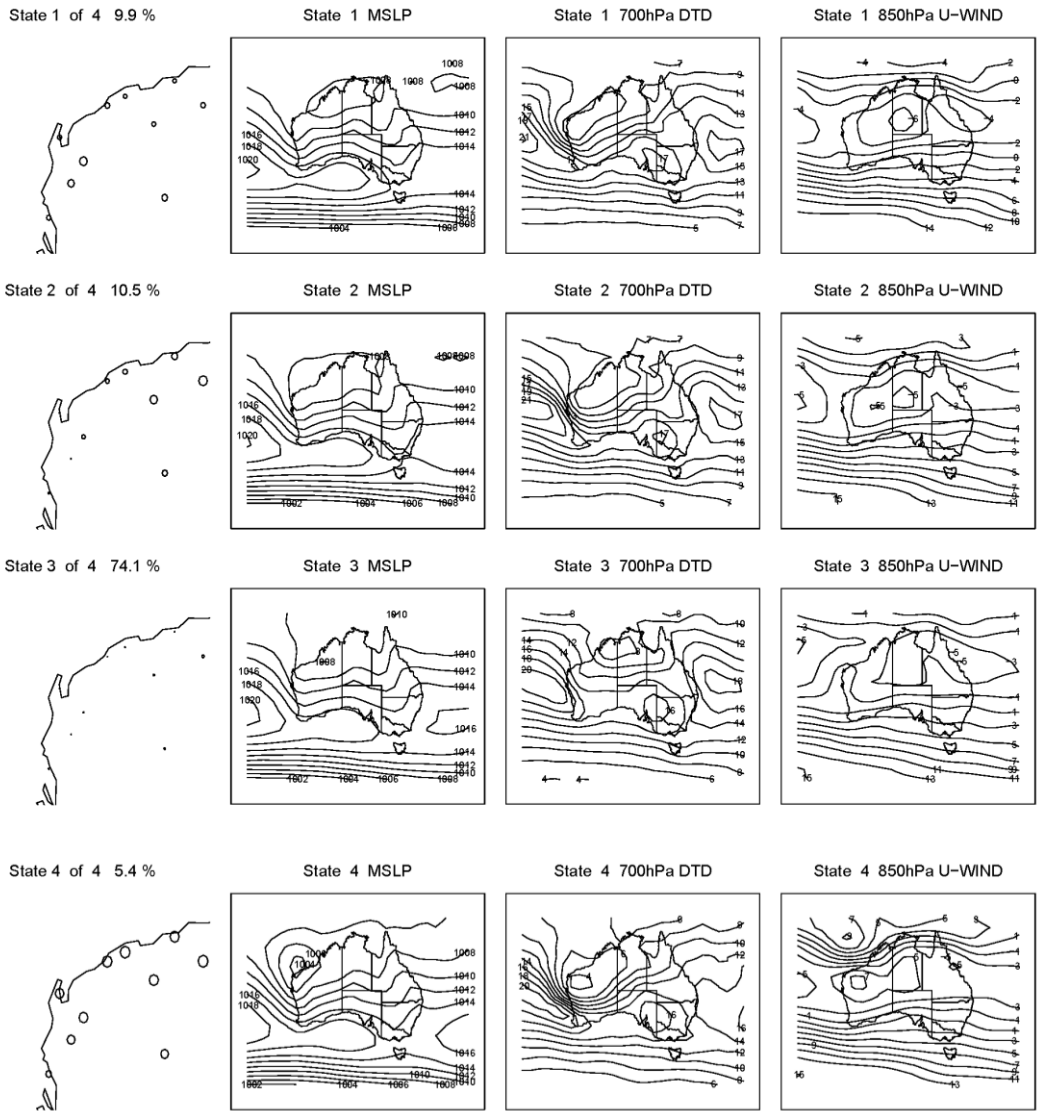

Figure C-4 Pilbara summer weather states as mean precipitation probability maps and corresponding composite atmospheric predictor plots.

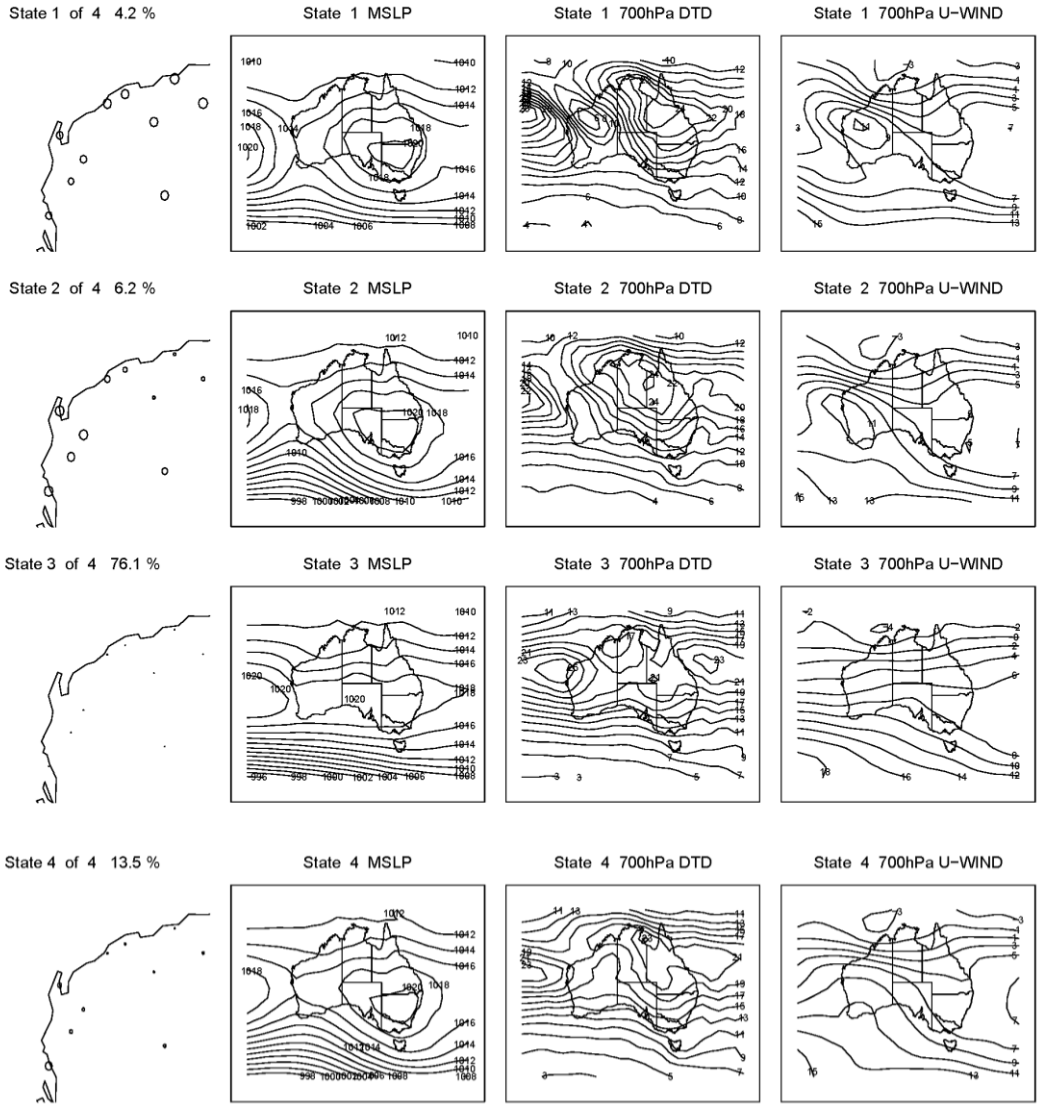

Figure C-5 Pilbara winter weather states as mean precipitation probability maps and corresponding composite atmospheric predictor plots.

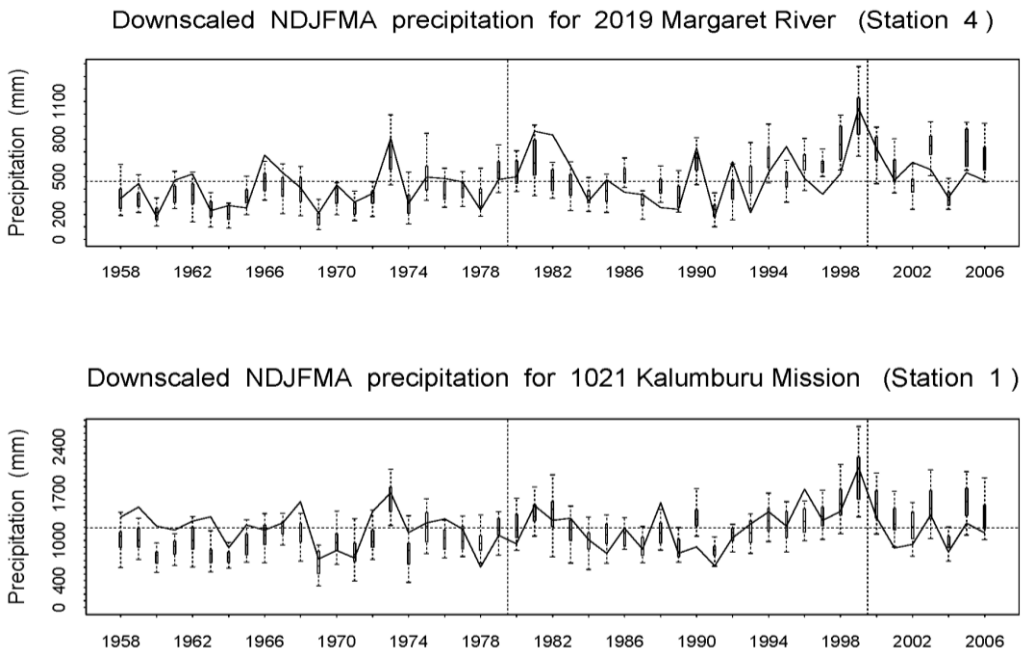

Figure C-6 NHMM simulations reproduce much of the observed interannual rainfall variability and the long-term trends, but also illustrate how extreme wet years can be underestimated. Illustrated here are November-April precipitation amounts for driest (upper plot: Margaret River) and wettest (lower plot: Kalumburu Mission) Kimberley rain gauges. Observed data is shown by solid lines, downscaled simulations by box-plots. Box–plots depict the range of 100 simulation trials (the edges of the box represent the 25th percentile and the 75th percentile of the simulations). The long-term observed mean is indicated by the horizontal dashed line. Vertical dashed lines separate the calibration period (1980/1 to 1999/2000) from the validation periods (1958/9 to 1979/80 and 2000/1 to 2006/7).

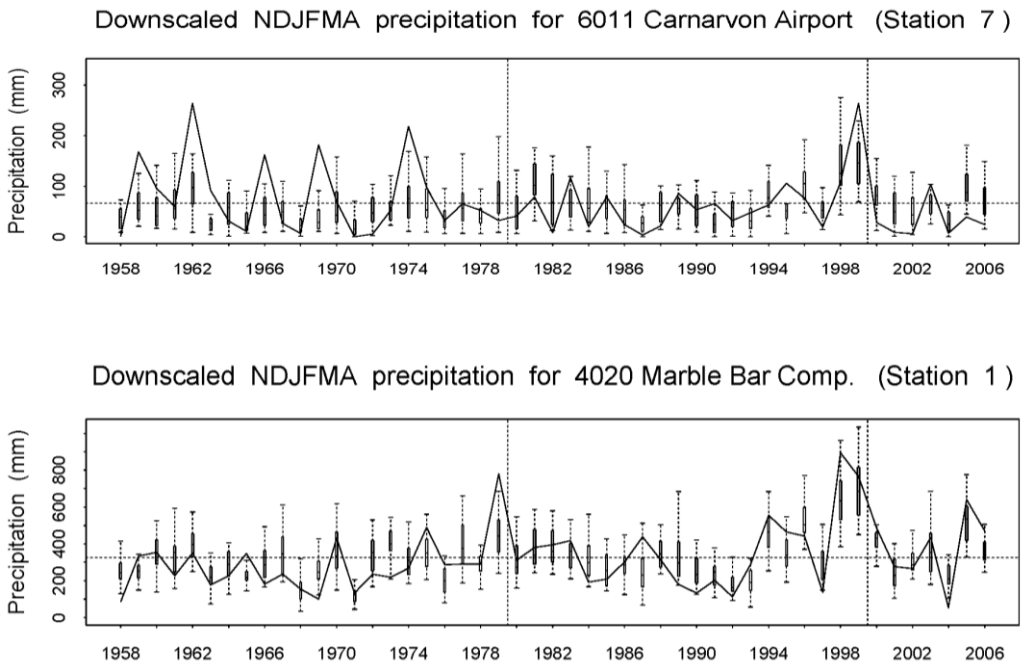

Figure C-7 As in Figure C-6 for sample Pilbara NHMM rain gauges. The Carnarvon Airport station data demonstrates how the model under-simulates several wet seasons (see 1962/63, 1966/67, 1969/70 and 1974/75), indicating that extremes-based methods, rather than the NHMM, are better suited to the task of modelling daily rainfall extremes.

Appendix D – Downscaled Rainfall and Temperature Results for NWWA

Table D-1 Projected proportional change in annual mean rainfall for nine sites in the Kimberley, as a proportion of present-day values (1962-1999). Values are given for mid-century (2047-2064) and end-of-century (2082-2099) periods under three SRES GHG scenarios (B1, A1B and A2). The range of results in each cell reflects the range of downscaled projections produced by the five GCMs, illustrating one source of uncertainty in the results.

STATION	PRESENT DAY	MID-CENTURY B1 (LOW)	MID-CENTURY A1B (MID-RANGE)	MID-CENTURY A2 (HIGH)	END OF CENTURY B1 (LOW)	END OF CENTURY A1B (MID-RANGE)	END OF CENTURY A2 (HIGH)
Kalumburu Mission	1	0.80–0.99	0.83–0.99	0.81–1.03	0.79–0.99	0.79–0.97	0.78–0.99
Halls Creek Airport	1	0.74–0.99	0.75–0.98	0.73–1.05	0.71–0.96	0.71–0.92	0.66–0.96
Lissadell	1	0.79–0.99	0.82–1.00	0.80–1.05	0.77–1.00	0.77–0.96	0.75–1.00
Margaret River Station	1	0.71–0.99	0.74–0.99	0.71–1.06	0.69–0.98	0.69–0.93	0.64–0.97
Broome Airport	1	0.72–0.98	0.73–0.97	0.69–1.06	0.68–0.95	0.68–0.93	0.61–0.96
Mount House Station	1	0.76–0.99	0.78–0.98	0.76–1.04	0.73–0.98	0.73–0.96	0.70–0.99
Udialla	1	0.72–1.00	0.74–0.97	0.71–1.05	0.70–0.97	0.70–0.93	0.65–0.96
Fossil Downs	1	0.72–0.99	0.73–0.98	0.71–1.05	0.69–0.97	0.68–0.95	0.63–0.95
Bidyadanga	1	0.70–0.97	0.74–0.98	0.70–1.04	0.68–0.96	0.68–0.93	0.62–0.94

Table D-2 Present-day and projected annual mean rainfall (in mm) for nine Kimberley stations. Values are given for mid-century (2047-2064) and end-of-century (2082-2099) periods under three SRES GHG scenarios (B1, A1B & A2). The range of results in each cell reflects the range of downscaled projections produced by the five GCMs, illustrating one source of uncertainty in the results.

STATION	PRESENT DAY	MID-CENTURY B1 (LOW)	MID-CENTURY A1B (MID-RANGE)	MID-CENTURY A2 (HIGH)	END OF CENTURY B1 (LOW)	END OF CENTURY A1B (MID-RANGE)	END OF CENTURY A2 (HIGH)
Kalumburu Mission	1260–1280	1030–1250	1070–1260	1030–1320	1010–1260	1010–1240	990–1260
Halls Creek Airport	630–640	470–620	480–610	470–660	450–610	450–590	420–600
Lissadell	670–680	530–660	550–670	540–710	520–660	520–650	510–670
Margaret River Station	530–550	390–530	400–520	380–560	380–530	370–500	340–520
Broome Airport	640–660	480–630	480–630	460–680	450–630	450–600	410–620
Mount House Station	860–890	660–860	690–880	660–920	640–870	640–850	620–860
Udialla	660–680	490–660	500–640	480–690	470–650	470–620	440–630
Fossil Downs	630–650	470–630	470–620	460–660	440–620	440–600	410–600
Bidyadanga	610–630	440–600	460–600	440–640	420–600	420–570	390–580

Table D-3 Projected change in annual mean rainfall for 10 sites in the Pilbara, as a proportion of present-day values (1962-1999), as per the description in Table D-1 above

STATION	PRESENT DAY	MID-CENTURY B1 (LOW)	MID-CENTURY A1B (MID-RANGE)	MID-CENTURY A2 (HIGH)	END OF CENTURY B1 (LOW)	END OF CENTURY A1B (MID-RANGE)	END OF CENTURY A2 (HIGH)
Marble Bar Comp	1	0.82–1.01	0.76–0.98	0.86–1.03	0.79–0.98	0.77–0.90	0.73–0.90
Port Hedland Airport	1	0.82–1.00	0.72–0.98	0.84–1.05	0.75–0.99	0.72–0.88	0.67–0.89
Coolawanyah	1	0.81–0.99	0.73–0.98	0.84–1.04	0.76–0.99	0.74–0.88	0.69–0.88
Learmonth Airport	1	0.87–1.00	0.78–1.00	0.88–1.06	0.81–1.00	0.78–0.94	0.73–0.93
Mardie	1	0.84–1.00	0.72–0.99	0.84–1.07	0.76–0.98	0.72–0.90	0.68–0.90
Karratha Station	1	0.83–0.99	0.71–0.99	0.84–1.07	0.74–0.97	0.73–0.89	0.67–0.88
Carnarvon Airport	1	0.91–1.01	0.86–1.00	0.92–1.05	0.87–1.01	0.86–0.97	0.82–0.99
Wandagee	1	0.88–0.99	0.78–0.99	0.87–1.07	0.80–1.03	0.79–0.92	0.74–0.96
Nyang Station	1	0.86–0.98	0.76–1.00	0.85–1.05	0.77–1.02	0.75–0.92	0.72–0.94
Mount Vernon	1	0.85–0.99	0.79–0.98	0.84–1.02	0.80–1.01	0.78–0.92	0.75–0.95

Table D-4 Present-day and projected annual mean rainfall (in mm) for 10 sites in the Pilbara, as per the description in Table D-2 above.

STATION	PRESENT DAY	MID-CENTURY B1 (LOW)	MID-CENTURY A1B (MID-RANGE)	MID-CENTURY A2 (HIGH)	END OF CENTURY B1 (LOW)	END OF CENTURY A1B (MID-RANGE)	END OF CENTURY A2 (HIGH)
Marble Bar Comp	430–490	350–470	330–460	370–500	340–460	330–420	310–420
Port Hedland Airport	300–360	250–340	220–340	260–380	230–340	220–300	210–310
Coolawanyah	420–480	340–460	300–450	350–500	310–460	310–410	290–410
Learmonth Airport	240–280	210–280	190–270	220–290	200–270	190–240	180–250
Mardie	310–360	260–350	220–340	260–390	230–340	220–300	210–310
Karratha Station	260–300	210–290	180–290	210–320	190–280	190–250	170–250
Carnarvon Airport	220–230	200–230	190–230	200–240	190–230	190–220	180–230
Wandagee	270–310	240–300	210–290	240–330	220–310	210–270	200–290
Nyang Station	310–360	270–350	240–340	270–380	240–360	240–310	230–330
Mount Vernon	300–320	250–310	230–310	250–330	240–320	230–290	220–300

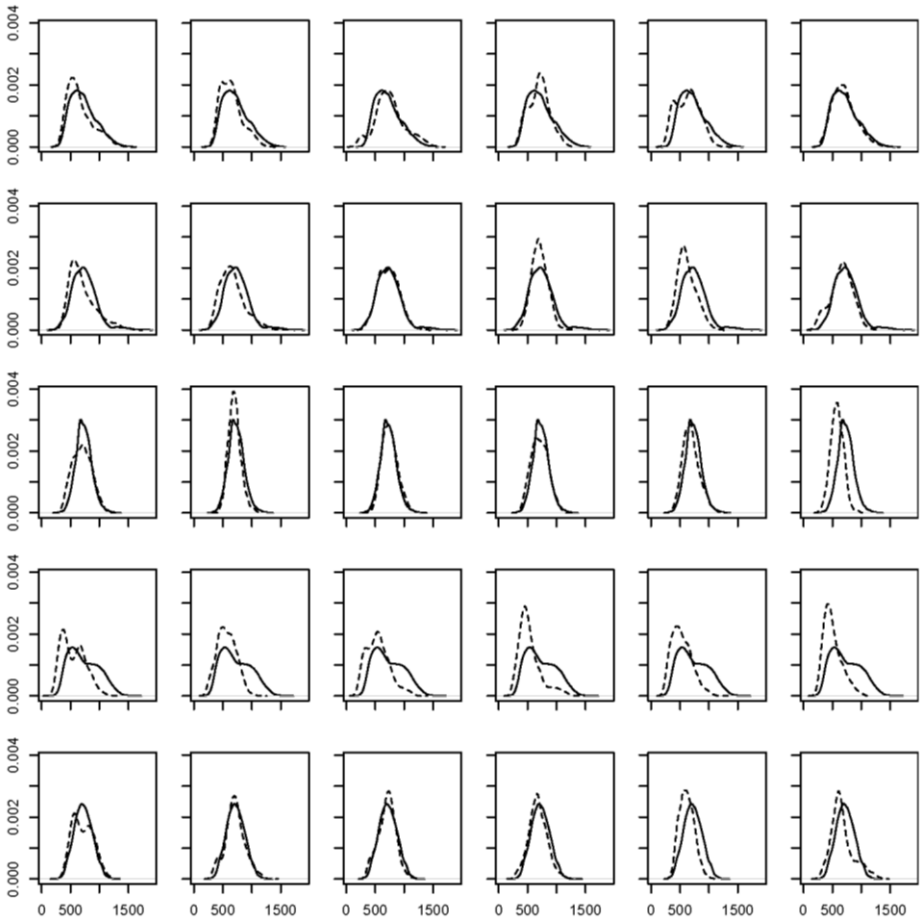

Figure D.1 The probability distribution of downscaled annual rainfall under current climate run (solid lines) compared to the projected climate (dashed lines). Results are averaged across nine Kimberly stations. A shift to the left indicates reduced rainfall in a future scenario. Rows from top to bottom represent the five GCMs (GFDL2.0, GFDL2.1, MIROC-medres, CSIRO Mk3.5 and MPI-ECHAM5) for six SRES scenario and period combinations (columns left to right: B1 mid-century, A1B mid-century, A2 mid-century, B1 end-century, A1B end-century and A2 end-century). The A1B or A2 emissions scenarios for the end of the century produce the most significant change, and suggest this region will be drier than the current period; most GCMs also produce a more peaked distribution (i.e., suggesting decreased interannual rainfall variance.)

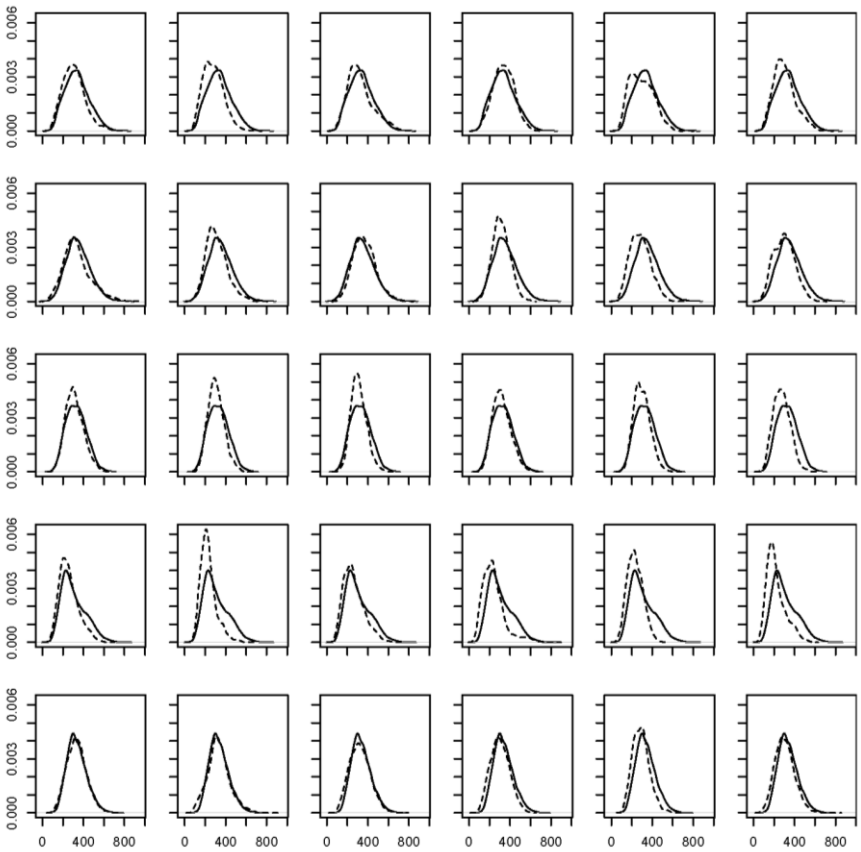

Figure D.2 As for the above, but for results averaged across the 10 Pilbara stations. In most cases an expected shift to drier conditions is projected for the end of the century, but only two global climate models project a more peaked rainfall distribution.

Table D-5 Kimberley summer weather state means and changes. First four data columns are mean frequency of respective weather state. Next four columns are the changes in weather state frequencies relative to the present climate (downscaled values [203CM] for the present day [1961-2000] relative to NCEP/NCAR Reanalysis [NNR] data; and global climate model projections for mid-century and end-of-century periods relative to downscaled present-day values).

PERIOD	DATA/GCM	STATE 1	STATE 2	STATE 3	STATE 4				
Full	NNR	0.09	0.28	0.31	0.31				
1st half	NNR	0.08	0.26	0.32	0.34	-0.01	-0.02	0.01	0.03
2nd half	NNR	0.10	0.31	0.31	0.29	0.01	0.03	0.00	-0.02
20C3M	GFDL2.0	0.10	0.30	0.30	0.29	0.01	0.02	-0.01	-0.02
20C3M	GFDL2.1	0.10	0.33	0.28	0.30	0.01	0.05	-0.03	-0.01
20C3M	MIROC	0.09	0.34	0.28	0.29	0.00	0.06	-0.03	-0.02
20C3M	MK35	0.10	0.31	0.29	0.29	0.01	0.03	-0.02	-0.02
20C3M	ECHAM5	0.10	0.32	0.28	0.30	0.01	0.04	-0.03	-0.01
B1_mid	GFDL2.0	0.09	0.29	0.32	0.30	-0.01	-0.02	0.02	0.01
B1_mid	GFDL2.1	0.10	0.32	0.29	0.30	0.00	-0.01	0.01	0.00
B1_mid	MIROC	0.09	0.33	0.29	0.29	0.00	-0.01	0.01	0.01
B1_mid	MK35	0.07	0.25	0.31	0.37	-0.03	-0.07	0.02	0.08
B1_mid	ECHAM5	0.10	0.32	0.29	0.29	0.00	0.00	0.00	0.00
A1B_mid	GFDL2.0	0.09	0.29	0.33	0.29	-0.02	-0.02	0.03	0.00
A1B_mid	GFDL2.1	0.08	0.29	0.31	0.32	-0.02	-0.03	0.03	0.02
A1B_mid	MIROC	0.08	0.36	0.30	0.26	-0.01	0.02	0.02	-0.03
A1B_mid	MK35	0.07	0.25	0.33	0.35	-0.04	-0.06	0.04	0.06
A1B_mid	ECHAM5	0.09	0.31	0.30	0.29	0.00	-0.01	0.02	-0.01
A2_mid	GFDL2.0	0.10	0.31	0.31	0.27	0.00	0.01	0.01	-0.02
A2_mid	GFDL2.1	0.10	0.31	0.29	0.30	0.00	-0.01	0.01	0.00
A2_mid	MIROC	0.10	0.37	0.30	0.24	0.00	0.02	0.02	-0.04
A2_mid	MK35	0.06	0.25	0.33	0.36	-0.04	-0.06	0.04	0.07
A2_mid	ECHAM5	0.10	0.30	0.29	0.31	0.00	-0.02	0.01	0.01
B1_end	GFDL2.0	0.09	0.33	0.32	0.26	-0.01	0.02	0.02	-0.03
B1_end	GFDL2.1	0.10	0.30	0.29	0.31	0.00	-0.02	0.02	0.01
B1_end	MIROC	0.09	0.34	0.29	0.29	-0.01	0.00	0.01	0.00
B1_end	MK35	0.06	0.24	0.31	0.39	-0.04	-0.08	0.02	0.10
B1_end	ECHAM5	0.09	0.28	0.30	0.33	-0.01	-0.04	0.02	0.03
A1B_end	GFDL2.0	0.08	0.29	0.35	0.29	-0.03	-0.02	0.04	0.00
A1B_end	GFDL2.1	0.08	0.28	0.31	0.33	-0.02	-0.04	0.03	0.03
A1B_end	MIROC	0.08	0.34	0.29	0.28	-0.01	0.00	0.02	-0.01
A1B_end	MK35	0.06	0.23	0.32	0.39	-0.04	-0.08	0.03	0.09
A1B_end	ECHAM5	0.08	0.28	0.33	0.31	-0.02	-0.04	0.04	0.02
A2_end	GFDL2.0	0.09	0.32	0.34	0.26	-0.02	0.01	0.04	-0.03
A2_end	GFDL2.1	0.08	0.30	0.32	0.30	-0.02	-0.02	0.04	0.00
A2_end	MIROC	0.06	0.30	0.31	0.33	-0.03	-0.04	0.03	0.04
A2_end	MK35	0.05	0.24	0.34	0.37	-0.05	-0.07	0.05	0.08
A2_end	ECHAM5	0.09	0.30	0.32	0.30	-0.01	-0.02	0.03	0.00

Table D-6 Kimberley summer atmospheric predictor means and changes. The first three data columns are the mean values of the respective atmospheric predictors. The next three columns are the changes in predictor values; downscaled values for the present day [1961-2000] relative to NCEP/NCAR Reanalysis [NNR] data; and projections for mid-century and end-of-century periods relative to downscaled present-day values.

PERIOD	DATA/GCM	N-S MSLP	V850	DTD850			
Full	NNR	0.22	0.20	13.47			
1st half	NNR	0.12	0.26	13.83	-0.10	0.06	0.36
2nd half	NNR	0.24	0.15	12.64	0.02	-0.05	-0.83
20C3M	GFDL2.0	0.13	-0.48	13.15	-0.09	-0.68	-0.32
20C3M	GFDL2.1	0.47	-0.21	10.25	0.25	-0.41	-3.22
20C3M	MIROC	0.31	-1.19	5.98	0.09	-1.39	-7.49
20C3M	MK35	0.25	-0.46	10.83	0.03	-0.66	-2.64
20C3M	ECHAM5	0.66	-0.58	10.07	0.44	-0.78	-3.40
B1_mid	GFDL2.0	0.12	-0.36	13.69	-0.01	0.11	0.54
B1_mid	GFDL2.1	0.40	-0.35	10.22	-0.07	-0.14	-0.03
B1_mid	MIROC	0.20	-1.18	5.92	-0.11	0.02	-0.06
B1_mid	MK35	0.23	0.12	13.27	-0.02	0.58	2.44
B1_mid	ECHAM5	0.62	-0.58	9.80	-0.04	0.00	-0.27
A1B_mid	GFDL2.0	0.03	-0.38	13.07	-0.10	0.09	-0.08
A1B_mid	GFDL2.1	0.44	-0.29	11.60	-0.03	-0.07	1.35
A1B_mid	MIROC	0.21	-1.20	5.67	-0.10	-0.01	-0.31
A1B_mid	MK35	0.23	0.04	13.10	-0.02	0.50	2.27
A1B_mid	ECHAM5	0.57	-0.65	9.88	-0.09	-0.07	-0.18
A2_mid	GFDL2.0	0.11	-0.45	12.22	-0.03	0.02	-0.93
A2_mid	GFDL2.1	0.50	-0.29	10.54	0.03	-0.07	0.29
A2_mid	MIROC	0.26	-1.38	5.41	-0.05	-0.19	-0.57
A2_mid	MK35	0.24	0.15	13.25	-0.01	0.60	2.42
A2_mid	ECHAM5	0.61	-0.55	10.18	-0.05	0.03	0.11
B1_end	GFDL2.0	0.17	-0.44	12.82	0.04	0.04	-0.34
B1_end	GFDL2.1	0.42	-0.32	10.37	-0.06	-0.11	0.12
B1_end	MIROC	0.22	-1.21	5.97	-0.09	-0.01	-0.01
B1_end	MK35	0.17	0.23	13.50	-0.08	0.69	2.67
B1_end	ECHAM5	0.63	-0.58	10.85	-0.02	0.00	0.78
A1B_end	GFDL2.0	0.03	-0.38	13.59	-0.10	0.10	0.43
A1B_end	GFDL2.1	0.35	-0.28	11.69	-0.12	-0.06	1.44
A1B_end	MIROC	0.12	-1.34	5.69	-0.19	-0.14	-0.29
A1B_end	MK35	0.25	0.18	13.90	0.00	0.63	3.07
A1B_end	ECHAM5	0.60	-0.65	11.36	-0.05	-0.07	1.29
A2_end	GFDL2.0	-0.05	-0.59	12.10	-0.18	-0.11	-1.05
A2_end	GFDL2.1	0.35	-0.30	10.60	-0.12	-0.08	0.34
A2_end	MIROC	-0.05	-1.12	6.27	-0.36	0.08	0.28
A2_end	MK35	0.28	0.30	14.36	0.03	0.75	3.53
A2_end	ECHAM5	0.67	-0.71	11.00	0.02	-0.13	0.94

Table D-7 Kimberley winter weather state means and changes. First four data columns are mean frequency of respective weather state. Next four columns are the changes in weather state frequencies relative to the present climate (downscaled values [203CM] for the present day [1961-2000] relative to NCEP/NCAR Reanalysis [NNR] data; and global climate model projections for mid-century and end-of-century periods relative to downscaled present-day values).

PERIOD	DATA/GCM	STATE 1	STATE 2	STATE 3	STATE 4				
Full	NNR	0.86	0.10	0.03	0.01				
1st half	NNR	0.86	0.10	0.03	0.01	0.00	0.00	0.00	0.00
2nd half	NNR	0.87	0.09	0.03	0.01	0.01	-0.01	0.00	0.00
20C3M	GFDL2.0	0.87	0.09	0.03	0.01	0.01	-0.01	0.00	0.00
20C3M	GFDL2.1	0.87	0.09	0.03	0.01	0.01	-0.01	0.00	0.00
20C3M	MIROC	0.87	0.09	0.03	0.01	0.01	-0.01	0.00	0.00
20C3M	MK35	0.87	0.09	0.03	0.01	0.01	-0.01	0.00	0.00
20C3M	ECHAM5	0.87	0.09	0.03	0.01	0.01	-0.01	0.00	0.00
B1_mid	GFDL2.0	0.87	0.09	0.03	0.01	0.00	0.00	0.00	0.00
B1_mid	GFDL2.1	0.87	0.09	0.03	0.01	0.00	0.00	0.00	0.00
B1_mid	MIROC	0.88	0.08	0.03	0.01	0.01	-0.01	0.00	0.00
B1_mid	MK35	0.89	0.08	0.03	0.01	0.02	-0.01	0.00	0.00
B1_mid	ECHAM5	0.88	0.08	0.03	0.01	0.01	-0.01	0.00	0.00
A1B_mid	GFDL2.0	0.88	0.08	0.03	0.01	0.01	-0.01	0.00	0.00
A1B_mid	GFDL2.1	0.89	0.08	0.03	0.01	0.02	-0.01	0.00	0.00
A1B_mid	MIROC	0.89	0.07	0.03	0.01	0.02	-0.02	0.00	0.00
A1B_mid	MK35	0.88	0.08	0.03	0.01	0.01	-0.01	0.00	0.00
A1B_mid	ECHAM5	0.88	0.08	0.03	0.01	0.01	-0.01	0.00	0.00
A2_mid	GFDL2.0	0.87	0.09	0.03	0.01	0.00	0.00	0.00	0.00
A2_mid	GFDL2.1	0.88	0.09	0.03	0.01	0.01	0.00	0.00	0.00
A2_mid	MIROC	0.89	0.07	0.03	0.01	0.01	-0.02	0.00	0.00
A2_mid	MK35	0.89	0.08	0.03	0.01	0.01	-0.01	0.00	0.00
A2_mid	ECHAM5	0.88	0.08	0.03	0.01	0.01	-0.01	0.00	0.00
B1_end	GFDL2.0	0.87	0.09	0.03	0.01	0.00	0.00	0.00	0.00
B1_end	GFDL2.1	0.88	0.08	0.03	0.01	0.01	-0.01	0.00	0.00
B1_end	MIROC	0.89	0.07	0.03	0.01	0.02	-0.02	0.00	0.00
B1_end	MK35	0.89	0.08	0.03	0.01	0.02	-0.01	0.00	0.00
B1_end	ECHAM5	0.88	0.08	0.03	0.01	0.01	-0.01	0.00	0.00
A1B_end	GFDL2.0	0.88	0.08	0.03	0.01	0.01	-0.01	0.00	0.00
A1B_end	GFDL2.1	0.89	0.07	0.03	0.01	0.02	-0.02	0.00	0.00
A1B_end	MIROC	0.90	0.06	0.03	0.01	0.03	-0.03	0.00	0.00
A1B_end	MK35	0.89	0.07	0.03	0.01	0.02	-0.01	0.00	0.00
A1B_end	ECHAM5	0.88	0.08	0.03	0.01	0.01	-0.01	0.00	0.00
A2_end	GFDL2.0	0.87	0.08	0.03	0.01	0.00	-0.01	0.00	0.00
A2_end	GFDL2.1	0.88	0.08	0.03	0.01	0.01	-0.01	0.00	0.00
A2_end	MIROC	0.90	0.06	0.03	0.01	0.03	-0.03	0.00	0.00
A2_end	MK35	0.89	0.08	0.03	0.01	0.01	-0.01	-0.01	0.00
A2_end	ECHAM5	0.88	0.08	0.03	0.01	0.01	-0.01	0.00	0.00

Table D-8 Kimberley winter atmospheric predictor means and changes. The first three data columns are the mean values of the respective atmospheric predictors. The next three columns are the changes in predictor values; downscaled values for the present day [1961-2000] relative to NCEP/NCAR Reanalysis [NNR] data; and projections for mid-century and end-of-century periods relative to downscaled present-day values.

PERIOD	DATA/GCM	MSLP	E-W MSLP	DTD700			
Full	NNR	1013.20	-0.24	17.36			
1st half	NNR	1013.07	-0.28	16.67	-0.13	-0.04	-0.69
2nd half	NNR	1013.31	-0.11	18.86	0.11	0.13	1.50
20C3M	GFDL2.0	1012.15	-0.43	17.09	-1.05	-0.19	-0.27
20C3M	GFDL2.1	1011.85	-0.37	15.66	-1.35	-0.13	-1.70
20C3M	MIROC	1012.96	0.39	13.65	-0.24	0.63	-3.71
20C3M	MK35	1015.63	0.45	16.11	2.43	0.69	-1.25
20C3M	ECHAM5	1012.76	0.04	18.70	-0.44	0.28	1.34
B1_mid	GFDL2.0	1012.13	-0.40	17.51	-0.02	0.03	0.42
B1_mid	GFDL2.1	1011.89	-0.26	15.06	0.04	0.11	-0.60
B1_mid	MIROC	1013.45	0.45	13.09	0.49	0.05	-0.56
B1_mid	MK35	1016.42	0.32	17.44	0.79	-0.13	1.33
B1_mid	ECHAM5	1013.10	0.10	19.38	0.33	0.06	0.68
A1B_mid	GFDL2.0	1012.44	-0.35	17.09	0.30	0.08	0.00
A1B_mid	GFDL2.1	1012.44	-0.32	17.31	0.59	0.04	1.65
A1B_mid	MIROC	1013.78	0.45	13.79	0.82	0.05	0.15
A1B_mid	MK35	1016.05	0.35	16.08	0.42	-0.10	-0.03
A1B_mid	ECHAM5	1013.02	0.16	18.80	0.26	0.12	0.10
A2_mid	GFDL2.0	1012.11	-0.41	17.31	-0.04	0.02	0.23
A2_mid	GFDL2.1	1012.06	-0.32	16.22	0.21	0.05	0.56
A2_mid	MIROC	1013.57	0.49	12.69	0.61	0.09	-0.96
A2_mid	MK35	1016.18	0.32	16.56	0.55	-0.13	0.45
A2_mid	ECHAM5	1013.15	0.14	18.94	0.38	0.10	0.24
B1_end	GFDL2.0	1012.07	-0.37	16.62	-0.07	0.06	-0.47
B1_end	GFDL2.1	1012.11	-0.34	16.45	0.25	0.03	0.78
B1_end	MIROC	1013.89	0.40	13.78	0.93	0.00	0.13
B1_end	MK35	1016.29	0.31	17.41	0.65	-0.14	1.31
B1_end	ECHAM5	1013.11	0.08	19.06	0.35	0.04	0.35
A1B_end	GFDL2.0	1012.29	-0.29	17.21	0.15	0.14	0.12
A1B_end	GFDL2.1	1012.44	-0.28	18.07	0.59	0.09	2.41
A1B_end	MIROC	1014.23	0.45	14.02	1.27	0.06	0.37
A1B_end	MK35	1016.43	0.32	16.57	0.80	-0.13	0.47
A1B_end	ECHAM5	1013.06	0.13	18.47	0.30	0.09	-0.24
A2_end	GFDL2.0	1012.23	-0.30	15.76	0.08	0.13	-1.33
A2_end	GFDL2.1	1012.31	-0.30	16.71	0.46	0.06	1.05
A2_end	MIROC	1014.31	0.47	13.51	1.35	0.08	-0.14
A2_end	MK35	1016.25	0.27	17.37	0.62	-0.18	1.26
A2_end	ECHAM5	1013.11	0.12	19.12	0.35	0.08	0.42

Table D-9 Pilbara summer weather state means and changes. First four data columns are mean frequency of respective weather state. Next four columns are the changes in weather state frequencies relative to the present climate (downscaled values [203CM] for the present day [1961-2000] relative to NCEP/NCAR Reanalysis [NNR] data; and global climate model projections for mid-century and end-of-century periods relative to downscaled present-day values).

PERIOD	DATA/GCM	STATE 1	STATE 2	STATE 3	STATE 4				
Full	NNR	0.11	0.11	0.73	0.05				
1st half	NNR	0.10	0.10	0.74	0.05	-0.01	-0.01	0.01	0.00
2nd half	NNR	0.11	0.12	0.72	0.05	0.00	0.01	-0.01	0.00
20C3M	GFDL2.0	0.12	0.11	0.70	0.07	0.01	0.00	-0.03	0.02
20C3M	GFDL2.1	0.12	0.12	0.69	0.07	0.02	0.01	-0.04	0.02
20C3M	MIROC	0.11	0.13	0.69	0.06	0.01	0.02	-0.04	0.01
20C3M	MK35	0.11	0.12	0.71	0.05	0.01	0.01	-0.02	0.00
20C3M	ECHAM5	0.12	0.11	0.70	0.07	0.01	0.01	-0.04	0.02
B1_mid	GFDL2.0	0.11	0.10	0.73	0.06	-0.01	-0.01	0.03	-0.01
B1_mid	GFDL2.1	0.12	0.10	0.71	0.07	0.00	-0.01	0.02	-0.01
B1_mid	MIROC	0.11	0.13	0.70	0.06	0.00	0.00	0.01	-0.01
B1_mid	MK35	0.10	0.09	0.77	0.04	-0.01	-0.02	0.05	-0.01
B1_mid	ECHAM5	0.11	0.11	0.71	0.07	-0.01	0.00	0.01	0.00
A1B_mid	GFDL2.0	0.12	0.10	0.73	0.05	0.00	-0.01	0.03	-0.02
A1B_mid	GFDL2.1	0.11	0.09	0.74	0.06	-0.01	-0.02	0.05	-0.02
A1B_mid	MIROC	0.10	0.13	0.72	0.05	-0.01	0.00	0.02	-0.01
A1B_mid	MK35	0.09	0.10	0.78	0.03	-0.02	-0.02	0.07	-0.02
A1B_mid	ECHAM5	0.11	0.11	0.71	0.06	0.00	0.00	0.01	0.00
A2_mid	GFDL2.0	0.13	0.11	0.70	0.06	0.01	0.00	0.00	-0.01
A2_mid	GFDL2.1	0.13	0.11	0.69	0.08	0.00	-0.01	0.00	0.00
A2_mid	MIROC	0.10	0.13	0.71	0.06	-0.01	0.00	0.01	-0.01
A2_mid	MK35	0.09	0.10	0.77	0.04	-0.02	-0.02	0.05	-0.01
A2_mid	ECHAM5	0.10	0.11	0.73	0.06	-0.02	-0.01	0.03	-0.01
B1_end	GFDL2.0	0.14	0.12	0.68	0.07	0.02	0.01	-0.02	0.00
B1_end	GFDL2.1	0.11	0.10	0.73	0.06	-0.02	-0.01	0.04	-0.01
B1_end	MIROC	0.11	0.13	0.70	0.06	0.00	0.00	0.01	0.00
B1_end	MK35	0.08	0.09	0.79	0.03	-0.03	-0.03	0.08	-0.02
B1_end	ECHAM5	0.11	0.10	0.74	0.05	-0.01	-0.01	0.04	-0.01
A1B_end	GFDL2.0	0.11	0.10	0.74	0.05	-0.01	-0.01	0.04	-0.02
A1B_end	GFDL2.1	0.10	0.09	0.76	0.05	-0.03	-0.02	0.07	-0.02
A1B_end	MIROC	0.10	0.12	0.73	0.05	-0.02	-0.01	0.04	-0.01
A1B_end	MK35	0.08	0.09	0.79	0.03	-0.03	-0.03	0.08	-0.02
A1B_end	ECHAM5	0.09	0.09	0.76	0.05	-0.02	-0.02	0.06	-0.02
A2_end	GFDL2.0	0.14	0.11	0.70	0.05	0.03	0.00	0.00	-0.02
A2_end	GFDL2.1	0.13	0.10	0.72	0.05	0.01	-0.02	0.03	-0.02
A2_end	MIROC	0.09	0.11	0.75	0.05	-0.02	-0.02	0.06	-0.02
A2_end	MK35	0.08	0.09	0.80	0.03	-0.03	-0.03	0.09	-0.03
A2_end	ECHAM5	0.10	0.10	0.74	0.06	-0.01	-0.01	0.04	-0.01

Table D-10 Pilbara summer atmospheric predictor means and changes. The first three data columns are the mean values of the respective atmospheric predictors. The next three columns are the changes in predictor values; downscaled values for the present day [1961-2000] relative to NCEP/NCAR Reanalysis [NNR] data; and projections for mid-century and end-of-century periods relative to downscaled present-day values.

PERIOD	DATA/GCM	E-W MSLP	U850	DTD700			
Full	NNR	-0.70	-1.46	13.19			
1st half	NNR	-0.78	-1.78	13.01	-0.08	-0.32	-0.18
2nd half	NNR	-0.62	-1.07	13.66	0.08	0.39	0.47
20C3M	GFDL2.0	-0.57	-1.68	15.28	0.13	-0.22	2.09
20C3M	GFDL2.1	-0.24	0.03	13.58	0.46	1.49	0.39
20C3M	MIROC	0.34	-0.56	10.48	1.04	0.90	-2.71
20C3M	MK35	-0.18	-0.24	13.22	0.52	1.22	0.03
20C3M	ECHAM5	-0.07	-0.36	12.03	0.63	1.10	-1.16
B1_mid	GFDL2.0	-0.63	-1.96	15.72	-0.06	-0.28	0.44
B1_mid	GFDL2.1	-0.30	-0.26	13.59	-0.06	-0.29	0.01
B1_mid	MIROC	0.31	-0.90	10.12	-0.04	-0.34	-0.36
B1_mid	MK35	-0.39	-1.17	13.21	-0.21	-0.93	0.00
B1_mid	ECHAM5	-0.07	-0.43	12.12	0.00	-0.07	0.09
A1B_mid	GFDL2.0	-0.69	-1.98	15.59	-0.12	-0.31	0.31
A1B_mid	GFDL2.1	-0.44	-0.44	14.23	-0.19	-0.47	0.65
A1B_mid	MIROC	0.33	-0.48	10.98	-0.02	0.08	0.50
A1B_mid	MK35	-0.47	-0.82	13.90	-0.29	-0.58	0.68
A1B_mid	ECHAM5	-0.08	-0.65	11.99	-0.01	-0.29	-0.04
A2_mid	GFDL2.0	-0.61	-1.44	15.08	-0.04	0.24	-0.20
A2_mid	GFDL2.1	-0.32	0.21	13.75	-0.08	0.18	0.17
A2_mid	MIROC	0.33	-0.40	10.79	-0.01	0.16	0.31
A2_mid	MK35	-0.33	-0.96	13.65	-0.15	-0.71	0.43
A2_mid	ECHAM5	-0.12	-0.65	12.38	-0.05	-0.29	0.35
B1_end	GFDL2.0	-0.56	-1.59	14.38	0.00	0.09	-0.91
B1_end	GFDL2.1	-0.35	-0.29	14.12	-0.10	-0.32	0.54
B1_end	MIROC	0.31	-0.50	10.56	-0.03	0.06	0.08
B1_end	MK35	-0.45	-1.19	13.86	-0.27	-0.95	0.65
B1_end	ECHAM5	-0.22	-0.81	12.26	-0.15	-0.45	0.23
A1B_end	GFDL2.0	-0.68	-2.16	15.15	-0.12	-0.48	-0.14
A1B_end	GFDL2.1	-0.50	-0.61	14.38	-0.26	-0.64	0.80
A1B_end	MIROC	0.28	-0.65	11.33	-0.06	-0.09	0.85
A1B_end	MK35	-0.49	-1.15	14.12	-0.31	-0.91	0.90
A1B_end	ECHAM5	-0.25	-1.01	12.81	-0.18	-0.65	0.78
A2_end	GFDL2.0	-0.64	-2.13	14.25	-0.07	-0.46	-1.04
A2_end	GFDL2.1	-0.46	-0.31	13.25	-0.21	-0.34	-0.33
A2_end	MIROC	0.29	-1.46	11.26	-0.05	-0.90	0.78
A2_end	MK35	-0.49	-1.22	13.93	-0.31	-0.98	0.71
A2_end	ECHAM5	-0.17	-0.70	12.43	-0.10	-0.34	0.40

Table D-11 Pilbara winter weather state means and changes. First four data columns are mean frequency of respective weather state. Next four columns are the changes in weather state frequencies relative to the present climate (downscaled values [203CM] for the present day [1961-2000] relative to NCEP/NCAR Reanalysis [NNR] data; and global climate model projections for mid-century and end-of-century periods relative to downscaled present-day values)

PERIOD	DATA/GCM	STATE 1	STATE 2	STATE 3	STATE 4				
Full	NNR	0.04	0.07	0.67	0.22				
1st half	NNR	0.04	0.07	0.67	0.22				
2nd half	NNR	0.05	0.08	0.65	0.22				
20C3M	GFDL2.0	0.04	0.07	0.66	0.22	0.00	0.00	-0.01	0.00
20C3M	GFDL2.1	0.04	0.07	0.66	0.22	0.00	0.00	-0.01	0.00
20C3M	MIROC	0.05	0.07	0.66	0.22	0.01	0.00	-0.01	0.00
20C3M	MK35	0.05	0.07	0.66	0.22	0.01	0.00	-0.01	0.00
20C3M	ECHAM5	0.05	0.07	0.66	0.22	0.01	0.00	-0.01	0.00
B1_mid	GFDL2.0	0.05	0.07	0.66	0.22	0.00	0.00	0.00	0.00
B1_mid	GFDL2.1	0.05	0.08	0.65	0.22	0.00	0.00	-0.01	0.00
B1_mid	MIROC	0.05	0.08	0.66	0.22	0.00	0.00	-0.01	0.00
B1_mid	MK35	0.04	0.07	0.67	0.22	0.00	-0.01	0.01	0.00
B1_mid	ECHAM5	0.05	0.07	0.66	0.22	0.00	0.00	0.00	0.00
A1B_mid	GFDL2.0	0.05	0.08	0.65	0.22	0.00	0.00	-0.01	0.00
A1B_mid	GFDL2.1	0.05	0.08	0.66	0.22	0.00	0.00	-0.01	0.00
A1B_mid	MIROC	0.04	0.08	0.66	0.22	0.00	0.00	-0.01	0.00
A1B_mid	MK35	0.04	0.07	0.68	0.22	0.00	-0.01	0.01	0.00
A1B_mid	ECHAM5	0.05	0.08	0.65	0.22	0.00	0.00	-0.01	0.00
A2_mid	GFDL2.0	0.05	0.07	0.66	0.22	0.00	0.00	0.00	0.00
A2_mid	GFDL2.1	0.05	0.08	0.65	0.22	0.00	0.00	-0.01	0.00
A2_mid	MIROC	0.05	0.08	0.65	0.23	0.00	0.00	-0.01	0.00
A2_mid	MK35	0.04	0.07	0.67	0.22	0.00	0.00	0.01	0.00
A2_mid	ECHAM5	0.05	0.08	0.65	0.22	0.00	0.00	-0.01	0.00
B1_end	GFDL2.0	0.05	0.08	0.66	0.22	0.00	0.00	-0.01	0.00
B1_end	GFDL2.1	0.05	0.08	0.66	0.22	0.00	0.00	-0.01	0.00
B1_end	MIROC	0.04	0.07	0.66	0.22	0.00	0.00	0.00	0.00
B1_end	MK35	0.04	0.07	0.67	0.22	0.00	-0.01	0.01	0.00
B1_end	ECHAM5	0.05	0.08	0.66	0.22	0.00	0.00	0.00	0.00
A1B_end	GFDL2.0	0.05	0.08	0.65	0.22	0.00	0.00	-0.01	0.00
A1B_end	GFDL2.1	0.05	0.08	0.65	0.22	0.00	0.00	-0.01	0.00
A1B_end	MIROC	0.05	0.08	0.65	0.22	0.00	0.00	-0.01	0.00
A1B_end	MK35	0.04	0.06	0.68	0.22	0.00	-0.01	0.02	-0.01
A1B_end	ECHAM5	0.05	0.07	0.66	0.22	0.00	0.00	0.00	0.00
A2_end	GFDL2.0	0.05	0.08	0.65	0.22	0.00	0.00	-0.01	0.00
A2_end	GFDL2.1	0.05	0.08	0.65	0.22	0.00	0.00	-0.01	0.00
A2_end	MIROC	0.05	0.08	0.65	0.22	0.00	0.00	-0.01	0.00
A2_end	MK35	0.04	0.06	0.68	0.21	0.00	-0.01	0.02	-0.01
A2_end	ECHAM5	0.05	0.08	0.66	0.22	0.00	0.00	0.00	0.00

Table D-12 Pilbara winter atmospheric predictor means and changes. The first three data columns are the mean values of the respective atmospheric predictors. The next three columns are the changes in predictor values; downscaled values for the present day (1961-2000] relative to NCEP/NCAR Reanalysis (NNR) data; and projections for mid-century and end-of-century periods relative to downscaled present-day values.

PERIOD	DATA/GCM	E-W MSLP	U700	DTD700			
Full	NNR	-0.45	3.70	20.72			
1st half	NNR	-0.50	3.87	19.41	-0.05	0.17	-1.31
2nd half	NNR	-0.34	3.31	22.60	0.11	-0.39	1.88
20C3M	GFDL2.0	-0.83	4.74	24.44	-0.38	1.04	3.72
20C3M	GFDL2.1	-0.71	4.25	22.20	-0.26	0.55	1.48
20C3M	MIROC	0.23	3.43	18.74	0.68	-0.27	-1.98
20C3M	MK35	0.28	4.99	20.74	0.73	1.29	0.02
20C3M	ECHAM5	-0.49	2.88	22.01	-0.04	-0.82	1.29
B1_mid	GFDL2.0	-0.83	4.68	25.35	0.00	-0.05	0.91
B1_mid	GFDL2.1	-0.63	3.64	22.47	0.08	-0.61	0.27
B1_mid	MIROC	0.29	3.51	18.69	0.06	0.08	-0.05
B1_mid	MK35	0.15	4.56	20.73	-0.14	-0.42	0.00
B1_mid	ECHAM5	-0.50	2.70	23.43	-0.01	-0.18	1.42
A1B_mid	GFDL2.0	-0.79	4.20	25.22	0.04	-0.53	0.78
A1B_mid	GFDL2.1	-0.71	3.42	24.76	0.00	-0.82	2.57
A1B_mid	MIROC	0.29	3.48	18.84	0.05	0.05	0.10
A1B_mid	MK35	0.14	4.67	19.79	-0.14	-0.32	-0.95
A1B_mid	ECHAM5	-0.43	2.87	23.01	0.06	-0.01	1.00
A2_mid	GFDL2.0	-0.83	4.52	25.36	0.00	-0.21	0.92
A2_mid	GFDL2.1	-0.69	3.60	23.74	0.02	-0.64	1.54
A2_mid	MIROC	0.36	2.99	17.71	0.13	-0.44	-1.04
A2_mid	MK35	0.12	4.94	20.86	-0.16	-0.05	0.12
A2_mid	ECHAM5	-0.45	2.75	23.14	0.04	-0.13	1.13
B1_end	GFDL2.0	-0.79	4.39	25.01	0.04	-0.35	0.57
B1_end	GFDL2.1	-0.72	3.93	23.95	-0.01	-0.31	1.75
B1_end	MIROC	0.24	3.40	18.89	0.01	-0.04	0.14
B1_end	MK35	0.13	4.77	20.69	-0.15	-0.21	-0.04
B1_end	ECHAM5	-0.49	2.94	23.85	0.00	0.06	1.84
A1B_end	GFDL2.0	-0.73	4.05	25.62	0.09	-0.68	1.18
A1B_end	GFDL2.1	-0.67	3.21	24.82	0.04	-1.03	2.62
A1B_end	MIROC	0.30	3.28	19.23	0.07	-0.15	0.49
A1B_end	MK35	0.13	4.21	19.31	-0.15	-0.78	-1.43
A1B_end	ECHAM5	-0.48	2.32	23.20	0.01	-0.56	1.19
A2_end	GFDL2.0	-0.74	4.40	24.26	0.09	-0.33	-0.18
A2_end	GFDL2.1	-0.69	3.58	24.57	0.02	-0.67	2.38
A2_end	MIROC	0.32	3.16	19.09	0.08	-0.27	0.35
A2_end	MK35	0.06	4.32	20.11	-0.22	-0.67	-0.63
A2_end	ECHAM5	-0.49	2.33	23.55	0.00	-0.55	1.54

Table D-13 Downscaled projected mean annual maximum and minimum temperatures in oC for nine Kimberley stations for mid-century (2047-2064) and end-of-century (2082-2099) periods for the SRES A2 GHG emissions scenario, relative to present day (1962-1999).

STATION	MINIMUM TEMPERATURE			MAXIMUM TEMPERATURE		
	PRESENT DAY	MID-CENTURY A2 (HIGH)	END OF CENTURY A2 (HIGH)	PRESENT DAY	MID-CENTURY A2 (HIGH)	END OF CENTURY A2 (HIGH)
Kalumburu Mission	21.0	23.0–23.6	25.0–25.7	34.4	36.0–37.2	37.5–38.8
Halls Creek Airport	20.3	22.4–23.2	24.7–25.7	33.6	35.5–36.5	37.5–38.6
Lissadell	21.5	23.6–24.4	25.8–26.8	35.3	37.1–38.2	38.9–40.1
Margaret River Station	20.5	22.6–23.4	24.9–25.8	34.6	36.6–37.5	38.5–39.7
Broome Airport	21.2	22.8–23.2	24.5–25.2	32.3	33.6–33.9	35.2–35.8
Mount House Station	19.7	21.7–22.3	23.9–24.6	34.2	35.9–37.0	37.6–38.9
Udialla	21.3	23.3–24.1	25.7–26.3	34.7	36.5–37.6	38.4–39.7
Fossil Downs	20.8	22.9–23.6	25.3–26.0	35.6	37.4–38.4	39.3–40.4
Bidyadanga	20.7	22.8–23.4	25.0–25.7	33.3	35.1–35.9	37.1–37.7

Table D-14. Downscaled projected mean annual maximum and minimum temperatures in oC for selected Pilbara stations for mid-century (2047-2064) and end-of-century (2082-2099) periods for an SRES A2 GHG emissions scenario relative to present day (1962-1999).

STATION	MINIMUM TEMPERATURE			MAXIMUM TEMPERATURE		
	PRESENT DAY	MID-CENTURY A2 (HIGH)	END OF CENTURY A2 (HIGH)	PRESENT DAY	MID-CENTURY A2 (HIGH)	END OF CENTURY A2 (HIGH)
Marble Bar Comp	20.4	22.5–23.4	25.3–25.9	35.2	37.3–38.4	39.3–40.8
Port Hedland Airport	19.7	21.7–22.5	24.3–24.8	33.3	35.2–36.2	37.3–38.4
Coolawanyah	19.2	21.4–22.2	24.0–24.7	33.1	35.3–36.3	37.2–38.7
Learmonth Airport	17.7	19.0–19.5	20.4–21.3	31.6	32.9–33.3	34.2–35.0
Mardie	19.0	20.6–21.0	22.3–23.0	34.2	35.8–36.0	37.2–37.9
Karratha Station	20.5	22.5–23.0	24.6–25.1	33.1	35.0–35.5	36.9–37.5
Carnarvon Airport	17.3	18.7–19.3	20.3–21.0	27.5	29.0–29.4	30.4–31.0
Wandagee	17.6	19.5–19.9	21.6–22.1	31.5	33.2–34.3	35.2–36.4
Nyang Station	18.1	20.1–20.6	22.4–22.9	33.4	35.3–36.4	37.4–38.6
Mount Vernon	17.3	19.4–20.2	22.1–22.7	32.1	34.1–35.3	36.0–37.6

Appendix E – Evaluation of Hot Spell Model for SWWA

Figure E-1 shows that the spatial pattern of thresholds estimated by the hot spell model using CCAM outputs (Figure E-1b) resembles that when using AWAP data (Figure E-1a). For example, southern parts of south Western Australia show relatively low threshold estimates (less than 30 °C), while the threshold estimate for the northern part are higher (above 35 °C). CCAM tends to underestimate the threshold by about 2-4 °C over the west and south coastal regions, and overestimates it by about 4 °C in north-east inland parts of south Western Australia (Figure E-1c).

The intensity of hot spells estimated from the CCAM data is largely consistent with that estimated from the AWAP-station data, with only minor overestimation of 2 °C over north-east inland SWWA (Figure E-1d-f).

Compared to the frequency of hot spells calculated from the AWAP and station data, the frequency of hot spells calculated from the CCAM data is slightly higher (1-2 events) over a large part of SWWA, and lower (by one event) in coastal regions (Figure E-1g-h).

For duration, there is a high level of consistency between the event lengths calculated from the CCAM and from the AWAP-station data, with only a 0 or 1 day difference over all of SWWA (Figure E-1j-l).

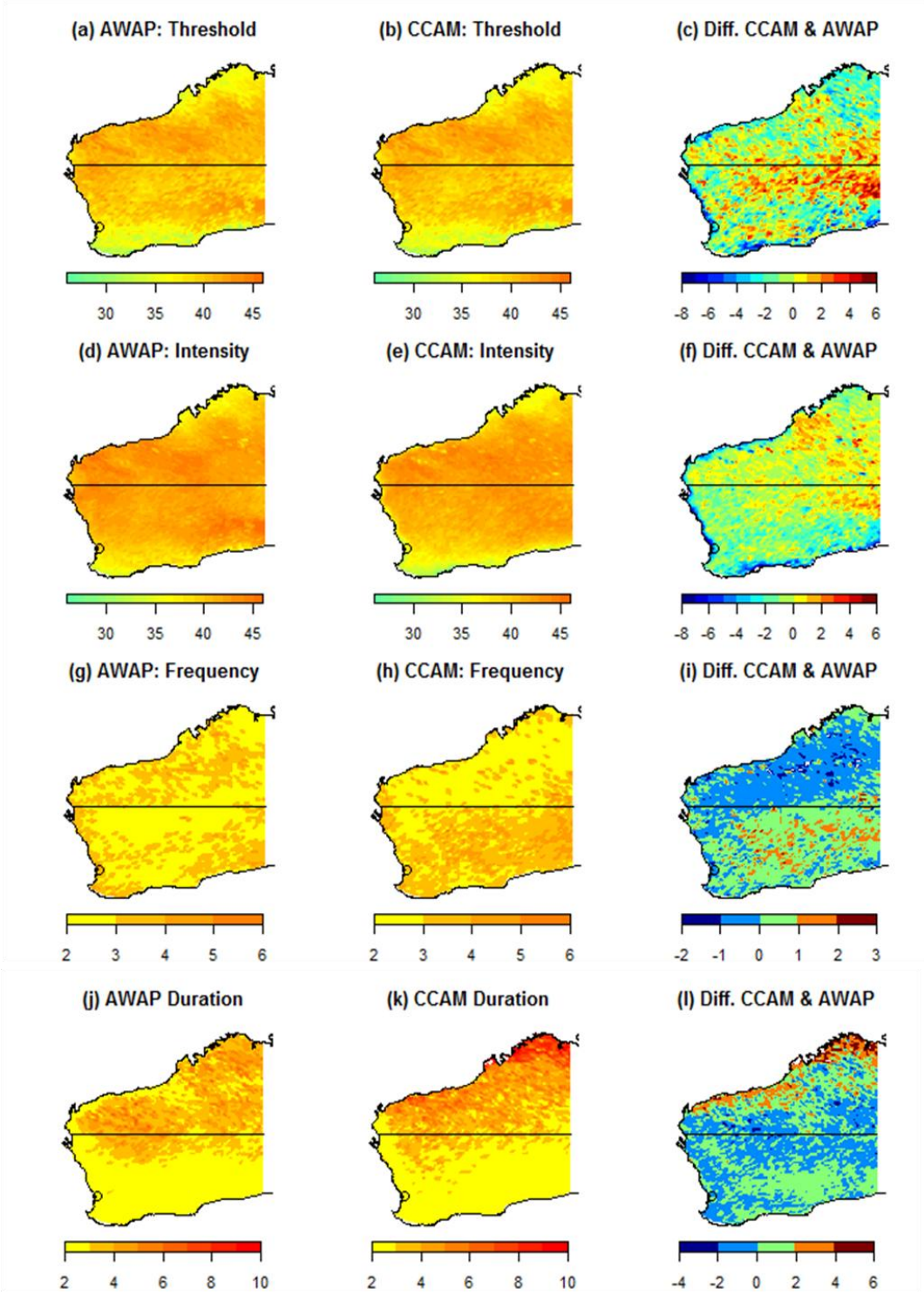

Figure E-1. Upper panel: spatial distribution of hot spell threshold estimates from the AWAP data (a); the CCAM data (b); and their difference (CCAM minus AWAP; c) during the 1981-2000 period; (d)-(f), same as (a)-(c), but for hot spell intensity; (g)-(i), same as (a)-(c), but for hot spell frequency. (d)-(f), same as (a)-(c), but for hot spell intensity; (j)-(l), same as (a)-(c), but for hot spell duration. Intensity is given in degrees Celsius, frequency in numbers of events, and duration in days. The black horizontal line at 25°S indicates the boundary between 'south Western Australia' (south of 25° S) and 'north Western Australia' (north of 25° S).

Appendix F – Evaluation of Hot Spell Model for NWWA

IOCI3 scientists evaluated the hot spell model's ability to reproduce the historical hot spell characteristics (intensity, frequency and duration) of north Western Australia by comparing model outputs with characteristics derived from summer (December through January) temperature observations at Port Hedland and Meekatharra airports for the period 1958-2011 (Figures F-1 and F-2). The estimated intensities (black curves) from the generalised Pareto distribution fit the data quite well (Figures F-1a and F-2a). The Poisson distributions (black curves) fit the observed frequencies well with two thirds of the Port Hedland and half of the Meekatharra observations for frequency falling on or within the area of the fitting (Figures F-1b and F-2b). Similarly, the geometric distribution fits (black curves) for these two stations are exceptionally good, with all observed durations falling within the area of the fitting (Figures F-1c and 2c).

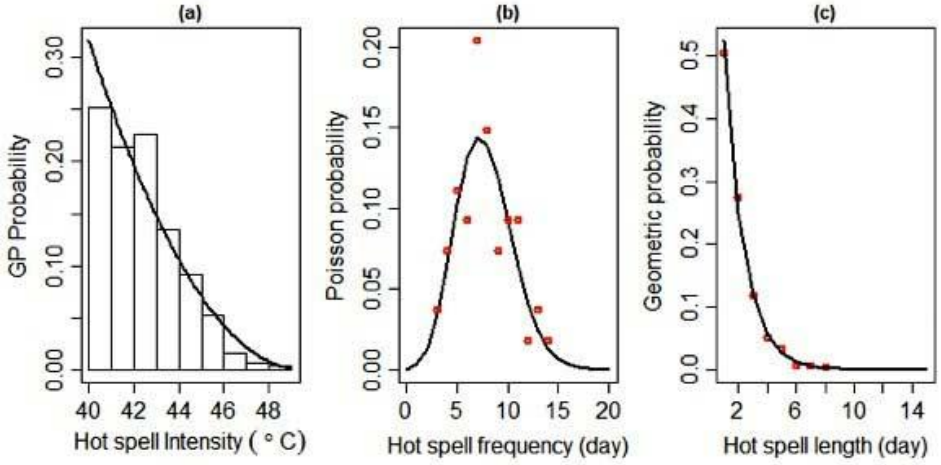

Figure F-1 Performance of distribution types chosen to model hot spell characteristics at Port Hedland Airport for summer (December through February) and the period 1958-2011. Hot spell model outputs are compared to station data obtained for the same period. (a) Histogram and estimated generalised Pareto distribution (black curve) for the intensity having a maximum excess within each of the hot spells; (b) empirical estimates (red circles) and estimated Poisson distribution (black curve) for the frequency of hot spells per summer; (c) empirical estimates (red circles) and estimated geometric distribution (black curve) for the duration of hot spell per summer.

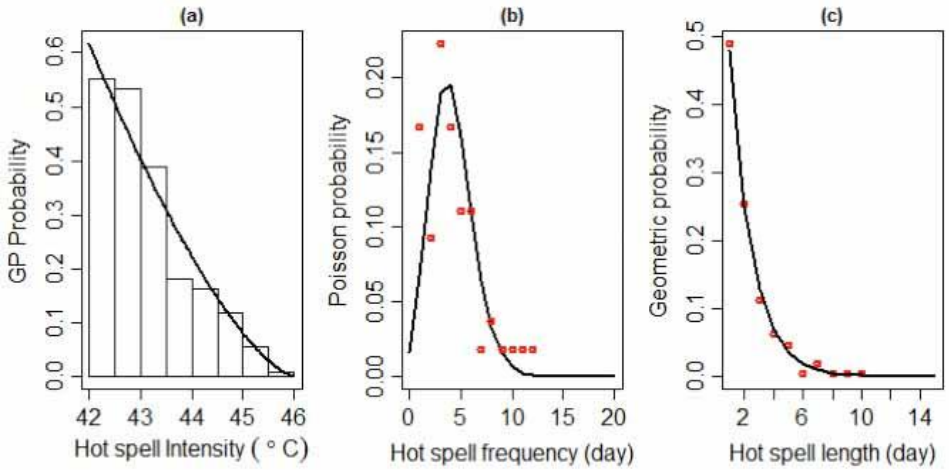

Figure F-2. As above, but for Meekatharra Airport.

Appendix G – Evaluation of CCAM Model Use in Hot Spell Simulations

Before producing projections for the characteristics of future north Western Australia hot spells, IOCI3 scientists compared ('observed') AWAP data and (modelled) CCAM outputs to test the hot spell model's ability to estimate north Western Australia hot spell characteristics for the present-day (1981-2010) climate.

Figure E-1 illustrates how the hot spell model results using AWAP data and CCAM output compare. The simulations produced using CCAM data overestimated thresholds by 2 to 5 °C in inland areas of north-western Australia, and underestimated hot spell thresholds by 3 to 6 °C along the south-western part of the Pilbara coast (Figure E-1c).

For hot spell intensity there is an overestimation of 0 to 2 °C and an underestimation of 2 to 5 °C (Figure E-1f).

For hot spell frequency, the CCAM simulations were consistent with the AWAP data in most of north-western Australia, with disparities of one or two events per summer. Along the Kimberly coastal region, this disparity was somewhat higher, from one to three events per summer (Figures E-1g-i).

As for duration, the CCAM simulations overestimated the length of hot spells along the Kimberly and Pilbara coastal regions by four to six days, and two to four days, respectively (Figures E-1j-l).